**PHD**

# CO Oxidation in Catalytic Hollow Fibres and Granular Catalysts: A Comparative Investigation of Catalyst Effectiveness

Nalette, Timothy

*Award date:*
2011

*Awarding institution:*
University of Bath

# CO Oxidation in Catalytic Hollow Fibres and Granular Catalysts: A Comparative Investigation of Catalyst Effectiveness

Timothy Arthur Nalette

A thesis submitted for the degree of Doctor of Philosophy

University of Bath
Department of Chemical Engineering

February, 2011



---

# Table of Contents

# List of Figures

# List of Tables

## Acknowledgements

The work presented in this thesis was carried out under the supervision of Dr. Semali Perera, Department of Chemical Engineering, University of Bath. The author would like to thank Dr. Perera for her support and guidance. Additionally, the author thanks Dr. Chin-Chih Tai for his support and technical assistance in the early phases of this research and Thomas Richards for his technical assistance in the laboratory at the university.

The author would also like to thank the Hamilton Sundstrand Division of United Technologies Corporation, US, for the financial support associated with the pursuit of this degree. Additionally, the author thanks Dr. David Wickham, Reactions Systems, LLC, for his encouragement, technical consultation, and review of various sections of this thesis.

The author would also like to thank his family for blessing him with five grandchildren during the conduct of this research and another to come shortly thereafter. I would also like to thank them for their unconditional love, continuous support, and encouragement in all my endeavors.

Finally, but foremost, I would like to thank God, the author and finisher of my faith, for ultimately providing me the wisdom and strength to finally see this through. I thank you for your provisions in all matters of life.

## Abstract

This research focuses on the development of novel catalytic hollow fibres, specifically aiming to demonstrate that catalytic reactions that have mass transfer limitations in the structure of the catalyst support can in many cases be incorporated into a hollow fibre structure with a higher activity, per unit volume and/or per unit mass of catalyst, than packed beds containing the same catalyst. Additionally, the hollow fibre configuration provides additional potential benefits relative to a packed bed such as lower reactor pressure drop, lower rates of catalyst attrition, and in many cases simpler reactor designs as catalyst retention is integral in the hollow fibre geometry and therefore retention screens and a means of providing a preload are eliminated.

Catalytic reactions investigated in this research dealt specifically with airborne contaminants of concern to the aerospace community, specifically ambient temperature oxidation of carbon monoxide and formaldehyde as it applies to closed systems such as spacecraft. However, the application of catalytic hollow fibre technology can be used for any reaction with internal mass transfer limitations and/or where pressure drop is a major consideration.

Candidate catalysts were selected based on a literature review, and the results of catalyst screening trials. Catalyst performance was compared to the baseline platinum on carbon catalyst used by the National Aeronautics and Space Administration (NASA) for trace contaminant control in existing closed loop life support systems. Based on the results of the catalyst screening trials, and research identified in the literature, a catalyst of platinum on titania, manufactured by the author, was selected for evaluation and development of catalytic hollow fibres. A commercially available catalyst, consisting of gold on titania and considered state of the art for the ambient temperature oxidation of carbon monoxide, was similarly investigated for comparison.

The selected catalysts were crushed to produce particles less than 50 microns in diameter and were mixed with various polymer solutions and subsequently used to produce the

catalytic hollow fibre structures using common hollow fibre spinning techniques. Polymers used in this research included polyethersulfone and polyvinylidenefluoride which were dissolved in 1-methyl-2-pyrrolidone. Precipitation of the polymer/catalyst spinning mixture was accomplished in a water bath for all samples. Catalyst concentrations investigated ranged from 70-90% (wgt.) in all fibres with the balance of the fibre consisting of polymer. Bore fluid compositions investigated included, 0, 70, 80, and 85% (wgt.) 1-methyl-2-pyrrolidone, in distilled water. The most significant increase in the catalyst effectiveness factor resulted when using a high solvent concentration in the bore fluid, with a corresponding increased porosity of the inner surface of the catalytic hollow fibre.

Multiple catalytic hollow fibres were combined to produce a catalytic hollow fibre module and tested in a differential reactor configuration to determine the internal effectiveness factor of each sample. The experimentally determined effectiveness factors of the catalytic fibres ranged from 0.001 to 0.062. The measured effectiveness factors for the original granular form of the gold and platinum catalysts were 0.058 and 0.040, respectively. In all cases, the internal effectiveness factors for the gold catalytic fibers were considerably lower than the granular form, ranging from 0.001- 0.034, due to degradation and/or poisoning of the gold catalyst during storage and manufacturing. The effectiveness factors measured for the platinum catalytic fibres ranged from 0.016 to 0.062, resulting in a maximum increase in the measured effectiveness factor of approximately 50% relative to the granular form.

In a comparative test of $Pt/TiO_2$ catalytic hollow fibres and granular catalysts with similar internal effectiveness factors conducted at a gas hourly space velocity of 110,400 $hr^{-1}$, the conversion of the granular form of the platinum catalyst was approximately 20% higher than the catalytic fibres. In the same test, the reaction rate per unit mass of the catalytic fibres was approximately 260% greater than the granular form. These results indicate that the catalytic hollow fibres result in a more efficient use of the catalyst which is expected due to the lower internal effectiveness factors of the granular catalyst for the ambient temperature oxidation of carbon monoxide.

# Nomenclature and Abbreviations

| | |
|---|---|
| $A_{CHF}$ | Cross sectional flow area of catalytic hollow fibre, $m^2$ |
| $A_{CCHF}$ | Exposed catalyst surface area on inner diameter of catalytic hollow fibre, $m^2$ |
| $A_r$ | Geometric surface area of catalyst structure available for diffusion, $cm^2$ |
| $a_c$ | Specific surface area of catalyst in reactor,$m^2/m^3$ |
| $a_p$ | Average pore radius in catalyst, cm |
| $C_a$ | Concentration of species *a*, moles $l^{-1}$ |
| $C_0$ | Inlet concentration, moles $l^{-1}$ |
| $[CO]_b$ | Concentration of CO in the bulk flow, moles $l^{-1}$ |
| $[CO]_s$ | Concentration of CO at the catalyst surface, moles $l^{-1}$ |
| $D$ | Diffusivity, $cm^2\ s^{-1}$ |
| $D_k$ | Knudsen diffusivity, $cm^2\ s^{-1}$ |
| $D_{AB}$ | Bulk diffusivity of binary gas mixture AB, $cm^2\ s^{-1}$ |
| $D_{CHF}$ | Diameter of catalytic hollow fibre, cm |
| $D_e$ | Effective diffusivity, $cm^2\ s^{-1}$ |
| $D_p$ | Effective particle diameter, cm |
| $g$ | Grams |
| $K$ | Degrees Kelvin |
| $k$ | Specific reaction rate constant, $s^{-1}$ |
| $k'$ | Pseudo rate constant, $l\ min^{-1}\ g^{-1}$ |
| $k''$ | Product of the pseudo rate constant and the catalyst density, $mins^{-1}$ |
| $k_b$ | Boltzmann constant = $1.38 \times 10^{-23}$ Joules/ºK |
| $k_c$ | Mass transfer coefficient, $cm\ s^{-1}$ |
| $k_d$ | Decay rate constant, $mins^{-1}$ |
| $k'_d$ | Specific decay constant, $g\ mol^{-1}$ |
| $L_i$ | Characteristic length of catalyst configuration *i*, where *i*=cylinder, CHF, etc, cm |
| $l$ | Liters |
| $l_{CHF}$ | Length of catalytic fibre, cm |
| *min* | Minutes |

| | |
|---|---|
| $MW_A, MW_B$ | Molecular weight of species A,B, g/mole |
| $M_T$ | Thiele modulus, dimensionless |
| $p$ | Pressure, atmospheres |
| $Re$ | Reynold's number, dimensionless |
| $Re_p$ | Packed bed, or particle, Reynold's number, dimensionless |
| $r_{p1}, r_{p2}$ | Radius of annular CHF configuration where subscripts 1 and 2 are ID and OD, respectively, cm |
| $S_p$ | Surface area of catalyst particle, $cm^2$ |
| $S_v$ | Specific surface area of catalyst particle, $cm^{-1}$ |
| $Sc$ | Schmidt number, dimensionless |
| $Sh$ | Sherwood number, dimensionless |
| $s$ | Seconds |
| $T$ | Temperature, K |
| $T_c$ | Critical Temperature, K |
| $t$ | Time, mins |
| $u_{bs}$ | Superficial bulk velocity, cm $s^{-1}$ |
| $V_b$ | Gas volume per mole at normal boiling point, $cm^3$ $gmol^{-1}$ |
| $V_{cat}$ | Volume of catalytic reactor, l |
| $V_p$ | Geometric volume of catalyst structure, $cm^3$ |
| $v_0$ | Volumetric flow rate at the reactor inlet, l $min^{-1}$ |
| $W$ | Weight of catalyst in packed bed or hollow fiber, g |
| $X$ | Fractional conversion of chemical reactant |
| | |
| **Greek Symbols** | |
| $\Omega$ | Overall effectiveness factor, dimensionless |
| $\Omega_{AB}$ | Collision integral for the molecular pair $AB$, dimensionless |
| $\varepsilon_B$ | Constants in the Lennard-Jones potential energy function for species A |
| $\varepsilon_B$ | Constants in the Lennard-Jones potential energy function for species A |
| $\varepsilon_{AB}$ | Constants in the Lennard-Jones potential energy function for molecular pair AB |

| | |
|---|---|
| $\eta_0$ | Initial internal catalyst effectiveness factor with deactivation, dimensionless |
| $\eta$ | Internal catalyst effectiveness factor, dimensionless |
| $\mu$ | Viscosity, g $cm^{-1}$ $s^{-1}$ |
| $\pi$ | Ratio of circumference to diameter of a circle, approximately 3.14 |
| $\rho$ | Gas density, g $cm^{-3}$ |
| $\sigma$ | Constriction factor for porous catalyst structure, dimensionless |
| $\sigma_{A,B}$ | Constants in the Lennard-Jones potential energy function for *A* or *B*, Å |
| $\sigma_{AB}$ | Constants in the Lennard-Jones potential energy function for gas pair *AB*, Å |
| $\tau$ | Tortuosity factor for catalyst structure, dimensionless |
| $\varphi$ | Porosity of catalyst structure |
| $\varphi_b$ | Void fraction of packed bed |
| | |
| **Abbreviations** | |
| *Å* | Angstroms |
| *ATCO* | Ambient temperature catalytic oxidizer |
| *Au* | Gold |
| *CHF* | Catalytic hollow fibre |
| *CO* | Carbon monoxide |
| *EDO* | Extended Duration Orbiter |
| *GHSV* | Gas Hourly Space Velocity, $hr^{-1}$ |
| *HCHO* | Formaldehyde |
| *IAQ* | Indoor air quality |
| *ISS* | International Space Station |
| *lpm* | l $min^{-1}$ |
| *NASA* | National Aeronautics and Space Administration |
| *PESF 1* | Polyethersulfone, Gafon 3100P |
| *PESF 2* | Polyethersulfone, Gafon 3000P |
| *Pt* | Platinum |
| *PVDF 1* | Polyvinylidenefluoride, Kynar 720 |
| *PVDF 2* | Polyvinylidenefluoride, Kynar 761 |

| | |
|---|---|
| *$SiO_2$* | Silicon dioxide |
| *SMAC* | Space maximum allowable concentration |
| *SOA* | State of the art |
| *sccm* | Standard $cm^3$ $min^{-1}$ |
| *slpm* | Standard l $min^{-1}$ |
| *TCC* | Trace contaminant control |
| *$TiO_2$* | Titanium dioxide |
| *μm* | Microns, $1x10^{-6}$ m |

# Chapter 1

## 1 Introduction

In heterogeneous catalysis, the active metal is supported on various structured supports such as granular supports, eg alumina, silica, titania, carbon, or other high pore volume, high surface area, granular or pelleted forms. Alternately, the structured support can also be in the form of monolith or honeycomb structures in which the active catalyst material is deposited on the surface of the structured passages which function as air flow channels. The primary advantage of a monolith, or honeycomb structure, is a significantly lower pressure drop as compared to a packed bed of granular catalyst (Farauto and Bartholomew 1997).

Reactions that are rate limited due to internal mass transfer within the structured support are occurring primarily at, or near, the outer surface of the supported catalyst. Therefore to more efficiently utilize the active catalyst material, it is desirable to deposit the catalyst metal only within the outer, active reaction zone of the catalyst support. In a pelleted or granular catalyst this is sometimes referred to as a "shell" like structure. In a monolith or honeycomb structure the active catalyst is contained in a thin layer, typically referred to as a "washcoat", which is applied to the surface of the flow channels of the structure to provide enhanced surface area. The thickness of the washcoat is typically controlled such that internal mass transfer limitations are negligible. However, if the washcoat is made sufficiently thick in an attempt to load more active catalyst metal in a given volume, the result is often similar to granular supports in that internal mass transfer limitations will develop as the thickness of the washcoat is increased (Farauto and Bartholomew 1997, Wei Lu et al. 2002).

To increase the reactivity of pelleted or granular supported catalysts with internal mass transfer limitations, the catalyst can be crushed to a size small enough to minimize or eliminate these limitations (Fogler 1999); however this typically results in an unacceptable pressure drop for industrial process applications as the pressure drop increase in a packed bed is inversely proportional to the catalyst particle diameter for

turbulent flow, and inversely proportional to the square of the diameter in laminar flow conditions (Perry and Chilton 1973).

A potential method of increasing the overall catalyst effectiveness is to encapsulate catalyst particles/powders into the walls of a porous hollow fibre structure, hereafter referred to as a catalytic hollow fibre (CHF). These structures are essentially physically equivalent to what is referred to in the literature as "mixed matrix membranes", whereby inorganic fillers are dispersed within polymeric membranes to enhance gas separation properties (Chung et al. 2007, Widjojo et al. 2008). In this research the following distinction is suggested. The catalytic hollow fibres are used as a means of incorporating catalyst particles within the polymer structure and essentially function as a packed bed – the polymer structure is acting as a component of the support for the catalyst. The reaction takes place via diffusion of reactants into the polymer/catalyst matrix and subsequent diffusion of reaction products out of the matrix. All bulk flow is in the bore of the fibres – there is no bulk flow through the polymer/catalyst wall. In mixed matrix membranes, the goal is to enhance the separation of components (in a gas or liquid phase) in the process stream through the incorporation of inorganic fillers, for example zeolites or alumina. The mixed matrix membranes therefore are used as membranes, with preferred separation occurring within the membrane structure, and not as a typical packed bed. These structures are discussed in more detail in Section 2.

In the CHF structure, if the resulting polymer/catalyst matrix is sufficiently porous, with pore diameters larger than typical granular supports, the catalyst particles can be fully utilized with an effectiveness factor similar to that of a packed bed of small catalyst particles. This approach has the potential of producing a high activity catalyst structure with minimal pressure drop. Additionally, the simplicity associated with a catalytic hollow fibre configuration allows packaging arrangements such as "reactive ductwork" significantly reducing the packaging volume associated with many industrial processes. A conceptual schematic for a catalytic hollow fibre module is depicted in Figure 1-1.

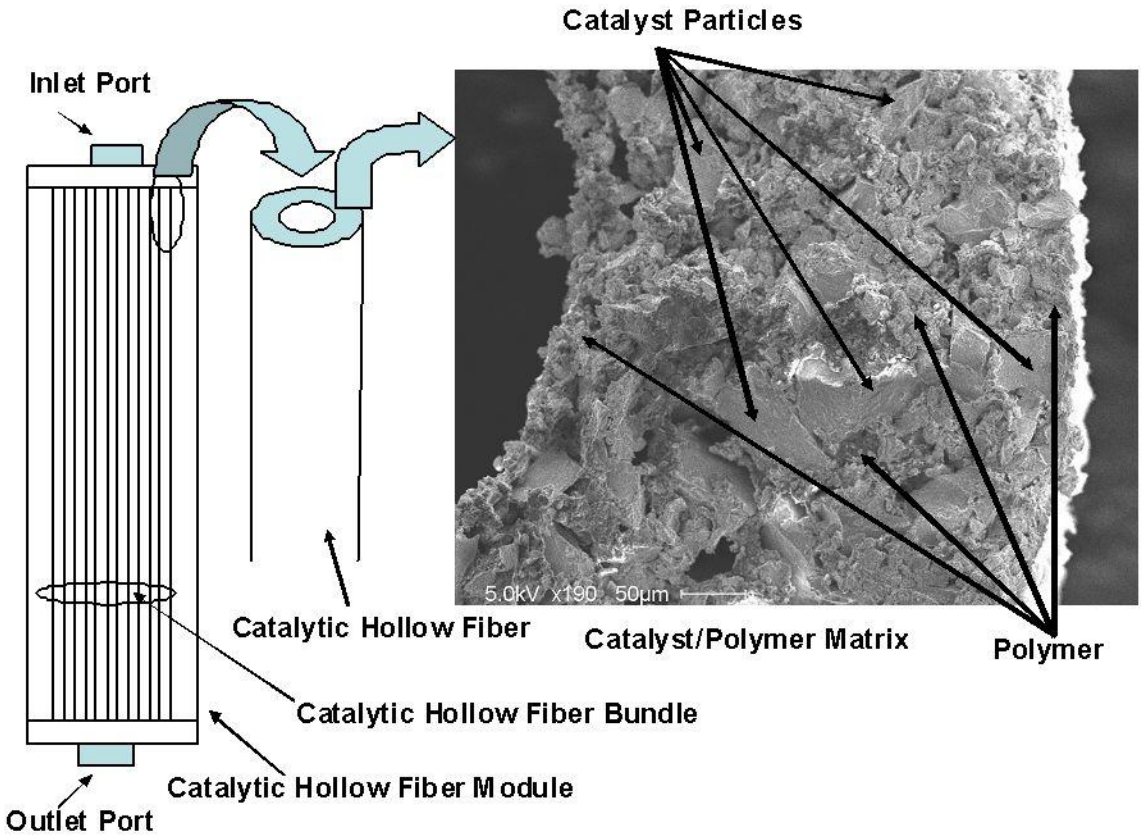


**Figure 1-1 Conceptual Schematic of a Catalytic Hollow Fibre Module**

The primary emphasis of this research is focused on the development of catalytic hollow fibres for use in trace contaminant control systems used in aerospace air revitalization systems in which reactor volume is a primary consideration, however due to similar considerations this technology may find applications in air quality control in office buildings where not only volume, but mass and cost of catalyst may also be important. Specifically, ambient temperature oxidation of selected contaminants, such as carbon monoxide and formaldehyde, which are not efficiently controlled by other technologies such as adsorption on activated carbon (Perry 1998), is investigated, and the effectiveness factors of the granular and CHF are compared.

### 1.1 Overall Objectives

The primary objective of this research is to produce a high activity catalytic hollow fibre reactor with increased effectiveness, by incorporating finely divided, highly effective

catalyst particles in the walls of porous hollow fibres. Since this research is applicable to catalytic reactions that are limited by internal mass transfer, a successful outcome is the demonstration of a catalytic hollow fibre that is more efficient (on a volumetric and/or catalyst mass basis) than conventional monolithic structures, ideally approaching that a packed bed of small catalyst particles where the size of the catalyst particles is sufficiently small such that a high internal effectiveness factor results. The obvious implication of this is a more efficient use of the catalyst in a configuration with a lower pressure drop than competing configurations.

**Specific aims of this research are:**

- Select candidate granular catalysts for comparison to the National Aeronautics and Space Administration's (NASA) existing contaminant control catalysts.
- Determine basic kinetic parameters and internal effectiveness factors for selected catalysts.
- Produce CHFs containing sufficiently small catalyst particles with an internal effectiveness factor approaching 0.95.
- Measure the internal effectiveness factor of the CHF structures and compare to the granular form of the same catalyst.
- Conduct a comparative test of a CHF module and a packed bed of the same catalyst and compare the results to the analytical prediction.
- Generate a list of recommendations for future research regarding CHF technology.

## 1.2 Research Methodology

Catalytic reactions of interest in indoor air quality control systems and trace contaminant control systems for space craft, and specifically ambient temperature catalysts for the oxidation of typical contaminants such as carbon monoxide and formaldehyde, are considered as model candidate reactions for evaluation in the catalytic hollow fibres.

A literature review was conducted to determine candidate catalysts which consist of granular, pelleted and monolithic forms. Comparative testing in the

"as received/manufactured" form was conducted to aid in the final selection of catalysts for further evaluation. Packed bed reactor testing was conducted, and kinetic parameters determined to aid in estimating the Thiele modulus and internal effectiveness factor of selected catalysts and the potential increase in the effectiveness factor for the CHF structures.

The selected catalysts were produced in a particle size that maximizes catalyst effectiveness and the catalyst particles were incorporated into the walls of hollow fibres. The oxidation reactions of interest were subsequently repeated to determine the internal effectiveness factors of the catalytic hollow fibre configuration as compared to the granular catalyst. Since the production of a volumetrically efficient reactor is the primary consideration in this research, reactant conversion as a function of gas hourly space velocity serves as the primary parameter for comparison of the two configurations. Additionally, the reaction rate, per unit mass of catalyst, was also measured to determine the efficiency of the CHF relative to the granular catalyst on a mass basis.

### 1.3 Thesis Overview

Chapter 2 of this thesis introduces the background for this research. The issue of trace contaminant control is introduced as it relates to aerospace life support systems and air revitalization specifically. Similar considerations and concerns are also presented related to indoor air quality applications. Contaminant classes, concentrations, and generation rates are also discussed to aid in understanding the rationale used in the research.

Chapter 2 also presents a detailed literature review, including NASA's history and rationale for the selection of currently used approaches, other approaches that NASA has investigated, and ambient temperature oxidation catalysts which target selected contaminants within spacecraft air revitalization systems. The review also addresses hollow fibre research associated with mixed matrix membranes and hollow fibre adsorbent structures.

Chapter 3 presents an overview of the experimental methodology used to address the comparison of packed bed and catalytic hollow fibre configurations. Catalyst selection, manufacturing and test procedures used in the support of this research are presented. Tests are conducted to determine basic kinetic parameters for $Pt/TiO_2$, $Au/Fe_2O_3$, and $Au/TiO_2$ catalysts and the effectiveness of the granular catalyst are calculated based on kinetic parameters, and catalyst geometry and structure. The low concentration (< 40ppm) of contaminants in this study allowed for the assumption of first order kinetics. Finally, the effectiveness factor for a potential CHF structure is analytically estimated.

Chapter 4 presents the development and test results of the CHF structures, including basic techniques and rationale associated with CHF manufacturing and the experimentally measured internal effectiveness factors for the CHF samples. The effectiveness factors are compared to those of the granular catalysts and an 18 hour test of a CHF fibre is conducted and modeled as a plug flow reactor. The results are then compared to a similar test conducted using an identical catalyst in a granular configuration.

Chapter 5 presents an overall discussion of the findings and conclusions of this research, in addition to providing recommendations for additional follow-on research associated with CHF applications.

# Chapter 2

## 2 Literature Review

Chapter 2 provides an overview of the pertinent literature as it relates to the development of the novel catalytic fibres. Specific contaminants, CO and HCHO are selected based on typical airborne contaminants encountered in space craft, however it is noted that the overall application of the catalytic fibre technology can be applied to other reactions as well. Historical and current methods of controlling these contaminants in space craft are presented, as well as relevant research associated with ambient temperature CO and HCHO oxidation catalysts.

As the selected catalyst is eventually to be encapsulated into a hollow fibre structure, the later sections in Chapter 2 provide a top level overview of common hollow fibre manufacturing approaches. Previous and current research that serves as the rationale for this research is presented. Finally, issues associated with fibre morphology are reviewed as they relate to the development of catalytic hollow fibres.

### 2.1 Airborne Contaminants

Exposure to airborne contaminants can result in numerous health issues, including various forms of respiratory system infection and irritation, potentially resulting in long term health effects and placing a burden on the health care system of many nations. As a result, government regulations have been developed in many countries to minimize the risk to employees by defining acceptable combinations of contaminant concentrations and exposure times for contaminants encountered in the work place. In addition to contaminants generated by various industrial processes, others are produced by the off-gassing of various volatile chemicals used in the manufacturing of office equipment and other workplace furnishings, such as laminated furniture and carpeting. Due to continually rising energy costs, specifically as it relates to the heating or cooling of air, reduced quantities of fresh air are used in ventilation systems thereby resulting in an

increased need to address air quality in the workplace. Many of these contaminants can also be present in houses, however higher ventilation in houses typically reduce the risk of such exposure to much lower levels than in the less well ventilated workplace environments (Yung et al. 2007, Oh and Hoflund 2006, Zhang et al. 2006).

Methods typically employed to control contaminant emissions include capturing or destroying the contaminant at the point of emission or through the incorporation of appropriate control technologies - usually installed in the heating, ventilation, and air conditioning (HVAC) system. These technologies include such things as carbon adsorption, absorption scrubbers, and oxidation reactors (thermal, catalytic, or photochemical) operating individually, or in combination, depending on the contaminant species present and their concentration (Yang et al. 2007, Kittrell 2002, Zhang et al. 2005).

A particularly unique trace contaminant problem exists in totally closed environments, such as spacecraft and submarines, where there is essentially no provision for providing fresh air ventilation. Since additional limitations exist due to the premium often placed on system power and volume requirements, highly efficient trace contaminant control systems are desirable.

The problem is further exacerbated in spacecraft due to the small free volume associated with such vehicles which provide little in the way of contaminant dilution. While many contaminants are controlled, or eliminated, in these applications through the careful selection of materials used in the construction of components, some off-gassing of volatile compounds is inevitable. Additionally, other less common contaminants may also be generated in significant quantities requiring control such as low molecular weight alcohols used in hand wipes, and metabolically produced contaminants such ammonia, methane, and methyl mercaptan from flatus.

## 2.2 Airborne Contaminants in Aerospace Closed Loop Life Support Applications

Closed loop air revitalization systems such as those employed on spacecraft must control trace contaminants at concentrations considered safe for personnel on board for mission durations ranging from approximate 7 days for a typical Shuttle mission, to 20 days for early lunar missions, and years for Mars missions, planetary habitats, and the International Space Station (ISS). In the US Space program, a large spacecraft airborne contaminant data base has been compiled over a span of approximately 40 years, and the number of contaminants that are monitored has grown as sampling and analytical techniques have matured (Perry 1998). Similar concerns exist in office buildings and aircraft as more air is recycled to reduce the costs associated with heating, ventilation, and air conditioning in buildings, and the compression of ambient air in commercial aircraft (Senkine 2002, Yu and Crump 1998). The terminology often used in these applications is referred to as trace contaminant control (TCC) in air revitalization applications, and indoor air quality (IAQ) in reference to terrestrial applications such as office buildings.

In TCC applications, some contaminants, such as $CO_2$, can rapidly rise to dangerous levels in a closed environment due to its relatively high generation rate resulting from human metabolism; however technologies to deal with them are well developed (NASA AMES Research Center 2004). Typically, organic compounds with sufficient adsorption potential can be efficiently controlled using activated carbon or zeolite adsorbents, or in the case of methane, high temperature catalytic oxidation. Some compounds such as CO and formaldehyde, which are not efficiently adsorbed on carbon or inorganic adsorbents are sometimes controlled by ambient temperature catalytic oxidation (Perry 2009a, Yang 2003).

IAQ applications, while similar in nature, are governed by a different set of criteria in defining the ultimate method of treatment. Since a significantly larger volume of air is processed, implementation costs are critical, whereas in manned space flight, performance, weight and volume are much stronger drivers in the design of the treatment system.

As indicated by Perry (1998), hundreds of contaminants have been identified in closed loop air revitalization systems encountered in aerospace applications, and mission duration is typically a major driver in the approach to trace contaminant control. For example on short missions, e.g. Shuttle, many compounds never reach the "space maximum allowable concentration", or SMAC, and for these contaminants no control is required. For contaminants that do reach their SMAC, a combination of activated charcoal and ambient temperature CO oxidation catalyst is used on the Shuttle. For longer term missions, such as the ISS, which are on the order of 5-10 years, many contaminants will reach their SMAC levels if control measures are not implemented. In this case, methane is the primary driver for the design of the TCC system since it is not easily adsorbed to any appreciable extent by activated carbon. The ISS therefore utilizes high temperature oxidation to control methane, and by default, many of the other contaminants are also oxidized which might otherwise be removed by activated carbon on shorter missions. The high temperature oxidation also eliminates the need to periodically launch and replace activated carbon beds since most of the other organic contaminants are also oxidized at the operating temperature of the high temperature reactor (Perry 1998).

### 2.3 Rationale for the Selection of Targeted Contaminants

The US is currently embarking on the design of a Shuttle replacement vehicle referred to as the Crew Exploration Vehicle, or CEV (NASA Exploration web site). The initial CEV missions include visits to the ISS, which is typically a 6-10 day mission, as well as a lunar transit mission which may last up to 20 days. For the initial CEV missions, methane doesn't reach its SMAC and therefore high temperature oxidation is not required since most of the other contaminants can be efficiently controlled using granular activated carbon. However, some low molecular weight contaminants do not load to any appreciable extent on activated carbon and therefore to minimize volume more efficient means of control are desired. Two such compounds are formaldehyde (HCHO) and carbon monoxide (CO). HCHO is classified as a carcinogen and therefore long term exposure is undesirable. CO is a poison that can bind with hemoglobin in the human

circulatory system, leading to CO poisoning and eventually death if no counter measures are implemented. CO and HCHO result from human metabolism, materials off-gassing, and are generated by the operation of certain electrical equipment (Perry 1998).

Formaldehyde has only recently been identified as a trace contaminant in closed life support systems and as a result no specific means of control had been historically implemented to control it concentration (Perry 2009a). On the International Space Station this is not an issue since the high temperature catalytic oxidation system in place to control the methane concentration will also effectively oxidize the formaldehyde, however the CEV currently doesn't plan on using a high temperature process for HCHO control and therefore an alternate means of control is desired.

On the US Space Shuttle, a 2% (wgt.) platinum on carbon (Pt/C) catalyst was selected for the control of CO. This selection was based on a study of commercially available catalysts in the late 1970s. The primary selection criteria at that time were minimum power and volume, and a 30 day operational life. At that time, 2% Pt/C demonstrated the best performance in that it was the only catalyst with sufficient activity at ambient temperature, over the range of required operating conditions. This catalyst is currently certified for 30 day shuttle missions (Lockheed Missiles and Space Company 1977).

To minimize energy requirements for the CEV mission duration mentioned above, it is undesirable to use high temperature catalytic oxidation. Additionally, the low loading of HCHO on activated charcoal results in the need to investigate alternate means of control. There currently exists a body of literature addressing ambient temperature oxidation of HCHO – primarily targeting IAQ applications, which is discussed in more detail in Section 2.4. Additionally, since the ambient temperature CO oxidation catalyst currently used on Shuttle was selected, the advent of the closed loop $CO_2$ lasers has resulted in much research in ambient/low temperature CO oxidation. It is the intent of this research to hopefully identify a catalyst that is active for both CO and HCHO (and possible other low molecular organic compounds) oxidation at ambient temperature to allow for the

efficient combination of these reactions in a single catalytic hollow fibre reactor, with potential applications in aerospace trace contaminant control and indoor air quality. Currently all NASA designed TCC systems utilize packed bed reactor configurations, primarily due to the fact that higher activity designs have been demonstrated with granular or pelleted catalysts as compared to monolith configurations (Perry 1998, Perry 2009a). This is believed to be primarily due to the limited mass of active catalyst material that can be deposited on the surfaces of the typical monolith structures. Additionally, there has been no incentive to investigate new approaches since mission durations have been well established for the last 15-20 years and the high cost associated with the certification of new technologies for TCC systems could not be justified.

A catalyst encapsulated in a hollow fibre matrix can provide numerous potential improvements over traditional packed bed reactors. If the catalyst effectiveness is low in the granular form, then much of the volume in a packed bed reactor is not utilized, i.e. - the interior of the catalyst support. Crushing the catalyst will expose more of the active metal but at the expense of much higher pressure drop. A hollow fibre matrix can encapsulate small catalyst particles in a porous structure that provides low pressure drop with high surface area, and the potential savings is a combination of more efficient utilization of catalyst in a fixed volume as well as reduced pressure drop relative to an equivalent packed bed reactor. Additional benefits may also be realized in the alternate packaging that a catalytic hollow fibre reactor offers – specifically in the sense that the hollow fibres could be housed directly in the ductwork, potentially reducing some of the capital costs associated with packed bed reactors in a chemical plant.

### 2.4 Ambient Temperature CO and HCHO Catalysts

In the mid 1970s NASA embarked on the design of the Space Shuttle with a variety potential mission scenarios, the longest of which was referred to as Extended Duration Orbiter (EDO), with mission lengths of up to 30 days. At that time HCHO was not identified as a contaminant that required treatment. Trace contaminant control was addressed primarily by three processes. Ammonia removal was determined adequate via

absorption in the water present in the condensing heat exchanger used to control cabin relative humidity, trace concentrations of organic contaminants were controlled via adsorption on granular activated charcoal, and CO was controlled through the use of a 2% (wgt.) Pt catalyst deposited on an activated carbon substrate (Perry 2009a). This reactor also incorporated a phosphoric acid impregnated carbon up stream of the catalyst to remove ammonia, a metabolically produced contaminant that would otherwise poison the catalyst. As previously noted on ISS missions, the primary means of controlling organic contaminants is via high temperature oxidation. This is primarily due to the fact that on long term missions, methane reaches its SMAC and requires elevated temperatures to oxidize. Additionally, using expendable carbon adsorption technologies would require re-supply which is costly due to the high launch costs and the on-orbit maintenance costs associated with changing sorbent canisters. Finally, it has only been since atmospheric contaminant data has become available from ISS, that concerns with HCHO contamination have been realized.

While high temperature oxidation of CO is common (with and without a catalyst), there are limited commercial applications of CO oxidation catalysts that operate at ambient temperature (Oh and Hoflund 2006, Taylor et al. 1999). A common catalyst, usually referred to as Hopcalite, is used extensively in protective masks for fire fighters primarily due to its high activity and low cost (Krämer et al. 2006), and consists of a mixture of manganese oxide and copper oxide for ambient temperature oxidation of CO. This catalyst has been extensively studied dating back to the early 1900's (Lamb et al. 1920, Farauto and Bartholomew 1997) however; it is easily deactivated by water vapor at concentrations typically encountered in closed loop life support systems (Lockheed Missiles and Space Company 1977).

An alternate method of ambient temperature CO oxidation that is currently being developed for closed, or semi-closed environmental control such as office buildings and commercial aircraft, is a photo-catalytic process that combines ultraviolet (UV) light and a photo catalyst such as titania dioxide (Hodgson et al. 2007, Sun et al. 2008). While this process may provide additional benefits such as microbial control and the oxidation of

other contaminants, including HCHO, ancillary equipment such as the UV light source and power requirements, in addition to the concerns associated with the potential release of mercury vapor from damaged UV light sources in microgravity closed systems, have resulted in limited interest by NASA for applications in aerospace TCC systems.

While CO and HCHO have low adsorption potentials on activated carbon (Perry 1998) making its use impractical, there are various commercial adsorbents being developed for the adsorption of HCHO, some with loadings as high as 20% by weight (Fukumoto et al. 2002, Nakayama et al. 2002). In most cases, the sorbent consists of pH basic compound that has been immobilized on a structural support, whereby the HCHO reacts via nucleophilic attack on the carbonyl carbon (Morrison and Boyd 1973). While the use of these sorbents may be practical in terrestrial applications, employing a separate, expendable system to control HCHO in long term space applications is not as attractive as combining it with another system, such as the CO oxidation catalyst if possible, assuming that the combination results in a reduction in total system weight and volume.

With the advent of closed cycle $CO_2$ lasers, a considerable body of literature exists related to low temperature CO oxidation catalysts (Hoflund and Gardner 1995, STC Catalysts Inc.). The high energy plasma of the laser results in decomposition of $CO_2$ into stoichiometric quantities of CO and $O_2$ which subsequently results in rapid power loss. To mitigate this phenomenon, low temperature CO oxidation catalysts have been developed to recombine the $O_2$ and CO, thereby maintaining the power output of the laser. While much of the research for this application is targeting stoichiometric concentrations of CO and $O_2$, more recently some of these catalysts are being evaluated for ambient temperature oxidation of CO and HCHO (STC Catalysts Inc., Schryer et al. 1990).

Combinations of a noble metal and a reducible metal oxide make up a class of catalysts referred to as NMRO (noble metal reducible metal oxide) catalysts, and in some combinations have been shown to possess a synergistic level of activity, which is higher than with either component alone (Schryer and Hoflund 1990). While much of the research related to $CO_2$ lasers has focused on $Pt/SnO_2/SiO_2$, additional catalysts that have

shown high activity include catalysts utilizing platinum or gold in combination with titanium dioxide and manganese dioxide supports (Alayon et al. 2009, Bond and Thompson 2000, Haruta 2003).

Under stoichiometric conditions, or in the presence of $CO_2$, Kielin (1998) reported $Pt/SnO_2/SiO_2$ to be the most active catalyst for CO oxidation, whereas with no $CO_2$ present, $Au/MnO_2$ appears to be preferred. Data presented for non-stoichiometric, $O_2$ rich gas mixtures, show an increased activity which further points to the potential suitability of these catalysts (Pt and Au based) as potential TCC candidates. His research also included evaluations of $MnO_2$, $Pt/MnO_2$, $Ag/MnO_2$, $Pd/MnO_2$, $Au/MnO_2$, $Au/CeO_2$, $Au/Fe_2O_3$, $Pt/SnO_2$, $Pt/Fe_2O_3$, and $Pt\text{-}Pd/SnO_2$ catalysts. Testing conducted with $Pt/SiO_2$ showed no activity for CO oxidation indicating that Pt alone is not responsible for the activity of the $Pt/SnO_2/SiO_2$ formulation. Kielin also noted that for Au and Pt with the highest activities, the optimum metal content by weight is 20-28% and 11-17%, respectively (the wt % numbers are based on the total weight of the noble metal and metal oxide only). When normalized based on the weight of the noble metal it is found that the activity of the Au catalyst is approximately twice that of the Pt catalyst.

In addition to CO oxidation, Kielin (1998) also investigated the oxidation of mixtures of CO and HCHO at 23 ºC. He reported that complete oxidation of an 8000 ppm HCHO in air continued for approximately 17 days at which time the activity began to decay due to saturation of the catalyst with HCHO (adsorption rate exceeding the rate of oxidation). Kielin also reported that Pt alone (not in combination with $SnO_2$) is capable of oxidizing HCHO which is discussed in more detail below.

Kielin's (1998) research elucidates the role of water in the oxidation of CO, specifically in that it acts as a catalyst, most likely in the form of hydroxyl radicals. However, in the stoichiometric applications it appears that only small amounts of water are desired for optimum activity, which may be a concern in TCC and IAQ applications in which the relative humidity is typically in the range of 35-70%. In Kielin's work he noted a significant decrease in catalyst activity when the relative humidity was greater than 15-

20%. For the $CO_2$ laser application this led to the use of silica gel as a catalyst support since it could serve as both a source and a sink for water, being pretreated to the optimum water content for the closed system application. The nominal test conditions in Kielin's research involved stoichiometric gas mixtures, reactor temperatures of 35-80 ºC, and space velocities on the order of 4,500-6,750 $hr^{-1}$.

It has also been shown that small amounts of promoters such as Fe and Ce can significantly increase the CO oxidation activity, while decreasing the decay rate of $Pt/SnO_2/SiO_2$ and $Au/MnO_2$ catalysts under stoichiometric conditions (Oh and Hoflund 2007). For the $Pt/SnO_2/SiO_2$, it is noted that 1% wt. Fe increased the activity approximately 2-fold at steady state conditions at 75 ºC. In the case of $Au/MnO_2$, 1% wt. Ce was found to increase the activity approximately 30% at 55 ºC. While this reference is not an exhaustive investigation in promoters it does indicate that additional activity can be obtained though the use of promoters. It should be noted that this reference also highlights the fact, which is not surprising, that activity and decay characteristics are strongly dependent upon numerous catalyst preparation, pretreatment, and reaction variables, and is often a reason for apparently conflicting results being reported by different researchers (Oh and Hoflund 2007, Perry and Wang 2007, Bond and Thompson 2000).

In TCC and IAQ applications, the typical range of ambient relative humidity is approximately 30-70 % and it is therefore advantageous if the catalyst can operate continuously with minimal degradation in activity in the presence of water vapor. Numerous researchers have shown that some combinations of NMRO catalysts maintain their catalytic activity over a range of inlet relative humidity (Kielin 1998). Oh and Hoflund (2007) have shown that some level of water vapor is advantageous to maintaining catalyst activity through a proposed active hydroxyl species responsible for the oxidation of chemi-sorbed CO on palladium oxides, while Kielin (1998) showed that pretreatment of a platinum catalyst with water vapor resulted in higher initial activity than un-treated catalyst. However, in the $CO_2$ laser applications, water is typically provided in small quantities to the gas mixture or directly to the catalyst as part of a

pretreatment process. As such there is limited literature on the effects of water vapor on these catalysts which is an obvious consideration for air purification applications.

The platinum/tin oxide catalyst mentioned in Kielin's work is commercially available from STC Catalysts Inc. in monolith structures, and will be evaluated in the preliminary screening work; however there is no data in the open literature on the effects of typical ambient humidity levels on this catalyst.

HCHO oxidation catalyst research targeting indoor air quality applications has identified platinum supported on tin oxide or titanium dioxide supports as the most promising. The STC Catalysts Inc. web site mentioned above lists both CO and HCHO oxidation capability at ambient temperature conditions using a $Pt/SnO_2$ catalyst. A $Pt/TiO_2$ catalyst has also been reported that is capable of oxidizing HCHO at 100 ppm and ambient temperatures (Peng and Wang 2007, Zang and Tanaka 2006, Zang and Tanaka 2005). In these studies 0.6-1% Pt (wgt.) was used on $TiO_2$ supports. A range of space velocities were investigated from 50,000-200,000 $hr^{-1}$, with 100% conversion noted up to 50,000 $hr^{-1}$.

Gold nanoparticles represent another class of potential ambient temperature oxidation catalysts. Brauer (2008) presents an excellent summary of the recent literature related to CO oxidation on gold nanoparticles, highlighting the facts that particle size, reaction temperature, sample substrate and deposition method influence the rate of reaction. While a variety of supports (eg. $SiO_2$, $TiO_2$, $Fe_2O_3$, and $CeO_2$) (summarized by Aguilar-Guerrero 2009) have been used in the studies of gold catalyzed CO oxidation, one consistently reported requirement is that the gold particle size be less than 5nm (Bond et al. 2006, Haruta 1997). Wang et al. (2009) also reports higher activities when reducible oxides are used as supports for the gold nanoparticles, as opposed to non-reducible oxides which is consistent with Kielin (1998), though Kielin work makes no mention of the gold crystallite size.

Haruta et al. (1989, 1993) reported complete oxidation of CO at temperatures as low as -70º C, while Huber (1977) reported some activity as low as -263 ºC. However it has also been reported that catalyst deactivation frequently occurs and is thought to be primarily attributed to gold crystallite agglomeration (eventually growth of larger gold clusters) and/or blockage of catalyst sites by carbonate species formed during the oxidation reaction (Aguilar-Guerrero and Gates 2008, Bond et al. 2006).

The use of gold for the ambient oxidation of HCHO is sparsely mentioned in the literature. Kielin (1998) had the longest test, lasting for approximately 17 days when deactivation was noted at 8000 ppm HCHO. Haruta (1996) found that gold deposited on $Fe_2O_3$ was as active as Pt on $Al_2O_3$ for the oxidation of 5000 ppm HCHO, with an oxidation efficiency of approximately 50% at 60 ºC, however no long term testing was conducted. Li et al. (2008) noted that Au on $Fe_2O_3$ completely oxidized 3.8 ppm HCHO in air at 80 ºC.

Based on a review of the literature for candidate catalysts, $Pt/SiO_2$, $Pt/TiO_2$, and Au nanoparticles on a reducible metal oxide support, are appropriate catalysts to be considered in further testing. Additional discussion on candidate catalyst selection and screening is presented in Section 3.2.

One obvious effect that requires additional investigation, prior to the selection of a catalyst for comparative testing in hollow fibre configurations, is that of gas mixture relative humidity. Nominal relative humidity levels will be investigated in the catalyst screening efforts. Additional catalyst deactivation studies are also required. Currently the US space program is targeting a Shuttle replacement vehicle referred to as the Crew Exploration Vehicle (CEV) which for all missions, including the first return to the moon in approximately 2020, in this case a catalyst life of at least 20 days is required. However for the IAQ applications, even longer catalyst life is desired. The initial target for catalysts for this study is those that maintain an acceptable activity for at least 30 days at a nominal humidity level of 50% - this provides a 50% margin on the life of the catalyst

for the CEV missions of approximately 20 days, while a 50% relative humidity represents a typical nominal range.

## 2.5 Overview of Catalytic Hollow Fibres

The emphasis of this research is the development of catalytic hollow fibre structures whereby small (less than 50 micron) catalyst particles are incorporated into porous hollow fibre structures. The novelty of the structure is that the porous catalytic hollow fibre is being used as an alternate means of providing a high surface area catalyst with high porosity and low internal diffusion resistance. Whereby traditional supports are either porous granular structures or monolith structures, the use of catalytic fibres provides potential advantages to packed beds in that similar, or higher, activities are theoretically possible in an equivalent volume with a lower pressure drop. Compared to traditional monolith structures, higher loadings of catalyst are possible due to the high porosity and relative thickness of the catalytic fibre structure into which small catalyst particles are encapsulated, and therefore higher activities may also be possible. The specific attributes of the catalytic hollow fibres are discussed in more detail in Section 2.5.4. To the author's knowledge this is the first reported investigation of this type of alternate catalyst structure.

Relative to this research it is important to clarify that the hollow fibre encapsulated catalysts are functioning as a packed bed reactor, and not a membrane. The basic configuration is similar to that of a shell and tube heat exchanger. In this analogy the reactant gases flow through the inner diameter, or bore, of the hollow fibre tubes and the reaction essentially takes place on the surface, and in the interior, of the tube "wall" into which the catalyst material has been encapsulated. There is no intended mass transfer through the walls of the hollow fibres, nor any intended separation of reactants/products by the hollow fibres. However there may be some diffusion through the wall of the hollow fibre into the "shell side" (reference Figure 1-1) which is essentially dead ended, its volume is minimal and as such has little influence on the interpretation of the experimental data.

In the manufacturing of the catalytic hollow fibres, micron size catalyst particles are mixed with a polymer solution to form a homogeneous slurry which is then formed into a hollow fibre structure that is similar to what is more conventionally referred to a mixed matrix membrane (see Section 2.5.2) (Chung et al. 2007), but at much higher inorganic loadings. A general overview of the hollow fibre manufacturing process and resulting structure is provided in the following sections.

### 2.5.1 Overview of Hollow Fibre Membranes

Hollow fibre membranes were initially developed by Dow Chemical in the 1960's and later commercialized by Dow, Monsanto, Du Pont, and others. Fibres are usually on the order of 25 microns to 2 mm in diameter. They can be made with a homogeneous dense structure (isotropic), or with a microporous structure having a dense permselective layer (anisotropic or asymmetric) on the outside and/or inside surface. Representative cross sections of isotropic and asymmetric membranes are shown in Figure 2-1. The fibres are packed into bundles and potted into tubes to form a membrane module. (Baker 2004).

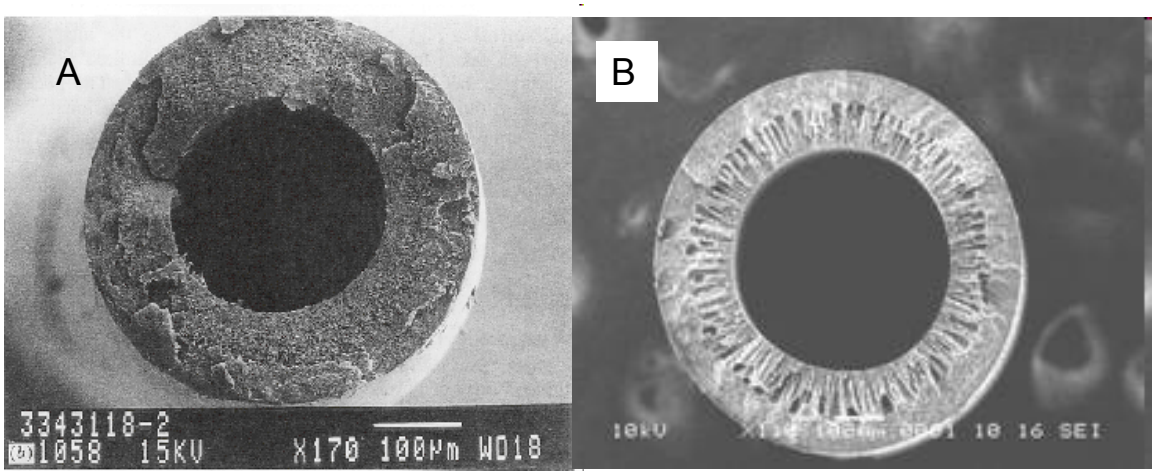


**Figure 2-1. Representative Cross Sections Isotropic (A) and Asymmetric (B) Hollow Fibres**

Due to the desire in this research for high pore volume to permit the inclusion of inorganic catalyst particles in the hollow fibre wall, the asymmetric structures are preferred.

There are three conventional synthetic-fibre spinning methods that can be applied to the production of hollow fibre membranes: (1) melt spinning, in which a polymer is extruded into a cooler atmosphere which induces phase transition and controlled solidification of the nascent fibre; (2) dry spinning, in which the spinning dope, consisting of the polymer(s) pre-dissolved in a volatile solvent mixture, is spun into an evaporative column; and (3) wet spinning, in which the polymer solution is spun into a liquid coagulating bath (Rubenfield 1967, Baker 2004).

The transformation of the polymer from a liquid state to the final solid state is referred to as phase inversion or immersion precipitation, and as implied in the three manufacturing approaches listed above, can be accomplished by (1) cooling the polymer solution to a temperature below its melting point (melt spinning), (2) evaporating the polymer solvent from the polymer/solvent solution (dry spinning), or (3) exchanging the polymer solvent with a coagulant (or non-solvent) in which the solvent is itself soluble, but in which the polymer isn't (wet spinning) (Baker 2004).

The invention of the wet spinning process, the most common of the manufacturing methods, is credited to Loeb and Sourirajan (1962), and has been extensively studied since. In fibre spinning, the polymer solution is extruded from a device referred to as a spinneret, which allows for fluid exposure/exchange with the polymer on both the outside diameter and inside diameter surfaces. The nature and composition of these fluids (among other parameters to be discussed in more detail in Section 2.5.4) strongly influence the morphology of the resulting hollow fibre structure (Wijmans et al. 1983, Reuvers and Smolders 1987, Laninovic 2005, Baker 2004).

As can easily be imagined, the spinning methods can be modified and/or combined, and when coupled with the variables associated with the overall manufacturing process, a wide variety of resulting fibre characteristics is possible for which there is an extensive body of literature. These parameters are varied to optimize membranes for various applications including reverse osmosis, micro-filtration, ultra-filtration, and gas separation (Koros and Fleming 1993, Michaels 1971).

### 2.5.2 Mixed Matrix Membranes

The latest membrane morphology emerging with the potential of enhanced separation factors involves mixed matrix membranes (MMMs) (Chung et al. 2007, Oh et al. 2009, Jiang et al. 2005). These membranes consist of an organic polymer and inorganic particle phases. The polymer provides mechanical advantages over fragile inorganic membranes, while the inorganic typically modifies the permeability and/or selectivity of a typical polymeric membrane.

The concept of MMMs for gas separation was first reported by Paul and Kemp (1973). In their work they reported a delayed diffusion time lag effect for $CO_2$ and $CH_4$ when adding 5A zeolite into rubbery polydimethyl siloxane (PDMS). Researchers at UOP (Kulprathipanja et al., 1988), observed superior separation performance for $O_2/N_2$ mixtures when increasing the silicalite content in cellulous acetate (CA) membranes. Additional research at UOP with MMMs for $CO_2/H_2$ separation using CA/silicalite MMMs demonstrated an almost 10 fold increase in the separation factor when compared to CA membranes without silicalite (Kulprathipanja et al. 1992).

Widjojo et al. (2008) demonstrated a method of fabricating double-layer mixed matrix hollow fibres. This work is primarily focused on reducing interfacial voids between the two layers while also demonstrating the potential of making competitive membranes using polyethersulfone as a replacement to the more expensive polyimide structures. Widjojo's research incorporated alumina, at varying ratios in the denser permselective layers of the hollow fibre as well as in the interior supporting structure of the fibre, resulting in a reduction of void formation at the interface of the asymmetric structure and higher adhesion of the two layers.

The addition of inorganics to polymer membranes adds yet another dimension to the manufacturing variables previously mentioned. The primary differences in the research of catalytic hollow fibres and mixed matrix membranes are two fold. The first is that the catalytic fibres incorporate higher mass loadings of inorganics compared to the MMMs, and secondly to obtain the enhanced separation effect offered by the inorganic in MMMs,

it is desirable to have a bond between the inorganic and the polymer to prevent bypass of the gas via Knudson diffusion around the inorganic particle (Jiang et al. 2005, Xiao et al. 2006, Husain and Koros 2007).

### 2.5.3 Hollow Fibre Adsorbers

In the context of this research, hollow fibre adsorbers specifically refer to the incorporation of regenerable adsorbents within the walls of the hollow fibre structure. These structures are then operated in a cyclic mode whereby a particular specie(s) is adsorbed into the adsorbent, while either flowing over the outside of the fibres (on the shell side), or through the bore of the lumen. Adsorption occurs via diffusion of the adsorbed species into the structure of the fibre and subsequently into the particular adsorbent incorporated into the fibre structure. In this regard, the morphology is similar to MMMs. Once the adsorbent is saturated, the fibre is regenerated using various modes such as temperature and/or pressure swing, or in the case of ion exchange resin sorbents, via chemical regeneration.

Lively et al. (2009) fabricated cellulose acetate hollow fibre adsorbents incorporating zeolites for $CO_2$ adsorption from flue gas of coal fired power plants. These fibres utilized an impermeable layer on the ID of the bore to allow either steam or water to flow through the bore, while the flue gas passes over the outside surface of the fibres. High heat and mass transfer rates are claimed due to the small diameter of the fibres and relatively thin cross section of the walls. During adsorption, water flows through the bore to maximize utilization of the zeolite sorbent by removing the exothermic heat of adsorption. Once the zeolite is fully loaded with $CO_2$, the zeolite is rapidly heated by passing steam through the bore of the hollow fibre

Avramescu et al. (2008) produced hollow fibres containing cation exchange particles via a phase inversion process for the purpose of separating lysozymes in chicken egg whites. These fibres were operated as a membrane (with flow through the fibre wall) and approximately 50% cation exchange material incorporated into the structure. Various additives were used in the manufacturing of the adsorbent fibres including PVP, PEG400

and glycerol to improve the fibre morphology but no details are given relative to specifics of the development process.

In 2004 The University of Bath, Domnick Hunter, and Hamilton Sundstrand began a collaboration to investigate the potential advantages of incorporating zeolites into hollow fibre structures for $CO_2$ adsorption for air revitalization for space craft life support applications. Researchers at the University of Bath (C. Tai, pers. comm., 11th April 2007) successfully demonstrated that 13X molecular sieve particles (1-2 micron diameter) could be efficiently encapsulated in the walls of a hollow fibre using a polymer matrix to successfully contain the molecular sieve, while simultaneously maintaining a sufficiently porous structure to permit the mass transfer of $CO_2$ into and out of the encapsulated molecular sieve. The goal of this collaborative effort was to demonstrate that similar $CO_2$ capacities (mass per unit volume) could be obtained in the hollow fibre configuration as compared to a traditional packed bed of 13X pellets. Figure 2-2 shows a typical breakthrough curve for the adsorption of $CO_2$ demonstrating the relative capacity of a packed bed of molecular sieve 13X and an equivalent volume of a hollow fibre sorbent bed where the molecular sieve is encapsulated in the walls of hollow fibres (adsorption breakthrough of $CO_2$ at equal $CO_2$ partial pressures is indicated by the blue and red lines for pellets and hollow fibre adsorbent, respectively).

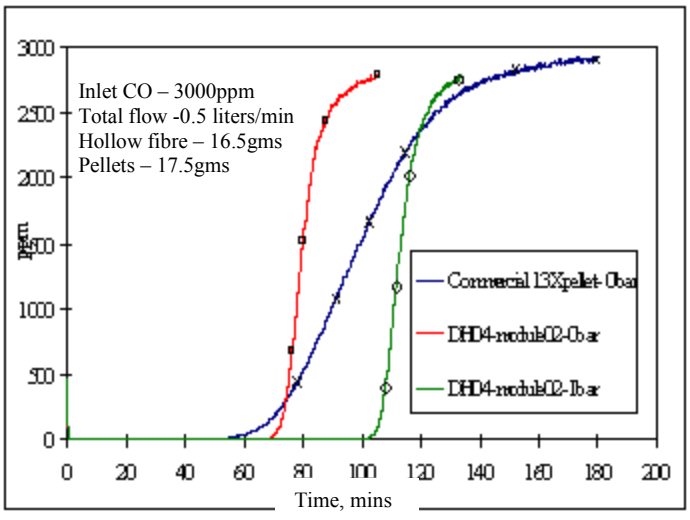


**Figure 2-2. Comparison of Conventional Packed Bed to HF Encapsulated Mol Sieve Sorbent (Tai 2007)**

It is interesting to note the efficient utilization of the mol sieve in the hollow fibre configuration as indicated by the steep breakthrough curve. The steeper breakthrough curve is indicative of higher mass transfer rates in the hollow fibre structure, relative to the packed bed configuration. From a volumetric perspective, the molecular sieve binder used in the pelleted form, which is approximately 30%, is "traded" for the polymeric binder of the hollow fibre configuration.

The encouraging adsorption results (comparable kinetics compared to a packed bed sorbent) obtained by Tai and Perera (2007) served as the impetus for investigating this type of structure as an alternate catalyst support.

### 2.5.4 Hollow Fibre Morphology

While this research has two major components – catalyst and hollow fibre, the primary research emphasis is focused on the development of a hollow fibre structure with appropriate morphology. This structure must maintain characteristics that inherently result in efficient access to the active catalyst material. Whereas the catalyst particles have been reduced to a particle size (<50 microns) that minimizes any internal mass transfer resistances, it is also required that they be uniformly dispersed in the hollow fibre structure at reasonable density (allowing adequate mass of catalyst) and that the internal structure be adequately porous throughout, resulting in high diffusion rates within the catalytic hollow fibre structure. The effect of catalyst particle size and membrane morphology as it relates to the catalyst effectiveness in the catalytic hollow fibre structures is discussed in Section 2.5.5.

Due to the inherent structure of asymmetric phase inversion membranes, it is important to control the morphology of the various sections of the resulting fibre structure. In this research the inner surface of the hollow fibre is exposed to the process stream and as such it is critical that the "skin" (in this case on the ID of the structure) that is typical of asymmetric phase inversion membranes be highly porous to maximize diffusion of reactants into the catalytic fibre structure. In most applications involving asymmetric

membranes this skin is the portion of the membrane that is used to effect the desired separation and may be non-porous for gas separation (applications requiring solution diffusion mechanism), or have a tightly controlled pore size for liquid separation which is accomplished by size exclusion (Baker 2004). While porosity is required for the catalytic fibres associated with this research, tight control of pore size is not important.

While many parameters affect the morphology of the final fibre (e.g. temperature of coagulant, polymer solution and bore fluid flow rate, coagulant type and concentration, polymer concentration, etc.) two important parameters that affect the morphology of the fibre are the nature and composition of the solvent used to dissolve the polymer, and the composition of the coagulant, or non-solvent, used to initiate the phase inversion, or precipitation, of the polymer (Koros and Fleming 1993). Variations in these parameters can result in a infinitely variable number of morphologies including, but not limited to, dense, porous or non-porous skins with various pore sizes and distribution, and a range of sub-structure (the fibre structure formed beneath the skin) morphologies ranging form highly porous, open cell, to dense closed cell. Additionally, in highly porous sub-structures macrovoids are common (Avramescu 2008, Baker 2004, Michaels 1971, Machado et al. 1999).

The phase inversion process involves a phase separation of a polymer solution in polymer rich and lean phases, which can be achieved by the immersion - precipitation technique. A polymer solution is immersed in a non-solvent (also referred to as a coagulant) bath, where a mass transfer process involving interchange of solvent/non-solvent occurs. The simplest system is formed by three components, polymer/solvent/nonsolvent, and is described by the ternary diagram shown in Figure 2-3.

The binodal curve delimitates the two-phase region, rich and lean polymer phases which have their compositions given by the tie lines. The spinodal curve represents the line where all possible fluctuations lead to instability. The region between binodal and spinodal corresponds to metastable compositions where phase separation by nucleation and growth takes place. The point where binodal and spinodal meet is referred to as the

critical point (C). If the precipitation path crosses the binodal below the critical point, nucleation of a polymer rich phase may initiate the phase separation process. If the precipitation path crosses the binodal above the critical point, nucleation of the polymer lean phase may occur. At high polymer concentrations, phenomena such as vitrification, gelation or crystallization can occur in the polymer solution interrupting the polymer lean phase growth (Macado 1999).

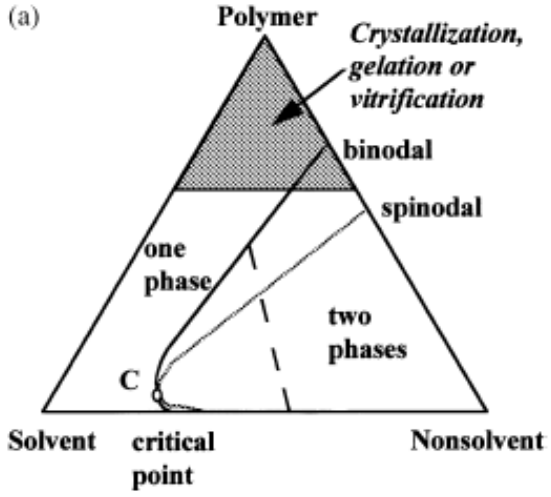


**Figure 2-3. Schematic Phase Diagram for Ternary Systems (Macado 1999)**

Higher polymer concentrations always result in reduced porosity and flux within a membrane and therefore for the highly porous morphology of membranes desired in this research, minimal polymer concentrations are desired. However, if the polymer concentration is too low, the inherent structural properties of the membrane will be lacking due to insufficient polymer connectivity and the resulting fibres will be weak and powdery. This is represented in the ternary phase diagram for a precipitation pathway that enters the two phase region below the critical point (Baker 2004).

The position, thickness, and location of the asymmetric film resulting from rapid demixing at the non-solvent interface, along with the pore structure of the skin and the under layer sections, can also be effected by varying the bath and bore solutions and/or casting solution compositions (Reuvers et al. 1987, Baker 2004).

Reuvers (1987) identified two different mechanisms occurring in phase separation by of ternary systems by immersion precipitation: instantaneous and delayed demixing. Instantaneous demixing is defined as phase separation that occurs immediately after immersion of the polymer solution in a non-solvent. The precipitation path crosses the binodal and two distinct phases are formed. Delayed demixing occurs when the precipitation path does not cross the binodal for some period of time following immersion in a non-solvent. Reuvers (1987) points out that instantaneous demixing usually results in a porous skin, while delayed demixing typically result in a dense skin.

The addition of non-solvent to a casting solution will move the solution towards the binodal and result in more rapid precipitation of the polymer. Since this skin will now act as a diffusion barrier, the rate of solvent/non-solvent exchange in regions below skin will be slowed, and as a result the morphology in the sub-layer will be affected.

The binodal for a ternary mixture of polyethersulphone (PESF), N-methylpyrrolidone (NMP), and water, indicates that for the ranges of polymer concentrations typically of interest (10-40%), the water (non-solvent) concentration is approximately constant at 10% (i.e. the binodal line is parallel to the 10% water concentration line) (Zeman and Tkacik 1988). As a result water is sometimes added to the spinning solution to effectively start the precipitation from a point on the ternary phase diagram that is close to the binodal.

Torrestiana-Sanchez et al. (1999) reports that addition of water to the polymer spinning solution increased the measured water flux in PESF hollow fibres, and shows fibre structures indicative of rapid demixing. In addition to water, other non-solvents may also be added such as alcohols and glycols, in addition to inorganic salts, acids, and bases as well as many organic acids. In general moving the polymer spinning solution closer to the binodal, through the addition of non-solvents to the spinning solution, generally results in rapid demixing, and suppression of macrovoids in the resulting sub-structure morphology of the fibre. (Wang et al. 1995, Wang et al. 1996, Laninvic 2005, Liu et al. 2003).

In addition to the addition of non-solvents to the spinning solution, the coagulant composition in the bore fluid, often pure water, can also be varied to include other so-called non solvents such as various alcohols, and/or solvents as well. The most important effect of varying the bore fluid as it relates to this research is to provide a highly porous structure, which typically results when the bore fluid has high solvent concentrations. Typical solvent concentrations reported to provide increased porosity in the inner skin, or in some cases even the prevention of skin formation, range from 30-90% (Xu and Qusay 2004, Liu et al. 2003, Chung et al. 2000, Qin and Chung 2004)

Modification of the coagulant bath fluid composition can also significantly impact the resulting fibre morphology. However, in most cases due to the cost, in addition to environmental and safety issues associated with the use of non solvents such as alcohols and solvents, water is the most common coagulant used in the coagulant baths used in fibre manufacturing (Baker 2004).

As stated earlier the number of permutations associated with the formation of hollow fibres is infinite. In this research emphasis is placed on producing a fibre morphology that is conducive to catalyst applications requiring a highly open, porous structure, and therefore high diffusivities within the structure. As a result, this research focuses on the porosity and thickness of the asymmetric skin located on the ID, the uniformity and porous nature of the sub-structure, and thickness and porosity of the asymmetric skin on the outer surface - though the porosity of this particular skin is not as critical as the skin on the ID since all of the mass transfer is between the hollow fibre structure and the process stream located in the ID.

### 2.5.5 Internal Effectiveness Factor

Increasing the effectiveness factor for internally mass transfer limited catalytic reactions is the primary focus of this research. As such, the general premise in this research is that if the catalyst particles can be made sufficiently small so as to minimize internal mass transfer resistances, and then these particles are dispersed in an alternate structure whose

pore structure is such that internal mass transfer resistances are negligible, then the catalyst material can be more efficiently utilized.

In general two types of effectiveness factors can be considered in heterogeneous catalysis. The first is the *overall* effectiveness factor which is defined as the ratio of the observed (or overall) rate of reaction to the rate of reaction that would result if the entire catalyst surface area was exposed to the *bulk concentration* of the reactants. The overall effectiveness factor thus must consider mass transfer from the bulk flow in addition to mass transfer from the external surface of the catalyst to the interior surface (Fogler 1999, Smith 1982). These considerations are depicted pictorially in Figure 2-4.

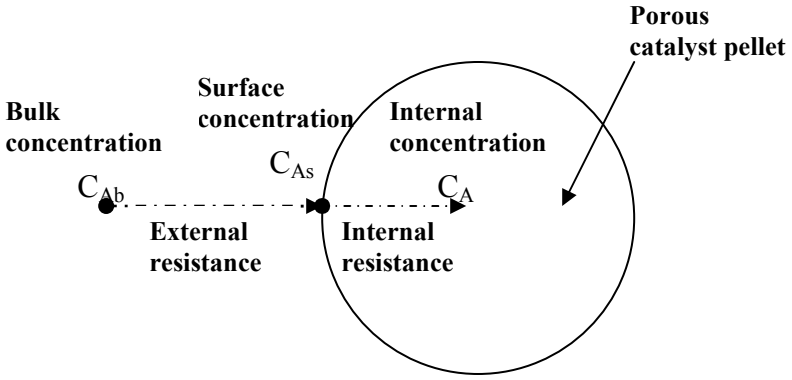


**Figure 2-4. Pictorial representation of mass transfer and reaction steps in a catalyst particle.**

Process parameters, such as required conversion and allowable pressure drop, will ultimately define the bulk concentration and resultant catalyst surface concentration of the reactants. For example, with a reaction system where low conversion is acceptable, a high flow rate may be acceptable, resulting in sufficiently turbulent flow such that the catalyst surface concentration is essentially equal to the bulk concentration. Conversely, if a high conversion is required, or laminar flow conditions exist, concentration gradients will exist in the bulk flow along the length of the reactor, as well between the bulk flow and catalyst surface at any position in the reactor.

While these process parameters are important, and therefore must be considered in the final design a reactor system, this research focuses specifically on the internal

effectiveness factor as it relates to the incorporation of granular catalysts in hollow fibre catalytic structures.

The second type of effectiveness factor, referred to as the *internal* effectiveness factor, is defined as the ratio of the observed (or overall) rate of reaction to the rate of reaction that would result if the entire catalyst surface area was exposed to the *external surface concentration* of the reactants. (At high flow rates where the bulk concentration and surface concentration are essentially equal, the overall and internal effectiveness factors are, by definition, equal).

The concept of a catalyst effectiveness factor was first introduced by Thiele (1939), where he noted that the activity of a catalyst particle was proportional to the particle size. Thiele developed a relationship, eventually referred to as the Thiele modulus ($M_T$), which is a grouping of the important parameters of a catalytic reaction system (reaction rate constant, diffusivity in the particle, reactant concentration in the surrounding fluid, average pore size and average pore length) and for a flat plate (slab) of catalyst sealed from reactants on one side and all ends, takes the dimensionless form (Smith 1981):

$$M_T = L_i\left(\frac{k}{D_e}\right)^{1/2} \qquad 2\text{-}1$$

where: $D_e$ = effective diffusivity, cm $s^{-1}$

$k$ = specific rate constant, $s^{-1}$

$L_i$ = a characteristic length which is dependent on the catalyst geometry and defined as the ratio of the volume to surface area of the specific catalyst structure, cm.

By definition the Thiele modulus is inversely proportional to the effectiveness factor and for values of $M_T$ greater than 4 (internal mass transfer is controlling), the effectiveness factor is approximately equal to $1/M_T$ (Aris 1957). While the Thiele modulus is derived from a material balance over a differential segment of a particular catalyst structure, Aris has shown that there is little variation between the resulting effectiveness factor if the proper values of the characteristic length, $L$ (which is dependent on the geometric structure of the catalyst), and $k$ (reaction order dependant) are used. In the region where mass transfer is limiting, it is easily seen from the inverse proportionality of the effectiveness factor and Thiele modulus, that the effectiveness is inversely proportional to the value of $L$. For example, if a catalytic reaction is strongly mass transfer limited, perhaps with a value of $M_T$ of 50 (effectiveness factor is 1/50 = 0.02), and the catalyst particle size is reduced by a factor of 10, the resulting value of $M_T$ is 5 and the effectiveness factor increase by a factor of 10. Estimates of the effectiveness factor for certain catalyst structures are further discussed in Section 3.4.3.

The usefulness of the Thiele modulus in this research is two fold – it provides for an analytical estimate of catalyst effectiveness (providing supporting analytical rationale for this research) and also points to the primary catalyst structural parameters which will affect the resulting catalyst effectiveness.

In regard to the structural properties of interest, it is clear from equation 2-1 that the characteristic length, $L$, and effective diffusivity, $D_e$, are the variables of interest. Since the same catalyst and reaction are assumed for the catalyst structures of interest, the rate constant is fixed.

The characteristic length is simply based on the geometry of the catalyst structure and provides a geometric proportionality to the diffusion path length of the structure. It is easily seen mathematically that due to the inverse proportional relationship of the Thiele modulus to effectiveness factor, that a smaller $L$ (shorter diffusion path length) results in higher effectiveness factors. However, in this regard there are two considerations. First, in granular catalyst applications typical in packed beds, a minimum value of $L$ is usually dictated due to pressure drop considerations and the associated increase in pumping power. Secondly, in the catalytic fibres associated with this research, the value of $L$ is proportional to the thickness of the hollow fibre wall and as such there is a practical minimum limitation of this wall thickness required to maintain adequate structural properties sufficient to allow handling of the fibres (the catalyst particle size is sufficiently small so that it is assumed to be essentially 100% effective and is therefore not considered in the calculation of the characteristic length. The required particle size to support this assumption is experimentally estimated in Chapter 3).

In addition to the straight forward mathematical and structure considerations associated with the characteristic length discussed above, there are other manufacturing considerations as well. In addition to the numerical value of $L_i$, the structural integrity of the resulting fibre is also influenced by a number of other parameters associated with the hollow fibre composition and morphology (e.g. polymer and catalyst content and ratio, type of polymer, presence or absence of macrovoids, etc) which are discussed in more detail in Chapter 4.

The final consideration associated with the characteristic length is simply the practical limitations associated with the manufacturing equipment – specifically the spinneret. Due to the cost associated with manufacturing of the spinneret it may not be practical to produce various spinnerets to optimize the value of $L$.

Therefore, the primary influence on effectiveness factor will be associated with the effective diffusivity, $D_e$, which includes a geometric correction factor that is applied to the diffusivity to account for the structure in which the gas is diffusing, and is a function

of the diffusivity of the contaminant in air, the catalyst porosity, tortuosity, and constriction factor:

$$D_e = \frac{D\varphi\sigma}{\tau} \qquad 2\text{-}2$$

where: $D$ = diffusivity, $cm^2\ s^{-1}$

$\varphi$ = pellet (catalytic fibre) porosity

$\tau$ = pellet tortuosity

$\sigma$ = constriction factor

The diffusivity within the structure must consider both bulk and Knudsen diffusion and at steady state is defined by equation 2-3 (Smith, 1981):

$$D = \frac{1}{(\frac{1}{D_{AB}} + \frac{1}{(D_k)_a})} \qquad 2\text{-}3$$

where: $D_{AB}$ = bulk diffusivity, $cm^2\ s^{-1}$

$(D_k)_a$ = the Knudsen diffusivity of species a, $cm^2\ s^{-1}$

The Knudsen diffusivity for diffusion in a circular pore of radius $a$ is (Smith 1981):

$$(D_k)_A = 9.70x10^3 a_p (\frac{T}{M_A})^{1/2} \qquad 2\text{-}4$$

where: $a_p$ = radius of pore, cm

$T$ = temperature, K

$M_A$= molecular weight of species $a$, $g\ mol^{-1}$

For a given temperature and molecular weight, it can be seen from equations 2-3 and 2-4, that when the pore radius is large (typically greater than 1000 Å), that the bulk diffusivity

is controlling and similarly when the pore radius is small, diffusion will be predominated by Knudsen diffusion.

The bulk diffusivity for a binary gas mixture (A, B) is derived from the kinetic theory of gases and has been statistically correlated by the *Chapman-Enskog formula* (Smith 1981):

$$D_{AB} = \frac{0.0018583 T^{3/2} \left(\frac{1}{M_A} + \frac{1}{M_B}\right)}{p_t \sigma_{AB}^{\ 2} \Omega_{AB}} \qquad 2\text{-}5$$

where : $D_{AB}$ = bulk diffusivity, $cm^2\ s^{-1}$

$T$ = temperature, K

$M_A$, $M_B$ = molecular weight of gases $A$ and $B$, $g\ mol^{-1}$

$p_t$ = total pressure of the gas mixture, atm

$\sigma_{AB}$, $\epsilon_{AB}$ = constants in the Lennard-Jones potential-energy function for the molecular pair $AB$; $\sigma_{AB}$ is in Å

$\Omega_{AB}$ = collision integral, which would be unity if the molecules were rigid spheres and is a function of $k_B T / \epsilon_{AB}$ for real gases ($k_B$ = Boltzmann constant)

As can be seen equation 2-5, the bulk diffusivity is independent of the catalyst structure and at a fixed temperature and pressure is only a function of the molecular species involved. From an analytical and theoretical perspective it is important to consider the relative value of both bulk and Knudsen diffusivities, since it is common in hollow fibres structures to produce pores many orders of magnitude larger than those typically found in granular catalyst supports (Baker 2004, Satterfield 1980). As such the bulk diffusivity can become the predominant diffusion mechanism and in the extreme represents the theoretical upper limit on diffusivity.

By inspection of equations 2-2 through 2-5, it is apparent that for a given reaction system (i.e. reacting species, concentrations, temperature, pressure and catalyst geometry) that the primary parameters of interest in developing catalytic fibres with high effectiveness

factors are those parameters directly associated with structural morphology properties of the fibres – specifically the porosity, tortuosity, constriction factor and pore size (via the Knudsen diffusivity). In this research typical values of these properties are taken from the literature and used to estimate the potential increase in effectiveness. Then based on experimentally determined effectiveness factors and microscopic examination of the manufactured catalytic fibres, manufacturing parameters can be varied in an attempt to maximize the effective diffusivity.

# Chapter 3

## 3 Experimental Approach and Catalyst Screening

Chapter 3 describes the experimental approach used in the screening of candidate catalysts identified in the literature search presented in Chapter 2. A description of each of the candidate catalysts is provided along with its source. A representative manufacturing procedure for catalysts fabricated by the author is also provided for reference purposes.

The rationale for the catalyst screening trials, test conditions, and a description of the test apparatus used in the oxidation screening trials for CO and HCHO is presented, followed by a discussion of the test results in dry and humidified air. Additionally, the effect of $CO_2$ on the oxidation of CO was investigated for one of the catalysts, $Pt/TiO_2$, to ascertain its impact. For HCHO oxidation, a carbon mass balance was completed to determine if any intermediates were formed as a result of partial oxidation.

Rationale is provided for the selection of catalysts, resulting from the screening trials, to be used in the development of catalytic hollow fibres (Chapter 4), and the concept of catalyst effectiveness factors is introduced and further discussed as it relates to the morphology and relative activities of the granular catalysts and catalytic hollow fibres.

For the selected catalysts, intrinsic reaction rate constants are determined experimentally and diffusivities are calculated to allow for estimates of the Thiele modulus and catalyst effectiveness factors to be calculated for representative catalyst structures. Effectiveness factors for selected catalysts are also measured experimentally and compared with the calculated values.

### 3.1 Catalyst Selection, Materials and Preparation

Based on the literature search, the catalyst screening focused on four Pt based catalysts: Pt supported on $TiO_2$, activated carbon, and two containing $SiO_2$. Additionally, "commercially" available gold catalysts were also selected for comparison.

The first platinum catalyst is the NASA ATCO catalyst, which is used as the baseline to which the other candidate catalysts are compared to. This catalyst consists of 2% wgt. Pt on 4x8 mesh (4.8 mm x 2.4 mm) granular carbon, and was provided by Hamilton Sundstrand as processed for NASA. The catalyst is manufactured by the Engelhard Corporation and subsequently processed by Hamilton Sundstrand. All ATCO catalyst used in this study was processed to the flight certified process specification prior to testing (SVHS 8740, 1979). Prior to this work there was no published data on this specific catalyst relative to its HCHO oxidation activity. This catalyst has served as the baseline for NASA for the ambient temperature oxidation of CO on the US Space Shuttle for approximately 30 years (SVHS 8740, 1979).

The second platinum catalyst is referred to as "Oxidation Catalyst", manufactured by STC Catalyst, Inc, Hampton Virginia, and was provided to Hamilton Sundstrand (HS) to support the initial screening trial. This catalyst, originally developed by NASA Langley Research, and eventually commercialized by STC Catalyst, Inc, claims ambient temperature catalytic activity for CO and HCHO oxidation. The specific composition of the STC catalyst is not known, but constituents are specified as $Pt/SnO_2$ on $SiO_2$ in the material safety data sheets provided by the manufacturer for the material. In the configuration supplied for this screening test the active components are deposited on a cordierite monolith structure. No additional catalyst processing was conducted, nor recommended by the supplier, prior to testing.

The third platinum catalyst is a Hamilton Sundstrand proprietary catalyst prepared by the author and originally targeted the selective oxidation of ammonia to nitrogen and water (Nalette et al. 2003, Wickham et al. 2005). This catalyst was selected since it is platinum based and contains $SiO_2$ which was highlighted as desired in the literature related to

closed loop $CO_2$ lasers (e.g. Kielin 1998). In the HS formulation the $SiO_2$ (Saint-Gorbain Norpro, SS61137, Ohio, U.S.A.) is the support for the Pt. The weight percent Pt in this catalyst is nominally 10% wgt. This catalyst is fabricated using a chloroplatinic acid (19.5 % wgt. platinum, Johnson Matthey, PA., U.S.A.) precursor. Standard wet incipient methods (Satterfield 1980) are used to deposit the Pt precursor, which is subsequently dried in air at 250 ºC and then reduced in hydrogen with a final temperature of 500ºC. Prior to testing, the catalyst is rinsed in deionized, distilled water to remove any residual chloride and then dried at 200 ºC in air. This catalyst is produced as a nominal 1/8 inch cylinder (nominal dimensions of 3 mm diameter by 6 mm length).

The forth platinum catalyst used a $TiO_2$ support (Saint-Gorbain Norpro, SS61120, Ohio, U.S.A.). This catalyst was also produced by the author using the same Pt loading, materials, and techniques discussed above for the $Pt/SiO_2$ catalyst. This catalyst is also produced as a nominal 1/8 inch cylinder (3 mm).

The platinum loading used in the catalysts manufactured by the author was selected as representative of the ranges of catalysts identified in the literature and is not intended to imply that they are optimized loadings or supports, or combinations thereof, but rather representative of the type of catalyst combinations identified by the author that are potential ambient temperature oxidation catalysts for CO and HCHO.

As a representative example of the incipient wetness process used to produce the 10% (wgt.) $Pt/TiO_2$ catalyst used in this research, 450 g of 1/8 inch (3 mm) cylindrical $TiO_2$ support (Saint-Gorbain Norpro, SS61120, Ohio, U.S.A.) is weighed after drying at 250 ºC to remove any residual water. Based on manufacturer data, the $TiO_2$ support has a pore volume of 0.45 $cm^3\ g^{-1}$, which results in a total pore volume of approximately 202.5 $cm^3$ (0.45 $cm^3\ g^{-1}$x 450 g). By trial and error it was observed that using approximately 5-6 % wgt less than the calculated volume of solution resulted in uniform wetting with “free liquid” just beginning to be observed when the solution was uniformly contacted with the $TiO_2$ support material. 255.5 g of a 19.5% wgt chloroplatinic acid (Johnson Matthey, PA., U.S.A.) solution with a density of 1.34 $g/cm^3$ (approximately 190.7 $cm^3$ of solution) was

added to the $TiO_2$ support which was subsequently dried under vacuum at 100 ºC in a rotary evaporator (Buchi Rotavapor R-114 with Buchi waterbath B-480) to evaporate any free liquid. The catalyst is then dried at 250 ºC in air in a convective oven (Blue M Electric DC-246A-FHP-1) for 2 hours, followed by reduction in a tube furnace (Applied Test Systems 3210) with a final temperature of 500 ºC. The catalyst is heated in the furnace and a nitrogen purge is used until the catalyst bed temperature exceeds 100 ºC to prevent condensation upon introduction of hydrogen (Aero All Gas, Hartford, CT). After exceeding 100 ºC, hydrogen is slowly introduced while the temperature continues to increase to 500 ºC at which time, the flow is switched to 100% (volume) $H_2$ and the furnace temperature is held at 500 ºC for 15 minutes and then allowed to cool in nitrogen. After cooling, the catalyst is rinsed in dionized, distilled water until no chloride is observed when testing the rinse water with 0.1 molar silver nitrate solution. After rinsing, the catalyst is dried at approximately 150ºC for at least 2 hours at which time it is ready for use.

In addition to the platinum catalysts discussed above, two "commercial" gold catalysts were also tested for comparison. The primary reason for the selection of Au catalyst is its noted activity in the literature at temperatures significantly below ambient. TDA Research (Wheatridge, CO., U.S.A.) provided one of the gold samples which is supported on $Fe_2O_3$, and is supplied in a granular form. No additional information on the chemical or physical nature of the catalyst was provided. In the "as received" form, the material is random granules, and due to a low inherent strength also contains a significant amount of dust and fine particles. As a result, the "as received" material was subsequently sieved to a 14 x 25 mesh (1.41 mm x 0.707 mm) particle size to provide a controlled range of particle sizes for testing. The sieved 14x25 mesh Au particles were used in all testing of the Au catalyst unless otherwise specified.

The second gold catalyst was supplied by Mintek (Randburg, Republic of South Africa) and consists of 1% wgt Au on $TiO_2$. This catalyst is supplied as 1.5mm diameter extrudates with an average length of 5 mm and a BET surface area of 40-50 $m^2 g^{-1}$ (Mintek data sheet).

The catalysts selected for the screening trials are summarized below in Table 3-1 and shown in Figure 3-1.

**Table 3-1 Summary of Candidate Catalysts used in Screening Trials**

| Catalyst | Source | Shape |
|---|---|---|
| 2% wgt Pt/Carbon | Englehard/processed by HS | 4x8 mesh (thin, flat, granular) |
| 10% wgt $Pt/SiO_2$ | HS | 1/8 inch cylinder |
| 10% wgt $Pt/TiO_2$ | HS | 1/8 inch cylinder 14x25 mesh granules, powder |
| $Pt/SnO_2/SiO_2$ | STC Catalyst, Inc | Monolith |
| $Au/FeO_2$ | TDA | 14x25 mesh granules, powder |
| 1% wgt $Au/TiO_2$ | Mintek | 1.5mm cylinder |


**Figure 3-1 Catalysts Used in Screening Trials**

Two different reactors were used in the catalyst screening trial depending on the size of the particles being tested to allow for a minimum of ten catalyst particles across the flow area of the reactors to minimize edge effects. In the initial catalyst screening trials, 0.015

liters of catalyst were tested in the 1.5 inch (3.8 cm) diameter reactor. When testing powder forms of the catalyst, the catalyst was dispersed in glass wool to aid in its retention and tested in a ½ inch (1.27 cm) diameter reactor. The two reactors are shown in Figure 3-2.

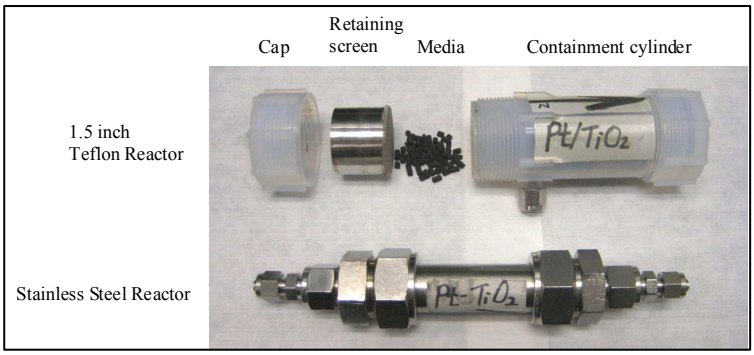


**Figure 3-2 Reactors Used In Catalyst Screening Trials**

### 3.2 Catalyst Screening Trials – Rationale for Test Conditions

The initial catalyst screening trials were conducted at approximate conditions of interest to trace contaminant control systems consistent with the historical design requirements of the U.S. space program. Basic design requirements consider two sources of contamination – the crew and the equipment. The generation rates for numerous contaminants, compiled over the history of the U.S space program, along with the space maximum allowable concentrations (SMAC), are summarized by Perry (1998). The SMAC values for CO and HCHO are listed as 10 mg $m^{-3}$ (8 ppm, ppm = mg $m^{-3}$ x 22.4 liter $mole^{-1}$ molecular $weight^{-1}$ ) and 0.10 mg $m^{-3}$ (75 ppb, ppb = ppm/1000) respectively. Nominal concentrations used in the catalyst screening trials were approximately 10 ppm and 100 ppb, for CO and HCHO respectively.

To determine an appropriate flow rate to be used in the screening trials, a gas hourly space velocity (GHSV) of 2500 $hr^{-1}$, which is the current NASA ATCO reactor design point (SSS 90-01, 1990), was used to estimate scaled flow rates and reactor volumes. However, at this space velocity the conversion of all catalysts was 100% and therefore a

relative comparison could not be made. To address this, the GHSV was increased until a conversion less than 100% was measured. A GHSV of 110,400 $hr^{-1}$ was determined sufficient to result in the desired range of conversions for the various catalysts. All of the catalysts were initially tested in the "as received" form and size, with the exception of the TDA $Au/Fe_2O_3$ catalyst which was sieved to remove dust, to 14x25 mesh (1.41 mm x 0.707 mm) as noted in Section 3.1.

The relative humidity of space craft is typically controlled to 30-70% (nominally targeting 50%) for crew comfort and also to minimize static charges for safety purposes. Therefore to determine if any of the catalysts are adversely affected by water vapor, additional screening tests were conducted at relative humidities ranging from approximately 30-50%.

A summary of the test conditions used in the initial catalyst screening trials is listed in Table 3-2.

**Table 3-2 Test Conditions in the Initial Candidate Catalysts Screening Trials**

| Parameter | Value |
|---|---|
| **Gas Hourly Space Velocity, $hr^{-1}$** | **110,400 -1,850,000** |
| **CO Concentration, ppm** | **Approximately 8 -10** |
| **HCHO Concentration, ppb** | **Approximately 100 – 300** |
| **Relative humidity, %** | **30 & 50** |
| **Reactor pressure, atm** | **1** |
| **Reactor temperature** | **ambient** |

### 3.3 Catalyst Screening Trials

This section provides the details of the test apparatus used in the CO and HCHO screening trials in addition to a discussion of the results obtained in preliminary screening trials of the candidate catalysts identified in Chapter 2. The effects of $CO_2$ and humidity are also discussed for some of the CO oxidation catalysts, while the effect of humidity is presented for the HCHO catalysts.

#### 3.3.1 CO Oxidation

##### 3.3.1.1 Description of CO Oxidation Test Apparatus

The test rig schematic used for CO oxidation experiments is presented in Figure 3-3 and photos of the test rig are presented in Figures 3-4 and 3-5.

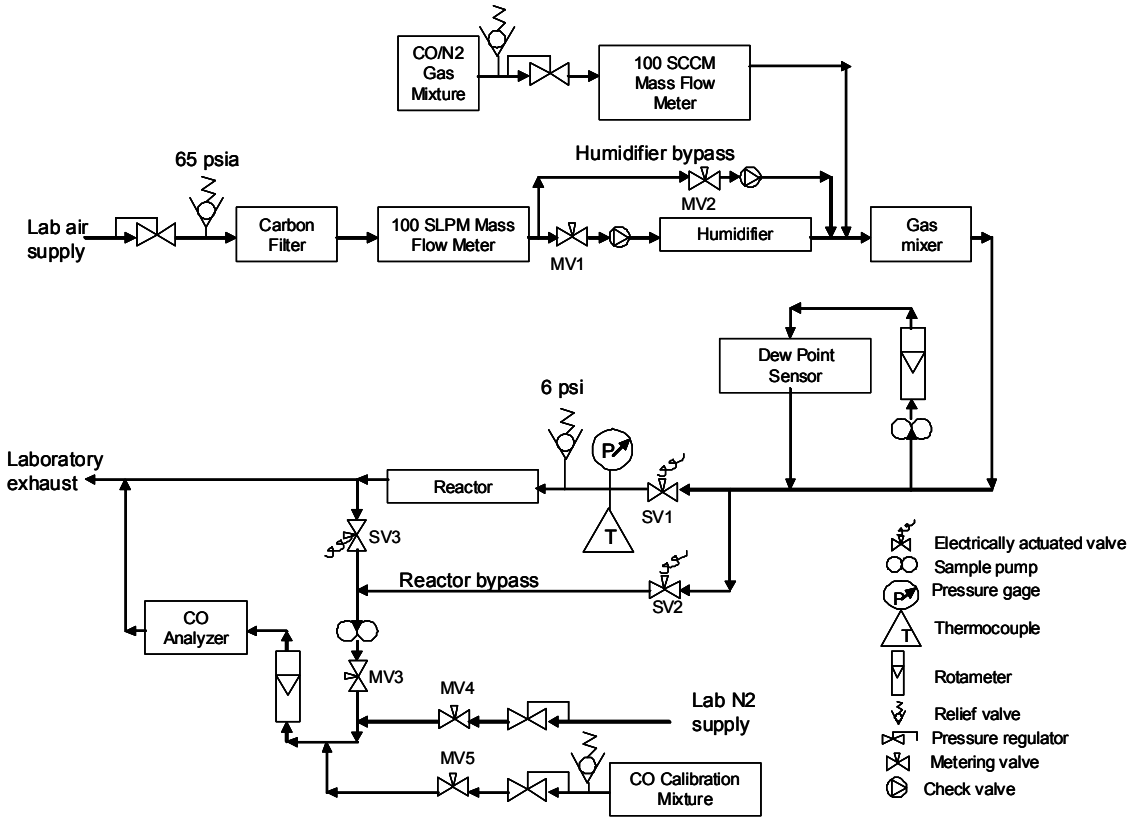


**Figure 3-3 Detailed Schematic Diagram of CO Oxidation Test Apparatus**

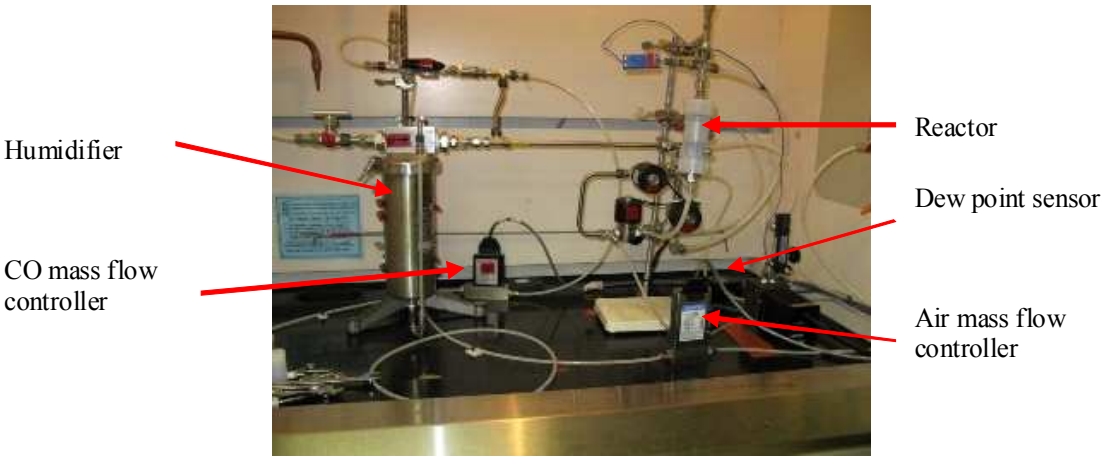


**Figure 3-4 CO Oxidation Test Apparatus**

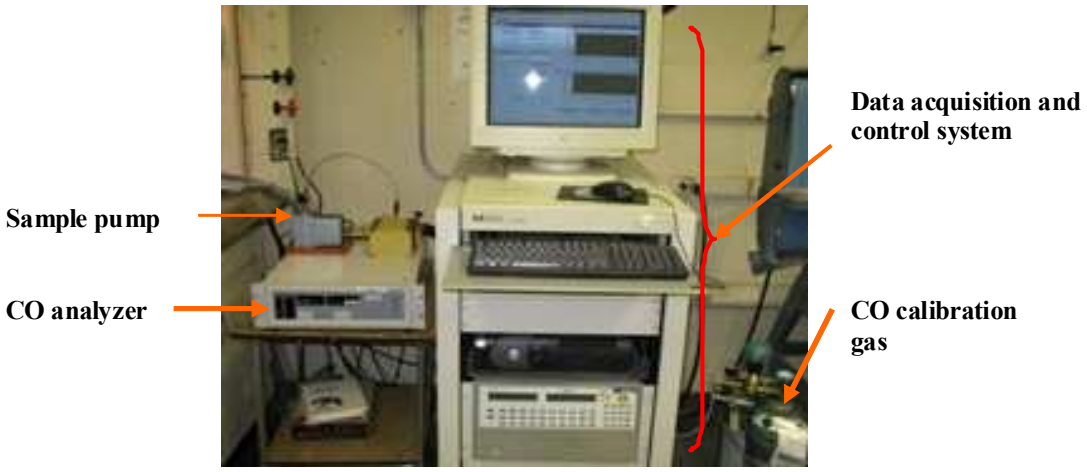


**Figure 3-5 CO Oxidation Data Acquisition and Control System**

Compressed laboratory air is supplied to the test rig and is filtered to remove any contaminants prior to being fed to the air mass flow controller. The air flow rate is controlled using a 100 slpm mass flow controller (Tylan model FC 2920V). For the dry air testing, the humidifier is bypassed by closing metering valve MV1 and opening metering valve MV2. A 4% (volume) $CO/N_2$ mixture (Matheson Tri-Gas, PA., U.S.A.) is added using a 100 sccm mass flow controller (Tylan model FC-260V-4S) and the flow rates of air and the CO mixture are adjusted to provide the desired inlet CO concentration and total flow rate.

For humidified tests, a portion of the air flow is directed through the humidifier by adjustment of metering valves MV1 and MV2 as required to provide the desired level of humidity (30-50% relative humidity). The humidifier is simply a water tank with a sparger tube installed to allow for saturation of part of the air flow to obtain the desired dew point/relative humidity. A General Eastern hygrometer (Model 1100AP system with 111D sensor) is used to measure the inlet dew point.

Conditions are allowed to stabilize during which time the reactor is bypassed by closing solenoid valve SV1 and opening solenoid valves SV2 and SV3. The flow rate to the CO analyzer is adjusted to approximately 0.5 l/min, while the excess flow is exhausted. After the test conditions stabilize, the flow is switched to the reactor by opening SV1 and closing SV2. A 50 ppm $CO/N_2$ calibration standard (Matheson Tri-Gas, PA., U.S.A.) was used to calibrate the CO gas analyzer (Horiba Model VIA-510). When investigating the effect of $CO_2$, an infrared $CO_2$ analyzer was used (Horiba Model VIA-510) and was installed in series with the CO analyzer. Test rig data acquisition and control was accomplished using a Hewlett Packard 3852 Data Acquisition and Control Unit, and HPVEE™ software.

#### 3.3.1.2 CO Catalyst Screening Trials in Dry Air

The reactor volume and geometry for the initial screening trials were arbitrarily fixed at approximately 15 $cm^3$, resulting in a required total flow of 27.6 slpm based on the desired GHSV of approximately 110,400 $hr^{-1}$ (per discussion in Section 3.2).

It was decided to run this test for approximately 16-18 hours since the relative throughput (moles of CO per unit volume of catalyst) under these conditions was identical to the total throughput of the full size Shuttle ATCO reactor over its operational life of 30 days (SSS 90-01, 1990). A comparison of the four platinum based catalysts and the two gold catalysts run in dry air is shown in Figure 3-6.

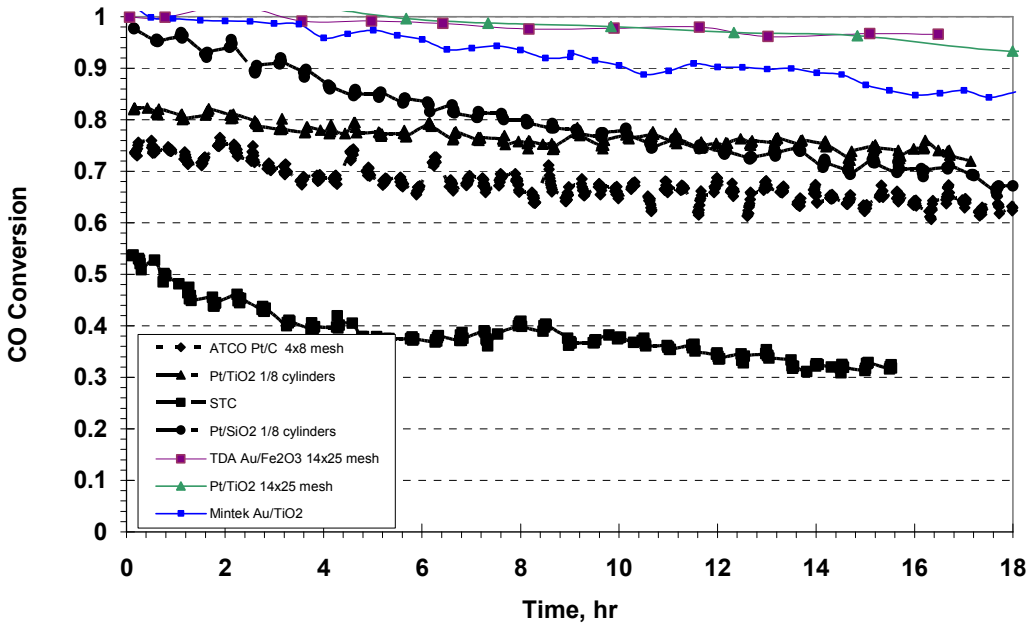


**Figure 3-6 CO Conversion vs Time; GHSV = 110,400 $hr^{-1}$; Inlet pCO = 10 ppm; Reactor volume = 15 $cm^3$; dry air.**

Of the four Pt based catalysts, the $Pt/SiO_2$ formulation has the highest initial activity in the "as received" (or manufactured form) for the first 9 hours at which time it was similar to the $Pt/TiO_2$ catalyst, and after approximately 12 hours, its conversion dropped slightly lower than the $Pt/TiO_2$ catalyst for the balance of the test. Since both of these catalysts had similar Pt loadings, the difference is initial activity is most likely due to differences in dispersion of the Pt.

The NASA baseline ATCO catalyst activity is slightly lower than the $Pt/TiO_2$ supported Pt catalyst for the entire duration of the test. The lower activity (relative to the $Pt/TiO_2$ and $Pt/SiO_2$ catalysts) of the ATCO catalyst is primarily attributed to its lower Pt content (i.e. 2% wgt vs. 10% wgt). As a result, it is very likely that the ATCO catalyst, if loaded with higher Pt content, would have higher conversions than observed, but in this testing the goal was to make a direct comparison with the current NASA catalyst and also select catalysts that have the potential for oxidation of both CO and HCHO.

The STC monolith had the lowest activity of all of the candidate catalysts which is not surprising since the relative mass of Pt is estimated to be considerably lower due to the lower mass of washcoat (and therefore lower Pt content, which is where the active metal is deposited) typical of monoliths relative to supported catalysts.

In the as received forms, the gold catalyst provided by TDA had the highest conversion, but it is also noted that its particle size is considerably smaller (0.0417 inch or 1.06mm – the average diameter of 14x25 mesh gold catalyst particles, vs. 0.125 inch or 3 mm diameter of the $TiO_2$ and $SiO_2$ catalyst supports) than the other granular forms, and as such the diffusion paths are considerably shortened. To make a relative comparison at these conditions, a similar size $Pt/TiO_2$ was prepared by crushing the 1/8" (3 mm) cylinders and sieving to 14x25 mesh. For the 18 hour test shown in Figure 3-6, it can be seen that the performance of the two similarly sized catalyst have similar performance. This test also demonstrates the difference in effectiveness of the two different sizes of $Pt/TiO_2$ catalysts, indicative of internal mass transfer resistance. Additionally, of the two "commercial" gold catalysts, the TDA catalyst ($Au/Fe_2O_3$) had a higher conversion than the Mintek catalyst ($Au/TiO_2$), although it is noted that the average size of the TDA material is smaller (14x25 mesh or 1.41 mm x 0.707 mm) which is nominally 1.06 mm diameter, whereas the as received Mintek catalyst is nominally 1.5 mm diameter).

To better understand the relative activity of similarly sized 14x25 mesh $Pt/TiO_2$ compared to the 14x25 mesh $Au/Fe_2O_3$ and 1.5 mm $Au/TiO_2$, an additional test using fresh catalyst samples was conducted at a higher space velocity and inlet CO partial pressure.

The Au catalyst received from TDA was sieved to a particle size of 14x25 mesh (1.41 mm x 0.707 mm) to remove any fines and the $Pt/TiO_2$ cylinders were crushed and sieved to 14x25 mesh. The Mintek catalyst was tested in the as received particle size. For this comparison a gas hourly space velocity of $1.85x10^6$ $hr^{-1}$ was chosen with an inlet partial pressure of CO of 40 ppm. These conditions resulted in conversions for all catalysts that were less than 100%. Additionally, having a conversion for the gold catalyst of

nominally less than 20% also allows for interpretation of the data as a differential reactor providing insight into the intrinsic kinetics, discussed in more detail in Section 3.4.1.2. Figure 3-7 shows the comparison of the 14x25 mesh $Au/Fe_2O_3$ and $Pt/TiO_2$ catalysts under these conditions.

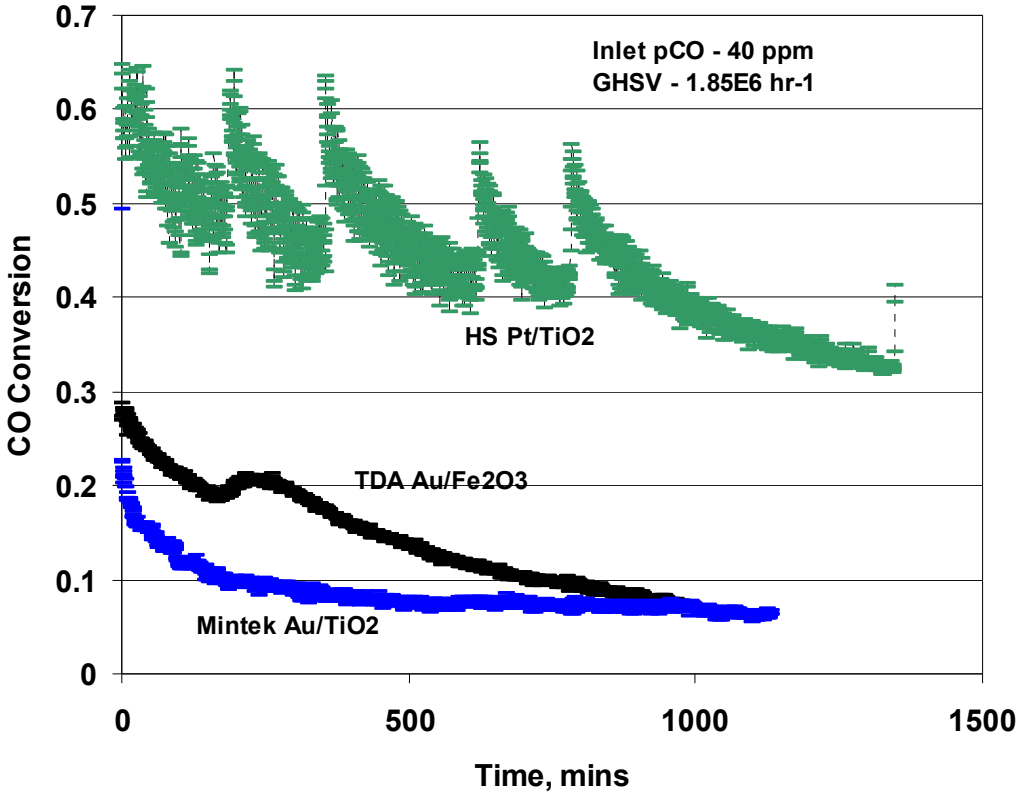


**Figure 3-7 Comparison of Au Catalysts and Pt/TiO2 with Similar Particle Sizes; GHSV = $1.85x10^6$ $hr^{-1}$; pCO = 40 ppm; dry air.**

Figure 3-7 indicates that the $Pt/TiO_2$ catalyst is nominally 3 to 5 times as active as the TDA Au catalyst. Since the composition of the TDA Au catalyst is unknown, no definitive assessment for the lower activity can be made, but most likely the metal content of Au is considerably lower than the 10% wgt used in the Pt catalyst since the Au catalyst is primarily targeting commercial applications such as gas masks, cigarette filters and diesel exhaust oxidation, and therefore the increased cost associated with higher metal contents is most likely not justified. This is also consistent with 1% wgt Au used in the Mintek Au catalyst. Additionally, the literature is consistent in that with many Au catalysts an increase in the size of the Au crystal has been observed over time due to a

form of Ostwald ripening where the growth of large particles occurs at the expense of smaller particles (Lu et al. 2007, Brauer 2008). It is thought that the reactive species result in a lifting of the Au from the surface providing the mobility necessary for sintering with nearby Au crystallites and the resulting growth of larger crystallites with lower catalytic activity. As a result, higher Au concentrations would most likely result in closer proximity of the Au nanoparticles and therefore the potential of increased rate of agglomeration into larger particles, and a corresponding reduction in catalyst activity.

A phenomenon observed in the comparison of the Au and Pt catalyst (Figure 3-7) not seen in the earlier screening tests, run at lower concentrations and lower space velocities, is the oscillatory nature (cyclic variations of CO conversion with time on stream) of the Pt catalyst. The data actually shows two distinct periods associated with this oscillation, one period is on the order of 5 minutes and indicated by the width of the band of data for the platinum, the second period is approximately 200 minutes (noted by periodic step change in CO conversion of approximately 0.15- 0.2 ppm, followed by a gradual decline in activity and then another step change). After approximately 800 minutes the amplitude of the oscillations began to subside and the oscillation associated with a 200 minute period was not observed for the balance of the test. This variation with time is most likely a result of irreversible poisoning which is gradually occurring with time.

The oscillatory nature of CO oxidation on Pt is well known (McCarthy et al. 1975, Liao and Wolf 1982, Eiswirth and Ertl 1996) and outside the scope of this thesis, however it can be briefly described as competing mechanisms of (1) CO oxidation with chemisorbed oxygen and (2) chemisorption of oxygen on the Pt surface. This has been described as a periodic reconstruction of the adsorbed species on the catalytic surface. This phenomenon has been described in detail by Cerasari (2000) and is summarized below.

1. On a prevalently O covered surface, CO adsorbs and reacts forming $CO_2$, consuming the oxygen.
2. Eventually a critical coverage is reached and “reconstruction” is initiated.

3. Upon “reconstruction”, new, highly coordinated empty sites are created which favor the adsorption of oxygen and reaction, consuming CO. As a result the CO concentration drops.
4. The cycle then repeats.

It should be noted that the exact conditions required for this behavior are not well understood presently, but it is believed to be present when the catalysts are operated near the maximum rate (McCarthy et al. 1975).

Deactivation with time on stream was observed for all the candidate catalysts and is not unexpected for either Pt or Au catalysts as it is well documented in the literature for both. For the platinum catalysts, the deactivation is generally attributed to poisoning by irreversible (at the ambient temperature of operation of interest in this research) adsorption of CO at the active sites of the catalyst. In dry air, the deactivation of the Au catalyst is generally attributed to gradual growth in the size of the Au crystallite to a size (typically considered to be > 5 nanometers) that is not active for CO oxidation. For the Pt on carbon ATCO catalyst, NASA had observed this deactivation and accounted for it in the sizing of the ambient temperature oxidation reactor in the early development phases of the ATCO catalyst. (Carlsson et al. 2002, Dwyer and Bennett 1982, Aguilar-Guerrero and Gates 2009, Denkwitz et al. 2009, Lockheed Missles and Space Company 1977).

#### 3.3.1.3 CO Catalyst Screening Trials in Moist Air

For NASA life support applications the relative humidity ranges from approximately 30% to 70%, with a nominal level of 50%, and it is therefore important to understand the magnitude of the effect of moisture on the catalytic activity of the candidate catalysts.

The effect of moisture on fresh Pt catalysts was determined at similar conditions (CO concentration and GHSV) as in the dry air testing except for the addition of water resulting in a relative humidity of 50%. The results are presented in Figure 3-8.

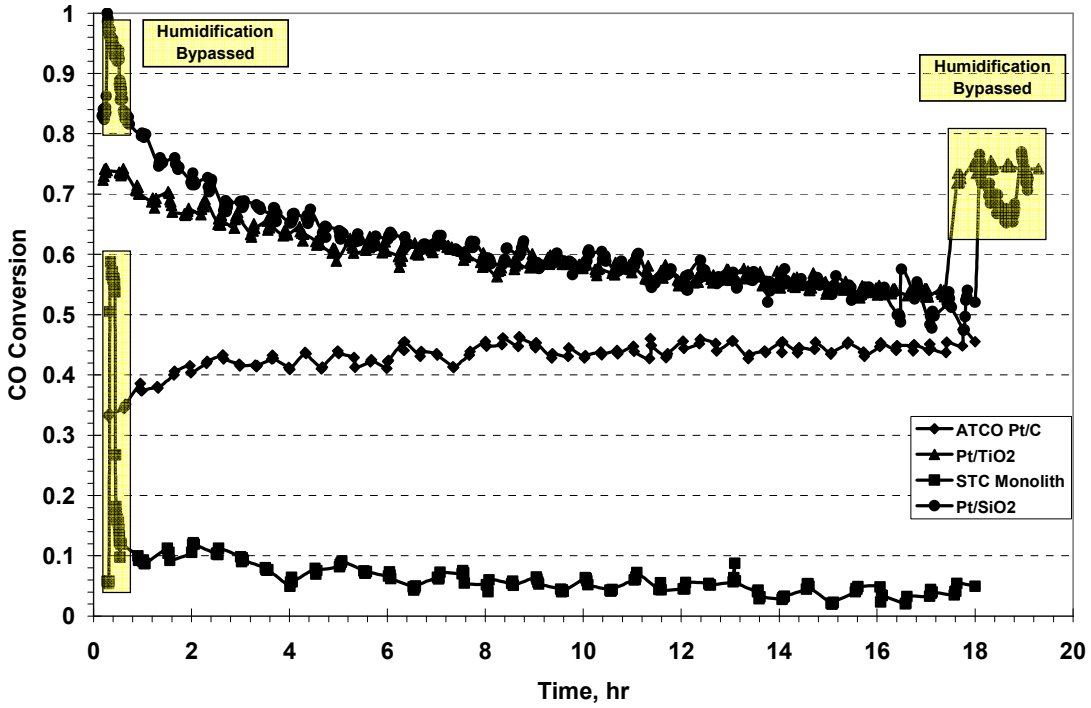


**Figure 3-8 Effect of Humidity on CO Conversion for Pt Catalysts with GHSV=110,400 $hr^{-1}$; Inlet pCO = 10 ppm; Reactor volume = 15 $cm^3$; 50% RH.**

While all catalysts showed a decrease in conversion efficiency relative to the dry air conditions, in moist conditions the decrease in the STC monolith performance was the most pronounced, and as a result was not considered a viable candidate for additional testing. Since the STC catalyst was initially developed for closed loop $CO_2$ lasers, it is thought that the amount of water (Keilin 1998) incorporated in those applications is considerably less than the amount associated with the continuous exposure as experienced in this test, and that competitive adsorption of water on the catalyst site overwhelmed the low mass of active catalyst metal, resulting in the observed large decrease in activity.

The general trend in relative activity of all the Pt catalysts was the same in dry air and 50% relative humidity: $Pt/SiO_2$ > $Pt/TiO_2$ > ATCO Pt/Carbon > STC monolith.

Again, consistent with the conversion in dry air, the primary reason for the observed differences in the relative CO conversion is attributed to the relative amounts of Pt metal between the various catalysts, with the STC having the least amount, whereas the ATCO is nominally 2% wgt and the $TiO_2$ and $SiO_2$ are both 10% wgt.

At the conclusion of the test, the humidity was removed for the $Pt/TiO_2$ and $Pt/SiO_2$ catalysts and the conversion quickly returned to levels consistent with the dry tests indicating that any observed poisoning due to the presence of water vapor was easily reversed. The rapid recovery of CO conversion upon the removal of water vapor is most likely due to a weakly adsorbed water bond on the catalyst surface, which is easily desorbed when the partial pressure of water is reduced in the gas phase. This is seen in three-way automotive catalyst systems containing platinum where the presence of water vapor inhibits CO oxidation at low temperatures but is easily reversed, and actually enhances CO oxidation, as the temperature is increased during normal operation (Lafyatis et al. 1998). Li et al. (2008) showed that the CO oxidation activity was positively and negatively affected at ambient temperatures and was dependent on the type of support, however in all cases, catalyst activity increased as the temperature increased, again presumably due to the desorption of adsorbed water.

Since it was previously shown (Section 3.3.1.2) that the 14x25 mesh $Pt/TiO_2$ and Au catalysts required testing at a higher space velocity ($1.85 \times 10^6$ $hr^{-1}$ vs. 110,400 $hr^{-1}$) to determine differences in relative activity, a similar test was attempted to determine the relative activity in the presence of water vapor. However initial attempts at testing these catalysts at a GHSV of $1.85 \times 10^6$ $hr^{-1}$ and a 50% relative humidity, resulted in such low conversions of the TDA gold catalyst that no direct comparison was possible. Therefore the space velocity was reduced to approximately 160,000 $hr^{-1}$ allowing for a relative assessment of the impact of water on the TDA and Mintek Au catalysts. Figure 3-9 presents the results of this test and shows that the poisoning effect of the water on the Au catalysts is also reversible upon removal of water vapor.

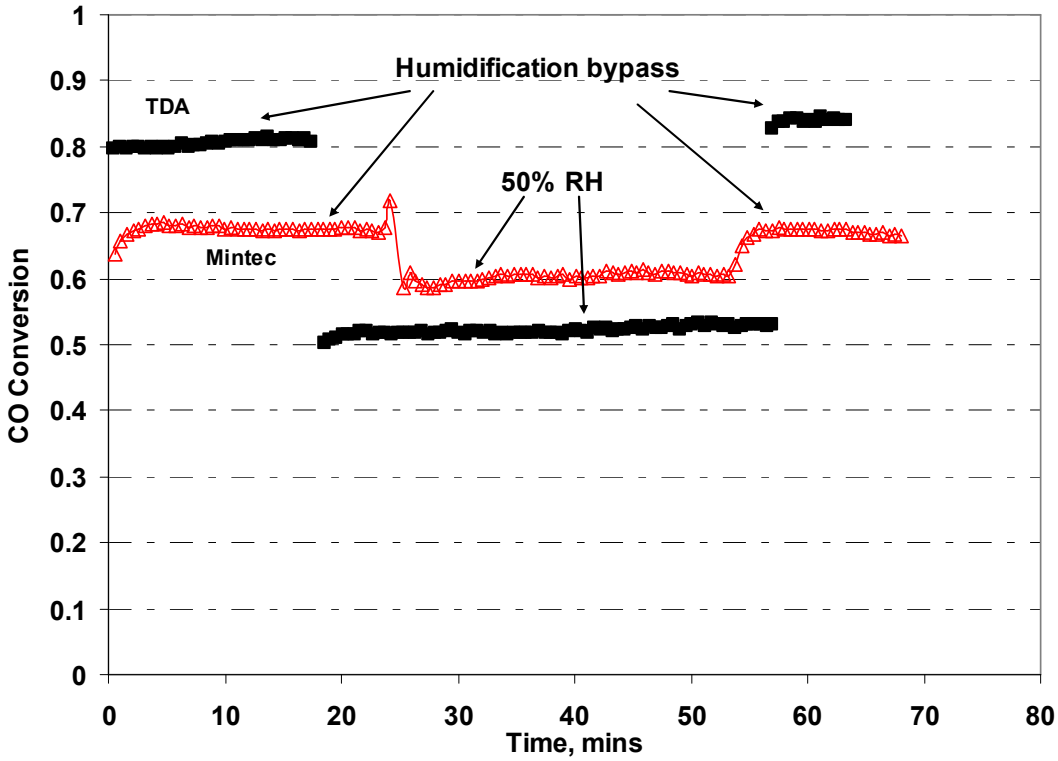


**Figure 3-9 Effect of Humidity on CO Conversion for TDA and Mintek Au Catalysts. GHSV = 160,000 $hr^{-1}$; Inlet pCO = 40 ppm; Reactor volume = 15 $cm^3$; 50% RH.**

At these conditions, the conversion of the 14x25 mesh (1.41 mm x 0.707 mm) $Pt/TiO_2$ catalyst remained at 100%, which is not surprising since the relative activity of the $Pt/TiO_2$ catalyst with similar particles sizes had previously been shown be 3 to 5 times higher than the Au catalyst (see Figure 3-7). The GHSV of the 14x25 mesh $PtTiO_2$ was then increased to 220,800 $hr^{-1}$, at 50% RH, and the conversion remained at > 0.99.

The effects of water on the oxidation of CO with Au catalysts in the literature are inconsistent, with some researchers indicating enhancement and others reporting a negative effect. While many of these inconsistencies can be attributed to the variations in the catalyst support and/or the method of manufacturing, in general it is reported that water has either no effect or an enhancing effect, on $Au/Fe_2O_3$ catalysts for low temperature CO oxidation (Bond and Thompson 2000, Olea et al. 2007, Haruta et al. 1987, Wu et al. 2004).

This apparent inconsistency is believed to be due to differences in test conditions reported in the literature. Haruta et al. (1987) presents data for Au/α-$Fe_2O_3$ where both temperature and relative humidity are varied, showing 100% conversion at 1% (volume) CO (10,000 ppm) at 0 ºC/dry and 30 ºC/76%RH, and less than 100% conversion at -70 ºC/dry. While this data shows that the catalyst was 100% active in the presence of water, the effect of temperature cannot be adequately separated from water vapor. Wu et al. (2004) presents data with 2000-4000 ppm CO showing 100% conversion in dry air and air saturated with water vapor at 28 ºC. However, both sets of data were run at a space velocity that is more than an order of magnitude lower than the lowest space velocity reported (Wu et al. 2004) to have less than 100% conversion (~38,000 $hr^{-1}$ vs. 700,000 $hr^{-1}$), and therefore it is very possible that any effect of water vapor is being masked by the lower space velocity.

While the specific mechanism of the observed poisoning effect is outside the scope of this research, it is clear that it is most likely due to competitive adsorption of water on the catalyst surface. This competition could be either with the sites occupied by $O_2$ or CO, but since the sites in this testing are saturated with $O_2$ (since this testing followed previous dry air testing and the $O_2$ concentration is >> stoichiometric), and the shift in performance was rapid, both in its initiation as well as upon the removal of water, it is most likely due to a competitive adsorption between $H_2O$ and CO.

#### 3.3.1.4 Effect of $CO_2$ on CO Oxidation on Pt/$TiO_2$

In NASA aerospace life support systems, $CO_2$ partial pressures are typically maintained at approximately 0.5% (5,000 ppm), and therefore a test was run to determine if this nominal concentration of $CO_2$ would adversely affect catalytic activity. This test was conducted with the Pt/$TiO_2$ catalyst (1/8", 3 mm cylinders) and the impact was evaluated at approximately 40 ppm inlet CO at 2 different flow rates. $CO_2$ was injected to bring the $CO_2$ concentration to approximate 0.5% (volume). Upon starting and stopping $CO_2$ flow, there was a transient response that appears to be a result of a weak competition for

adsorption sites on the catalyst/support. Upon initiation of $CO_2$ flow (see Figure 3-10) there is an initial spike in effluent CO concentration, but then it drops slightly lower than it was prior to the initiation of flow. It is believed that the $CO_2$ initially displaces some of the CO but then the previously existing equilibrium is re-established. Upon stopping the $CO_2$ flow, there is an immediate drop in effluent CO concentration which is thought to be a result of any residual adsorbed $CO_2$ being replaced by CO, and then the concentration recovers to similar levels existing prior to stopping the $CO_2$ flow. While a minor transient effect is observed, it is considered negligible relative to the catalyst activity. The test results are shown below in Figure 3-10. A similar finding has been reported for CO oxidation on Au catalysts (Steyn et al. 2007).

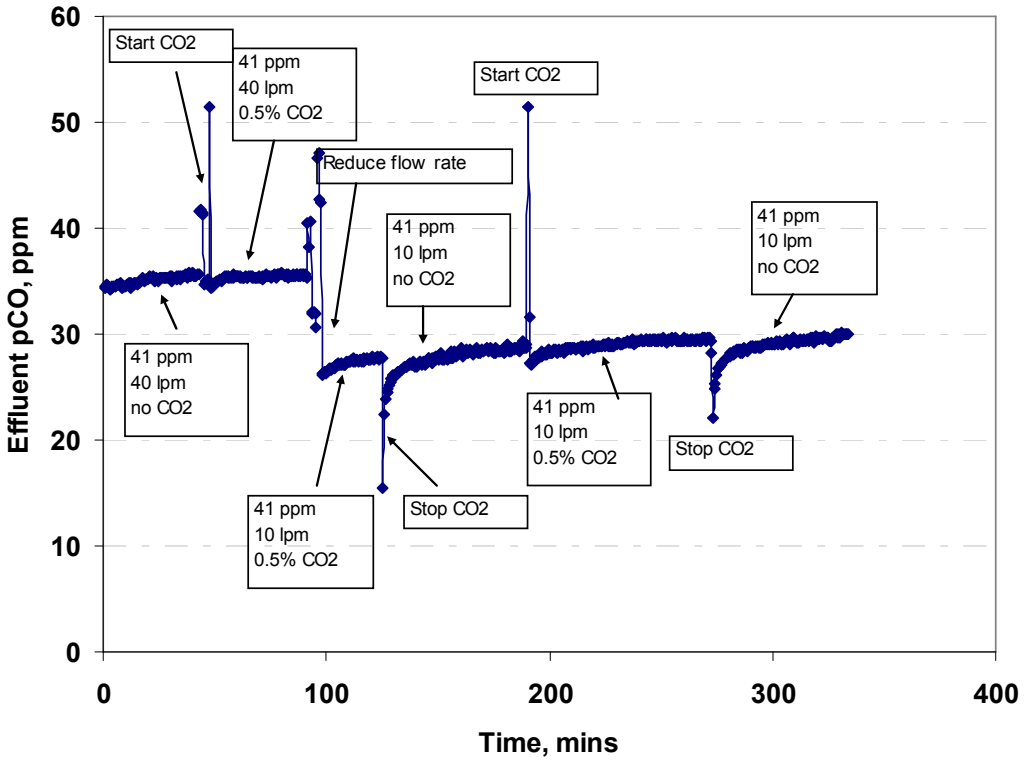


**Figure 3-10 Effect of 0.5% (volume) $CO_2$ on CO Oxidation on 1/8"(3 mm) Cylindrical $Pt/TiO_2$**

### 3.3.1.5 Summary of CO Screening Tests

The measured rates of reaction for the CO oxidation screening trials in dry air are summarized in Table 3-3 for the various candidate catalysts.

**Table 3-3 Measured Average* Reaction Rates for the Candidate CO Oxidation Catalysts; 15 $cm^3$ Plug Flow Reactor; 10 ppm inlet CO; GHSV = 110,400 $hr^{-1}$**

| Summary of Catalyst Screening at 10 ppm CO in Dry Air | | | |
|---|---|---|---|
| Catalyst | Mass, g | Rate, moles CO $hr^{-1}g^{-1}cat$ | Rate, moles CO $hr^{-1}cm^{-3}$ |
| ATCO | 7.2 | $6.36 \times 10^{-5}$ | $3.05 \times 10^{-5}$ |
| $Pt/TiO_2$ – 1/8" cylinder | 14.3 | $3.64 \times 10^{-5}$ | $3.48 \times 10^{-5}$ |
| $Pt/TiO_2$ – 14x25 mesh | 13.4 | $5.12 \times 10^{-5}$ | $4.57 \times 10^{-5}$ |
| $Pt/SiO_2$ – 1/8" cylinder | 12.9 | $4.18 \times 10^{-5}$ | $3.61 \times 10^{-5}$ |
| STC monolith | 11.5 | $2.27 \times 10^{-5}$ | $1.74 \times 10^{-5}$ |
| $Au/Fe_2O_3$ – 14x25 mesh | 12.8 | $5.47 \times 10^{-5}$ | $4.46 \times 10^{-5}$ |
| Mintek 1.5 mm x 5 mm cylinder (as received) | 16.4 | $3.77 \times 10^{-5}$ | $4.13 \times 10^{-5}$ |

*time averaged rate from Figure 3-6

As previously stated for NASA applications, the volume of the catalyst bed is more important than catalyst weight however, rates based on catalyst mass are also given for reference purposes.

Of the platinum catalysts, the Hamilton Sundstrand (HS) $Pt/SiO_2$ had the highest average rate (on a volumetric basis) when tested in the "as manufactured" form (1/8", 3 mm cylinders), though not significantly higher than the HS $Pt/TiO_2$ catalyst. The difference in activities is most likely attributable to differences in dispersion of the platinum within the support. While the surface area of both is similar (155 $m^2\ g^{-1}$ for $TiO_2$ vs. 141 $m^2\ g^{-1}$ for $SiO_2$), the $SiO_2$ support has a median pore diameter of 102 angstroms while the $TiO_2$ median pore diameter is 150 Å. The larger pore diameter of the $TiO_2$ will allow easier penetration of the precursor salts during preparation of the catalyst, whereas the smaller pore diameter of the $SiO_2$ will preferentially deposit the salts closer to the surface.

Since there are more references in the literature to $Pt/TiO_2$ then $Pt/SiO_2$ for the oxidation of HCHO, and the average rates for CO oxidation for the two are similar, a relative

comparison of similarly sized (14x24 mesh) particles of $Pt/TiO_2$ and Au catalysts were made. At the nominal condition (GHSV = 110,400 $hr^{-1}$) the average rate of the Pt catalyst was similar to, or slightly greater than, the Au catalysts.

Since the measured rates for the HS $Pt/SiO_2$ and HS $Pt/TiO_2$ 1/8" (3 mm) catalyst cylinders are similar and they both have the same Pt content, it is assumed that the $Pt/SiO_2$ would most likely have a similar rate if crushed and sieved to a similar particle size.

All of the catalysts show some level of deactivation during the testing in dry air. Similarly, deactivation was also occurring during the humid testing, though the test duration of the Au catalysts in humid conditions may not have been sufficient to observe any significant deactivation. Deactivation is not unexpected as CO is a known poison for Pt based catalysts (Farauto and Bartholomew 1997).

All of the candidate catalysts were negatively affected by the presence of water vapor, though the effect was quickly reversed by the removal of the water for the $Pt/TiO_2$, $Pt/SiO_2$ and Au catalysts. This is not unexpected at ambient temperature as the literature reports negative effects of water vapor on platinum and gold catalysts which can typically be reversed by removal of water or increased temperature which effectively desorbs any adsorbed water species (Bond et al. 2006, Lafyatis et al. 1998) The reversibility of the other catalysts was not measured but there is no reason to believe that they would not react similarly. This data indicates that the effect of water vapor on catalyst activity needs to be considered in the sizing of ambient temperature CO oxidation reactors.

In the presence of $CO_2$, the $Pt/TiO_2$ catalyst showed only a slight transient response and CO oxidation activity eventually returned to the same levels that existed before the addition of $CO_2$. As a result, the impact due to the presence of $CO_2$ in aerospace life support applications is considered negligible.

In summary, the general trend in catalyst activity (on a volume basis) for the candidate catalysts is similar in both dry and humid conditions: 14 x 25 mesh (1.41 mm x 0.707 mm) $Pt/TiO_2$ > 14 x 25 mesh (1.41 mm x 0.707mm) $Au/Fe_2O_3$ > 1.5x5 mm $Au/TiO_2$ > 1/8" (3 mm) $Pt/SiO_2$ > 1/8" (3 mm) $Pt/TiO_2$ > 4 x 8 mesh (4.76 mm x 2.78 mm) Pt/Carbon (NASA ATCO) > STC monolith.

### 3.3.2 HCHO Oxidation

Due to the limited availability of the HCHO test rig, HCHO oxidation tests were conducted primarily to determine the relative activity of the candidate catalysts for the ambient temperature oxidation of HCHO. The catalysts previously tested for ambient temperature CO oxidation tests were utilized with the following exceptions: 1) Since neither of the Au catalysts were available at the time of testing, they were not experimentally evaluated for HCHO oxidation activity, and 2) shortly after the initiation of the HCHO testing, the CO oxidation results indicated that the STC catalyst had considerably lower activity than the other catalysts in both dry and humid conditions. Due to the low relative activity and the fact that the catalyst material was not commercially available in a form amenable to incorporation in the catalytic fibre structures, the STC catalyst was dropped from further evaluation/consideration.

#### 3.3.2.1 HCHO Oxidation Test Apparatus

The HCHO oxidation test set up accommodated simultaneous testing of all candidate catalysts, using a series of 3-way valves (V1 – V3) on the outlet of each reactor to select the individual reactors for HCHO analysis of the effluent. A single, common synthetic air stream (20% by volume O2, 80% by volume N2) was used in all tests. The nitrogen came from boil-off from a liquid nitrogen tank. The oxygen was supplied from ultra-pure oxygen gas-cylinders from Matheson Tri-Gas (PA., U.S.A.). HCHO, and in some cases water vapor, were injected into the feed stream to the desired concentrations. In this fashion, the inlet concentration was the same to all reactors and required only a single

inlet measurement (via V4). Detailed schematics and pictures of the HCHO oxidation test rig are shown below in Figures 3-11 to 3-14.

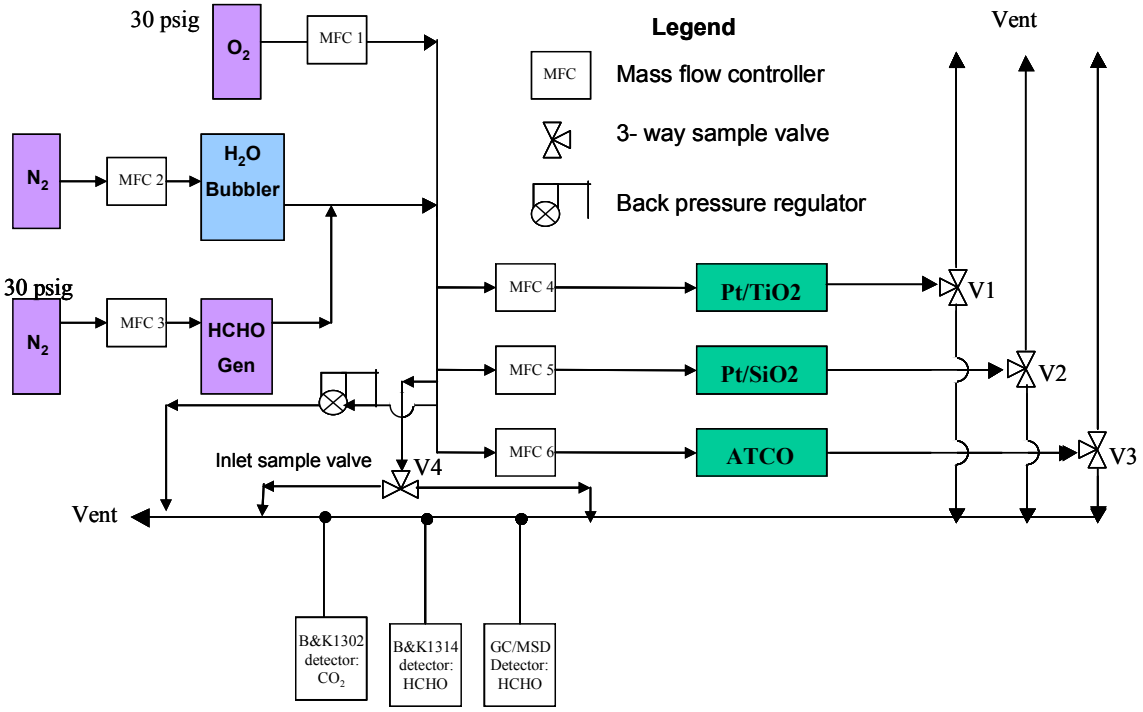


**Figure 3-11 Detailed Schematic Diagram of HCHO Oxidation Test Apparatus**

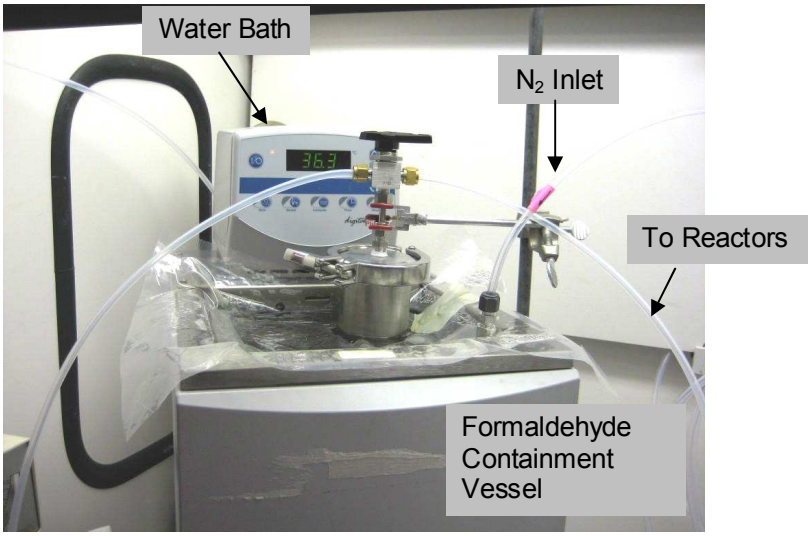


**Figure 3-12 Formaldehyde Generator**

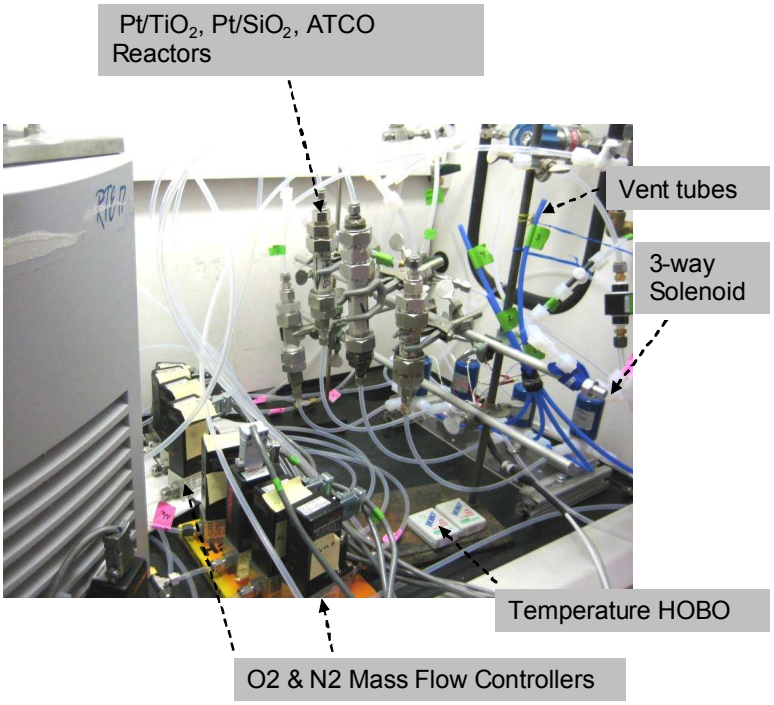


**Figure 3-13 HCHO Test Reactors and Flow Set Up**

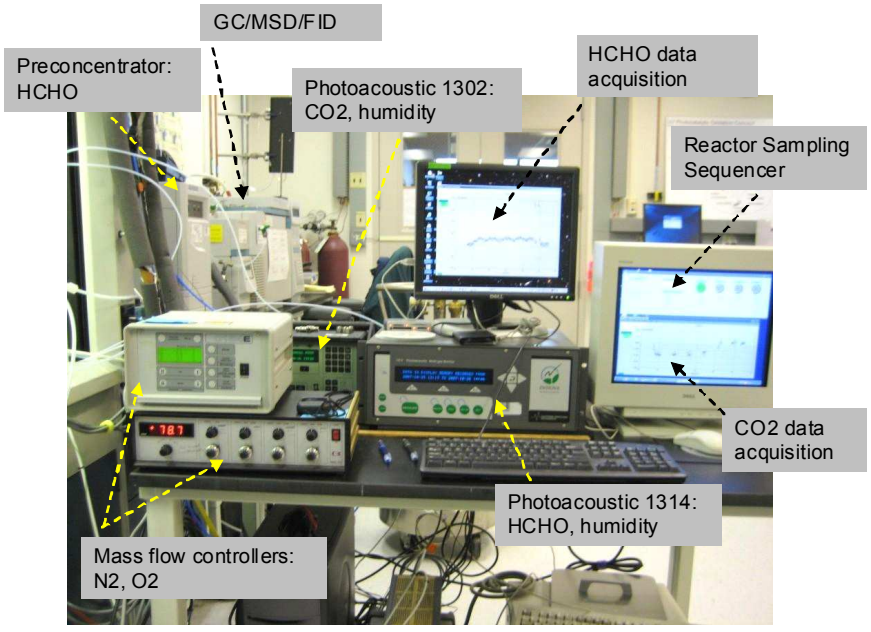


**Figure 3-14 HCHO Test Rig Data Acquisition System**

The gas flow rate was measured with a Wet-Test meter (Shinagawa Corp. Model W-NK) and controlled with mass-flow-controllers. Mass flow controllers MFC 1, MFC 2, and MFC 3 were used to set the total flow to the reactors. A total flow in slight excess to that required for the reactors assured adequate pressure at the inlet of the reactor mass flow controllers (MFC 4 – MFC 6). The excess flow was bled from the system through the back pressure regulator which was set to 10 psia (nominal recommendation for the mass flow controllers). For the humid tests, the required nitrogen flow was split between MFC 2 and MFC 3.

Formaldehyde was generated by vaporizing paraformaldehyde (Fisher Scientific, U.S.A.). Formaldehyde generation is based on controlled diffusion of formaldehyde vapor. The formaldehyde generator consists of a vial, in which a quantity of paraformaldehyde is deposited, a diffusion tube attached to the vial, a containment vessel and a temperature controlled water bath. The vial is secured inside the containment vessel which is immersed in the water bath. Nitrogen carrier gas, preheated to the water bath operating temperature, enters the containment vessel and sweeps away formaldehyde from the end of the diffusion tube/vial before finally leaving the containment vessel.

Formaldehyde concentration was determined using a photoacoustic detector (Bruel & Kjaer Multigas Model 1314) and an Entech Preconcentrator/GC-MSD (Entech Preconcentrator 7100A/Agilent 5973) detector system. The photoacoustic detector was used in all tests. For formaldehyde sensing the Preconcentrator/GC-MSD is restricted to sampling humidity-free gas streams. The minimum detection limit for formaldehyde is about 20 ppb (parts per billion) for the photoacoustic detector and $\leq$1 ppb for the Preconcentrator/GC-MSD detector (manufacturer's claim). Calibration of these detectors was performed with a Dynacalibrator (Model 230) and a certified paraformaldehyde permeation tube.

To determine if any intermediates were formed during the screening tests for HCHO oxidation, the effluent carbon dioxide was measured to allow for a carbon mass balance to be performed. Carbon dioxide was measured by a photoacoustic detector (Bruel &

Kjaer Multigas Model 1302) with a minimum detection limit of 10 ppb (manufacturer's claim). A certified carbon dioxide gas cylinder from Matheson Tri-Gas (U.S.A.) was used to calibrate the detector.

A Preconcentrator/GC-FID detector (Entech Preconcentrator 7100A /Agilent 6890N) was used for quantification of possible organic products and background species whose quantification limit is < 100 ppt (parts per trillion). The actual limit is set by the carbon content of the species. In the HCHO testing, water vapor content of all gas streams was quantified by the two photoacoustic detectors.

#### 3.3.2.2 HCHO Catalyst Screening Trials

Based on the results of the CO oxidation screening tests, the ATCO, $Pt/SiO_2$, and $Pt/TiO_2$ catalysts were selected for evaluation as ambient temperature oxidation catalysts for HCHO. Tests were conducted in dry air at GHSVs ranging from 6,000 – 120,000 $hr^{-1}$ and at 30% RH, all at ambient temperature. Most of the tests were conducted at an inlet HCHO concentration of approximately 100 ppb while one test was conducted at an inlet HCHO concentration of approximately 300 ppb at a GHSV of 120,000 $hr^{-1}$. Since no significant deactivation was noted during the testing, the same catalyst was used for all tests. Data for the three catalysts are presented in Figures 3-15 through 3-17.

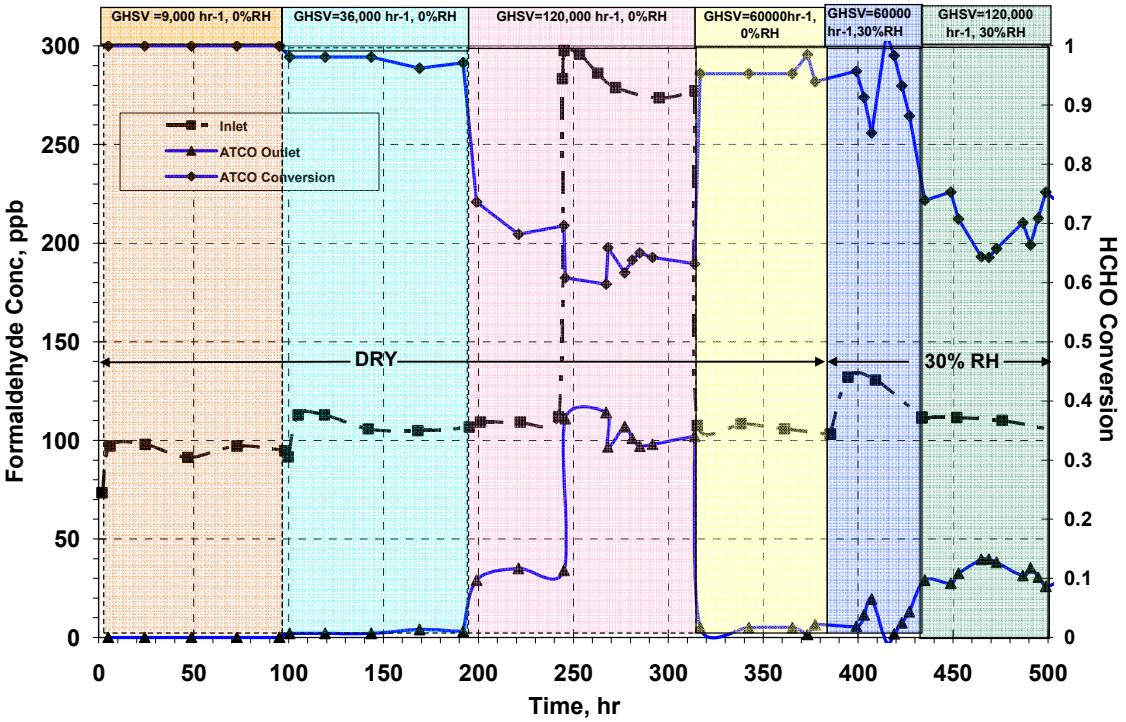


**Figure 3-15 Screening Test for HCHO Oxidation on ATCO Catalyst**

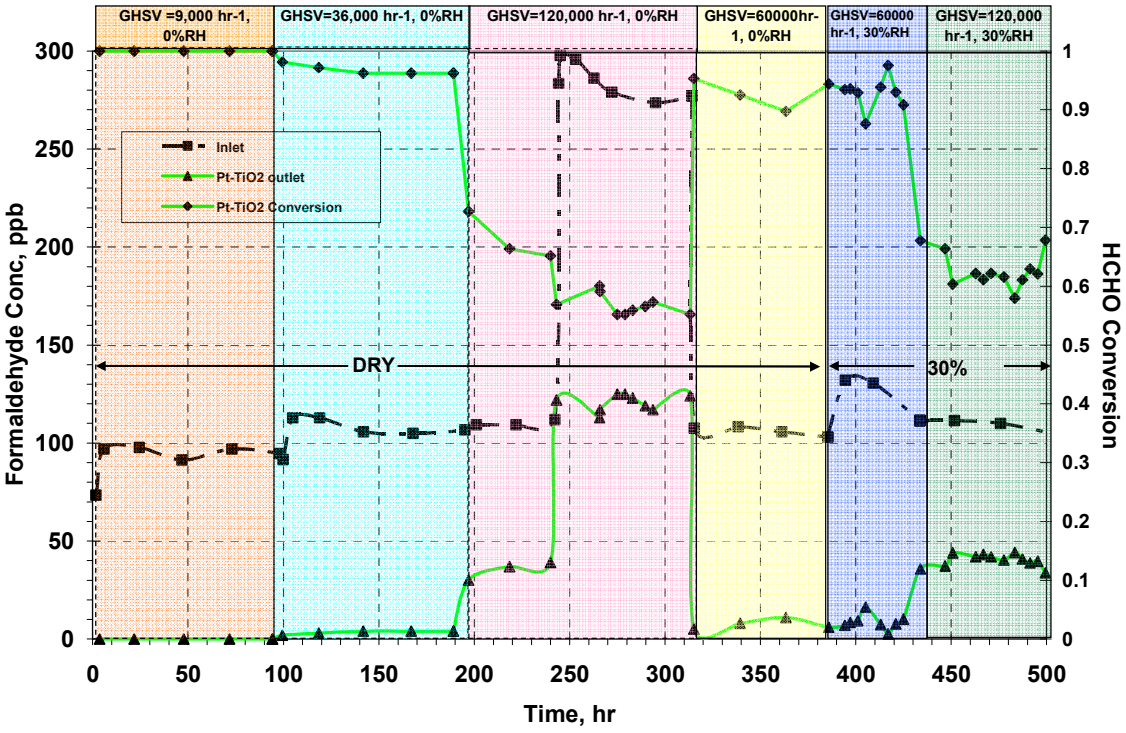


**Figure 3-16 Screening Test for HCHO Oxidation on Pt/TiO2 Catalyst**

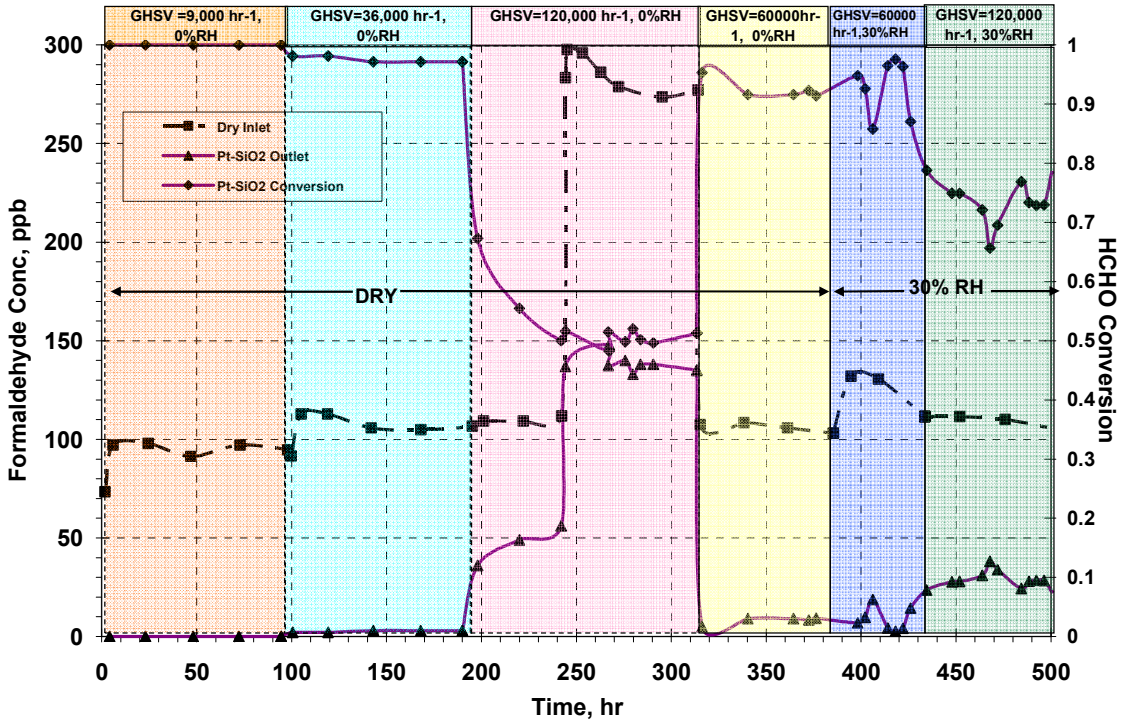


**Figure 3-17 Screening Test for HCHO Oxidation on Pt/SiO2 Catalyst**

### 3.3.2.3 HCHO Catalyst Screening Trials

Since a common inlet stream was used for all three catalysts, a direct comparison of performance can be made on a time basis from the graphs. For the three catalysts tested, there were no significant differences noted in performance over the range of conditions tested. At high space velocities, the $Pt/SiO_2$ performance was slightly lower than the others, however with the introduction of moisture, the oxidation efficiency increased to levels consistent with the others. In general the effect of moisture was relatively small and not as pronounced as in the CO oxidation screening tests. Upon changing the inlet HCHO concentration to 300 ppb, at approximately 250 hours into the test, there was no significant change in conversion.

In addition to the oxidation efficiency, the outlet $CO_2$ concentration was also measured to allow for a mass balance to verify complete oxidation of the HCHO to $CO_2$ and water.

The outlet $CO_2$ concentrations for the three catalysts are shown below in Figure 3-18 and shows that the HCHO is completely oxidized to $CO_2$ within expected experimental accuracy. For complete oxidation of HCHO, the outlet $CO_2$ concentration should be identical to the inlet HCHO concentration. The initial lower than expected $CO_2$ concentration is believed to be due to an initial adsorption of the $CO_2$ and/or HCHO as the surface species come to equilibrium on the catalyst surface, whereas the spike noted at approximately 80 hours into the test can be traced to an approximate 5° C increase in ambient temperature, most likely resulting in desorption of adsorbed $CO_2$ from the catalysts. These results are consistent with the work of Zhang et al. (2005) in which they report > 99.7 % conversion of HCHO to $CO_2$ on $Pt/TiO_2$ at room temperature with GHSVs of 50,000-200,000 $hr^{-1}$.

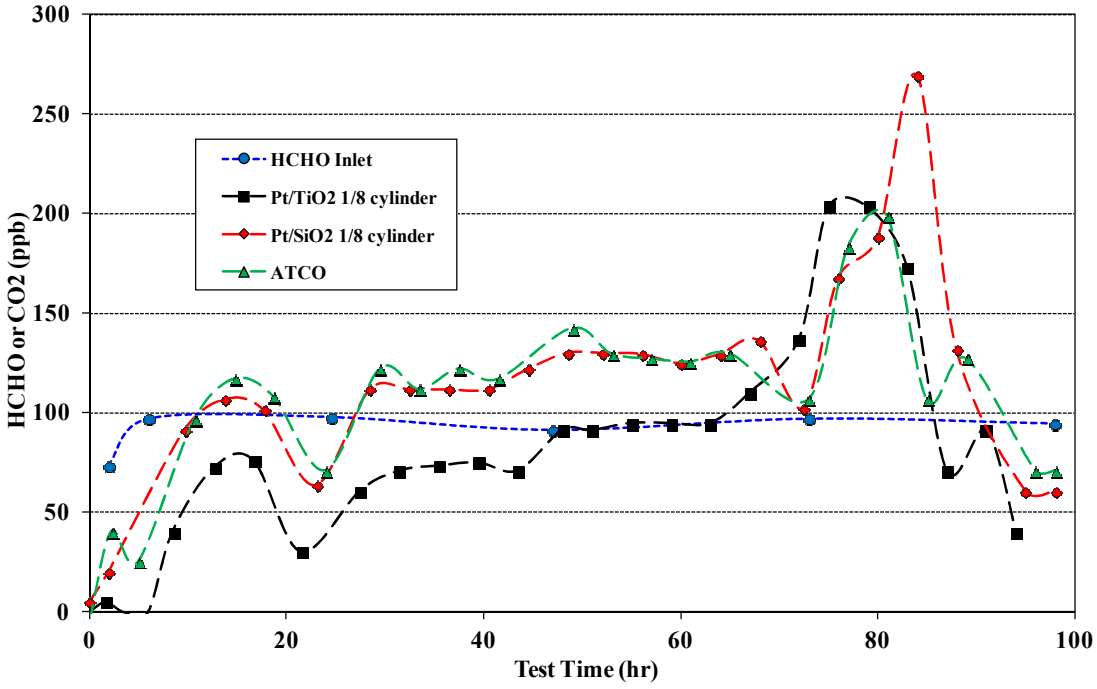


**Figure 3-18 Carbon Mass Balance during HCHO Oxidation**

### 3.3.3 Catalyst Selection Resulting from Screening Process

$Pt/SiO_2$ and $Pt/TiO_2$ catalysts had the highest oxidation efficiencies for CO of the platinum based catalysts that were evaluated and similar oxidation efficiencies for HCHO. However, since there is considerably more research reported in the literature for the

oxidation of HCHO using $Pt/TiO_2$, it was selected for additional evaluation in catalytic hollow fibres, noting that $Pt/SiO_2$ would most likely perform similarly.

Two "commercial" gold based catalysts were tested for CO oxidation and in all dry air testing, the TDA $Au/Fe_2O_3$ performed better than the Mintek $Au/TiO_2$, however the TDA Au catalyst showed a higher reduction in performance in the presence of water vapor. Additionally, TDA was unable to provide sufficient material for fibre manufacturing and therefore the Mintek $Au/TiO_2$ catalyst was selected as representative of the state of the art of commercially available gold CO oxidation catalysts to be used in the development of catalytic fibres. Utilizing the Mintek material also provided a more direct comparison of the catalytic material since in both cases (Pt and Au) the catalyst support was $TiO_2$, though it is noted that the characteristics (e.g. surface area, pore size, pore volume and pore size distribution) of the catalyst supports are most likely different.

In order to be able to achieve a higher catalyst effectiveness through the incorporation of catalyst particles in the hollow fibre, two conditions must exist: the first condition is that for the reaction of interest, the granular catalyst must have significant internal mass transfer resistance (actually the diffusion rate needs to be much slower than the rate of reaction) and therefore the rate of reaction can be enhanced through the use of a smaller catalyst particle. Second, by producing the catalyst in a small enough particle size to essentially eliminate any internal mass transfer resistance within the catalyst particle, it must be incorporated into a hollow fibre and the resulting catalytic hollow fibre structure must be sufficiently porous so as not to introduce a similar resistance to that which originally existed in the pores of the granular form of the catalyst. The efficient utilization of catalysts is typically discussed in terms of catalyst effectiveness, as discussed in more detail in Section 3.4.

### 3.4 Catalyst Effectiveness

Catalyst effectiveness factors can be used to estimate the potential benefit of using catalytic hollow fibre structures as an alternate to traditional catalyst support structures.

If the catalyst particle size is small enough, its effectiveness factor will be maximized, however this will often result in an unacceptably high pressure drop in a packed bed configuration (Farrauto and Bartholomew 1997, Fogler 1999).

In catalytic reactions where the active catalyst metal is deposited on a porous support, the internal effectiveness factor is a measure of how far a reactant diffuses into a catalyst pellet before reacting, and is defined as the ratio of the actual overall rate of reaction to the rate of reaction that would result if the entire internal surface were exposed to the external surface conditions (concentration and temperature). Effectiveness factors are usually correlated with the Thiele modulus, which is large when diffusion limits the overall rate of reaction, and is small when the surface reaction is rate-limiting. (Fogler 1999). The Thiele modulus is discussed in more detail in Section 3.4.3.

Inherent in the definition of the effectiveness factor (and therefore the Thiele modulus) is the ratio of reaction kinetics (i.e. rate constant) to diffusion parameters (in this case - gas diffusivity and morphology of the catalyst support) and therefore values of the reaction rate constant and diffusivity are necessary to estimate the effectiveness factor.

### 3.4.1 Estimate of Reaction Rate and Deactivation Constants for the Oxidation of CO in Dry Air on $Pt/TiO_2$ and Au Catalysts

This section presents an overview of the basic theory for kinetics and specifically as it relates to the rate equation for a first order reaction with deactivation, resulting in a generalized form of the rate equation to which experimental data can be compared. Intrinsic rate constants and deactivation constants for CO oxidation are determined experimentally using catalyst powder (< 50 microns) dispersed in a glass wool plug which is tested as a differential reactor.

#### 3.4.1.1 Kinetic Theory with Deactivation

The rate of a chemical reaction is proportional to the concentration of the reacting species and generally represented by equation 3-1:

$$-r_a = [k_a(T)]\,a(t)[fn(C_a, C_b.....)] \qquad 3\text{-}1$$

where: $r_a$ = rate of reaction of species a

$a$ = activity (=1 without deactivation, with deactivation $a$ is function of time)

$k_a$ = specific reaction rate constant (which is a function of temperature $T$ ), $s^{-1}$

$C_a$ , $C_b$ …= concentrations of reacting species *a, b..,*, mol $l^{-1}$

For the oxidation reactions and low concentrations of contaminants studied in this research, the rate of reaction can be considered first order in contaminant concentration (McCarthey et al. 1975, Dewil et al. 2005, Xu et al. 2007). Additionally, at the low concentrations associated with this research, the oxygen is present at concentrations much greater than stoichiometric and therefore can be considered constant and combined with the rate constant. This results in a rate equation that is a function of a single species with a pseudo rate constant, *k'*, and dropping the subscript "*a*" since the rate is essentially a function of CO concentration only. The low concentration of CO also allows the reaction to be considered isothermal and therefore equation 3-1 for CO oxidation can be re-written as:

$$-r_{co} = k'\,a(t)[CO] \qquad 3\text{-}2$$

For many reactions where poisoning occurs due to adsorption of reactants or products, the conversion decreases at an approximate linear rate with time, and the activity is considered to follow a first order decay law (Fogler 1999):

$$a = e^{-k_d t} \qquad 3\text{-}3$$

where: $k_d$ = decay constant, $mins^{-1}$

$t$ = time, $min^{-1}$

Using the design equation for a packed bed reactor combined with the rate law for a first order reaction yields:

$$v_0 \frac{d[CO]}{dW} = -k' a(t)[CO] \qquad 3\text{-}4$$

where: $v_o$ = inlet volumetric flow rate, $l\ min^{-1}$

$W$ = weight of catalyst, g

Combining equations 3-3 and 3-4 and solving for the case where the activity is uniform throughout the reactor yields:

$$-k_d t = \ln\left(\frac{v_0}{Wk'}\right) + \ln\left(\ln\left(\frac{[CO]_0}{[CO]}\right)\right) \qquad 3\text{-}5$$

where $[CO]_0$ is the inlet concentration of CO in mole $l^{-1}$.

From equation 3-5 it can be seen that if the assumptions of first order decay rate and first order reaction are reasonable then a plot of $\ln\left(\ln\left(\frac{[CO]_0}{[CO]}\right)\right)$ as a function of time should yield a straight line with a slope of $-k_d$ and a y-intercept of $-\ln\left(\frac{v_0}{Wk'}\right)$ (Fogler 1999).

### 3.4.1.2 Experimental Determination of Kinetic Constants for CO Oxidation

To estimate the specific rate and decay constants, a differential reactor was fabricated using catalyst particles that were crushed to less than 50 μm in diameter and dispersed in a matrix of glass wool which was subsequently formed into a plug and run in a ½ inch (1.27 cm) diameter reactor. Test conditions were adjusted to allow operation as a differential reactor with conversions of 5-15% during the tests. For most reactions, differential reactor assumptions are valid for conversions up to 25% with less than 5%

error (Smith 1981). To satisfy these criteria, tests which were run at a total flow rate ($v_o$) of 40 l $min^{-1}$ for the $Pt/TiO_2$ and $Au/TiO_2$ catalysts and 10 l $min^{-1}$ for the $Au/Fe_2O_3$ catalysts, both at an inlet concentration of 40 ppm CO. The results for the Pt and Au catalysts are shown in Figures 3-19 to 3-21. Though the TDA Au catalyst was not available during the development of catalytic fibres, the kinetic data had already been obtained and is therefore included only for reference purposes.

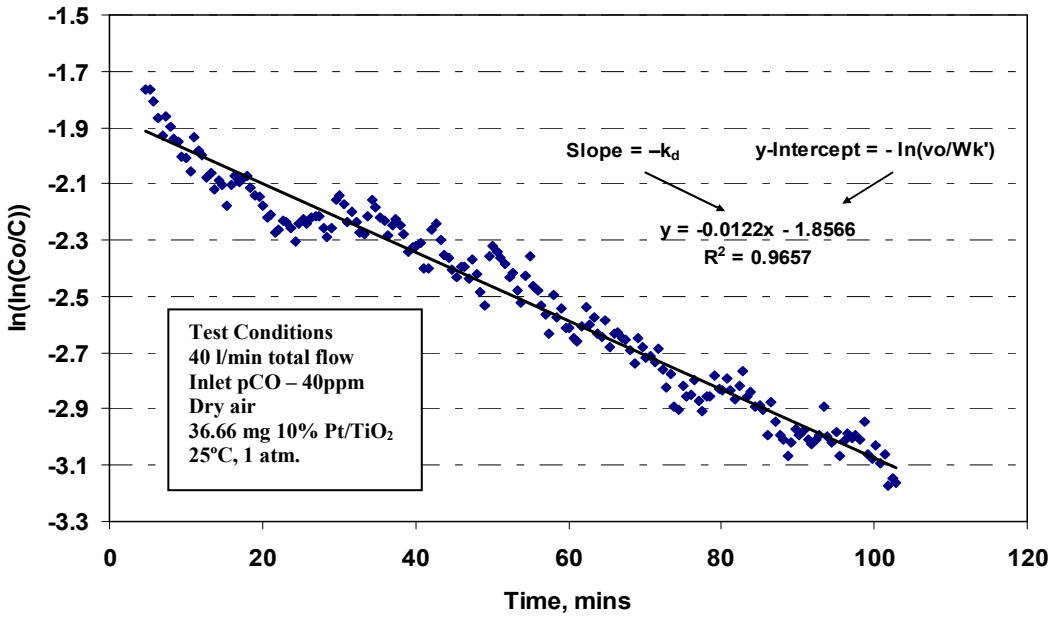


**Figure 3-19 Estimate of Specific Rate Constant and Decay Constant for CO Oxidation on 10% wgt $Pt/TiO_2$ Powder Catalyst**

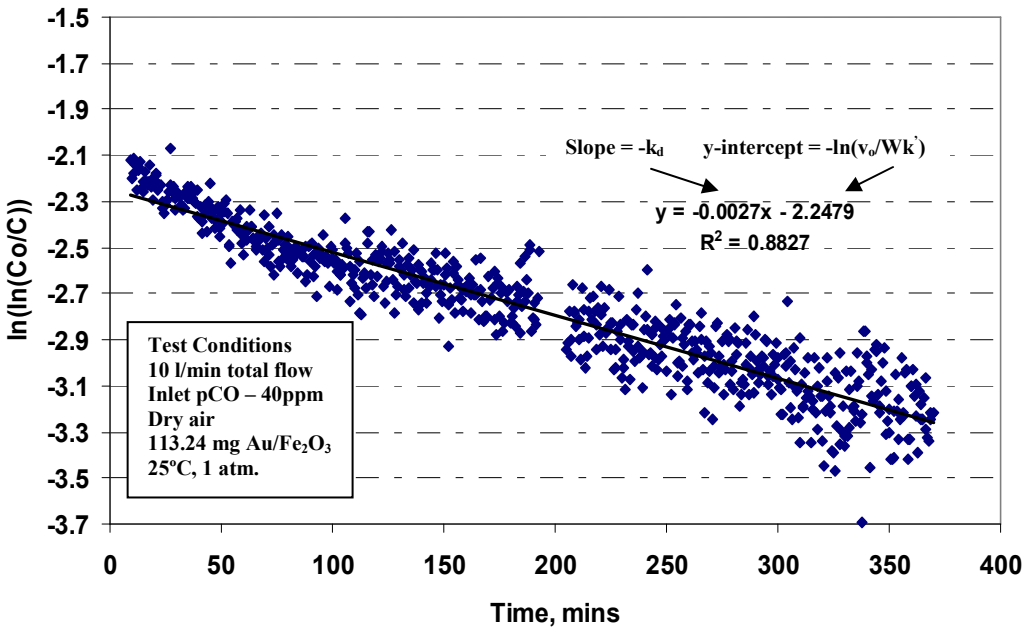


**Figure 3-20 Estimate of Specific Rate Constant and Decay Constant for CO Oxidation on $Au/Fe_2O_3$ Powder Catalyst**

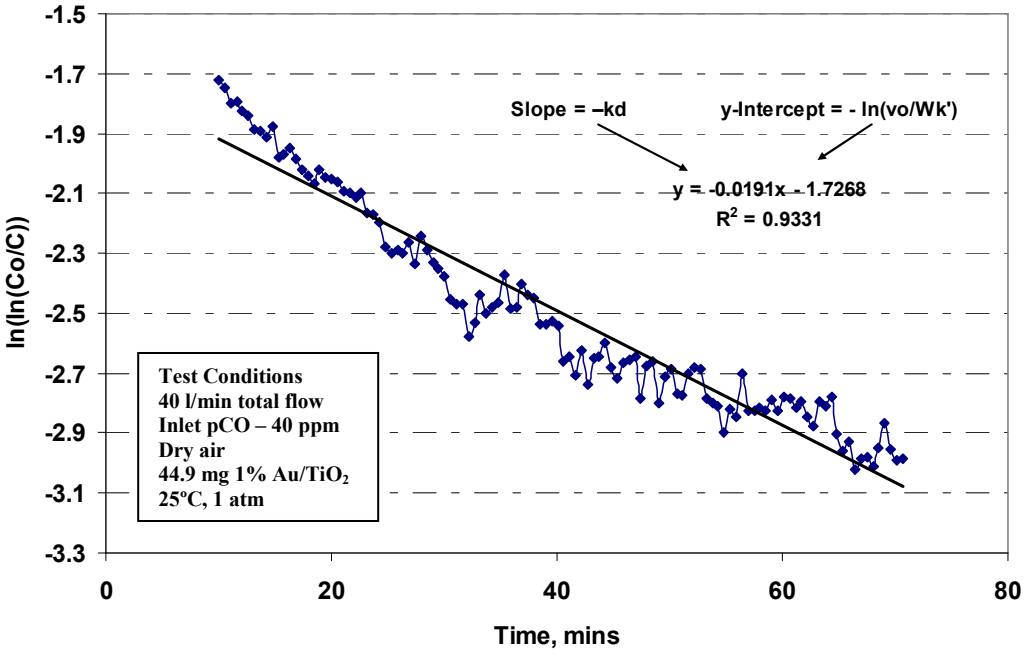


**Figure 3-21 Estimate of Specific Rate Constant and Decay Constant for CO Oxidation on $Au/TiO_2$ Powder Catalyst**

From Figures 3-19 through 3-21, the rate constants and decay constants for the $Pt/TiO_2$ and Au catalysts were calculated using the appropriate values for inlet flow rate and catalyst weight and are listed in Table 3-4. An example calculation is given in Appendix. 1.

**Table 3-4 Estimate of Decay Constant and Rate Constant for CO Oxidation on $Pt/TiO_2$ and Au Catalysts – Dry Air**

| Catalyst/reactant | $k_d$ ($mins^{-1}$) | $k'$ (l $min^{-1}$ $g^{-1}$) |
|---|---|---|
| **$Pt/TiO_2$/CO** | **0.0122** | **161.6** |
| **$Au/Fe_2O_3$/CO** | **0.0027** | **37.3** |
| **$Au/TiO_2$/CO** | **0.0191** | **158.4** |

Bamwenda et al. (1997) reported CO oxidation rates for $Pt/TiO_2$ that range from approximately $5x10^{-6}$ to $2x10^{-8}$ mol $s^{-1}$ $g^{-1}$. The maximum rate constant calculated from Bamwenda's data is approximately 0.73 l $min^{-1}$ $g^{-1}$ which is lower than the results reported in Table 3-4 by a factor of approximately 200. This difference is primarily attributed to differences in platinum loading (the catalyst in Table 3-4 has 10 times more platinum – 10% wgt vs.1% wgt), $TiO_2$ surface area (the catalyst in Table 3-4 has approximately 3 times the surface area, 155 vs. 50 $m^2$ $g^{-1}$), and differences in preparation methods, which is the subject matter of Bamwenda's paper, which for some of the catalysts is reported to result in variations of the rate constant of up to 3 orders of magnitude.

No rate constants were identified for $Au/Fe_2O_3$ catalysts in the literature but Bamwenda et al. (1997) lists data from which a maximum rate (for the range of data reported) can be estimated of 2.93 l $g^{-1}$ $min^{-1}$ for $Au/TiO_2$. As with the $Pt/TiO_2$, for the various $Au/TiO_2$ catalysts in Bamwenda's research, they also report a large variation (5 orders of magnitude) in measured reaction rates. Denkwitz et al. (2009) reports rates for various $Au/TiO_2$ catalysts as high as 46 liter $min^{-1}$ $g^{-1}$ . Aguilar-Guerrero and Gates (2009) also report on the large variation of kinetic parameters in the reported data in the literature for supported gold catalysts for CO oxidation. In light of these variations, and the lack of specific information on the "commercial" Au catalyst formulations, the experimentally determined values for the Au catalysts listed in Table 3-4 are considered reasonable.

### 3.4.2 Estimate of Reaction Rate Constants for the Oxidation of HCHO in Dry Air on $Pt/TiO_2$

This section presents a modification to the reaction rate equation previously developed in Section 3.4.1.1. for the case when there is no measurable deactivation. In a similar fashion the rate equation is combined with the design equation for a plug flow reactor to determine the rate constant for HCHO oxidation from experimental data. In this case, the data from the HCHO screening trials is used directly. As previously noted, none of the Au catalysts were available at the time of the HCHO testing so no experimental work was done in that regard. Additionally, since the $Pt/TiO_2$ catalyst is selected for incorporation into the catalytic hollow fibre structures, it is the only catalyst from the screening trial for which HCHO rate constants are calculated.

#### 3.4.2.1 Kinetic Theory without Deactivation

To estimate the reaction rate constant (also assumed as first order) for the oxidation of HCHO equation 3-4 is used with the activity set equal to one since there was no significant indication of catalyst deactivation as:

$$v_0 \frac{d[CO]}{dW} = -k'[CO] \qquad 3\text{-}6$$

which upon integration yields:

$$\ln \frac{C}{C_0} = -k' \frac{W}{v_0} \qquad 3\text{-}7$$

Equation 3-7 can be re-written in terms of the volume of catalyst instead of the weight of catalyst as:

$$\ln \frac{C}{C_0} = -k'' \frac{V_{cat}}{v_0} \qquad 3\text{-}8$$

where the ratio $\frac{V_{cat}}{v_0}$ is the residence time and $k'' = k'$ multiplied by the density of the catalyst. Therefore a plot of $\ln\frac{C}{C_0}$ versus the residence time will yield a straight line with a slope of $k''$. Data from Figure 3-16 was averaged at each of the flow rates (different residence times) and used to estimate the reaction rate constant. The results are shown below in Figure 3-22.

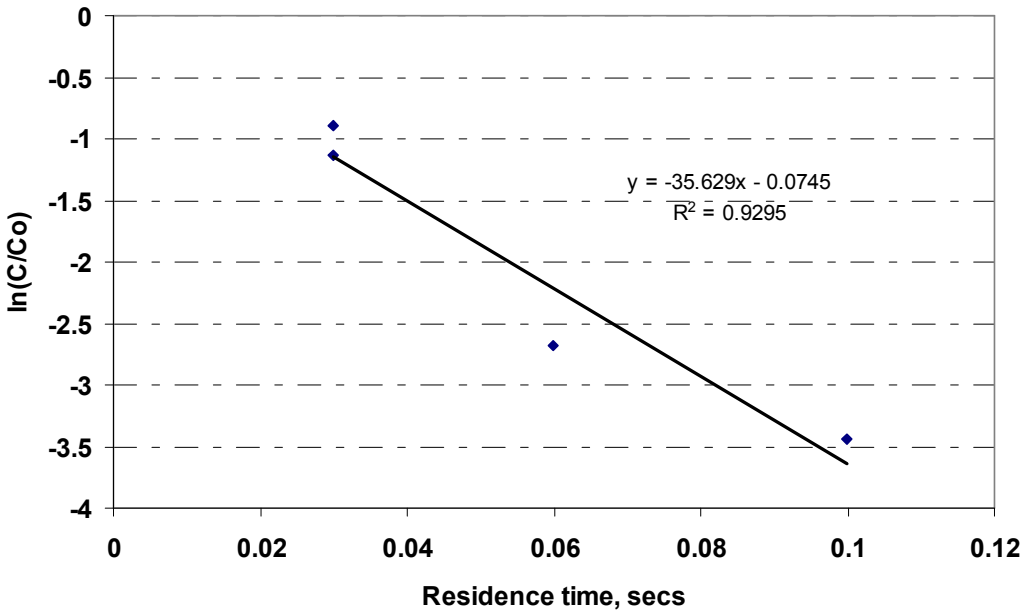


**Figure 3-22 Estimate of Reaction Rate Constant for the Oxidation of HCHO in Dry Air on Pt/$TiO_2$**

The variation in data is primarily due to the accuracy of the analysis at the low ppb levels of HCHO, however the estimated rate constant calculated from the slope of Figure 3-22, 35.6 $s^{-1}$ is in excellent agreement with the average published value of 35.9 $s^{-1}$ from Dewil et al. (2005) (based on relative Pt content and estimated internal effectiveness factor discussed in Section 3.4.3). No kinetic data specific to the oxidation of HCHO on Au catalysts was found in the literature.

### 3.4.3 Estimate of Diffusivities and Thiele Modulus for Catalyst Structures

The Thiele modulus ($M_T$) is a measure of pore diffusional resistance and has been extensively correlated to the effectiveness factors ($\eta$) for various reaction orders and catalyst geometries (Levenspiel 1972). Assuming first order reaction kinetics on Pt catalysts for the oxidation of CO and HCHO at low concentrations in air (McCarthy et al. 1974, Dewil et al. 2005), $M_T$ and $\eta$ can be estimated from equations 3-9 and 3-10.

$$M_T = L_i\left(\frac{k}{D_e}\right)^{1/2} \qquad 3\text{-}9$$

$$\eta = \frac{1}{M_T} \text{ (for } M_T > 4)^* \qquad 3\text{-}10$$

where: $D_e$ = effective diffusivity (discussed below), $cm^2\ s^{-1}$

$k$ = specific rate constant, $s^{-1}$

$L_i$ = a characteristic length which is dependent on the catalyst geometry ($i$ is based on the shape of the catalyst, cylindrical, spherical, etc) and is defined by equation 3-11, cm.

$$L_i = \frac{V_p}{A_r} \qquad 3\text{-}11$$

where $V_p$ = the volume of the catalyst structure (in this case the pellet or the catalytic fibre), $cm^3$

$A_r$ = the exterior surface available for reactant penetration and diffusion, $cm^2$.

* For $0.4 < M_T < 4$, $M_T$ can be obtained graphically from reaction engineering text books such as Levenspiel (1972) or Fogler (1999). At $M_T < 0.4$, $\eta \approx 1$.

For the cylindrical Pt/$TiO_2$ catalysts tested, the length is approximately twice the diameter and including the ends of the cylinder in the calculation of the the exterior surface, the effective length $L$ is given by:

$$L_{cyl} = \frac{4\pi r^3}{10\pi r^2} = 0.4 r_p \qquad 3\text{-}12$$

where $r_p$ = the radius of the cylinder, cm.

For the cylindrical hollow fibre structures, $A_r$ is based on the inside diameter of the fibre, and $V_p$ is the volume associated with the solid portion of the hollow fibre structure and therefore $L$ is given by:

$$L_{CHF} = \frac{(r_{p2}^2 - r_{p1}^2)\pi l}{2\pi r_{p1} l_{CHF}} = \frac{(r_{p2}^2 - r_{p1}^2)}{2 r_{p1}} \qquad 3\text{-}13$$

where $r_{p1}$ = the radius associated with the inside diameter of the hollow fibre bore, cm

$r_{p2}$ = the radius associated with the outside diameter of the hollow fibre bore, cm

$l_{CHF}$ = the length of the hollow fibre, cm

The CHF structures used in the initial phases of this research had a nominal inside diameter of 0.8 mm and a nominal outside diameter of 2 mm. The Pt/$TiO_2$ cylinders had a nominal diameter of 3.175 mm and an aspect ratio (length to diameter ratio) of approximately 2. Based on these values the following characteristic lengths, $L_i$, are calculated for the CHF and catalyst structures. (A sample calculation for a CHF structure is given in Appendix 1).

$L_{CHF}$ = 0.105 cm

$L_{Pt\_cylinder}$ = 0.0635 cm

$L_{Au\_granule}$ = 0.0176 cm (TDA)

$L_{Au\_cylinder}$ = 0.057 cm (Mintek)

It is clearly seen that the unidirectional diffusion path (from inside diameter to the outside diameter) of the CHF structure results in an effective length which is 65% larger than that of the cylindrical catalyst structure for which diffusion is multidirectional – radially from the outer surface in addition to axially from the ends of the cylinders. This longer characteristic length must be physically modified (by changes in the ID and OD of the fibre) and/or off-set by the effective diffusivity of the CHFs in order for the resulting structures to have an increased efficiency (higher effectiveness factor) relative to the supported granular catalyst structures.

In equation 3-9, $D_e$ is the effective diffusivity and includes a geometric correction factor which is applied to the diffusivity to account for the structure in which the gas is diffusing, and is a function of the diffusivity of the contaminant in air, the catalyst porosity, tortuosity, and constriction factor, and is defined by equation 3-14:

$$D_e = \frac{D\varphi\sigma}{\tau} \qquad 3\text{-}14$$

where: $D$ = diffusivity, $cm^2\ s^{-1}$

$\varphi$ = catalyst porosity

$\tau$ = catalyst tortuosity

$\sigma$ = constriction factor

The diffusivity within the structure must consider both bulk and Knudsen diffusion and at steady state is defined by equation 3-15 (Smith, 1981):

$$D = \frac{1}{\left(\frac{1}{D_{AB}} + \frac{1}{(D_k)_A}\right)} \qquad 3\text{-}15$$

where: $D_{AB}$ = bulk diffusivity of binary gas mixture $AB$, $cm^2\ s^{-1}$

$(D_k)_A$ = the Knudsen diffusivity of species $A$, $cm^{2\ -1}$

The bulk diffusivity for a binary gas mixture (A, B) can be calculated using the *Chapman-Enskog formula* (Smith 1981):

$$D_{AB} = \frac{0.0018583 T^{3/2} \left( \frac{1}{M_A} + \frac{1}{M_B} \right)^{1/2}}{p_t \sigma_{AB}^{\,2} \Omega_{AB}} \qquad 3\text{-}16$$

where: $D_{AB}$ = bulk diffusivity, $cm^2\ s^{-1}$

$T$ = temperature, ºK

$M_A$, $M_B$ = molecular weight of gases, $g\ mol^{-1}$

$p_t$ = total pressure of the gas mixture, atm

$\sigma_{AB}$, $\epsilon_{AB}$ = constants in the Lennard-Jones potential-energy function for the molecular pair $AB$; $\sigma_{AB}$ is in Å

$\Omega_{AB}$ = collision integral, which would be unity if the molecules were rigid spheres and is a function of $k_B T / \epsilon_{AB}$ for real gases ($k_B$ = Boltzmann constant)

$$\sigma_{AB} = \frac{1}{2}(\sigma_A + \sigma_B) \qquad 3\text{-}17$$

$$\varepsilon_{AB} = (\varepsilon_A \varepsilon_B)^{1/2} \qquad 3\text{-}18$$

Since the Lennard-Jones potential-energy function is used, the equation is strictly valid only for nonpolar gases.

The force constants for CO and air were taken from Smith (1981), while constants for HCOH were calculated using the following relationships (Smith 1981)

$$\sigma = 1.18 V_b^{1/3} \qquad 3\text{-}19$$

$$\frac{k_B T}{\varepsilon} = 1.30 \frac{T}{T_C} \qquad 3\text{-}20$$

where: $k_B$ = Boltzmann's constant

$T_c$ = critical temperature, K

$V_b$ = volume per mole at normal boiling point, $cm^3\ gmol^{-1}$

The bulk diffusivities calculated using equation 3-16 for CO:air and HCHO:air mixtures are:

$$D_{CO:air} = 0.196\ cm^2\ s^{-1}$$
$$D_{HCHO:air} = 0.176\ cm^2\ s^{-1}$$

A representative calculation is given in the Appendix.

The Knudsen diffusivity for diffusion in a circular pore of radius $a_p$ is (Smith 1981):

$$(D_k)_A = 9.70x10^3 a_p \left(\frac{T}{M_A}\right)^{1/2} \qquad 3\text{-}21$$

where: $a_p$ = radius of pore, cm

$T$ = temperature, K

Values of $D_k$ for CO and HCHO, calculated from equation 3-21, for representative catalyst particles and the catalytic hollow fibre structure are presented below in Table 3-5. The pore size used to estimate $D_k$ for the CHF was taken from the hollow fibre adsorbent work of Tai (2007). Since no pore size data was available from the manufacturer of the $Au/Fe_2O_3$ catalyst, the value was back-calculated based on an experimentally determined effectiveness factor, which was used to subsequently calculate the Thiele modulus, which allowed for the calculation of the effective diffusivity and ultimately the pore size.

**Table 3-5 Estimated Knudsen Diffusivity in Various Catalyst Structures**

| Structure | $(D_k)_{CO}$ ($cm^2\ s^{-1}$) | $(D_k)_{HCHO}$ ($cm^2\ s^{-1}$) | $a_p$,(cm x $10^8$) |
|---|---|---|---|
| CHF | 1.108 | 1.070 | 3500,average (Tai 2007) |
| $Pt/TiO_2$ | 0.024 | 0.023 | 75 (St.Gorbain data sheet) |
| $Fe_2O_3$ | 0.114 | 0.110 | 360 (exp estimate from measured effectiveness) |
| $Au/TiO_2$ | 0.049 | 0.048 | 155 (manufacturer data) |

It is clear from the relative values of the Knudsen and bulk diffusivities that the small pores in the catalyst supports are the primary resistance (Knudsen diffusion) in supported catalysts, whereas in the CHF the larger pores result in the bulk diffusion being the primary resistance. The calculated diffusivity (by equation 3-15), prior to applying a geometric correction associated with the structure, for the CHF and $TiO_2$ structures for CO and HCHO are given in Table 3-6.

**Table 3-6 Estimated Diffusivities of CO and HCHO in the CHF, $TiO_2$, and $Fe_2O_3$ Structures**

| Structure | $D_{CO}$ ($cm^2\ s^{-1}$) | $D_{HCHO}$ ($cm^2\ s^{-1}$) |
|---|---|---|
| CHF | 0.167 | 0.151 |
| $Pt/TiO_2$ | 0.020 | 0.020 |
| $Fe_2O_3$ | 0.072 | 0.068 |
| $Au/TiO_2$ | 0.039 | 0.038 |

To calculate the effective diffusivities, a geometric correction is necessary based on the structure of the catalyst support material. Typical values for the porosity, tortuosity, and constriction factors for porous catalysts are given by Fogler (1999) and were used in the estimation of the diffusivity for the CHF and $TiO_2$ structures:

$\varphi = 0.4$

$\tau = 4$ ( typical range is 2-8)

$\sigma = 0.8$

While the average values were used for both structures, inspection of a typical SEM photo of the CHF structures reveals long radial "finger" like pores which would effectively reduce the tortuosity of the fibre structures, however this would result in an increase in the value of *De* and therefore to be conservative in the estimation of the potential benefits of a CHF, the average values for catalyst support structures were used in the calculation for $D_e$ for the two structures. Note that the value of $D_e$ for the $Au/Fe_2O_3$ catalyst is based on a measured effectiveness factor, and then calculated from the relationship of the Thiele Modulus. Values of $D_e$ for the various catalysts are listed in Table 3-7.

**Table 3-7 Estimated Effective Diffusivities of CHF, $TiO_2$, and $Fe_2O_3$ Structures**

| Structure | $(D_e)_{CO}$ ($cm^2\ s^{-1}$) | $(D_e)_{HCHO}$ ($cm^2\ s^{-1}$) |
|---|---|---|
| **CHF** | **0.0134** | **0.0121** |
| **$Pt/TiO_2$** | **0.0016** | **0.0016** |
| **$Fe_2O_3$** | **0.0053** | **0.0054** |
| **$Au/TiO_2$** | **0.0031** | **0.0030** |

With the values for the specific rate constant, effective length and effective diffusivity, the Thiele Modulus can be estimated using previously defined equations 3-9 and 3-10:

$$M_T = L_i\left(\frac{k}{D_e}\right)^{1/2} \qquad 3\text{-}9$$

$$\eta = \frac{1}{\mathrm{M_T}}\,(for M_T > 4) \qquad 3\text{-}10$$

Since the rate constants shown in Table 3-4 are based on the density of the catalyst, it must be multiplied by the density to obtain the dimensionless units of the Thiele Modulus. The density of the cylindrical $TiO_2$ catalyst is 0.954 g $cm^{-3}$, while that of the fibres as initially fabricated is 0.598 g $cm^{-3}$, which is the density of the catalyst in the final module configuration (i.e. the value includes the inefficiency of the packing density of the fibre bundle structure). The CHF catalyst density used in this estimate in based only on initial studies and is further investigated during the development of the final catalytic fibre structures in Section 4.

In the estimation of the Thiele Modulus for the $Au/TiO_2$ CHF structures, the initial density of the $Pt/TiO_2$ CHF structure was used since it was assumed that the catalytic metal would not significantly alter the density of the final structure. Similarly the same effective diffusivity for CO in the structure was used in the calculation.

As noted above, there was insufficient data (pore size) from the supplier of the $Au/Fe_2O_3$ catalyst to analytically estimate its effectiveness factor so it was measured directly and the measured values are reported in Section 3.5. The estimates of the Thiele Modulus ($M_T$) and effectiveness factors ($\eta$) for the $Pt/TiO_2$ and $Au/TiO_2$ cylinders and CHF configurations are listed in Table 3-8, while an example calculation is presented in the Appendix (testing was not conducted for HCHO due to the lack of test rig availability).

**Table 3-8 Estimates of Thiele Modulus and Effectiveness Factors for Various Catalysts and Catalyst Structures**

| Structure | Catalyst | Reaction | $M_t$ | $\eta$ |
|---|---|---|---|---|
| CHF | $Pt/TiO_2$ | CO oxidation | 36.4 | 0.028 |
| 1/8 inch $TiO_2$ cylinder | $Pt/TiO_2$ | CO oxidation | 80.6 | 0.012 |
| CHF | $Au/TiO_2$ | CO oxidation | 36 | 0.028 |
| 1.5mm $TiO_2$ cylinder | $Au/TiO_2$ | CO oxidation | 55 | 0.018 |
| CHF | $Pt/TiO_2$ | HCHO oxidation | 4.4 | 0.23 |
| 1/8 inch $TiO_2$ cylinder | $Pt/TiO_2$ | HCHO oxidation | 9.5 | 0.116 |

Based on the estimates of the effectiveness factors of the various structures for both reactions it is clear that in both cases internal mass transfer resistances exist. However due to the high rate of reaction of the CO oxidation relative to HCHO, and the fact that the effective diffusivities are similar (primarily due to similar molecular weights), the effectiveness factor for the CO oxidation reaction in both structures is approximately an order of magnitude lower than the HCHO. The potential increase in catalyst effectiveness factors for the reactions based on the use of CHF structures range from a factor of approximately 1.6 to 2.3. The validation of these assumptions will be determined experimentally and are discussed in Chapter 4.

## 3.5 Experimentally Determined Effectiveness Factors for $Pt/TiO_2$ and $Au/Fe_2O_3$ Catalysts for CO oxidation.

The effectiveness factors for the "as received" $Pt/TiO_2$, $Au/Fe_2O_3$, and $Au/TiO_2$ catalysts were also determined experimentally using a differential reactor configuration with an inlet pCO of approximately 40ppm CO and are listed in Table 3-9.

**Table 3-9 Experimentally Measured Effectiveness Factors for Granular $Pt/TiO_2$ and Au Catalysts for CO Oxidation at 40 ppm CO**

| Catalyst/Structure | $\eta$ |
|---|---|
| 1/8 inch $Pt/TiO_2$ cylinder | 0.040 |
| 14x24 mesh $Au/Fe_2O_3$ granular | 0.184 |
| 1.5 mm $Au/TiO_2$ cylinder | 0.058 |

The measured effectiveness for the $Pt/TiO_2$ and $Au/TiO_2$ catalysts is approximately 3 times the estimated value in Section 3.4.3. This is not unreasonable based on the assumptions used in calculating the effective diffusivity – specifically as the assumptions relate to catalyst structure morphology, e.g. tortuosity, constriction factor, and pore diameter. The relative value of the measured effectiveness factor for the Au catalyst is primarily a result of the smaller particle size and resulting smaller characteristic length.

The effect of particle size was also noted in the initial screening shown in Figure 3-6 (Section 3.3.1.2) which shows an approximate 75% average conversion for the 1/8" $TiO_2$ and > 95% conversion using 14x24 mesh (1.41 mm x 0.707 mm) particles of the same catalyst under the same test conditions.

Since the Thiele modulus is defined as being proportional to the ratio of a "reaction rate" to a "diffusion rate", when deactivation is occurring the reaction rate is changing with time and therefore the Thiele modulus and effectiveness factor also change with time. In measuring the effectiveness factors of the various forms of catalysts, test durations were relatively short, typically 10-20 minutes, and therefore deactivation during the test was negligible. Therefore the reported values represent the initial effectiveness factor. In longer term tests, deactivation needs to be considered and is discussed for longer term comparative tests in Section 4.2.12.

### 3.6 Estimate of Maximum Catalyst Particle Size Required to Obtain a Catalyst Effectiveness Factor of 0.95

The maximum particle size required to essentially eliminate internal mass transfer resistance can be estimated by combining the experimentally determined catalyst effectiveness factors from Section 3.5 and the definition of the Thiele modulus, equation 3-9. From equation 3-9, the ratio of the Thiele module for two different sized catalyst particles of the same material reduces to:

$$\frac{M_{T1}}{M_{T2}} = \frac{L_{i1}}{L_{i2}} \qquad 3\text{-}22$$

Where the subscripts *1* and *2* refer to different catalyst particle sizes. The radius of the particle is calculated from the definition of the characteristic length, $L_i$, which depends on the geometry of the catalyst particle as previously defined in Section 3.4.3.

Since the Thiele modulus is non-linear below a value of 4, it can be calculated analytically or obtained graphically as a function of the effectiveness factor. For an effectiveness factor of 0.95 (therefore negligible internal mass transfer resistance), $M_T$ = 0.9 (Fogler 1999). For high values of the Thiele modulus (i.e., the low effectiveness factors consistent with the catalysts used in this research) the measured values of the effectiveness factor can be used to calculate the Thiele modulus from equation 3-10.

$$\eta = \frac{1}{\mathrm{M_T}} (for M_T > 4) \qquad 3\text{-}10$$

Additionally, if it is assumed that the crushed catalyst particles are spherical; the equivalent length (based on the definition of equation 3-11) for a spherical catalyst particle is:

$$L_{sphere} = \frac{V_p}{A_r} = \frac{\frac{4}{3}\pi r_{sphere}^3}{4\pi r_{sphere}^2} = \frac{r_{sphere}}{3} \qquad 3\text{-}23$$

Combination of equations 3-22 and 3-23 allow for the estimation of the particle size required to achieve essentially eliminate internal mass transfer control (i.e. a catalyst effectiveness factor of 0.95 or greater), based on the data from a single experiment in which the effectiveness factor has been determined:

$$r_{shere2} = \frac{3M_{T2}L_{sphere1}}{M_{T1}} \qquad 3\text{-}24$$

For the cylindrical $Pt/TiO_2$ catalyst, the characteristic length was previously calculated as 0.0635 cm. The measured effectiveness factor for this catalyst is 0.040, which from equation 3-10 yields a Thiele modulus = 25. As stated above, for an effectiveness factor of 0.95, the Thiele modulus is 0.9. The estimated maximum particle to eliminate internal mass transfer is then calculated from equation 3-24.

$$r_{shere2} = \frac{3M_{T2}L_{sphere1}}{M_{T1}} = \frac{3(0.9)(0.0635\,\text{cm})}{25} = 0.00686\,\text{cm}$$

The resulting maximum catalyst particle sizes required for an effectiveness factor of 0.95, based on the measured effectiveness factors for the various catalysts summarized in Table 3-9, are listed in Table 3-10.

**Table 3-10 Estimated Maximum Catalyst Particle Size to Achieve an Effectiveness Factor of 0.95**

| Catalyst/Structure | $\eta$ | $M_T$ | $L_1$, cm | $L_2$, cm | $r_{sphere}$, cm | $r_{sphere}$, µm |
|---|---|---|---|---|---|---|
| 1/8 inch $Pt/TiO_2$ cylinder | 0.040 | 25 | 0.0635 | 0.00229 | 0.00686 | 68.6 |
| 14x24 mesh $Au/Fe_2O_3$ granular | 0.184 | 5.4 | 0.0176 | 0.00292 | 0.00874 | 87.4 |
| 1.5 mm $Au/TiO_2$ cylinder | 0.058 | 17.2 | 0.057 | 0.00298 | 0.00893 | 89.3 |

### 3.7 Conclusions from the Catalyst Screening Evaluation

Platinum catalysts using higher metal content and alternate supports have been shown to be more active than the baseline NASA catalyst of Pt/carbon for the ambient temperature oxidation of CO. Two of these, $Pt/TiO_2$ and $Pt/SiO_2$ had similar activities, however the $Pt/TiO_2$ catalyst was chosen for incorporation into the CHF structures since there was considerably more literature associated with its use for ambient temperature oxidation of formaldehyde. No significant difference in HCHO oxidation was observed.

In addition to the platinum catalysts, two gold catalysts were also tested as representative of the state of the art gold catalysts for ambient temperature CO oxidation. $Au/Fe_2O_3$ was more active than $Au/TiO_2$ in the "as received" form when tested in dry air, but the reverse is true in the presence of water vapor. For equal particle sizes at low space velocities the $Au/Fe_2O_3$ performed similar to the $Pt/TiO_2$ catalyst, however at higher space velocities the $Pt/TiO_2$ catalyst was considerably more active. Due to the lack of availability of the HCHO test rig, none of the gold catalyst material was evaluated for ambient temperature HCHO oxidation.

All of the catalysts were negatively affected by water vapor, however all catalysts recovered completely upon the removal of water vapor, however it is critical that this effect be factored into any application as it the magnitude of the impact on performance is not negligible.

The effect of a 0.5% (by volume) $CO_2$ concentration on CO oxidation activity was also investigated on the $Pt/TiO_2$ and was found to have only a temporary, and negligible effect on CO oxidation activity. Similar findings were noted in the literature for a gold based catalyst at 0.2% (volume) $CO_2$ concentration.

Effectiveness factors were estimated for both CO and HCHO oxidation reactions and analytically it is predicted that both reactions will benefit from smaller catalyst particle size due to internal mass transfer resistance. However due to the much higher rate of the CO oxidation reaction, relative to HCHO oxidation, and similar diffusivities, the effectiveness factor for the CO oxidation reaction is much lower. Additionally, maximum catalyst particle sizes were estimated that would essentially eliminate internal mass transfer control within the supported catalyst.

Due to the high activity of the $Pt/TiO_2$ noted in the CO oxidation testing, and significant literature references to it being used for ambient temperature HCHO oxidation, it was selected for use in the development of catalytic hollow fibre structures. Of the two gold catalysts, the $Au/TiO_2$ was selected for catalytic fibre development since it is the only one that was made available by the manufacturer in sufficient quantities. Basic characteristics of the two catalysts selected for incorporation into catalytic hollow fibre structures are summarized below in Table 3-11.

**Table 3-11 Catalysts Selected for Development of Catalytic Hollow Fibres**

| Catalyst | Manufacturer | Metal Content Wgt. % | Average pore diameter, Å | Reaction rate constant ($l\ min^{-1}\ g^{-1}$) |
|---|---|---|---|---|
| $Pt/TiO_2$ | Nalette | 10 | 150 | 161.6 |
| $Au/TiO_2$ | Mintek | 1 | 310 | 158.6 |

# Chapter 4

## 4 Experimental Approach and Development of Catalytic Hollow Fibres

Hollow fibre adsorbents incorporating 13X mol sieve desiccants were previously shown by Tai and Perera (2007) to offer enhanced kinetics when compared to 1/8 inch (3 mm) granular forms. They investigated various polymer/solvent systems and manufacturing parameters including polymer concentrations, polymer type, solvents, air gap, drying temperature, etc. An open structure consisting of 20% (wgt.) polyethersulphone and 80% 13X (wgt.), was easily fabricated using conventional dry/wet spinning techniques, and when dried at 200 ºC resulted in a hollow fibre adsorbent with comparable adsorption kinetics to granular forms of 13X. Tai and Perera's research (inorganic content of resultant fibre, polymer selection, and manufacturing process) served as the starting point for the manufacturing of catalytic hollow fibres (CHF), with the 13X being replaced by candidate catalyst particles in this research. However, the nominal porosity obtained in their hollow fibre adsorbents proved insufficient to obtain a sufficiently open porosity on the inner diameter of their fibres and therefore novel approaches to increasing the porosity of the inner surface were investigated in this research.

Catalysts selected for incorporation into hollow fibre structures included 10% $Pt/TiO_2$ (manufactured by Nalette) and 1% $Au/TiO_2$ (Mintek, South Africa) which resulted from the literature search in Chapter 2 and the catalytic screening trials discussed in Chapter 3.

The initial CHF development effort focused on the determination of a suitable catalyst content and the production of physically stable fibre structures. Once a structure with acceptable structural integrity was produced, manufacturing parameters (e.g. fibre dimensions, molecular weight and type of polymer, addition of non-solvent additives and pore former materials, and bore fluid composition) were modified in an attempt to maximize the catalytic effectiveness factors. Due to the inherent expense associated with the platinum and limited availability of Au catalyst samples, an extensive parametric development program was not practical, often requiring modifying multiple parameters during the development process.

Following the production of catalytic fibre samples, fibre modules were produced and tested in a differential reactor configuration to determine the catalyst effectiveness factor for the ambient temperature oxidation of CO using the test apparatus discussed in Chapter 3 (Section 3.3.1.1). Catalytic fibre effectiveness factors were measured for the CO oxidation reaction at a concentration of 40 ppm CO and are calculated as the ratio of the rates of reaction of the catalytic fibre to that previously measured for the catalyst powder at the same conditions.

For the $Pt/TiO_2$ fibres, the maximum increase in measured effectiveness factor was found to be approximately 50% greater than the effectiveness factor for the corresponding granular form of the catalyst, while the maximum effectiveness factor for the $Au/TiO_2$ fibres was less than 10% of the Au granular catalyst. Due to the limited amount of Au catalyst made available in support of this research, only three samples could be produced, limiting the amount of development associated with the Au catalyst, however this also highlights the significant difference in the manufactured fibres potentially resulting from minor changes in the catalyst support characteristics (e.g. in this case the Pt catalyst support had a surface area approximately 3 times the Au support while both catalysts were dispersed on $TiO_2$ as discussed in Section 3.1).

The catalytic hollow fibres that were developed and tested for catalytic effectiveness are summarized in Table 4-1. The measured effective factors for the granular catalyst structures are included for reference purposes.

**Table 4-1 Summary of Catalytic Hollow Fibres Formulations and Measured Effectiveness Factors**

| CHF Sample | Catalyst | Polymer* | Polymer/Solvent Ratio | Catalyst/Polymer Ratio | % NMP in Bore** | Effectiveness Factor**** |
|---|---|---|---|---|---|---|
| C1 | 10% $Pt/TiO_2$ | PESF1 | 20/80 | 80/20 | 0 | 0.016 |
| C2 | 10% $Pt/TiO_2$ | PESF1 | 18/72.6*** | 83/17 | 85 | 0.036 |
| C3 | 10% $Pt/TiO_2$ | PESF1 | 18/82 | 83/17 | 85 | 0.058 |
| C4 | 10% $Pt/TiO_2$ | PESF1 | 20/80 | 80/20 | 85 | 0.025 |
| C5 | 10% $Pt/TiO_2$ | PESF1 | 17.5/82.5 | 85/15 | 85 | 0.041 |
| C9 | 10% $Pt/TiO_2$ | PESF2 | 18/82 | 83/17 | 80 | 0.030 |
| C10 | 10% $Pt/TiO_2$ | PESF2 | 14/86 | 83/17 | 80 | 0.062 |
| C11 | 10% $Pt/TiO_2$ | PESF2 | 16/84 | 83/17 | 80 | 0.050 |
| C12 | 1% $Au/TiO_2$ | PESF2 | 16/84 | 83/17 | 80 | 0.001 |
| C14 | 10% $Pt/TiO_2$ | PVDF1 | 14/86 | 83/17 | 80 | 0.034 |
| C15/70 | 1% $Au/TiO_2$ | PVDF2 | 14/86 | 83/17 | 70 | 0.002 |
| C15/80 | 1% $Au/TiO_2$ | PVDF2 | 14/86 | 83/17 | 80 | 0.014 |
| $C16^t$ | 8.2% $Pt/TiO_2$ | PESF1 | 13.3/80.8** | 14.6/85.4 | 85 | 0.015 |
| --N/A-- | Pt granular | N/A | N/A | N/A | N/A | 0.040 |
| --N/A-- | Au granular | N/A | N/A | N/A | N/A | 0.058 |

*PESF1 – polyethersulfone Gafon 3100P (Solvay), PESF2 - polyethersulfone Gafon 3000P (Solvay)
PVDF1 – polyvinylidenefluoride Kynar 720 (Arkema), PVDF2 – polyvinylidenefluoride Kynar 761 (Arkema)
** Balance $H_2O$
*** Balance 4.7% $H_2O$, 4.7% polyvinylpyrrolidone
**** Based on catalyst mass in catalytic fibre
t – Hollow fibre with $TiO_2$ support which was impregnated with platinum catalyst precursor after manufacturing

## 4.1 Catalytic Fibre Materials, Characterization Equipment, and CHF Fabrication Methods

This section presents a summary of the materials used in the manufacturing of the catalytic hollow fibres, characterization equipment, test apparatus and manufacturing

approach and equipment. Additionally a representative example of the specific method for making fibres is also presented.

### 4.1.1 Materials

All the $Pt/TiO_2$ catalysts used in this research contained 10 % (wgt.) platinum and were manufactured as 1/8 inch (3mm) cylinders by Nalette (2007) using standard incipient wetness techniques previously discussed in Section 3.1. The $Au/TiO_2$ contains 1 % (wgt.)Au and was provided by Mintek (South Africa) as 1.5 mm cylinders. Though not used after the initial fibre development, a single batch of $Pt/SiO_2$ catalyst (also manufactured by Nalette) was also evaluated in the initial development activity.

The prepared catalysts were ground, using a Retsch ball mill (Model PM 100), and the resulting powder sieved to less than 350 microns in the initial fibre development while subsequent fibre development sieved the crushed catalyst powder to less than 50 microns.

Four different polymers were used in the fabrication of the catalytic hollow fibres including two polyethersulfone (PESF) materials designated Gafon 3100P and Gafon 3000P (Solvay), and two polyvinylidenefluoride materials designated Kynar 720 and Kynar 761 (Arkema). The polymers were fully dissolved in 1-methyl-2-pyrrolidone (NMP) (Sigma-Aldrich) prior to the addition of the catalyst material.

A single CHF sample (designated C2) was produced whereby the NMP solvent was reduced and a corresponding amount of a 50/50 mixture (by weight) of water and polyvinylpyrrolidone (PVP) was added to the polymer/NMP mixture. The laboratory grade distilled water acted as a non-solvent and the PVP (molecular weight 1000, Sigma-Aldrich) as a pore-former.

In addition to the CHFs discussed above in which the catalysts were manufactured prior to incorporation into the CHF, a single sample was also produced using non-catalytic $TiO_2$ powder. After manufacturing the hollow fibre structure, the non-catalytic fibre with

$TiO_2$ was impregnated with a platinum salt and subsequently reduced to evaluate this alternate method of producing a CHF.

### 4.1.2 Characterization Equipment

Scanning electron micrographs (SEM) photos of prepared catalytic hollow fibres were taken to examine samples in cross section in addition to the interior and exterior surfaces to ascertain surface porosity. Samples were prepared by breaking the hollow fibres after scoring with a razor blade. All samples were mounted on conductive carbon tape and gold sputtered for 1-3 minutes prior to inspection by SEM. SEMs were taken with either a model JSM-6480LV (JEOL, University of Bath) or model JSM-5800LV (JEOL, Hamilton Sundstrand).

BET surface area and CO chemisorption measurements were performed by Reaction Systems LTD (Bolder CO) using a Micromeritics FlowSorb II 2300 surface area analyzer to investigate the potential of polymer blockage of the catalyst pores and also of catalyst site occlusion by the polymer. To perform a BET surface area analysis, the sample is crushed and weighed and placed in a u-shaped sample cell. The cell is then installed in the unit and a flow of 30% $N_2$ in He is directed through the cell at a flow rate of approximately 90 $cm^3$ $min^{-1}$. A heating mantle is placed over the cell and it is used to heat the sample to 150 °C for one hour to remove adsorbed water. After degassing, the cell is immersed in a Dewar of liquid nitrogen, causing a monolayer of $N_2$ to adsorb onto the surface of the sample. The transient reduction in $N_2$ concentration exiting the sample cell is detected by a thermal conductivity detector (TCD) and used to determine the quantity of $N_2$ adsorbed on the sample. Finally, moles of $N_2$ are converted to surface area using a factor of 1.62E-19 $m^2$/molecule $N_2$ (Satterfield 1980).

CO chemisorption was determined using the Micromeritics FlowSorb II 2300 surface area analyzer. The sample is crushed and placed in the sample cell and reduced in $H_2$ at 150 C for one hour, and then cooled in He to ambient temperature. This is followed by injection of 10 microliter quantities of CO into the He and measuring the quantity of CO

that passed through the sample following each injection. The injections are repeated until CO is no longer being adsorbed. The amount of adsorbed CO is assumed proportional to the available platinum.

Catalytic hollow fibre modules were produced by potting the CHF catalytic fibres in a tube, which after curing of the potting, were tested in a differential reactor mode using the CO oxidation test apparatus discussed in Section 3.3.1.1. The CO oxidation rate was measured and normalized to an equivalent inlet CO concentration of 40 ppm. In most experiments, the number of CHFs used to produce a module was between 7 and 10, and typically 3.5 inches (8.9 cm) long. Testing to determine the effectiveness factor was done in dry air and the flow was adjusted as required to obtain differential reactor conversions, typically in the range of 10-20 percent. The effectiveness factor was then calculated as the ratio of the rate of CO oxidation for the CHF structure to that of the powder.

### 4.1.3 CHF Fabrication Equipment and Methods

The device used in the fabrication of the catalytic hollow fibres was fabricated by researchers in the Department of Chemical Engineering at the University of Bath and is shown schematically in Figure 4-1. The primary components consist of a stainless steel feed vessel, spinneret and coagulation bath. The polymer/catalyst dope (or casting solution) is fed under pressure, produced by a pressurized nitrogen gas supply, to the spinneret which also has a port to which a bore fluid is simultaneously pumped to form the inner (hollow) opening of the hollow fibre. The extruded casting solution is then precipitated in the coagulation bath.

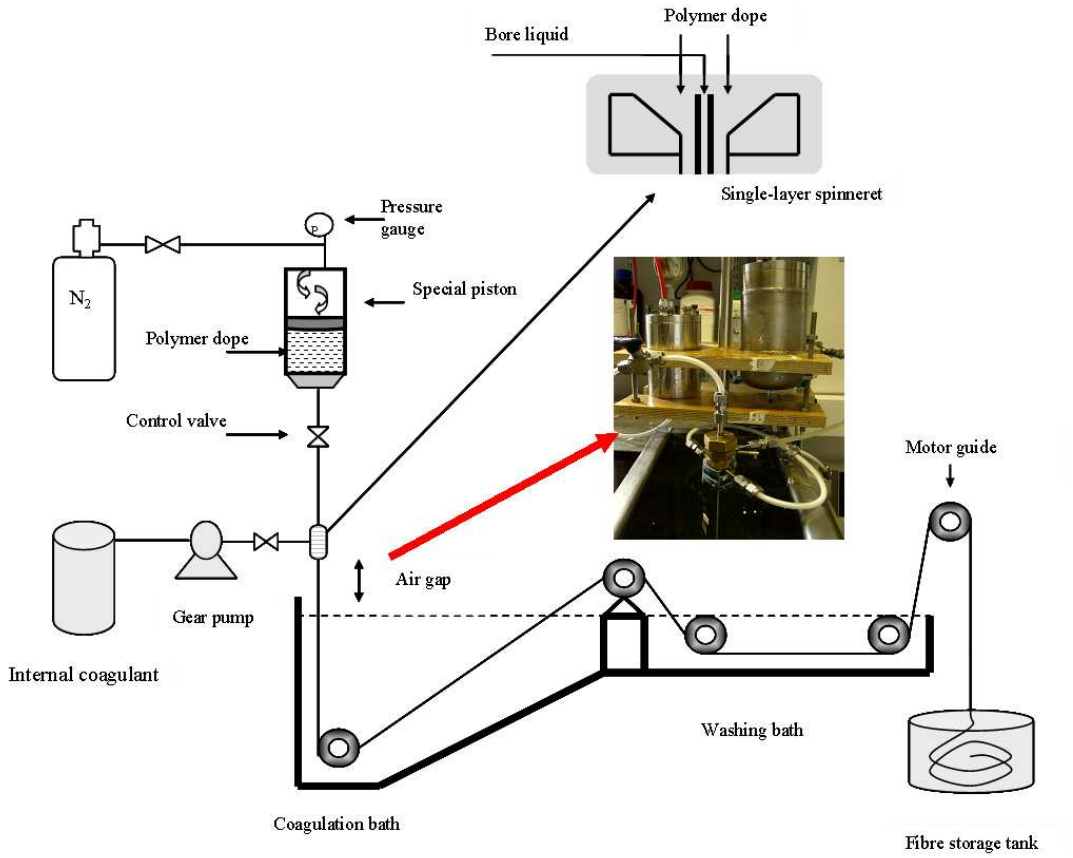


**Figure 4-1 Catalytic Hollow Fibre Manufacturing Schematic**

Two different spinnerets were used depending on the desired size of the fibres. In the initial development phases a spinneret (designated spinneret 1) with a 1.0 mm diameter bore and an outside diameter of 3.2 mm. CHF sample C1 is the only experimental fibre produced using spinneret 1. All subsequent CHF structures used a spinneret (spinneret 2) with a bore diameter of 0.8 mm and outside diameter of 1.9 mm. Details of a typical spinneret are shown in Figure 4-2.

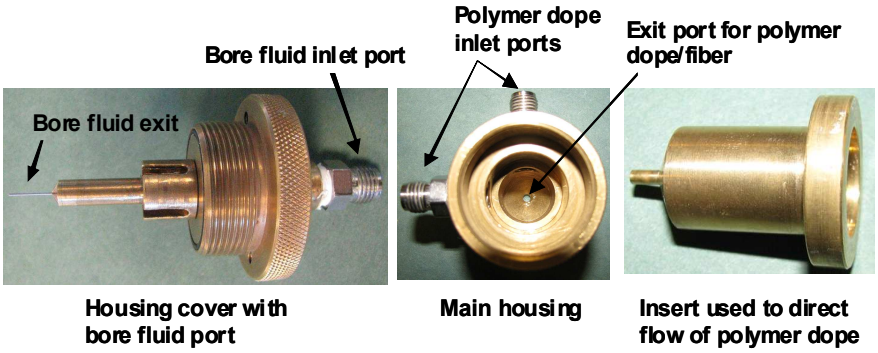


**Figure 4-2 Hollow Fibre Spinneret Elements**

The air gap refers to the distance between the exit of the spinneret and the surface of the coagulant bath and allows for the potential of relaxing stresses in the polymer dope as it is forced through the spinneret, drawing (or stretching) of the fibre as a result of gravitational forces, partial evaporation of a volatile solvent, partial precipitation of casting solution in contact with the bore fluid, or a combination there of, prior to contact with the coagulant bath. Depending on the polymer/solvent system being used, the effect of the air gap can be significant, affecting the resulting morphology and dimensions of the produced fibres (Koros and Fleming 1993, Baker 2004). Based on earlier work by Tai and Perera (2007), the initial fibre development utilized a 5 cm air gap; however the bulk of the fibres investigated in this thesis used a zero air gap as it proved to provide a more stable manufacturing due to the high solvent concentrations eventually used in the bore fluid which was required to produce a more open structure on the inside diameter of the hollow fibre structures.

The manufacturing of all of the catalytic hollow fibres followed the same general procedure with slight changes in manufacturing parameters to determine the effect on the measured catalyst effectiveness factor in the resulting fibres. Specific variable effects are discussed in more detail in the following sections while the general procedure and a representative example are presented below.

The general procedure of producing catalytic hollow fibre structures consists of the preparation of the polymer/solvent/catalyst dope (mixture) which is then forced through a spinneret and subsequently coagulated in a coagulant bath. The polymer solution is prepared by dissolving the polymer in solvent at the desired mass ratio (typically in the range of 20/80 polymer/solvent weight ratio). The desired amount of catalyst is then added to the polymer/solvent solution to obtain the final desired ratio of catalyst to polymer in the resultant fibres. The polymer/solvent/catalyst dope mixture is vigorously stirred using an IKA WERKE stirrer for a minimum of 24 hours to obtain a homogeneous dispersion. After stirring, the polymer dope/catalyst dispersion is slowly rotated until used to manufacture the catalytic fibres. Prior to spinning fibres the polymer/solvent/catalyst dope mixture is degassed by applying a vacuum for a minimum of 30 minutes to remove any gas entrained during the mixing process.

The polymer/solvent/catalyst mixture is then transferred to a feed vessel that is pressurized to drive the mixture into the spinneret device used to form the hollow fibre structure. A bore fluid (distilled water or distilled water/solvent mixture) is simultaneously fed to the inlet of the bore in the spinneret. The polymer/solvent/catalyst mixture then exits the spinneret contacting the coagulant bath to initiate (with zero air gap) or complete (in the event where an air gap is used) the precipitation (sometimes referred to as phase inversion) of the casting mixture. The fibres are then soaked in water for at least 24 hours, which is periodically replaced with fresh water, to extract the residual solvent from the fibre structures. The fibres are then air dried at room temperature for approximately 24 hours and then dried at the desired final temperature.

The manufacturing details of CHF sample C1 (reference Table 4-1) are provided as an example of a typical CHF. A 20 wgt. % polymer solution was prepared by dissolving 20 g of polyethersulfone (PESF) Gafon 3100P (Solvay) in 80 g of NMP and mixed until the PESF was fully dissolved. To produce a final catalyst/polymer weight ratio of 80/20, 64 g of crushed $Pt/TiO_2$ catalyst was mixed with 80 grams of the PESF/NMP solution. Pure water, used as the bore fluid, and the PESF/NMP/catalyst were concurrently fed through spinneret 1 with a 5 cm air gap prior to entering the pure water coagulant bath.

After soaking in water for 24 hours, the resulting fibres were dried in air for 24 hours. After drying in air at room temperature, the fibres were cut and bundled together with Teflon tape to minimize twisting of the fibres during final drying.

The final drying of the C1 fibres was done at 180 ºC for approximately 24 hour in pure nitrogen to minimize potential oxidation of the polymer. The dried fibres were then cut to approximately 4 inches (10.2 cm) in length and 37 fibres were potted in a module prior to testing the CO oxidation effectiveness. The finished module is shown in Figure 4-3.

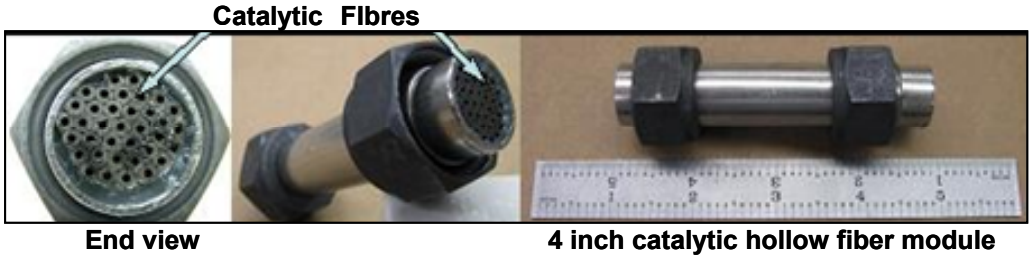


**Figure 4-3 Catalytic Hollow Fibre Module – 37 C1 Fibres**

### 4.2 Development of Experimental Catalytic Hollow Fibres

This section presents the development activity associated with establishing the basic requirements of the experimental catalytic hollow fibre structures: specifically as it relates to catalyst particle size, fibre drying requirements, and polymer/catalyst ratio. Additionally, basic CO oxidation activity of chopped hollow fibres is also presented.

Once a sufficiently robust CHF fibre was developed, the balance of the development activity focused on increasing the catalytic activity (as determined by measuring catalyst effectiveness factor for CO oxidation) based on attempting to alter the morphology of the CHF structures.

While Tai and Perera's (2007) and Tai's (2007) research focused on the incorporation of adsorbents in hollow fibre structures, the research in this thesis is aimed at incorporating high loadings of catalyst material into hollow fibre structures and to the best of the

author's knowledge represents original research that has not been previously reported in the literature.

### 4.2.1 Determination of Appropriate Catalyst Particle Size and Polymer/Catalyst Ratio

As a starting point in the manufacturing of the CHF structures, the previous work of Tai and Perera (2007) was referenced for the determination of an appropriate initial ratio of polymer/solvent/catalyst. In their work, successful fibres were developed using a polymer/solvent weight ratio of 20/80, and a final molecular sieve/polymer weight ratio of 80/20.

If the catalyst particles are small enough to achieve an effectiveness factor of 1, i.e. 100% of the catalyst is utilized in the reaction, it is obvious that maximizing the amount of catalyst in the CHF structures, and therefore maximizing the catalyst weight percent is desired. Additionally, maximizing the polymer concentration in the initial polymer/solvent mixture will maximize the density of the final structure. The resulting maximum "catalytic density" (defined as the mass of catalyst per unit length of fibre) of the final CHF structure is therefore achieved by maximizing the amount of catalyst used in the final polymer/solvent/catalyst dope while also maximizing the initial polymer concentration in the polymer/solvent solution.

However, there are also competing manufacturing and fibre morphology issues in attempting to maximize polymer and catalyst concentrations. The most obvious issue in this regard is that high concentrations of polymer and catalyst both result in an increase in mixture viscosity potentially resulting in a polymer/solvent/catalyst that cannot easily be processed without high pressure, specialized equipment. Additionally, excessively high catalyst content (typically in the range of 85-90 % , by weight) results in fibres that are brittle and therefore damaged during handling.

Alternately, since it is desirable to have a CHF structure with low mass transfer resistance (to allow for rapid diffusion of process gas within the fibre wall structure), a low polymer concentration is desired, which upon polymer precipitation will result in a more open, porous structure than would be achieved with a higher polymer concentration. However, if the polymer concentration is too low, the resulting structure will be void of structural integrity since it is the interconnectivity of the polymer strands in the fibre that provides the necessary integrity.

All of the initial fibres in this research were manufactured using water as both the external coagulant (non-solvent) and bore fluid. Spinneret 1 and an air gap of 5 cm were used in the initial fabrication, and all catalyst particles were crushed and sieved to less than 350 μm (while it was estimated in Section 3-6 that a maximum catalyst particle diameter of approximately 137 μm was required to achieve a catalyst effectiveness factor of 0.95, the initial CHF structures were manufactured prior to conducting the necessary kinetic experiments needed for those calculations).

The polymer/solvent weight ratio was targeted at 20/80 and catalyst weight percents were targeted at 70, 80 and 90%, however it was subjectively determined that at 90% catalyst, the polymer/solvent/catalyst mixture was too viscous to process so additional solvent was added resulting in a final maximum catalyst content of 87 weight percent being investigated. The incorporation of additional solvent also resulted in a reduction of the polymer content of the starting polymer/solvent mixture to 15 weight percent.

The compositions of the hollow fibres fabricated in the initial manufacturing process are summarized in Table 4-2.

**Table 4-2 Composition of the Initial Catalytic Hollow Fibres**

| Sample | Catalyst particle size, μm | Polymer/Solvent Weight ratio | Catalyst/Polymer final weight ratio | Weight Percent Catalyst/Support |
|---|---|---|---|---|
| A | < 350 | 15/85 | 87/13 | 10%Pt/$TiO_2$ |
| B | < 350 | 20/80 | 80/20 | 10%Pt/$TiO_2$ |
| C | < 350 | 20/80 | 70/30 | 10%Pt/$TiO_2$ |

Bore fluid – pure water
Air gap – 5 cm
Dried in air at 200 ºC

While Pt/$SiO_2$ fibres were attempted, they essentially crumbled after drying and as a result it was decided to continue development with only the Pt/$TiO_2$ catalyst; however the Pt/$SiO_2$ fibres were used to investigate the cause of the poor fibre integrity discussed in Section 4.2.2.

Pictures of the catalyst structures used in the initial manufacturing and representative hollow fibres are shown in Figure 4-4.

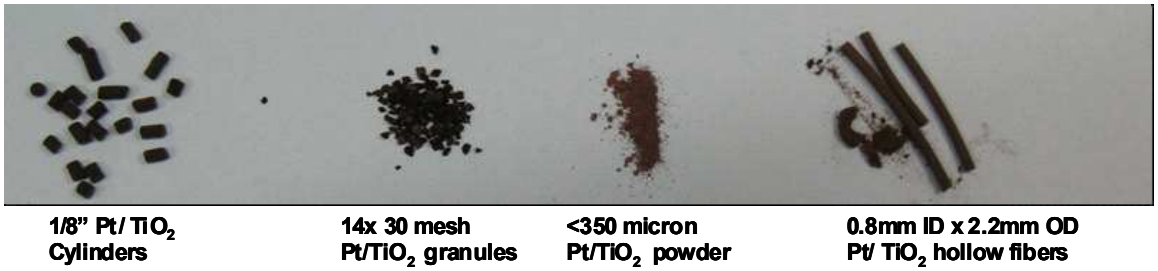


**Figure 4-4 Representative Pt/$TiO_2$ Catalyst Structures and Resultant Catalytic Hollow Fibres**

After air drying at room temperature for 24 hours, the fibres were subsequently dried overnight in a convection oven for 24 hours at 200 ºC. All of the initial CHFs produced using this technique were qualitatively determined to be insufficient to fabricate CHF modules primarily due to the lack of structural integrity. Of all of the initial samples produced, sample C, 70% (wgt.) Pt/$TiO_2$/30% (wgt.) PESF, was the most robust, but even

this sample was considered too weak structurally to produce a module. While it is not surprising that the low polymer content (less than 20% by wgt.) of the fibres resulted in fragile fibre structures, it was not clear what resulted in inferior structural strength at the higher polymer content (20-30 % by wgt.). Pictures of representative initial CHF structures are shown in Figure 4-5.


**Figure 4-5 Effect of Catalyst/Polymer Ratio on CHF Structures after Drying at 200º C**

To investigate the cause of the structurally inferior CHF structures in the initial manufacturing, SEM photographs of the 70% and 87% $TiO_2$ structures were taken which reveal two potential reasons for the lack of structural integrity of the initial CHF samples. Figure 4-6 shows typical cross sections of the fibres showing the relative dimensions of the catalyst particles and hollow fibre wall.

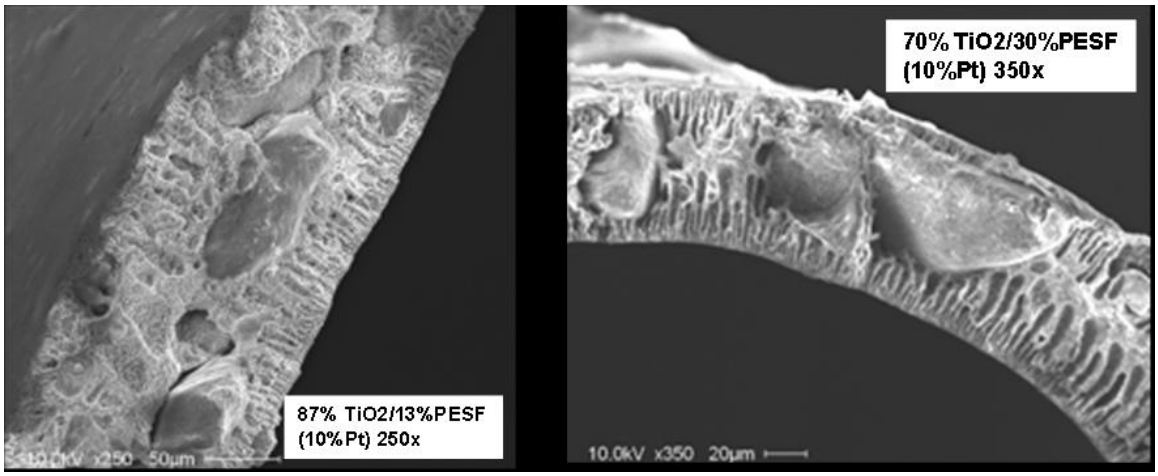


**Figure 4-6 Representative Fibres Depicting Excessive Particle Size Relative to Fibre Thickness**

It is clear that the relative dimensions (nominal 350 micron catalyst particles) of the catalyst particle to resulting fibre wall thickness can result in particles spanning more than half the thickness of the fibre wall thickness and therefore little or no polymer to tie the structure together, resulting in fibres that are easily fractured.

This problem is further exasperated at the higher catalyst mass fractions as more catalyst particles are available to span the fibre wall cross section. In some cases, the resulting fibre cross sections are only slightly thicker than a single catalyst particle. Additionally, at catalyst concentrations above 80%, the resulting high viscosity of the polymer dope made the spinning process extremely inefficient as much of the polymer/solvent/catalyst mixture remained on the walls of the polymer dope feed vessel, and therefore 80% (wgt.) of catalyst was determined as an approximate maximum.

While the SEM photographs of the CHFs shown in Figure 4-6 for an intact sample of fibre show a uniform, continuous porous polymer structure, effectively encapsulating the catalyst particles, SEM micrographs of resulting CHF powder samples shown in Figure 4-7 from the same batch of fibres show the lack of a continuous polymer structure.

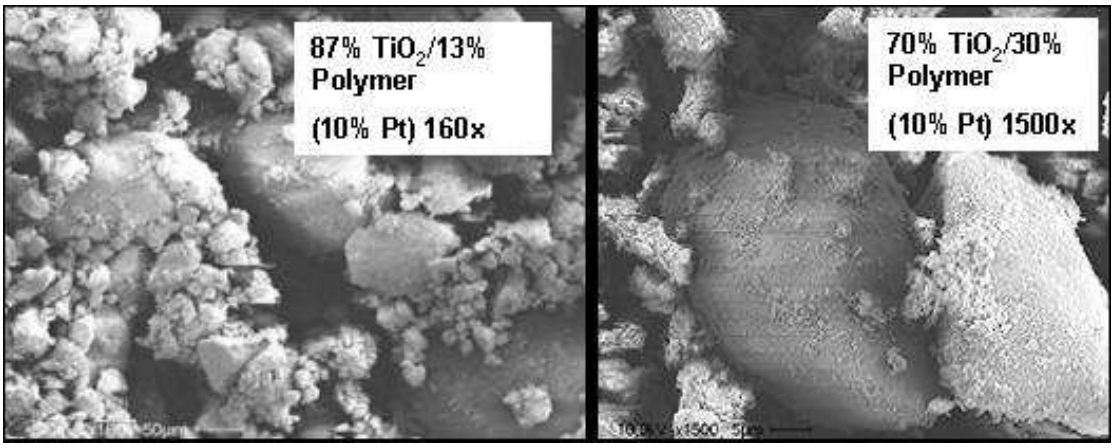


**Figure 4-7 Initial CHF Powder Showing Inadequate Polymer Connectivity**

This lack of polymer "connectivity" could have been a result of one or more of the following - high catalyst loadings, large catalyst particles, or chemical alteration of the polymer structure.

The issue of catalyst particle size and catalyst loading can be adjusted by physical means (i.e. a reduction in catalyst particle size and catalyst mass fraction), thereby minimizing the potential of large particles forming natural fracture points. However, it is believed that in the presence of the dispersed platinum catalysts, the polymer structure may be partially oxidized at 200 ºC in air (the final drying condition used in the manufacturing of these samples).

### 4.2.2 Characterization of Initial CHF Structures by FTIR

To investigate the possibility of oxidation further, FTIR (Nicolet, model Avatar 360 FT-IR) spectra were run on samples of catalytic hollow fibres containing $TiO_2$ and $SiO_2$ catalyst and compared to pure PESF polymer. While the CHF containing $TiO_2$, which was more stable from a structural point of view, shows many of the same peaks as the pure PESF in the IR spectra, many of the characteristic peaks of the PESF are absent in the spectra of the CHF containing $SiO_2$. Specifically, the carbon-hydrogen and

carbon=carbon double bonds of the ether, in addition to the S=O bonds of the sulphonic group are non-exist (Pavia et al. 1996). These differences, indicative of the degradation of the PESF, are highlighted in the FTIR spectra shown in Figure 4-8.

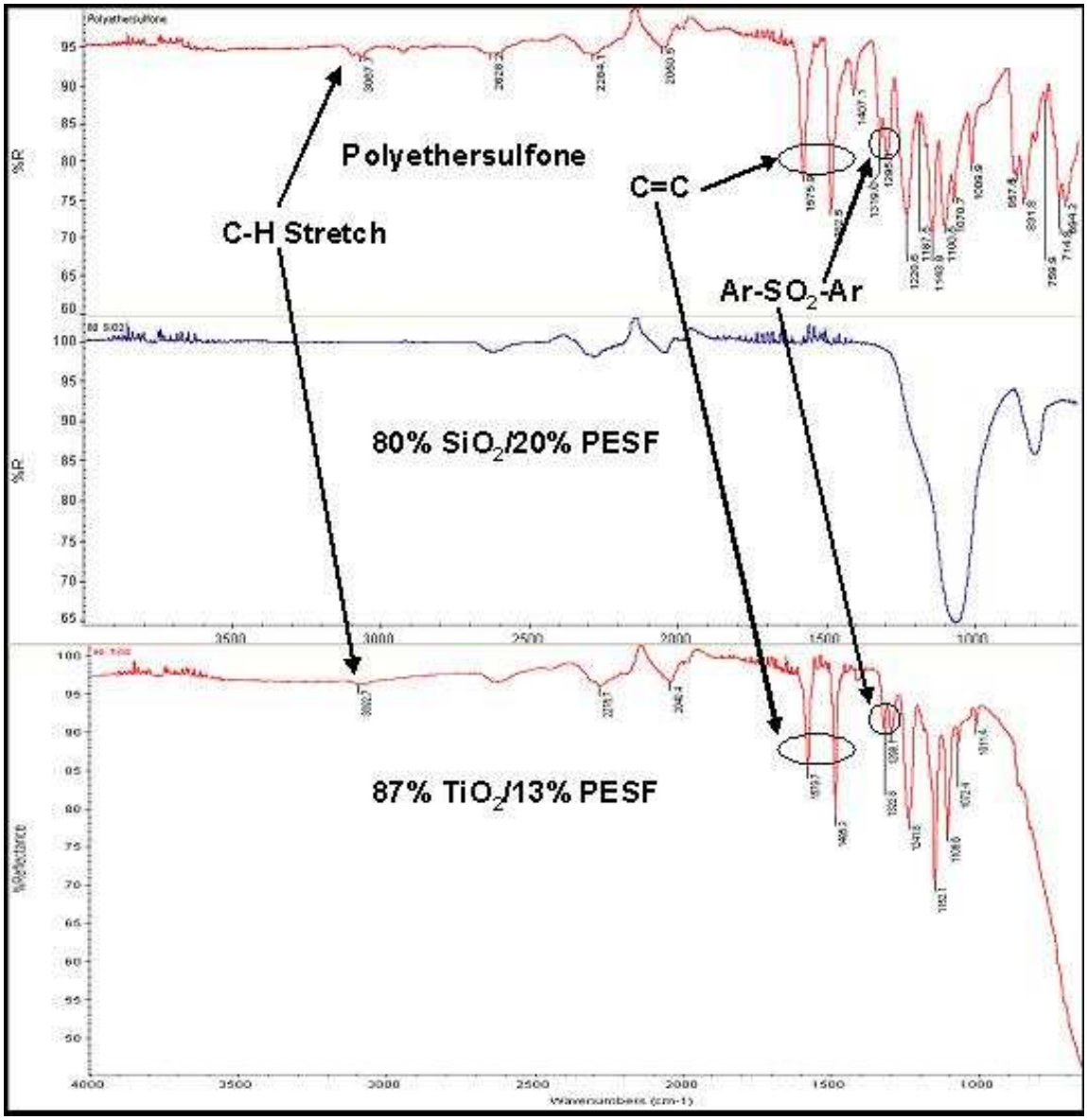


**Figure 4-8 FTIR Spectra Comparison of Pt/TiO2 CHF, Pt/SiO2 CHF, and PESF Showing Potential Oxidation of PESF after Exposure to Air at 200 ºC**

To evaluate the impact of these parameters, subsequent manufacturing was done with smaller catalyst particles (< 50 μm - which also addresses the desired higher effectiveness associated with smaller catalyst particles) and limited the catalyst mass loadings to 80 -

83% (wgt), with all elevated temperature drying done in a nitrogen environment to eliminate the potential of polymer oxidation – the impact of these changes is discussed in Section 4.2.4.

### 4.2.3 CO Oxidation Activity of Initial $Pt/TiO_2$ Chopped CHF Structures

Though the initial fibres were brittle and not satisfactory for the production of hollow fibre modules, an initial assessment of CO conversion was made to ascertain the relative activity of the $Pt/TiO_2$ CHF structures relative to the baseline granular catalyst. This was accomplished by chopping the fibres to an approximate length of 2-3 mm, sieving any dust, and testing the oxidation of CO in a 15 $cm^3$ packed bed reactor to allow a direct comparison to the previous granular catalyst baseline activity tests (Section 3.3.1.2)

These tests were conducted in dry air at a GHSV of 110,400 $hr^{-1}$, with inlet CO concentrations of 10, 20, and 40 ppm. Figure 4-9 shows the outlet CO concentration as a function of inlet concentration, while Figure 4-10 show the normalized rate of reaction, for the baseline granular material, and catalytic fibre material for 70 and 87 weight percent catalysts (there was insufficient material to evaluate the 80% (wgt.) catalytic fibres).

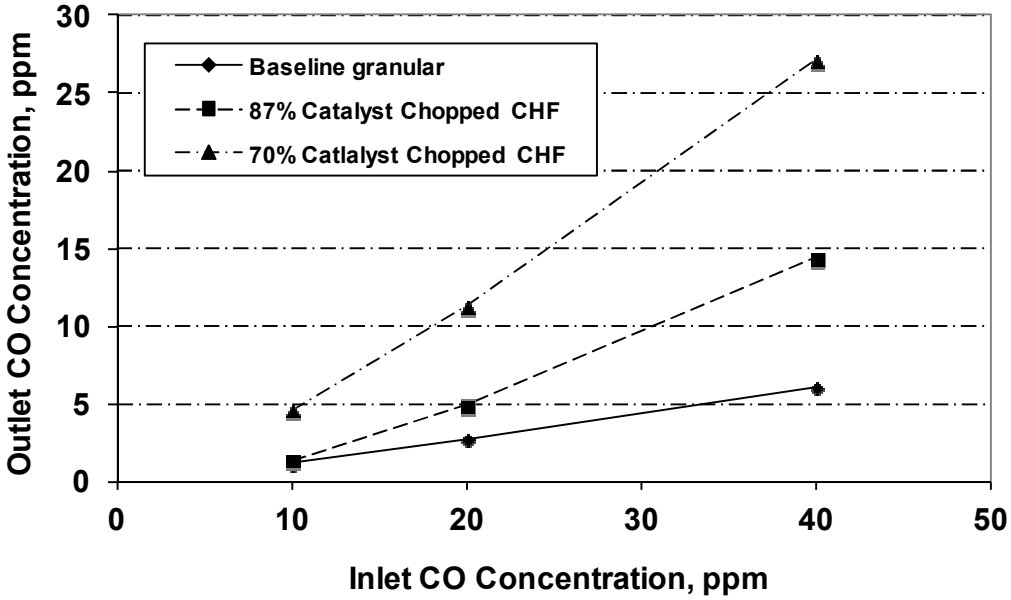


**Figure 4-9 Comparison of Initial "Chopped" Catalytic Fibre Material to Baseline Granular Catalyst – 15 $cm^3$ Bed Volume, GHSV of 110,400 $hr^{-1}$**

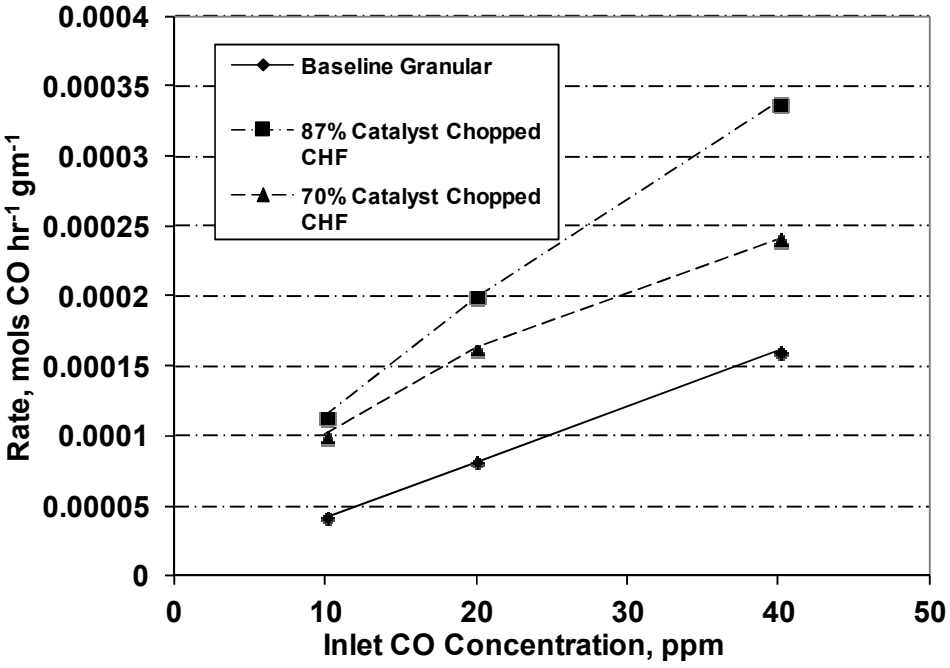


**Figure 4-10 Rate of Reaction Initial "Chopped" Catalytic Fibre Material and Baseline Granular Catalyst – 15 $cm^3$ Bed Volume, GHSV of 110,400 $hr^{-1}$**

While Figure 4-9 clearly shows that the fibres are not as efficient from a volumetric perspective, Figure 4-10 shows that the normalized rate of CO oxidation is higher for the catalytic fibres, demonstrating a more efficient use of the catalyst mass (14.3 g for granular, 5.1 g for 87 % (wgt.) CHF, and 3.6 g for 70 % (wgt.) CHF). Not surprisingly, Figure 4-10 also shows that higher concentrations of catalyst in the fibre are preferred as they result in higher rates of reaction.

Due to the weak structure and low packing density of the initial fibres, the desired volumetric efficiency was not achieved, however if a similarly open structure can be achieved with a dense packing of hollow fibres, the volumetric efficiency of the fibres can be increased. However, it should also be noted that this method (i.e. chopped fibres) of testing takes advantage of multi-directional diffusion in the chopped fibres (i.e. from the inside, outside and ends of the chopped fibre structures), and therefore a shorter characteristic length than what would be possible with an actual hollow fibre structure in which all diffusion will be from the inside surface.

### 4.2.4 Effect of Reduced Catalyst Particle Size and Nitrogen Drying

To investigate the potential of producing more robust catalytic hollow fibres, the $Pt/TiO_2$ granular material was crushed to produce smaller particle sizes. The crushed particles were subsequently sieved through a 50 μm screen prior to mixing with the polymer/solvent solution. The CHFs were manufactured using a weight ratio 20% polymer/80% NMP solvent, with a final weight ratio of 80% catalyst/20% polymer.

The bore fluid and coagulant bath were both water and a 5 cm air gap was used between the spinneret and coagulant bath. After soaking the resultant fibres in water to remove residual solvent all fibres were dried in nitrogen, except for the room temperature drying which was done in air. The bulk of the particles were determined to be on the order of 1-2 microns as seen in the SEM shown in Figure 4-11.

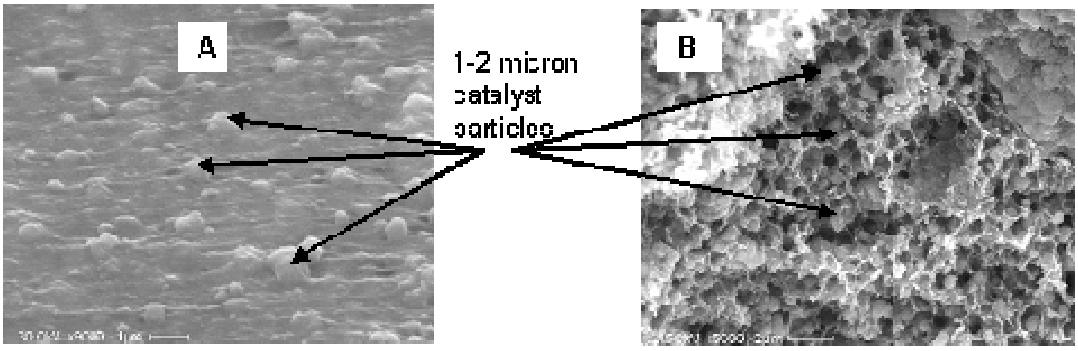


**Figure 4-11 Representative Catalyst Structures Produced Showing 1-2 µm $Pt/TiO_2$ Particles (A – surface, B – internal structure)**

To determine the effect of the drying temperature and the potential of reducing polymer degradation due to elevated temperature drying in air, small samples of produced fibres were dried at room temperature, 80 ºC, and 120 ºC – all for a minimum of 24 hours, with all elevated temperature drying done in a nitrogen environment. The three fibre structures samples were then examined using scanning electron microscopy. Cross sections and surface morphologies are shown in Figures 4-12 through 4-14.

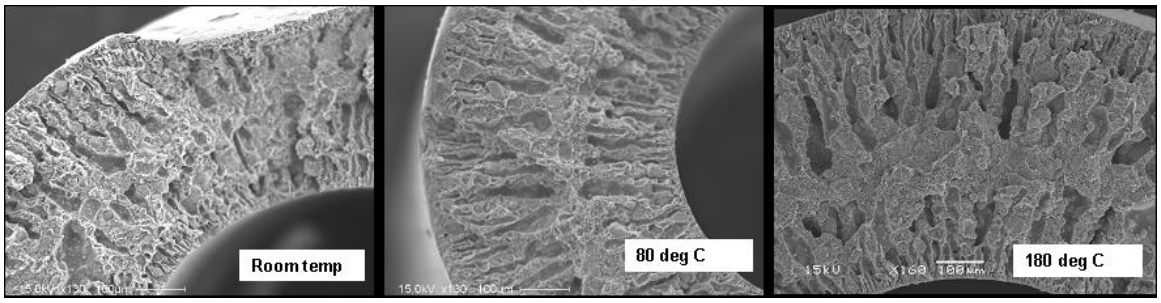


**Figure 4-12 Effect of Nitrogen Drying Temperature on C1 Fibre Morphology Cross Sections - Room Temperature, 80 ºC, and 180 ºC.**

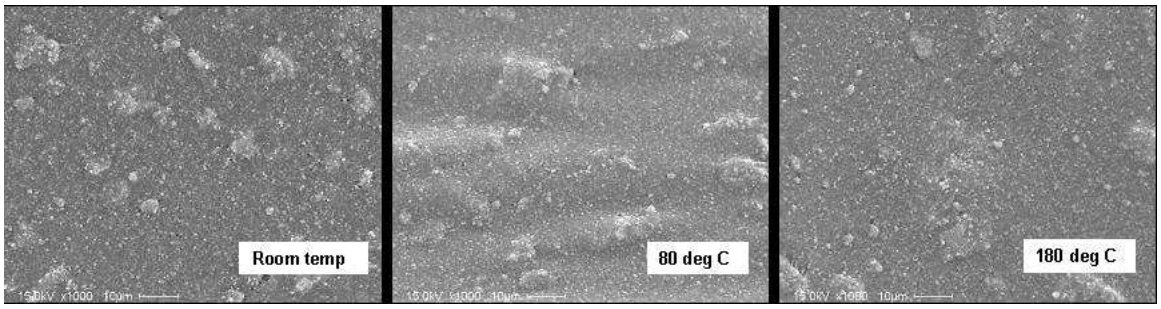


**Figure 4-13 Effect of Nitrogen Drying Temperature on C1 Fibre Morphology Inside Diameter Surfaces, Room Temperature, 80 ºC, and 180 ºC.**

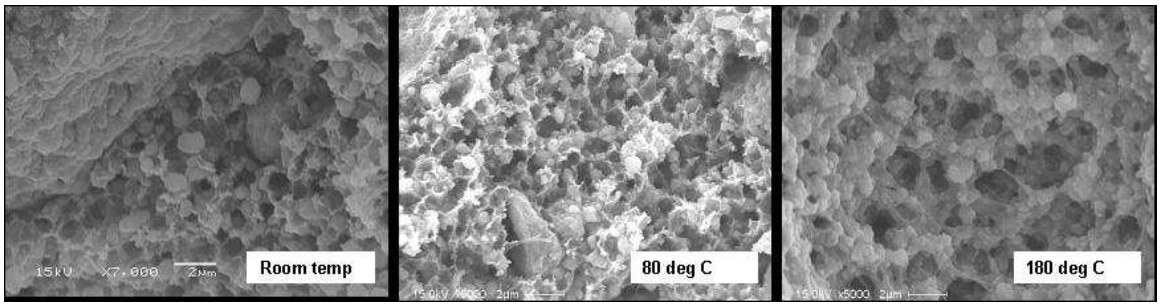


**Figure 4-14 Effect of Nitrogen Drying Temperature on C1 Fibre Morphology Macro-void Surfaces, Room Temperature, 80 ºC, and 180 ºC.**

As can be seen from the SEM photos, the differences in fibre morphology are negligible when dried from room temperature to 180 ºC. In all structures typical "finger-like" macro-voids are formed across the structure during the rapid demixing process (Oh et. al., 2009). The substructure contains pores that are nominally 1-2 μm in diameter, while the inner surfaces appear dense with low porosity. The most significant finding from this experiment is that the fibre structures were intact upon drying in nitrogen at 80 ºC and 180 ºC, presumably due to limiting the potential of partial oxidation of the polymer.

Based on the results from this experiment, all subsequent CHFs were produced using catalyst particles sieved to less than 50 μm and dried in a nitrogen environment.

### 4.2.5 CO Oxidation Activity of $Pt/TiO_2$ Initial Catalytic Hollow Fibres

Catalytic hollow fibres manufacture as discussed in Section 4.2.3 were used to produce the hollow fibre membrane module, previously shown in Figure 4-3 and designated as CHF sample C1, for CO oxidation activity testing. The module consisted of 37 hollow fibres at 3.7 inches (9.4 cm) in length. The fibres were potted using silicon potting to prevent bypass in the module and tested at the same space velocity and concentration range as the baseline granular material to provide a direct comparison of catalytic activity. The results of the comparative testing are shown in Figures 4-15 and 4-16, and include baseline granular catalyst, 87% $Pt/TiO_2$ chopped fibres and the CHF module containing sample C1.

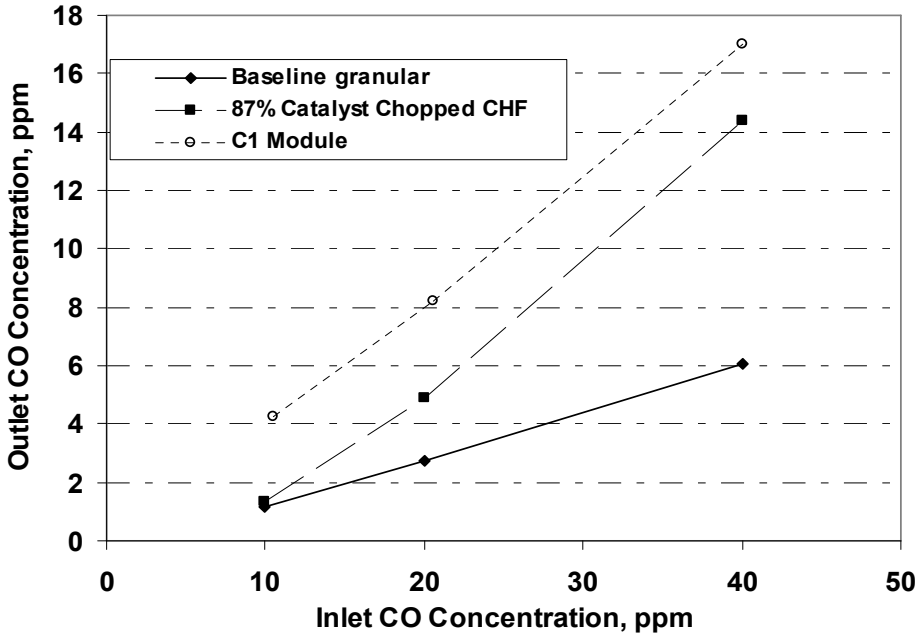


**Figure 4-15 Relative Activity of $Pt/TiO_2$ Catalyst – Baseline Granules, 87% wgt $Pt/TiO_2$ Chopped CHF, and C1 CHF Module – GHSV 110,400 $hr^{-1}$**

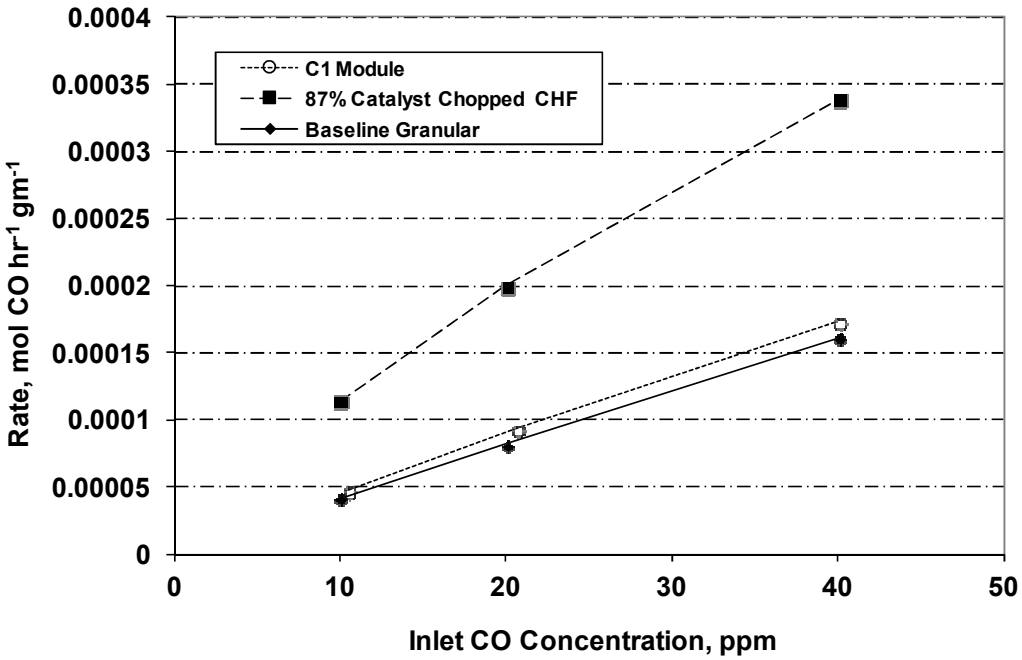


**Figure 4-16 Specific Reaction Rate of $Pt/TiO_2$ Catalyst - Baseline Granules, 87% wgt $Pt/TiO_2$ Chopped CHF, and C1 CHF Module - GHSV 110,400 $hr^{-1}$**

It is clear from Figure 4-15 that the granular form of the catalyst is the most active from a volumetric perspective, while the CHF module is the least active. Comparing the specific reaction rates in Figure 4-16 shows similar efficiencies for the CHF module when compared to the baseline granular, both of which are lower than the chopped catalytic fibres.

The difference in specific rate of the CHF structures is most likely attributed to the more open structure of the chopped fibres which results from the lower polymer concentration relative to the C1 CHF (13% vs. 20%, wgt.), the shorter diffusion path length resulting from chopping the fibres and testing them in a packed bed configuration, and a higher mass fraction of catalyst in the chopped fibres . The shorter diffusion path length (or shorter characteristic length, *L*, previously defined in Section 3.4.3) results from the fact that diffusion can occur from all surfaces of the chopped fibre (inside, outside, and both ends), whereas for the module diffusion is only from the surface of the inner diameter of the fibres.

Since the C1 CHF module and baseline catalyst have similar specific reaction rates, under these test conditions the utilization of the catalyst on a mass basis is similar. However a differential reactor test is more appropriate to determine an effectiveness factor since the above test has a large axial concentration gradient and therefore a varying partial pressure driving force along the length of the reactor.

As previously discussed in Section 2.5.5, the effectiveness factor is defined as the ratio of the observed rate to the rate that would result if the entire catalyst surface was exposed to the external surface concentration of the reactants. A differential test of module C1 resulted in a measured effectiveness factor of approximately 0.016 versus 0.040 for the granular catalyst. The low effectiveness factor could be caused by a low effective diffusivity or a blocking of active catalyst sites either by filling pores of the catalyst support or covering individual catalyst sites within the pores.

### 4.2.6 Investigation of Morphology Modifications to Increase Effective Diffusivity of Pt/$TiO_2$/Polyethersulfone CHF Structures

As previously shown in Figure 4-13, the surface area of the inside diameter of 3 samples (C1) of CHF structures dried at various temperatures indicates that in all cases there is minimal surface porosity. Similarly, inspection of the cross sections shown in Figure 4-12 reveals a dense asymmetric layer on the inner and outer surfaces. This is due to rapid coagulation of the polymer by the water in the bore fluid and coagulant bath (Baker 2004) as the polymer de-mixes too fast to allow for any appreciable segregation into polymer lean and polymer rich phases which is more typically seen in the substructure (e.g. as seen in Figure 4-14). Since the surface area of the inside of the hollow fibre is the area through which all of the diffusion of reactants occurs, modifications to fibre morphology focused on the surface area of the inside of the fibre. Additionally, the diffusional path length (ie characteristic length, $L$) was examined by generating a fibre with a shorter cross section thickness.

In summary, three modifications to the manufacturing approach were evaluated, including reduced polymer content of final fibre, incorporation of high solvent concentration in the bore fluid, and the ratio of inner to outer diameter of the spinneret – all of which were aimed at increasing the catalytic effectiveness factor of the final fibre structure. Additionally, a single CHF sample investigated the effect of the addition of a water (a non-solvent additive) and PVP (a pore former) to the initial polymer/solvent/catalyst mixture.

It is well known that increasing the solvent concentration in the bore fluid will affect the surface properties of the asymmetric skin on the inside of the fibre (Xu and Qusay 2004, Qin and Chung 2004). In an initial attempt to maximize the porosity, 100% NMP was used with spinneret1 (larger diameter) to see the effect relative to the initial fibres, however these could not be produced easily as the demixing, which now occurred totally due to water flux from the coagulant bath from the outer surface of the fibre, was too slow to allow for adequate fibre strength to develop during precipitation in the coagulation bath prior to the breaking of the fibre structures under their own weight.

To allow for sufficient fibre strength to be developed during the manufacturing process, the solvent concentration was reduced to 85% (wgt) in the bore. Sample C4 was produced in this fashion and otherwise had an identical composition to the initial fibre C1. Representative SEM micrographs of the C4 fibres are shown in Figures 4-17 and 4-18.

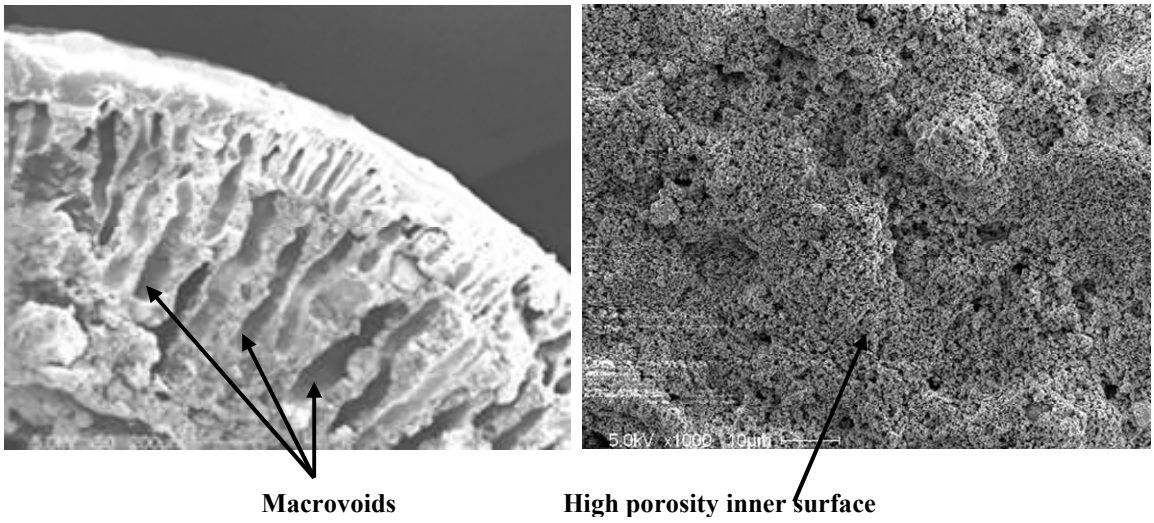


**Figure 4-17 Effect of 85% wgt NMP in Bore Fluid on Resulting C4 CHF Morphology Cross Section (L) and Inner Surface (R)**

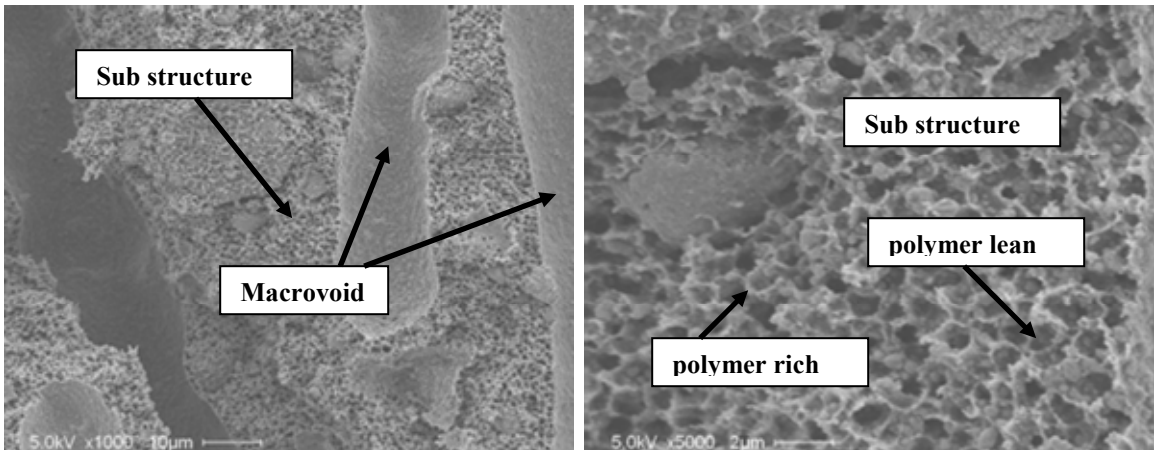


**Figure 4-18 Effect of 85% wgt NMP in Bore Fluid on C4 CHF Sub-structure Morphology Cross Section with Macrovoid (L) and Sub-Structure (R)**

As can be seen in Figure 4-17, a significant number of macrovoids are present as a result of the rapid influx of water from the coagulant bath. Additionally, the dense skin on the inner surface is essentially eliminated and a highly porous inner surface is obtained. Figure 4-18 shows a representative cross section indicating that a dense skin is still formed on the surface area associated with macrovoids, while other sections of the interior structure apart from the macrovoids, have the typical polymer lean and polymer rich characteristics that result in an open porous substructure.

The addition of the solvent to the bore fluid resulted in an increase in measured effectiveness factor from 0.016 for C1, to 0.025 for C4. Due to the slow demixing of the C4 fibre (from the surface containing the bore fluid) and the high solvent concentration in the bore fluid, the bore of the fibre was non uniform and in many cases collapsed. To produce a more robust structure and also reduce the diffusional path length, all subsequent fibres were produced with spinneret 2. The smaller diameter and shorter cross sectional length associated with spinneret 2 allows for faster coagulation of the fibre and the development of adequate strength of the fibre, prior to breaking under its own weight. Simultaneously it was decided to also attempt a lower polymer content in the fibres as this would increase porosity of the resulting fibre and therefore increase the diffusion rate.

Additionally, due to the low concentration (15%, wgt.) of water in the bore fluid, there is minimal precipitation of the polymer in the air gap prior to contacting the water bath. Elimination of the air gap allowed for the precipitation of the polymer mixture immediately upon exiting the spinneret, thereby allow for sufficient fibre strength to develop during manufacturing. This approach increased the yield of CHFs significantly and therefore all subsequent CHFs were manufactured with out an air gap.

CHF sample C5 was produced with a final polymer to catalyst weight ratio of 15/85, as a weight ratio of polymer to catalyst of 13/87 had previously been determined to result in fibres with poor mechanical strength. However, as a result of the increase in viscosity associated with the higher catalyst in the final C5 mixture relative to C1, additional NMP solvent had to be added to the mixture, which ultimately reduces the overall density of the final CHF structure. As a result of the additional solvent, the polymer to solvent weight ratio that resulted was 17.5/82.5. The bore fluid composition was maintained at 85% (wgt.) NMP in water. SEM micrographs of C5 cross section and substructure are shown in Figure 4-19 and the inner surface is shown in Figure 4-20.

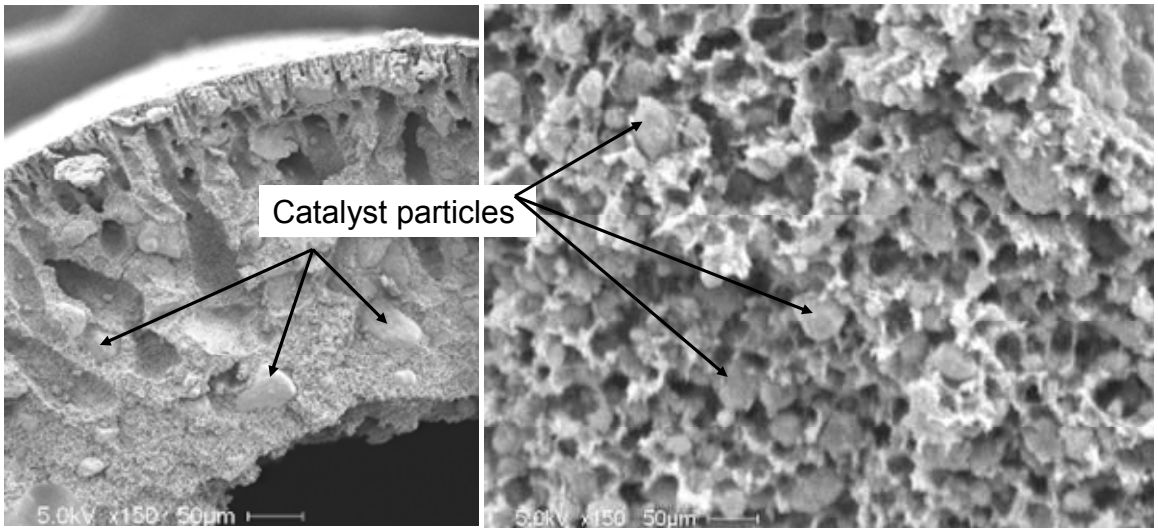


**Figure 4-19 C5 Cross Section (L) and Substructure (R)**

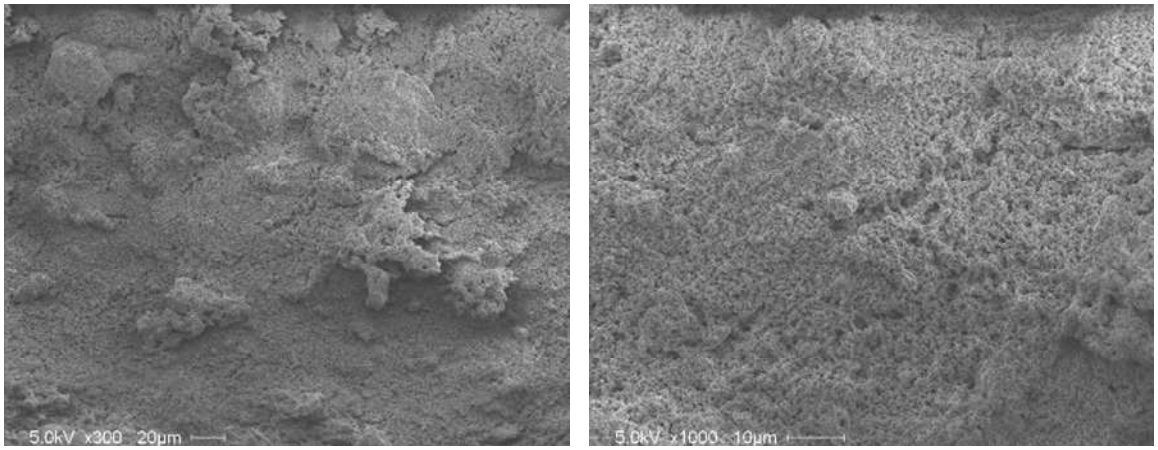


**Figure 4-20 C5 Inner Surface**

While the slight reduction in polymer content did not result in any significant morphology differences, the combination of shorter diffusion path length and lower polymer content resulted in an increase in the measured effectiveness factor from 0.025 for C4 to 0.041 for C5.

While C5 had the highest effectiveness factor of the samples manufactured thus far, the lower polymer content of 15% (wgt.) resulted in fibres that had marginal strength, so the polymer concentration was increased slightly to 17% (wgt.) with 83% (wgt.) catalyst. While still requiring caution during handling so as not to break the fibres, the resulting

CHF structures were sufficiently strong to allow test modules to be fabricated. This weight ratio of polymer to catalyst of 17/83 was used to produce all subsequent fibres.

As a result of the slight reduction in catalyst content 85% (sample C5) to 83% (wgt) (sample C3), the polymer content of the initial polymer/solvent mixture could be increased slightly to 18% (wgt.) without becoming too viscous to allow CHF structures to be produced. This resulted in a theoretical final "catalyst density" for C3 that was similar to C5. This "theoretical" catalyst density is proportional to the product of the catalyst content in the final structure to the polymer content in the polymer/solvent dope (i.e. a pseudo proportionality constant: 83x18=1494 for C3 vs. 85x17.5 = 1487 for C5). C3 also utilized 85% (wgt.) NMP in the bore fluid. The measured effectiveness factor for C3 is 0.058. SEM micrographs of C3 are shown in Figures 4-21, which shows a relatively uniform porous internal surface.

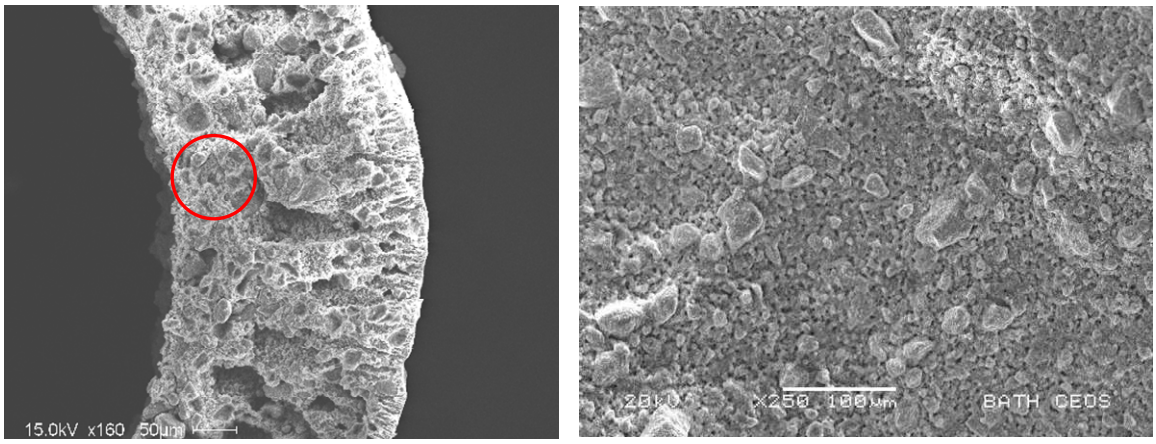


**Figure 4-21 C3 Cross Section (L) and Internal Surface (R)**

While only relatively minor changes were made in fibre dope compositions, the increase in the measured effectiveness factor for C3 was approximately 50% greater than C5 (0.058 for C3 vs. 0.041 for C5). While there are no significant differences in morphology that can easily be seen in the SEM micrographs of the two samples, the relative densities of the actual fibres (measured as mass of catalyst per unit length of fibre) is 0.014 g/cm for C3 vs. 0.017 for C5, indicating that additional manufacturing parameters are affecting

the final structure. This is believed to be primarily due to slight variations in viscosity as a result of the changes in the polymer/catalyst/solvent mixture composition of the fibres.

While these changes may at first appear to be minimal it is well known that slight variations in the dope composition can produce major differences in the resulting fibre (Baker 2004). Since the fibre wall thickness of C5 and C3 are similar, it is concluded that the lower density of C3 must therefore be more porous than C5, leading to the higher measured effectiveness factor.

The simultaneous incorporation of a non-solvent additive and pore former were investigated in the manufacturing of CHF sample C2 to determine if the porosity of the CHF could be increase further. In general, the use of non-solvent additives, which in this sample was water, moves the casting solution towards the binodal region of the ternary phase diagram, and often results in the suppression of macrovoids. (see Section 2.5.4). Since the macrovoid regions are effectively void of catalyst, they can be considered as an inefficient use of part of the volume of the fibre wall, however there is a trade off since they also provide a means of rapid mass transfer towards the outside diameter due to their large (relative to the rest of the structure) pore sizes.

Similarly, polyvinylpyrrolidone (PVP) is also often used as a pore former and has also been shown to suppress the formation of macrovoids in the production of hollow fibre membranes (Yang, Chung, and Santoso 2007). In sample C2, 4.7 % ( wgt.) PVP (molecular weight 1000) and 4.7 % (wgt.) $H_2O$ were added to the casting solution, while the amount of NMP solvent was reduced accordingly to maintain 18 % (wgt.) polymer. Figure 4-22 shows the resulting fibre in which a significant number of macrovoids still remain. It is possible that a higher water concentration is required to suppress the macrovoids to any noticeable extent since up to approximately 10% (wgt.) water can be added prior to reaching the binodal point on the ternary phase diagram (Zeman and Tkacik 1988). The measured effectiveness factor for CHF sample C2 was 0.036, indicating no benefit of the water and PVP at the concentrations investigated.

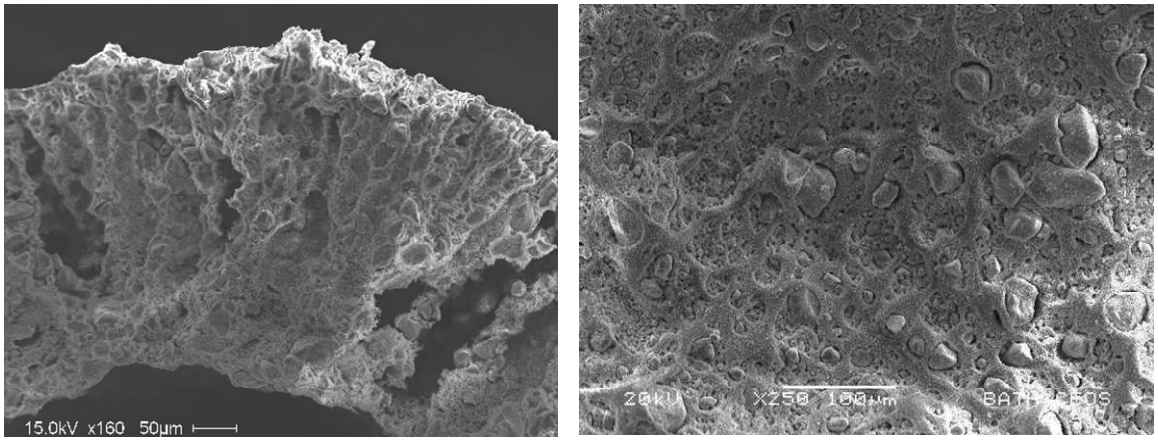


**Figure 4-22 Effect of the Addition of Water and PVP to the Casting Solution Cross Section (L) and Internal Surface (R) for CHF Sample C2**

In summary, in the evaluation of CHF samples C1-C5, it is noted that the use of solvent in the bore fluid at 85 weight percent significantly increased the apparent porosity of the inner surface of the hollow fibre. Additionally, reducing the "catalytic density" (catalyst weight per unit length of CHF) of the final structure increases porosity and therefore diffusion rates within the structure, resulting in higher effectiveness factors. It is also noted that changes in the ratios of components in the casting dope may not always produce the expected results as it relates to the final density, most likely a result of varying flows in the spinneret required to establish a stable CHF structure. The results for samples C1-C5 are summarized in Table 4-3.

**Table 4-3 Summary of Manufacturing Parameters and Effectiveness Factors for Pt/$TiO_2$/Polyethersulfone (Gafon 3100P, ~ 55,000 molecular weight)**

| CHF Sample | Spinneret ID/OD, mm | Catalytic Density g Catalyst/cm CHF | Polymer/Solvent Ratio | Catalyst/Polymer Ratio | % NMP in Bore | Effectiveness Factor |
|---|---|---|---|---|---|---|
| C1* | 1.0/3.2 | 0.026 | 20/80 | 80/20 | 0 | 0.016 |
| C2** | 0.8/1.9 | 0.016 | 18/72.6 *** | 83/17 | 85 | 0.036 |
| C3** | 0.8/1.9 | 0.014 | 18/82 | 83/17 | 85 | 0.058 |
| C4* | 1.0/3.2 | 0.034 | 20/80 | 80/20 | 85 | 0.025 |
| C5** | 0.8/1.9 | 0.017 | 17.5/82.5 | 85/15 | 85 | 0.041 |

* Air gap = 5 cm
** Air gap = 0 cm
*** Balance 4.7% $H_2O$, 4.7% polyvinylpyrrolidone

While the percentage increase in effectiveness factor of the CHF structures, relative to the 1/8 inch (3 mm) $Pt/TiO_2$ cylinders is consistent with initial estimates (see Section 3.4.3 and Table 3-8), it was decided to investigate the potential occlusion of active platinum sites by blocking of catalyst pores and/or covering of the active metal within the pore structures of the catalyst.

### 4.2.7 Comparison of BET Surface Area Measurement of $Pt/TiO_2$ Powder and CHF Sample C1.

After the fabrication of CHF sample C1 and subsequent testing which revealed a lower than desired effectiveness factor, the BET surface area of $Pt/TiO_2$ powder and CHF C1 was measured to evaluate the potential of gross blockage of the catalyst pore structure. The measurements on the powder were repeated three times – twice with preconditioning at 150 ºC and once at 300 ºC. This served the purpose of not only desorbing any water from the structure but also demonstrated an acceptable temperature for preconditioning of the fibres since the upper temperature limit of the polymer is approximately 200 ºC due to its glass transition temperature of approximately 225 ºC. The three measurements for the powder resulted in a measured surface area of 109.3 $m^2 g^{-1}$, with less than 1% variation between the three measurements. The CHF sample average surface area was 84.8 $m^2 g^{-1}$ $Pt/TiO_2$, which is within 3% of what would be estimated based on 80% (wgt.) of catalyst in the CHF structure.

The surface area of the powder is approximately 70-75% of the $TiO_2$ support which is not unexpected due to the high temperature reduction (500 ºC) of the catalyst as the titania is partially converted from the higher surface area anatase form to the lower surface area rutile form (D. Heneghan, Saint-Gobain NorPro, pers. comm., 4th October 2007). While these results imply that the pores of the catalyst are not significantly blocked by polymer filling, it is possible that the inner surfaces of the catalyst support have some level of coating on them, essentially directly covering the active metal while still providing access to the high surface area of the catalyst support. Additionally, a nominal diameter of a polyethersulphone molecule is estimated to be 200-250 Å

(W. Koros, Georgia Tech, pers. comm., 6th January 2010) which, while larger than the nominal pore size of approximately 150 Å for the $TiO_2$ support, it is possible that some of the larger pores in the support may be partially blocked.

To further investigate the potential of occluding catalyst sites as a result of polymer penetration into the catalyst support pore structure, higher molecular weight polymers were used to produce additional CHF structures and CO oxidation effectiveness factors and CO chemisorption measurements were made on all the samples.

### 4.2.8 Effect of Higher Molecular Weight Polyethersulfone, Initial Polymer Content, and PVDF on CHF Structure and Effectiveness Factor

To investigate the possibility of partial pore blockage, a higher molecular weight polyethersulfone polymer (designated as PESF 2), which has a molecular weight of approximately 63,000, (Sovay 3000P) was evaluated in addition to two polyvinylidenefluoride (PVDF) polymers with molecular weights of 220,000 (PVDF 1, Kynar 720) and 450,000 (PVDF 2, Kynar 761).

In addition to investigating the potential of partial catalyst pore blockage, the higher molecular weight PESF allowed for direct assessment of the effect of increased molecular weight, while the use of PVDF provided a comparison of effectiveness factors resulting from a different polymer.

The effect of the catalyst content in the initial polymer/solvent/catalyst was also investigated for the PESF 2 polymer for a constant catalyst wgt percent in the final CHF structure.

#### 4.2.8.1 Effect of Higher Molecular Weight PESF on $Pt/TiO_2$ CHF Structures

Sample C9 was produced using 18 % (wgt.) polymer in the initial (PESF2) polymer/solvent mixture and proved difficult to spin. It is noted that the higher molecular

weight polymer increases the viscosity of the mixture and it was difficult to establish a uniform flow of polymer/catalyst/solvent from the spinneret during the casting process.

Additionally, it was decided to decrease the NMP solvent concentration in the bore fluid from 85% to 80% (wgt.) since fibre manufacturing is more stable with lower concentrations of solvent in the bore fluid. SEM micrographs showing the cross section, internal surface, and external surface of the C9 CHF are shown in Figures 4-23 and 4-24.

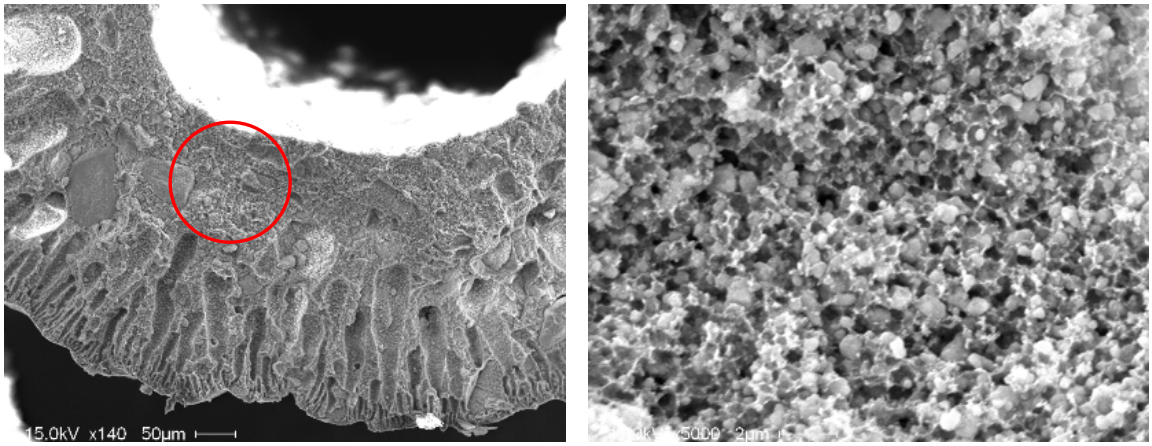


**Figure 4-23 CHF Sample C9 Cross Section (L) and Substructure (R) PESF2/NMP Weight Ratio – 18/82**

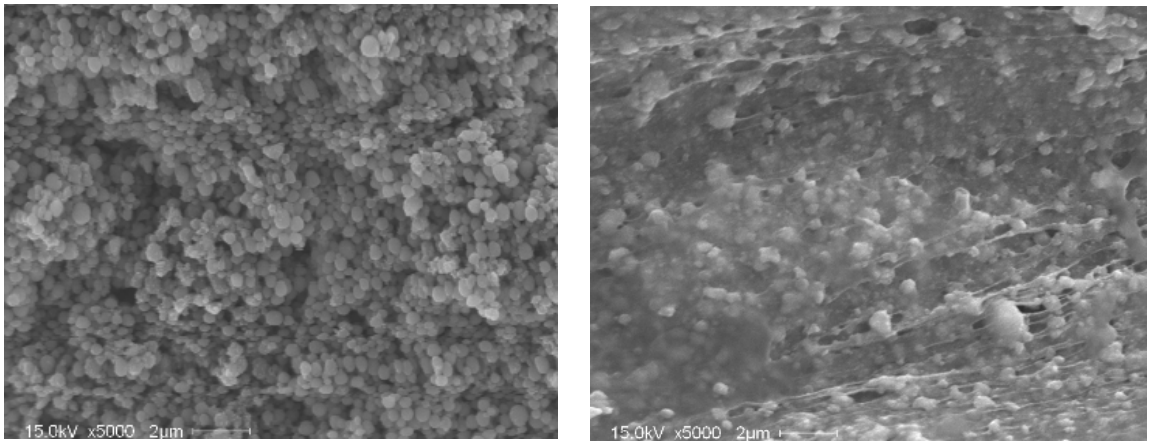


**Figure 4-24 Sample C9 Inner Surface (L) and External Surface (R) for PESF2/NMP Weight Ratio =18/82**

The measured CO oxidation effectiveness factor for C9 is 0.030, which is approximately 50% of the comparable C3 fibre made with the lower molecular weight polymer. By inspection of the inner surface of CHF C9 (Figure 4-24) it is clearly seen that the slight reduction in the concentration of NMP in the bore fluid had no apparent effect in reducing the surface porosity of the internal surface of the fibres, and therefore the measured reduction in effectiveness factor is attributed to the increase in PESF molecular weight. It can also be inferred that since the effectiveness factor decreased with the higher molecular weight PESF, that blockage of catalyst sites and/or pores is most likely not occurring to any significant extent and therefore not contributing to the observed catalyst activity. The higher molecular weight polymer would be less likely to enter the pore structure of the catalyst, and therefore the effectiveness would have been expected to increase with increased molecular weight if blockage of the pores or catalysts sites was occurring.

While the SEM micrographs of C3 and C9 reveal no significant, visually observed differences in CHF morphology, the structure closest to the ID of the fibre appears to have a higher density with PESF 2 compared to PESF 1 (reference sections highlighted by a red circle in Figures 4-21 (L) and 4-23 (L)). This is believed to be a result of the higher viscosity associated with higher molecular weight which would result in less separation of the polymer into polymer rich and polymer lean and therefore increased density of polymer. Additionally, the higher viscosity would also result in less polymer migrating into the solvent rich bore fluid, also result in a potentially higher concentration of polymer at the inner surfaces of the fibre (Baker 2004).

#### 4.2.8.2 Effect of the Initial Polymer Concentration in $TiO_2$/PESF 2 CHF Structures

Three CHF samples were produced with PESF 2 to investigate the effect of the concentration in the initial polymer/solvent mixture – 14, 16, and 18 % wgt polymer. In these 3 samples the final polymer/catalyst weight ratio was constant at 17/83.

CHF sample C9 was produced using an initial polymer/solvent weight ratio of 18/82, whereas sample C10 used a ratio of 14/86 and C11 used 16/84. All 3 samples used 80% (wgt.) NMP (balance was water) as the bore fluid. Representative SEM micrographs are shown in Figures 4-25 and 4-26.

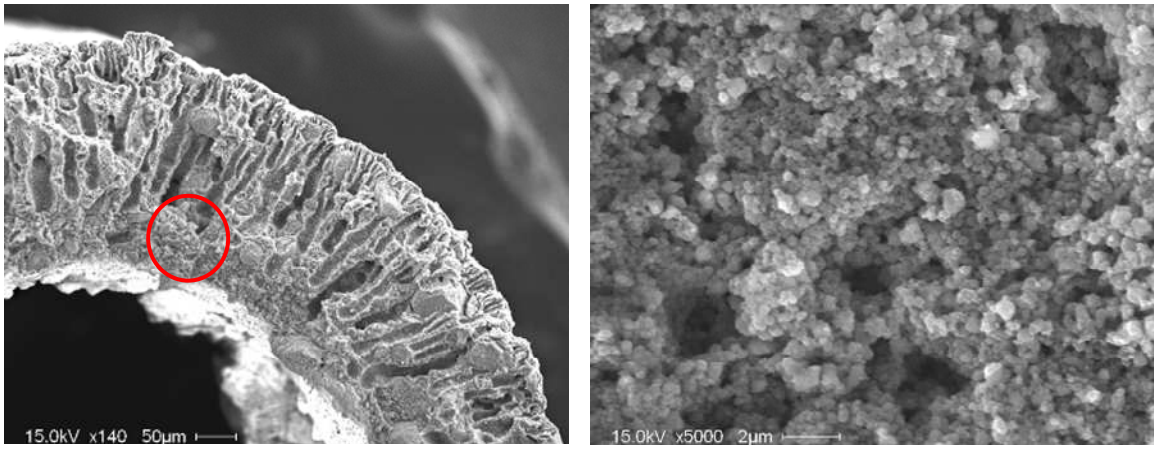


**Figure 4-25 Sample C10 Cross Section (L) and Internal Surface (R) PESF2/NMP Weight Ratio =14/86**

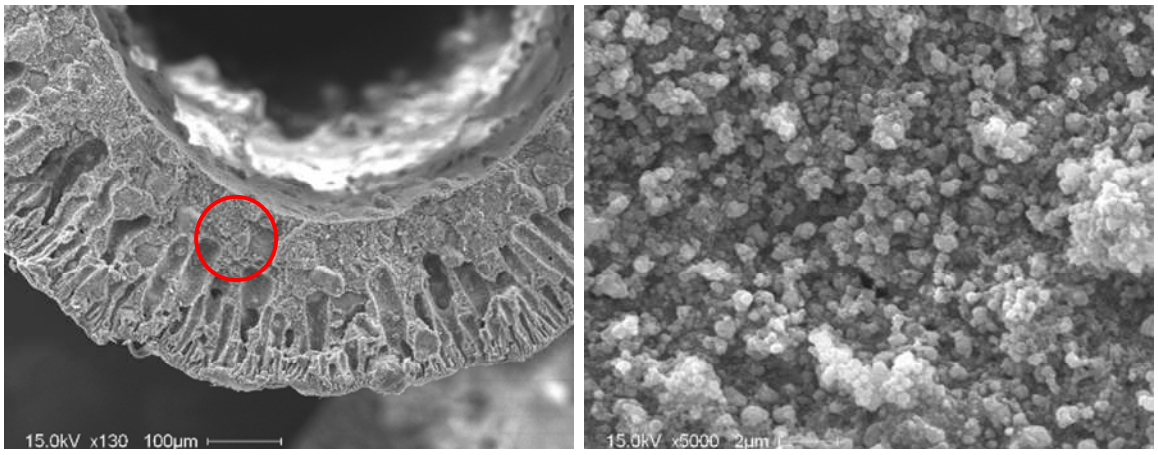


**Figure 4-26 Sample C11 Cross Section (L) and Internal Surface (R) PESF2/NMP Weight Ratio = 16/86**

It is again noted that no significant differences are observed in the general morphology of samples C10 and C11, relative to previous CHF samples. However, the measured effectiveness did change considerably for C10 and C11, having an effectiveness factor of 0.062 and 0.050, respectively, whereas the effectiveness factor of C9 is 0.030. This trend

is not unexpected as it is consistent with a higher porosity resulting from a reduction in the amount of polymer in the polymer/solvent dope, and was generally observed with samples produced with PESF 1. The variation in porosity can be qualitatively seen in the micrograph cross sections highlighted with the red circles in Figures,4-23, 4-25 and 4-26, for CHF samples C9-C11, respectively.

It is noted that as the concentration of PESF 2 in the initial polymer/solvent mixture was reduced it was possible to achieve values of the effectiveness factor similar to those achieved with PESF 1, however this is achieved at the expense of fibre strength as the lower polymer content of the PESF 2 fibres resulted in considerably weaker fibres compared to those with similar effectiveness factors that were produced using PESF 1.

#### 4.2.8.3 Comparison of $TiO_2$/PESF 2 and $TiO_2$/PVDF 1 CHF Structures

As part of the investigation into thepotential blockage of catalyst pores and/or catalyst sites, an alternate polymer with a molecular weight considerably higher than PESF was also investigated. CHF sample C14, was produced using a polymer/solvent weight ratio of 14/86 containing polyvinylidenefluoride with a molecular weight of 220,000 (Kynar 720, PVDF 1). The relative constituent composition of sample C14 is identical to that used in sample C10, however the resulting measured catalyst effectiveness factor of C14 is 0.034 (compared to 0.062 for C10). The decrease in measured effectiveness with increased molecular weight of polymer is consistent with that previously observed with PESF 1 and PESF 2 CHF structures. Additionally the characteristics of the macrovoids in C14 are considerably different than those of other samples. In C14 the quantity, size and distribution of macrovoids is considerably lower than that observed in other CHF samples which may also be affecting the effective diffusivity of CO in the structure, though additional tests are required to validate this possibility. A representative cross section and the internal surface is shown in Figure 4-27.

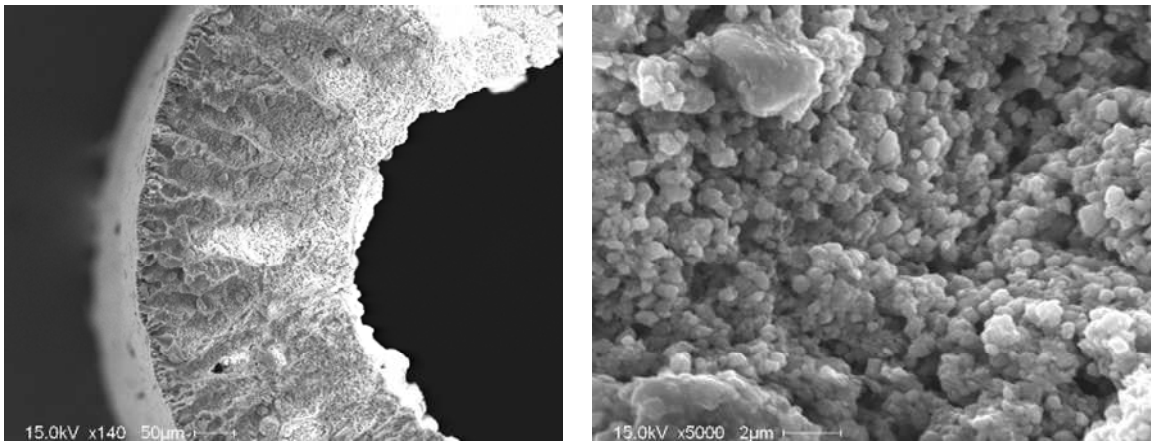


**Figure 4-27 Sample C14 Cross Section (L) and Internal Surface (R) PVDF1/NMP Weight Ratio =14/86**

#### 4.2.8.4 Summary of Effects of Polymer Molecular Weight, Polymer Type, and Initial Polymer Concentration

In summary, by testing various molecular weight polymers (at a constant constituent weight ratio), it does not appear that the polymer is blocking the pores of the catalyst or covering the catalytic sites to any appreciable extent based on measured catalyst effectiveness factors. This is further investigated through CO chemisorption measurements and is discussed in 4.2.10. The increase in molecular weight of the PESF polymers resulted in a decrease in the measured effectiveness factor at equal constituent concentrations, while for a given molecular weight polymer, decreasing the polymer content resulted in an increase in measured effectiveness factor.

The effects of polymer molecular weight, polymer type and initial polymer concentration used in the manufacturing of $Pt/TiO_2$ catalysts are summarized in Table 4-4.

**Table 4-4 Summary of the Effect of Polymer Molecular Weight, Polymer Type,and Initial Polymer Concentration on Measured Effectiveness Factor-Weight Ratio of $Pt/TiO_2$ Catalyst/Polymer = 83/17**

| CHF Sample | Spinneret ID/OD, mm | Polymer | Catalyst Mass in CHF, g $cm^{-1}$ | Polymer/Solvent Ratio | % NMP in Bore | Effectiveness Factor |
|---|---|---|---|---|---|---|
| C3 | 0.8/1.9 | PESF 1 | 0.014 | 18/82 | 85 | 0.058 |
| C9 | 0.8/1.9 | PESF 2 | 0.015 | 18/82 | 80 | 0.030 |
| C10 | 0.8/1.9 | PESF 2 | 0.009 | 14/86 | 80 | 0.062 |
| C11 | 0.8/1.9 | PESF 2 | 0.012 | 16/84 | 80 | 0.050 |
| C14 | 0.8/1.9 | PVDF 1 | 0.011 | 14/86 | 80 | 0.034 |

### 4.2.9 $Au/TiO_2$ Catalytic Hollow Fibres

Due to the limited availability of "commercial" gold catalysts, only three samples of CHF structures were produced. In all cases the weight ratio of the catalyst to polymer in the final structure is fixed at 83/17. Sample C12 used PESF 2 and provides a direct comparison to the $Pt/TiO_2$ sample, C11. Samples C15/70 and C15/80 used the highest molecular weight of all samples ( PVDF 2 - Kynar 761, molecular weight = 450,000). The designation of /70 and /80 in sample C15 refers to the weight percent of NMP in the bore fluid.

In terms of ease of manufacturing, sample C15 was superior to all other samples produced in this research. This is due to the high flexural modulus of the PVDF, however upon drying the fibres, they were easily broken and would crumble if not handled with extreme caution. The final weak structure is primarily due the low tensile strength (approximately 5,000 psi) of PVDF coupled with a low relative weight percent of polymer to solvent of 14/86. The low polymer content was required to maintain a reasonable viscosity of the final catalyst/polymer/solvent mixture to enable manufacturability of the fibres.

However, most importantly, the measured effectiveness factors for the gold catalysts were extremely low, achieving approximately 24% of the effectiveness factor of the granular form in one sample, while the effectiveness factor in the other two samples was essentially zero. An additional literature search was conducted to try and understand why

the effectiveness factors for the CHFs produced with gold catalysts were so low. Raphulu et al., 2009, reported specifically on the Mintek gold material stating that deactivation occurs even in storage, having tested samples that were stored in air, nitrogen and under vacuum, over the course of 12 months. Under vacuum storage conditions they observed an approximate 60% degradation in % CO conversion after one month of storage, and by month 12 the same sample had degraded to less than 5% of its original activity. One indication of catalyst degradation noted by Raphulu et al. is a colour change from whitish-gray to purple over time, which has been associated with particle size increase and reduction of oxidic gold to metallic gold.

Additionally, Raphulu et al., 2009, also indicated the loss of surface hydroxyl groups as another reason for the degradation in catalytic activity, though it had also been suggested that the gold catalyst be dried before use. It was also observed upon crushing the catalyst prior to incorporating it into the CHF structures that it was primarily purple in colour and that only a thin layer on the outer surface appeared to be "whitish-gray". Pictures of fresh catalyst, powder prepared for incorporation into the fibres and the final $Au/TiO_2$ fibres are shown in Figure 4-28, clearly showing a purple colour in the produced CHFs.

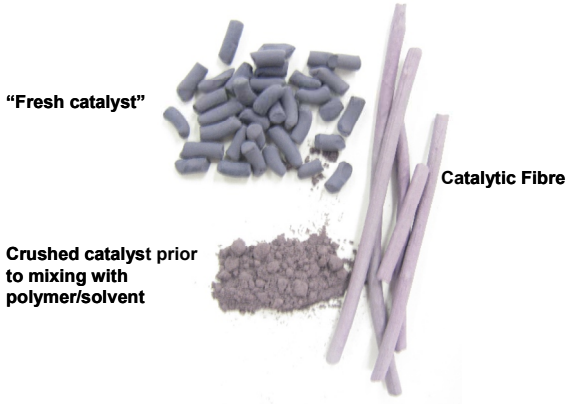


**Figure 4-28 Variation in Colour of the $Au/TiO_2$ Catalyst at Different Stages of CHF Manufacturing Indicating Potentially Degraded Catalyst**

Based on these observations, it appears that the "as received" gold catalyst may have been largely deactivated upon receipt since it essentially appeared purple when initially crushed. Additionally, the degradation noted, even during storage, by Raphula et al. (2009) presents an issue relative to the applicability of gold catalysts to NASA life

support systems since there are often long term storage requirements and a large range of storage environments.

In addition to the potential of catalyst degradation prior to use, it is also noted that sulfur is a known poison for gold catalysts as indicated on 3M Corporation web site (3M Corporation 2010), and it is also very probably that the sulfur groups in the polyethersulfone reacted with the gold catalyst during manufacturing, also contributing to the observed low reactivity (M. Shaw, University of Connecticut, pers. comm., 2nd July, 2010).

Since there is no sulfur present in the PVDF polymer, and its measured effectiveness factor was also low, it is most likely that the bulk of the observed low activity in this case is due to a degraded catalyst in the original $Au/TiO_2$ sample. This is also discussed further in Section 4.2.10. The results for the $Au/TiO_2$ fibres are summarized in Table 4-5.

**Table 4-5 Summary of Manufacturing Characteristics and Effectiveness Factor for $Au/TiO_2$ CHF Structures**

| CHF Sample | Spinneret ID/OD, mm | Polymer | Catalyst Mass in CHF, g $cm^{-1}$ | Polymer/Solvent Ratio | % NMP in Bore | Effectiveness Factor |
|---|---|---|---|---|---|---|
| C12 | 0.8/1.9 | PESF 2 | 0.016 | 14/86 | 80 | 0.001 |
| C15/70 | 0.8/1.9 | PVDF 2 | 0.012 | 14/86 | 70 | 0.002 |
| C15/80 | 0.8/1.9 | PVDF 2 | 0.012 | 14/86 | 80 | 0.014 |

### 4.2.10 CO Chemisorption of Catalytic Hollow Fibre Structures

To investigate the potential of blocking active catalyst sites within the catalyst pore structures with polymer, CO chemisorption measurements were conducted on all of the catalytic hollow fibre structures. When the CO uptake is normalized based on the catalyst content of the various platinum catalysts, six of the nine samples are in good agreement with what would be expected based on CO chemisorption on the powder. The three samples (C2, C5, and C14) that do not seem to correlate well with the powder may be due to fibres samples that were not representative of the bulk fibres , i.e. samples from the initial stages of CHF manufacturing where the flow rates of polymer/solvent/catalyst

dope and bore fluid are being adjusted to stabilize the fibre structure. In general, the CO chemisorption values do not show any trend with the measured effectiveness factor for the $Pt/TiO_2$ CHF structures which is not unexpected since the former is an "equilibrium" measurement, while the later is a "kinetic" measurement.

The CO chemisorption data for the gold catalyst essentially indicate no capacity for CO after the fibres are manufactured, and are believed most likely a result of using degraded catalyst in the manufacturing of the $Au/TiO_2$ CHF structures. It is also unlikely that the lack of CO adsorption is due to polymer getting into the pore structure of the $Au/TiO_2$ support since the pore size is similar to that used in the $Pt/TiO_2$ and the polymer used in sample C15 had the highest molecular weight of all polymers used. The data from the CO chemisorption measurements are listed in Table 4-6.

**Table 4-6 Summary of CO Chemisorption Measurements of Catalytic Hollow Fibres**

| Sample No. | Catalyst | wt (g) | CO uptake (mole/gCHF) | CO uptake ratio (mole/g catalyst) | CO uptake ratio mole/gm catalyst/powder |
|---|---|---|---|---|---|
| Powder | Pt/TiO2 | 0.067 | 6.32E-05 | 6.32E-05 | 1.00 |
| C1 | Pt/TiO2 | 0.1052 | 4.84E-05 | 6.05E-05 | 0.96 |
| C2 | Pt/TiO2 | 0.0629 | 1.30E-04 | 1.57E-04 | 2.48 |
| C3 | Pt/TiO2 | 0.0795 | 4.60E-05 | 5.54E-05 | 0.88 |
| C4 | Pt/TiO2 | 0.07915 | 5.25E-05 | 6.56E-05 | 1.04 |
| C5 | Pt/TiO2 | 0.0716 | 3.76E-05 | 4.42E-05 | 0.70 |
| C9 | Pt/TiO2 | 0.0953 | 5.27E-05 | 6.35E-05 | 1.01 |
| C10 | Pt/TiO2 | 0.0643 | 6.12E-05 | 7.37E-05 | 1.17 |
| C11 | Pt/TiO2 | 0.0897 | 5.53E-05 | 6.66E-05 | 1.06 |
| C12 | Au/TiO2 | 0.082 | 2.35E-07 | 2.83E-07 | 0.03 |
| C14 | Pt/TiO2 | 0.0947 | 2.39E-05 | 2.88E-05 | 0.46 |
| C15/70 | Au/TiO2 | 0.1017 | 1.69E-08 | 2.04E-08 | 0.00 |
| C15/80 | Au/TiO2 | 0.0828 | 7.48E-08 | 9.01E-08 | 0.01 |
| Powder | Au/TiO2 | 0.1209 | 1.01E-05 | 1.01E-05 | 1.00 |

### 4.2.11 Investigation of Impregnation of Platinum into $TiO_2$/Polyethersulfone Fibres

A final sample of $Pt/TiO_2$ CHF was manufactured with fibres produced using non catalytic $TiO_2$ powder in which platinum was deposited after the production of the fibres. In this sample, C16, the crushed $TiO_2$ support (Saint-Gorbain Norpro, SS61120, Ohio,

U.S.A.) was incorporated into hollow fibre structures using the same general techniques discussed in Section 4.1.3, with the addition of water as a non solvent to the initial polymer/solvent mixture. These fibres were available from early development work and not optimized, however they did allow for a CHF structure to be evaluated in which platinum was deposited after fibre manufacturing, providing additional insight, though limited, into a potential alternate means of producing catalytic hollow fibre structures.

Due to the fact that the "non-catalyzed" $TiO_2$ had not been exposed to the same temperatures (500 ºC) as was typically done during the normal reduction of the platinum procurer salts, and because the addition of water resulted in an increase in the viscosity of the casting solution, the solution required dilution with additional solvent to obtain an appropriate viscosity for fibre manufacturing. As a result the final composition of the solvent/polymer/water mixture was 80.8 % (wgt.) NMP, 13.3 % (wgt.) PESF 1, and 5.9 % (wgt.) water. The weight percent of the final fibre structure was 16 % (wgt.) PESF 1 and 84 % (wgt.) $TiO_2$.
To incorporate the platinum in the fibres, the dried fibres were soaked in a 19.5 % (wgt.) chloroplatinic acid solution (Johnson Matthey, PA., U.S.A.). The excess solution was drained from the fibre and nitrogen was forced through the bore of the fibres to remove excess solution. The initial weights indicated an approximate platinum loading of about 20 % (wgt.) would result if all of the impregnated platinum solution remained in the structure after reduction.

Since the typical high temperature (approximately 500 ºC ) hydrogen reduction was not possible without destroying the PESF polymer, the reduction was accomplished using a solution of excess sodium borohydride (J.T. Baker,U.S.A.) during which much of the platinum was released due to poor adhesion and the vigorous decomposition of the sodium borohydride. After approximately 30 minutes of soaking in borohydride solution, the fibres were soaked in a solution of ammonia carbonate (J.T. Baker, U.S.A.)) to aid in the removal of residual acid, and then rinsed in distilled water until no chloride could be detected in the rinse water when tested with 0.1 molar silver nitrate solution.

The fibres were then dried at 140 ºC and the resulting Pt content of the CHF was calculated to be 8.2% (wgt.), indicating that the original excess Pt solution that was most likely trapped in the polymer structure was subsequently release during the reduction process. The final catalyst content (based on the weight of $TiO_2$ and platinum) was calculated to be 85.4% (wgt.). SEM micrographs of the C16 cross section and inner surface are shown in Figure 4-29.

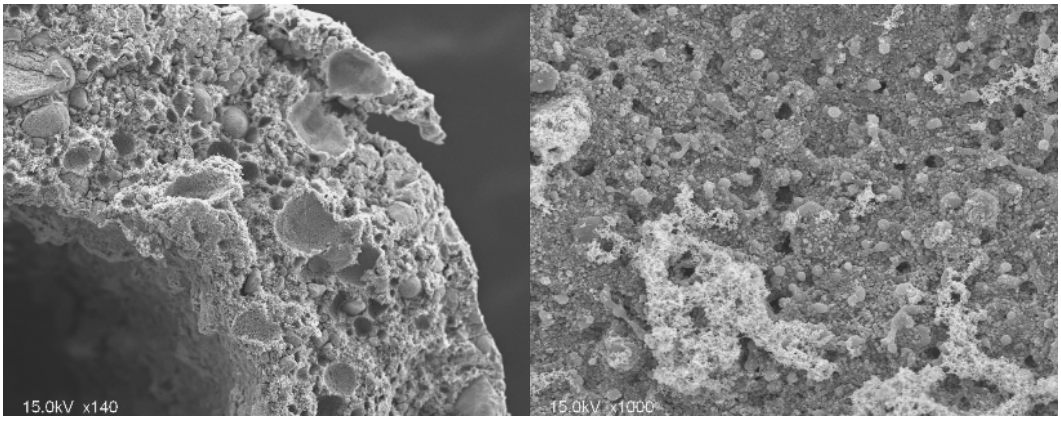


**Figure 4-29 SEM Micrographs Showing C16 Cross Section (L) and Inner Surface (R)**

A CHF module of C16 fibres was tested as a differential reactor and had a measured effectiveness factor of 0.015, similar to the C1 initial fibres. While it is worth noting that the cross section shown in Figure 4-29 is relatively void of macrovoids, and the inner surface is porous (consistent with the use of high concentrations of NMP in the bore fluid), it is not clear why the measured effectiveness factor is not greater. Since the catalyst was produced by a significantly different process (i.e. post impregnation of platinum precursor solution and reduction in solution with sodium borohydride), it is conceivable that this alternate method of producing this CHF sample results in a significantly different catalyst. However, as a first attempt at investigating an alternate method of producing catalytic fibres, there was no apparent benefit, though due to the limited research in this regard it is recommended that additional research be conducted to more thoroughly investigate alternate methods of producing CHF structures.

### 4.2.12 Comparative Test of the Baseline Granular Catalyst and CHF Module

A CHF module was fabricated to compare its performance with that of the granular catalyst. The most direct comparison of performance of the two structures is accomplished by testing at the same gas hourly space velocity and with structures that had similar measured effectiveness factors. CHF sample C2 was selected as there was adequate fibre quantity to allow for a test module, and its measured effectiveness factor was 0.036 as compared to 0.040 for the 1/8 inch (3 mm) $Pt/TiO_2$ baseline granular catalyst.

Test conditions were similar to the catalyst screening trials (to allow for a direct comparison), with a target inlet concentration of 10 ppm CO, a GHSV of 110,400 $hr^{-1}$ and dry air. The C2 CHF module consisted of 22 fibres and was 4.25 inches (10.8 cm) in length. The tubes were potted in a ½ inch (1.27 cm) outside diameter tube with an inside diameter of 7/16 inch (1.11 cm). The empty tube volume was calculated to be 10.5 $cm^3$ which was used to calculate the required flow rate of 19.32 l $min^{-1}$ required to obtain the same GHSV that was used in the initial screening trials of the baseline granular catalyst. The results for the comparative test are shown in Figure 4-30.

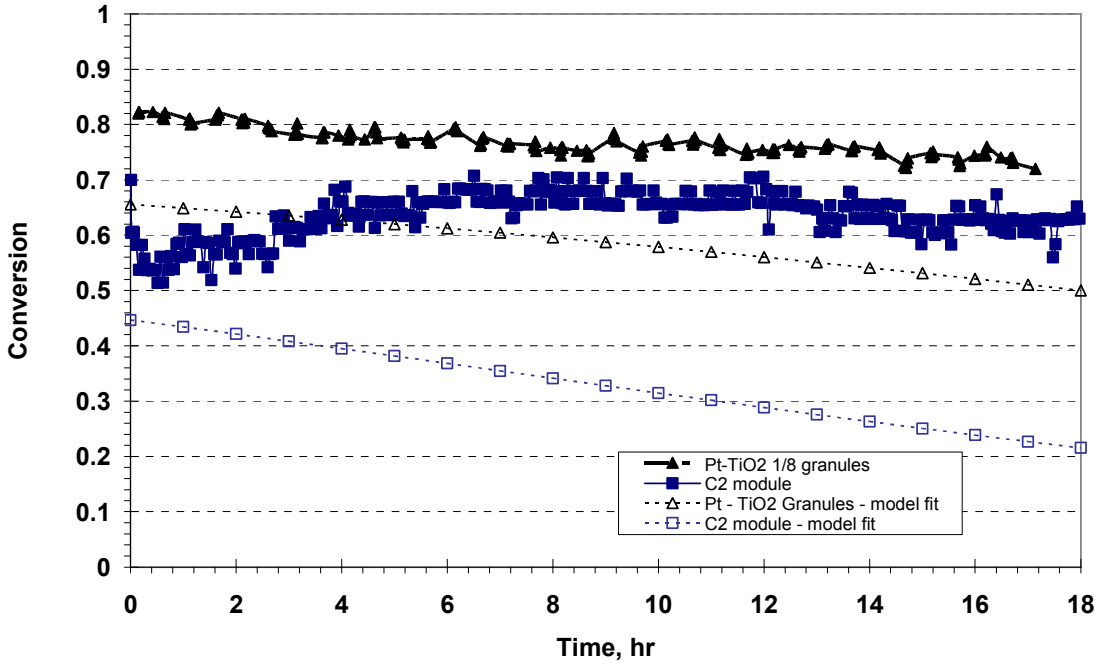


**Figure 4-30 Performance and Model Fit Comparison of C2 CFH Module to Baseline Granular Catalyst**

The average rates of CO oxidation measured during the 18 hour tests are $3.35 \times 10^{-5}$ and $8.85 \times 10^{-5}$ moles CO $hr^{-1}$ $g^{-1}$ of catalyst for the baseline granular $Pt/TiO_2$ and the C2 CHF module, respectively. While the differences in specific rates measured for the two catalyst configurations appear to indicate that the CHF module is more efficient than would be expected based on similar test conditions and effectiveness factors, the different geometries of the test items need to be considered. Specifically, since the CO oxidation reaction is fast, the rate of mass transfer from the bulk fluid to the surface of the catalyst must be considered to determine the controlling step. This is most easily done by comparison of the mass transfer coefficients of the two reactor geometries, which can be estimated from standard dimensionless convective mass transfer parameters (Bennett and Myers 1974, Fogler 1999).

The initial low conversion observed in the CHF structure is thought to be due to temporary poisoning of the active catalyst sites from solvents contained in the silicon potting materials used to fabricate the CHF module. As air is flowed through the module any adsorbed species from the potting are eventually desorbed from the surface.

The Reynolds number is used to determine the flow regime of the reactor configuration which will aid in determining the appropriate correlation of the Sherwood number which is then used to calculate an estimated mass transfer coefficient.

#### 4.2.12.1 Estimate of the Conversion for the Baseline Granular Catalyst

For a packed bed, the Reynolds number is defined as:

$$Re_p = \frac{D_p u_{bs} \rho}{\mu(1-\varphi_b)} \qquad 4\text{-}1$$

where: $Re_p$= particle Reynolds number, dimensionless

$D_p$= effective particle diameter, cm

$u_{bs}$= superficial bulk velocity, cm $s^{-1}$

$\rho$= gas density, g $cm^{-3}$ = 0.0012g $cm^{-3}$ for air

$\mu$= viscosity, g $cm^{-1}$ $s^{-1}$ = 0.000164 g $cm^{-1}$ $s^{-1}$ for air

$\varphi_b$=void fraction of the packed bed, assumed = 0.33 (Perry and Chilton, 1973)

For irregular particles, the effective particle diameter is defined by:

$$D_p = \frac{6}{S_v} \qquad 4\text{-}2$$

where: $S_v$= specific surface = the inverse of the characteristic length, $L$, previously defined for the 1/8 inch cylinders by equations 3-11 and 3-12, and equal to 0.635 cm.

$$D_p = \frac{6}{1/0.635\,\text{cm}} = 0.381\ \text{cm}$$

For the cylindrical 1.5 inch (3.81 cm) reactor at a flow rate of 27.6 l $min^{-1}$, the superficial velocity is 39.38 cm $sec^{-1}$ and therefore the particle Reynolds number is

$$Re_p = \frac{0.381\,\text{cm}(39.38\,\text{cm s}^{-1})(0.0012\,\text{g cm}^{-3})}{0.000164\,\text{g cm}^{-1}\,\text{s}^{-1}\,(1-0.33)} = 163.4$$

The Sherwood number, which can be used to estimate the mass transfer coefficient, is defined by the Frössling correlation (Fogler 1999):

$$Sh = \frac{k_c D_p}{D_{AB}} = 2 + 0.6 Re_p^{1/2} Sc^{1/3} \qquad 4\text{-}3$$

where: $k_c$ = mass transfer coefficient, cm $s^{-1}$

$D_{AB}$ = bulk diffusivity of CO in air = 0.196 $cm^2$ $s^{-1}$ (see Section 3.4.3)

$Sc$ = Schmidt number, dimensionless

The Schmidt number, $Sc$, is defined by:

$$Sc = \frac{\mu}{\rho D_{AB}} = \frac{0.000164\,\text{g cm}^{-1}\,\text{s}^{-1}}{0.0012\,\text{g cm}^{-3}(0.196\,\text{cm}^2\,\text{s}^{-1})} = 0.7 \qquad 4\text{-}4$$

The mass transfer coefficient for the packed bed reactor is then calculated by rearrangement of equation 4-3.

$$k_c = \frac{D_{AB}}{D_p}(2 + 0.6 Re_p^{1/2} Sc^{1/3}) = \left(\frac{0.196\,\text{cm}^2\,\text{s}^{-1}}{0.381\,\text{cm}}\right)\left(2 + 0.6(163.4)^{1/2}(0.7)^{1/3}\right) = 4.54\,\text{cm s}^{-1}$$

The relative rate of mass transfer from the bulk flow to the reaction rate can be determined by comparing the value of the product of the mass transfer coefficient and specific surface area to the product of the specific reaction rate and internal effectiveness factor.

The specific surface area of the packed bed reactor is calculated based on the void volume of the packed bed and the effective particle diameter $D_p$ (Fogler 1999):

$$a_c = \frac{6(1-\varphi_b)}{D_p} \qquad 4\text{-}5$$

where: $a_c$= specific surface area, $m^2\ m^{-3}$

$\varphi_b$= void fraction of packed bed (assumed = 0.33)

By substitution of the assumed void fraction and previously calculated effective diameter from Equation 4-2, the specific area of the packed bed configuration is then calculated as:

$$a_c = \frac{6(1-0.33)}{0.00381\,\text{m}} = 1055\,\text{m}^2\ \text{m}^{-3}$$

The product of the mass transfer coefficient and the specific surface area is then calculated as:

$$k_c a_c = 4.54\ \text{cm s}^{-1}\ (1\ \text{m})(100\ \text{cm})^{-1}\ (1055\ \text{m}^2\ \text{m}^{-3}\ ) = 47.9\text{s}^{-1}$$

The specific reaction rate constant is calculated as the product of the reaction rate (calculated in Section 3.4.1.2), 161.6 ($l\ min^{-1}\ g^{-1}$), and the density of the packed bed reactor, 954 $g\ l^{-1}$.

$$k = k'\rho_b = 161.6\ \text{l min}^{-1}\ \text{g}^{-1}\ (954\ \text{g l}^{-1})(1\ \text{min})(60\ \text{s})^{-1} = 2569\ \text{s}^{-1}$$

The measured internal effectiveness factor for the granular catalyst was measured as $\eta$=0.04. The product of the specific reaction rate and internal effectiveness factor is:

$$\eta k = 0.04(2569\ \text{s}^{-1}) = 102.8\ \text{s}^{-1}$$

Since the relative rates of mass transfer and reaction are the same order of magnitude, both must be considered in analysis of the data. Under these conditions the overall rate of reaction is equal to the rate of mass transfer to the catalyst surface and also equal to the rate of reaction on, and within, the catalyst which can be calculated based on the measured effectiveness factor (as discussed in Chapter 3), specific reaction rate, surface concentration, activity, and assuming a first order reaction can be calculated from (Smith 1981):

$$r_{CO} = \overbrace{k_c a_c \left([CO]_b - [CO]_s\right)}^{\text{Rate of mass transfer to the catalyst surface}} = \overbrace{\eta k a [CO]_s}^{\text{Rate of reaction}} \qquad 4\text{-}6$$

where: $k_c$ = mass transfer coefficient, cm $s^{-1}$

$a$ = activity

$a_c$= specific surface area, $m^2$ $m^{-3}$

$k$ = specific reaction rate, $s^{-1}$

$\eta$ = internal effectiveness factor, dimensionless

$[CO]_b$ = Bulk fluid concentration of CO , mole $l^{-1}$

$[CO]_s$ = Concentration of CO on the exterior catalyst surface, mole $l^{-1}$

Since the internal effectiveness factor is inversely proportional to the square root of the reaction rate (Section 3.4.3), and the rate is changing with time due to changes in the catalyst activity, the effectiveness factor changes with time. For a catalytic reaction with strong pore diffusional resistance, the effect of changes in catalytic activity on the internal effectiveness factor can be calculated as (Levenspiel 1972, Levenspiel 1984):

$$\eta = \frac{1}{L_i}\sqrt{\frac{D_e}{ka}} = \eta_0 a^{-\frac{1}{2}} \qquad 4\text{-}7$$

where: $D_e$ = effective diffusivity, $cm^2\ s^{-1}$

$k$ = specific rate constant, $s^{-1}$

$L_i$ = a characteristic length

$\eta_0$ = the effectiveness factor at time = 0.

Substituting equation 4-7 into the right hand side of equation 4-6 gives the following relationship for the rate of reaction based on the initial catalyst effectiveness factor and catalyst activity.

$$r_{CO} = k_c a_c \left([CO]_b - [CO]_s\right) = \eta_0 k a^{\frac{1}{2}} [CO]_s \qquad 4\text{-}8$$

Equation 4-8 can be solved by the elimination of the surface concentration, which is the only unknown. Solving for the surface concentration in terms of the measurable bulk concentration yields:

$$[CO]_s = \frac{[CO]_b}{1 + \dfrac{\eta_0 k a^{\frac{1}{2}}}{k_c a_c}} \qquad 4\text{-}9$$

Substituting the surface concentration from equation 4-9 into the right hand side of equation 4-8 results in the following form of the rate equation:

$$r_{CO} = \left( \frac{\eta_0 a^{\frac{1}{2}}}{1 + \dfrac{\eta_0 k a^{\frac{1}{2}}}{k_c a_c}} \right) k[CO]_b = \Omega k [CO]_b \qquad 4\text{-}10$$

where: Ω = Overall, activity dependant, effectiveness factor and is defined by:

$$\Omega = \frac{\eta_0 a^{\frac{1}{2}}}{1 + \frac{\eta_0 k a^{\frac{1}{2}}}{k_c a_c}} \qquad 4\text{-}11$$

The rate of reaction from equation 4-10 can be combined with the design equation for a plug flow reactor allowing for the concentration, or conversion, to be estimated as a function of the overall effectiveness factor, incorporating the effects of internal and external mass transfer and deactivation:

$$v_0 \frac{dC}{dV} = \Omega k C \qquad 4\text{-}12$$

Integration of equation 4-12 with the assumption of separable kinetics and uniform activity through the reactor allows for the simple solution:

$$\ln \frac{C}{C_0} = \Omega k \frac{V_{cat}}{v_0} \qquad 4\text{-}13$$

The ratio of outlet to inlet concentration at any time is therefore:

$$\frac{C}{C_0} = e^{\frac{-\Omega k V_{cat}}{v_0}} \qquad 4\text{-}14$$

The conversion is defined as:

$$X = 1 - \frac{C}{C_0} \qquad 4\text{-}15$$

Combining equations 4-14 and 4-15 gives the conversion as a function of time for a plug flow reactor, incorporating internal and external mass transfer and catalyst deactivation:

$$X = 1 - e^{\frac{-\Omega k V_{cat}}{v_0}} \qquad 4\text{-}16$$

In the calculation of the decay constant in Sections 3.4.1.1 and 3.4.1.1, it was assumed that the decay constant was independent of the concentration of the poisoning specie(s) to simplify the analysis, however it is most likely proportional to the concentration of the poisoning specie(s), assumed in this case proportional to the inlet CO concentration (Fogler 1999). If the decay constant is considered directly proportional to concentration and assuming that an average CO partial pressure is a reasonable first assumption (uniform activity in reactor) then the decay constant for the 18 hour test conditions can be estimated from the results obtained in differential reactor tests in Section 3.4.1.2 from:

$$k_{d(18\ hr\ test)} = k_{d(diifferntial\ test)} \frac{[CO]_{average\ during\ 18\ hr\ test}}{[CO]_{during\ differntial\ test}} = 0.0122\ \text{min}^{-1} \left( \frac{5.7\ \text{ppm}}{38\ \text{ppm}} \right) = 0.00183\ \text{min}^{-1} \qquad 4\text{-}17$$

The average partial pressure for the 18 hour test is based on the average conversion for the test and represents the numerical average partial pressure over the catalyst.

For the packed bed reactor test, the volume was 15 $cm^3$ (0.015 l) and the flow rate was 27.6 l $min^{-1}$ (0.46 l $s^{-1}$). The activity, previously defined by equation 3-3,is

$$a = e^{-k_d t} \qquad 3\text{-}3$$

Using the adjusted value for the decay constant from equation 4-17 and substituting the appropriate values for the 18 hour packed bed test,he estimated overall effectiveness factor can be estimated as a function of time calculated from equation 4-11:

$$\Omega = \frac{\eta_0 e^{\frac{k_d t}{2}}}{1 + \frac{\eta_0 k e^{\frac{k_d t}{2}}}{k_c a_c}} = \frac{0.04 e^{\frac{-0.00183\,\mathrm{min}^{-1}}{2} t}}{1 + \frac{0.04(2569\,\mathrm{s}^{-1}) e^{\frac{-0.00183\,\mathrm{min}^{-1}}{2} t}}{47.9\,\mathrm{s}^{-1}}} \qquad 4\text{-}18$$

Therefore, the estimated conversion as a function of time can be estimated by combining equations 4-16 and 4-18 and is compared to the data in Figure 4-30.

While the slope (associated with deactivation of the catalyst) of the line associated with the model prediction is similar to that of the data, the initial predicted conversion is considerably lower than that which was measured. At approximately 9 hours the predicted conversion is approximately 76% of that which was measured. There are many possible explanations for the discrepancy; however the primary cause is believed to be a result of potential non - uniform flow in the differential reactor used to obtain the kinetic constants. The powdered catalyst was spread in a thin layer of glass wool which was then rolled and inserted in a tubular reactor between additional layers of glass wool on the top and bottom of the catalyst to hold the sample in place during testing. Since the packing density of the glass wool could not easily be controlled in this manner is it possible that flow was not uniform. If a portion of the catalyst was not exposed to the flow as a result then it doesn't participate in the reaction and therefore a lower conversion would result. As a result the measured kinetic constants would be inaccurate – the rate constant would be lower and the decay constant would be higher. To investigate the potential effect of this possibility, a rough approximation was made based on the outlet concentrations being reduced by 20 percent of what were measured and the resulting initial conversion increased from the original predicted value of 0.65 to 0.74. This also modified the decay constant as well but the change in the predicted slope was not significant.

Additional inaccuracies in the kinetic constants may be due to experimental variations in the rate constants for various catalyst batches. The measured specific rate constant was based on the original batch of $Pt/TiO_2$ catalyst, whereas a number of additional batches of catalyst were produced during the conduct of this research and the "acceptance" criteria

for the catalyst was simply a check of conversion at the conditions presented in Figure 4-9, as opposed to a rigorous measurement of the specific rate of all batches of catalyst.

Alternately, it is possible that other basic assumptions used in developing the model are incorrect such as separable kinetics of the activity and rate, uniform activity throughout the reactor, a non linear affect of CO concentration on the activity, and the assumed first order of the CO oxidation reaction. However, it is the author's belief though that the primary discrepancy is associated with the issue of flow distribution.

#### 4.2.12.2 Estimate of Conversion for the CHF Module in Comparative Test

A similar analysis for the CHF is accomplished using similar dimensionless mass transfer correlations; however the differences in geometry of the granular and CHF structures must be factored into the analysis. The primary geometrical considerations are that the CHF structure is modeled as a group of parallel tubes and the mass transfer area is the area of exposed catalyst on the inside diameter surface of the CHF.

The Reynolds number for the catalytic hollow fibre geometry is calculated based on the velocity in the fibres and the bore diameter of the fibres:

$$Re = \frac{D_{CHF} u_{bs} \rho}{\mu} \qquad 4\text{-}19$$

where: $D_{CHF}$ = CHF diameter, cm

$u_{b\,s}$= superficial bulk velocity, cm $s^{-1}$

$\rho$ = gas density, g $cm^{-3}$ = 0.0012 g $cm^{-3}$ for air

$\mu$= viscosity, g $cm^{-1}$ $s^{-1}$ = 0.000164 g $cm^{-1}$ $s^{-1}$ for air

To achieve the desired equivalent GHSV of 110,400 $hr^{-1}$ used in the granular catalyst test discussed above, the flow rate in the comparative test for the CHF module was

19.32 l $min^{-1}$. Based on 22 fibres with a nominal diameter of 0.8 mm, the superficial velocity is calculated as:

$$u_{bs} = \frac{v_0}{A_{CHF}(\#\ fibres)} = \frac{19.32\,\text{l}\,\text{min}^{-1}(1000\,\text{cm}^3\,\text{l}^{-1})\,4}{60\ \text{s}\,\text{min}^{-1}(3.14)(0.08\,\text{cm})^2(22)} = 2913\,\text{cm}\,\text{s}^{-1}$$

The Reynolds number is then calculated from equation 4-19 as:

$$Re = \frac{0.08\,\text{cm}(2913\,\text{cm}\,\text{s}^{-1})(0.0012\,\text{g}\,\text{cm}^{-3})}{0.000164\,\text{g}\,\text{cm}^{-1}\,\text{s}^{-1}} = 1705$$

This is in the laminar flow regime, and therefore the Sherwood number is constant and is a function of the bulk diffusivity (0.196 $cm^2$ $s^{-1}$ for CO in air) and the fibre diameter (0.08 cm) (Bennet and Meyers 1974):

$$Sh = 3.6 = \frac{k_c D_{CHF}}{D_{AB}} \qquad 4\text{-}20$$

Rearranging equation 4-20, and solving for mass transfer coefficient, $k_c$,

$$k_c = \frac{3.6(D_{AB})}{D_{CHF}} = \frac{3.6(0.196\,\text{cm}^2\,\text{s}^{-1})}{0.08\,\text{cm}} = 8.82\,\text{cm}\,\text{s}^{-1}$$

The specific surface area of the CHF structure is based on the exposed surface area of catalyst particles on the inner diameter surface of the CHF structure. Since the actual exposed catalyst surface area cannot be easily measured it was estimated based on a visual examination of the inner surface of the C2 CHF to be approximately 75% of the total surface area of the inner surface of the fibres:

$$A_{CCHF} = 0.75\pi D_{CHF}\,(l_{CHF})\,(1\text{m})^2\,(100\text{cm})^{-2}\,(\#\ of\ fibres) \qquad 4\text{-}21$$

where: $A_{CCHF}$ = Exposed surface area of catalytic hollow fibre, $m^2$

$D_{CHF}$ = Diameter of catalytic hollow fibre, cm

$l_{CHF}$ = length of the catalytic hollow fibres, cm

$\#\ of\ fibres$ = number of fibres in the module

Substituting the appropriate values for the CHF test articles yields:

$A_{CCHF}$ = 0.75(3.14)(0.08 cm)(4.25 in)(2.54 cm $in^{-1}$) )$(1m)^2$ $(100cm)^{-2}$ (22)=0.0045 $m^2$

The specific surface area, $a_c$ is calculated by dividing the exposed surface area of the catalyst particles in the hollow fibre module by the volume of the module, 10.5 $cm^3$ (0.0000105 $m^3$):

$$a_c = \frac{0.0045\ \text{m}^2}{0.0000105\ \text{m}^3} = 428.6\ \text{m}^2\ \text{m}^{-3}$$

The product of the mass transfer coefficient and the specific surface area is then calculated as:

$$k_c a_c = 0.0882\ \text{m s}^{-1}(428.6\ \text{m}^2\ \text{m}^{-3}) = 37.8\ \text{s}^{-1}$$

For the C2 CHF sample used to manufacture the test fibre module, the CHF density was measured at 360 g $l^{-1}$ (based on the mass of the catalyst and the empty tube volume of the module). The specific rate constant for the CHF module is calculated as:

$$k = k'\rho_b = 161.6\ \text{l min}^{-1}\ \text{g}^{-1}\ (360\ \text{g l}^{-1})(1\ \text{min})(60\text{s})^{-1} = 969.6^{-1}$$

The measured initial internal effectiveness factor for C2 CHF module was $\eta_0$ = 0.036. The product of the specific reaction rate and internal effectiveness factor for the CHF is:

$$\eta_0 k = 0.036(969.9\ s^{-1}) = 34.9\ s^{-1}$$

As was the case with the packed bed test, mass transfer from the bulk and intra-pellet mass transfer must be considered in the analysis of the data. In a similar fashion, the CHF module can be modeled as a plug flow reactor and for the comparative test at a GHSV of 110,400 $(hr)^{-1}$, the volume of the reactor was 0.0105 liters and the flow rate was 19.32 l $min^{-1}$ (0.322 l $s^{-1}$). The average CO partial pressure in along the length of the module was 7.65 ppm resulting in a pressure corrected decay constant of 0.00246 $mins^{-1}$. The overall CHF effectiveness factor incorporating mass transfer and deactivation is then given by 4-22 (same form as for granular catalyst – equation 4-18):

$$\Omega = \frac{\eta_0 e^{-\frac{k_d}{2}t}}{1 + \frac{\eta_0 k e^{-\frac{k_d}{2}t}}{k_c a_c}} = \frac{0.036 e^{-\frac{0.00246\ min^{-1}}{2}t}}{1 + \frac{34.9\ s^{-1} e^{-\frac{0.00246\ min^{-1}}{2}t}}{37.8\ s^{-1}}} \qquad 4\text{-}22$$

The conversion as a function of time can then be predicted by substituting the overall effectiveness factor from equation 4-20 into equation 4-16. The results of this prediction are also shown for the CHF structure in Figure 30.

The estimated conversion at 9 hours into the test for the CHF structure is approximately 50% of the model prediction. In addition to the potential inaccuracies associated with obtaining the basic kinetic parameters as noted above in the analysis of the granular catalyst test case, additional variables potentially affecting the accuracy of the analysis for the CHF structures include the exposed catalyst surface area on the inner diameter of the CHF and the actual density of the catalyst. The exposed area used in this calculation is simply an estimate based on limited subjective inspection of the SEMs of the inner surface and the catalyst density is based on the original formulation of the polymer/catalyst spinning mixture. In using a high concentration of NMP solvent in the bore side of the hollow fibre spinneret, it is possible that the solvent allowed for rinsing

of some fraction of the polymer in the fibre which would result in increased exposed catalyst surface area as well as an increased catalyst percentage beyond that which was originally specified in the polymer/catalyst mixture. Given the nature of these potential variations, the relative values of the calculated and measured conversions are reasonable.

An average overall effectiveness factor for the two tests can be calculated based on the average conversions measured during the test by substituting the measured conversions into equation 4-16 for the two sets of tests and then solving for the overall effectiveness factor. In doing so, the measured overall effectiveness factors for the granular and CHF configurations are 0.018 and 0.032, respectively, whereas the initial internal effectiveness factors were 0.040 for the granular catalyst and 0.036 for the CHF structure. Since the relative rates of mass transfer and reaction are similar for the CHF structure this is not unexpected, as the rate of reaction becomes more strongly controlled by the catalyst – if mass transfer was much faster the overall effectiveness factor would approach the internal effectiveness factor of 0.036. Similarly, in the granular form, the bulk mass transfer is approximately half the reaction rate and therefore mass transfer from the bulk flow is a significant part of the overall resistance.

### 4.2.13 Conclusions of Catalytic Fibre Structure Development

Catalytic hollow fibres incorporating a 10% (wgt.) $Pt/TiO_2$ catalyst were successfully produced with internal effectiveness factors that were up to 50% higher than the internal effectiveness factor for the same catalyst when tested in a granular form in a packed bed reactor for the ambient temperature oxidation of CO. While similar CHF structures were produced incorporating a 1% (wgt.) $Au/TiO_2$, the measured effectiveness factors were much lower than the granular form of the catalyst which is believed to be primarily due to degradation of the Au catalyst during storage and/or fabrication of the hollow fibre structures.

The average overall effectiveness factor for a CHF structure was measured to be approximately 78% greater than the granular form of the catalyst in which the internal effectiveness factors were similar. These measurements are based on an 18 hour

comparative test run at equivalent gas hourly space velocities and demonstrate the importance of the reactor design. The primary reason for the differences in the measured overall effectiveness factors result from the differences in the relative magnitude of the rates of mass transfer and chemical reaction for the two reactor configurations.

For the 10% $Pt/TiO_2$ CHF structures, 80-85% (wgt.) of catalyst, with the balance being the polymer, is an approximate maximum amount of catalyst, which results in the minimum amount of polymer needed to produce a CHF structure with adequate mechanical strength. Minimizing the polymer content also maximizes the porosity of the structure thereby increasing the rate of diffusion within the CHF structure.

For the 10% Pt/TiO2 catalyst, at concentrations of 70-90% (wgt.) in the CHF structure, oxidation of the polymer is possible at elevated temperatures (at, or above, approximately 200 ºC) due to the activity of the $Pt/TiO_2$ catalyst and its intimate contact with the polymer, and therefore high temperature operation should be avoided during processing or use. It was determined in this research that drying in an inert atmosphere resulted in CHF structures with good mechanical properties, whereas drying in air at 200 ºC resulted in mechanically weak structures.

Based on CO chemisorption data, polymers with a molecular weight of 50,000 to 220,000 do not penetrate the catalyst structures nor result in any appreciable coverage of the active catalyst sites. For the range of molecular weights tested in this research, polyethersulfone produced CHF structures with better mechanical properties than CHFs produced using polyvinylidenefluoride, presumably due to the higher tensile strength of polyethersulfone. At constant polymer content, higher molecular weight polymers result in a reduction in catalyst effectiveness factor. It is believed that this is primarily due to a higher density structure that results from lower diffusion rates of the polymer during the precipitation of the casting solution.

While an extensive evaluation of the effects of various manufacturing parameters was not possible due to the cost of the platinum catalyst used in the this research, of all the

parameters investigated, the most significant, observable, morphology change in this research resulted from the incorporation of high (80-85%, wgt.) concentrations of NMP in the bore fluid. At the high concentrations of catalyst investigated in this research (80-90% by weight), many of the parameters typically investigated in the research associated with hollow fibre membrane morphology, appear to have minimal effect on the observable morphology of the final CHF structure. This is presumably a result of the incorporation of large concentrations of inorganic materials which results in the interruption of the thermodynamics of the precipitation (phase inversion) process.

# Chapter 5

## 5 Overall Conclusions and Recommendations for Future Research

This chapter summarizes the overall conclusions resulting from the catalyst selection process and the subsequent production and experimental evaluation of catalytic hollow fibre (CHF) structures incorporating selected catalysts. The experimental results indicate the potential of increasing the internal effectiveness factor of certain catalysts by incorporating them into hollow fibre structures and therefore recommendations are suggested for future research to more fully examine the potential of these new catalytic structures. Though not unexpected, a comparative test of a granular packed bed of catalyst and catalytic hollow fibre module demonstrates the importance of the reactor configuration and flow regime as it relates to the overall effectiveness factor of the reactors.

### 5.1 Catalyst Selection - Conclusions

In the research associated with this thesis, the selection of catalysts for incorporation into hollow fiber structures focused on a specific trace contaminant control application associated with closed loop life support systems, however the potential application of CHFs can be applied to any catalyst system operating within the physical limits of the structures, where pressure drop is too high or an increase in catalyst effectiveness is desired.

The reactions of interest studied in this research focused on the ambient temperature oxidation of carbon monoxide and formaldehyde (HCHO) at concentrations of approximately 10 ppm and 100 ppb, respectively. Higher concentrations of platinum were shown to more effective from a volumetric perspective for the oxidation of CO. Due to limited test rig availability, limited testing of HCHO was conducted, and it was observed that there was little difference in catalyst activity (for the oxidation of HCHO) between the catalysts tested.

Of the candidate catalysts tested, 10% (wgt.) $Pt/TiO_2$ and 10% (wgt.) $Pt/SiO_2$ had the highest volumetric efficiencies, however since the bulk of the literature related to the ambient temperature oxidation of HCHO was based on $Pt/TiO_2$ catalysts, it was selected for evaluation in the CHFs.

Commercial state of the art (SOA) catalysts were also investigated and based on the literature and manufacturer data, 1% $Au/TiO_2$ (Mintek, South Africa) was selected as a representative SOA catalyst for the ambient temperature oxidation of CO. Samples of gold catalyst were not available at the time that HCHO screening trials were conducted. However, it was noted during the testing of the Au catalysts, that the specific Mintek catalyst used in this research has a very limited shelf life which may result in it not being preferred if it will not be put into use shortly after manufacturing.

Since the rate of reaction for CO oxidation is very fast, external and internal mass transfer need to be considered in the configuration of the reactor to optimize the use of the catalyst.

In closed loop life support applications, $CO_2$ is typically present at concentrations of up to 0.5% (vol.), which was shown to have a negligible effect on the oxidation of CO. Additionally; water vapor is typically present at concentrations associated with 30-70% relative humidity. In HCHO oxidation testing at 30% relative humidity, the effect of moisture was found to be negligible, however at 50% relative humidity a decrease in CO conversion of approximately 25% was noted for the 10% $Pt/TiO_2$ catalyst, while for the Mintek 1% $Au/TiO_2$ catalyst the conversion decreased by approximately 10% at the conditions tested. As a result, any design applications for ambient temperature CO oxidation need to account for this shift in activity. All the catalysts tested showed some level of deactivation for CO oxidation during testing which also would need to be factored into the final design of a reactor. No deactivation was observed in the HCHO oxidation studies.

The comparison of catalysts in this research showed that ambient temperature CO oxidation catalysts can easily be produced that exceed the activity of the catalysts currently used by NASA for trace contaminant control applications. Furthermore, it is noted that HCHO, another contaminant of concern in closed loop life support applications, can also be easily oxidized at ambient temperatures with platinum based catalysts at the conditions of interest (100ppb and nominal levels of relative humidity) in NASA's closed loop life support systems.

Finally, it was shown that due to the high reaction rate of CO oxidation on the 10% $Pt/TiO_2$ catalyst, that catalyst particles with a diameter no larger than 60 microns are preferred to achieve 95% utilization of the active catalyst material.

### 5.2 Catalytic Hollow Fibre Development - Conclusions

Catalytic hollow fibres were easily produced containing up to 83% catalyst with sufficient mechanical strength to allow handling and assembly into hollow fibre modules. However, it was noted during the development of the fibre that the nature of the catalyst support affects the manufacturability of the CHF and manufacturing parameters need to be adjusted accordingly to achieve the desired results. In this research it was noted that fibre manufacturing procedures used by other researchers to produce other types of mixed matrix hollow fibre structures did not directly translate to the hollow fibres produced in this research. This is not surprising due to the varying physical and chemical properties of the various inorganics that can be used as catalyst supports, in addition to numerous solvent and polymer systems that can be used to produce the fibres. Parametric considerations such as pore volume and chemical interaction between the surfaces of the inorganic and the solvent, or potential chemical interaction of the active catalyst and polymer require investigation at the onset of attempting to produce CHF structures.

Catalytic hollow fibres containing 83% (wgt.) of 10% (wgt.) $Pt/TiO_2$ were produced with internal effectiveness factors 50% greater than those measured for the same catalyst in a 1/8 inch (3 mm) cylindrical geometry. It was also noted that a much more efficient use

(by a factor of 2-3) of catalyst could be achieved in the CHF structure relative to the cylindrical form. This is primarily due to the fact that the internal effectiveness factors for the catalyst are very low to begin with so that only a small fraction of the active metal is used at the conditions tested in this research.

In comparative tests run at equivalent gas hourly space velocities, the measured average overall effectiveness of the CHF configuration was approximately 78% higher than the equivalent granular packed bed configuration. Since the internal effectiveness factors for both catalyst configurations were similar, the primary reason for the lower overall effectiveness factor of the granular configuration was due to different flow dynamics for the two reactor configurations that were tested, resulting in the bulk mass transfer rate being the primary resistance in the packed bed reactor. This test, and the analysis of the data, highlights the importance of separating mass transfer in the bulk from mass transfer in the catalyst structure when interpreting the kinetic data.

Three primary parameters were identified which result in the highest measured internal effectiveness factor for the CHF structures: ratio of catalyst/polymer, composition of the bore fluid, and wall thickness of the CHF. Of these three parameters, the composition of the bore fluid had the largest observed impact on the measured effectiveness factors for the CHFs. Maximizing the mass ratio of catalyst to polymer results in the maximum mass of catalyst being available in the minimum volume while simultaneously minimizing the amount of polymer which produces a higher porosity and higher rates of diffusion within the structure, however practical minimum quantities of polymer of 14-20% are required for adequate mechanical strength. Reducing the wall thickness of the CHF reduces the length of the internal mass transfer zone, and therefore a more efficient utilization of the catalyst is achieved. Finally, incorporating high concentrations of solvent, approximately 80-85% (wgt.), in the bore fluid results in a porous surface on the inside diameter of the hollow fibres, significantly increasing the rate of diffusion of reactants in the resulting structure.

CO chemisorption data indicates that there is no significant blocking of the catalyst surfaces for the polymers tested with molecular weights of 50,000 – 200,000. Lower molecular weight polymers are preferred which is believed to be due to their lower viscosity allowing for more separation into polymer lean and polymer rich sections within the polymer during the rapid precipitation of the polymer. SEM photo appear to indicate that the inner section of the CHF wall is less dense with lower molecular weight polymers. Additionally, polyethersulfone produced CHFs with superior mechanical properties when compared to CHFs produced using polyvinylidene, presumably due to the higher tensile strength of the polyethersulfone.

### 5.3 Recommendations for Future Research

- **Investigation into the effect of the final "catalytic density"** The catalytic density of the CHF fibre, based on a unit length basis, is a combination of the catalyst/polymer ratio and the initial polymer/solvent ratio. If the catalyst/polymer ratio is decreased, the resulting fibre will be less brittle, and easier to handle. The lower catalyst content will also reduce the viscosity of the casting solution, and therefore higher polymer/solvent ratios can be used such that the final catalytic density can be increased beyond what was investigated in this research. This may also decrease the macrovoid formation within the CHF structure resulting in a more efficient utilization of the volume of the CHF structure. Tests with constant catalytic density but produced with variations in the polymer/solvent ratio and polymer/catalyst ratio are suggested.

- **Incorporation of porous fillers.** The incorporation of solvent in the bore fluid appears to have a significantly increased the porosity of the inner surface of the CHF structures, however the adjacent substructure remains dense for an approximate thickness of 50-100 μm. The incorporation of porous fillers, perhaps in the form of porous nanotubes, may provide additional pore structure in this region, resulting in an increase in diffusion rates. If double layer fibres are

produced, the porous filler material could be preferentially distributed in the inner region if desired to locate the porous filler material in the region of interest.

- **Additional catalysts and reactions.** While this research focused on a specific application to trace contaminant control for aerospace life support systems, any application in which pressure drop is important may benefit from the hollow fibre geometry. Additionally, other less expensive catalysts used in many commercial applications should be investigated where cost is more of a driver.

- **Multiple layer structures.** By using a multiple layer spinneret design, CHF structures can be produced with multiple layers with varied composition and constituents. This provides a significant opportunity for optimization and customization of CHF structures. Different compositions in the layers can be investigated to determine the effect on fibre strength and catalytic activity of the CHF structure. A low polymer concentration in an inner layer will maximize diffusion rates, while the polymer concentration in the outer layer can be increased to provide the necessary strength for handling purposes. In this way the density adjacent to the inner surface may be able to be positively affected. Finally, different catalysts can be incorporated in the different layers, thereby providing a variation of a series type reactor.

- **Comparative testing with monolithic reactor geometries.** Typical monolith reactors are primarily used in applications where pressure drop and/or particulate fouling would result in unacceptable performance in a packed bed configuration. Other applications include catalysts with low internal effectiveness factors where only thin layers of the active catalyst material participate in the reaction of interest. The thickness of the catalyst layer in many of these applications is on the order of 70-200 μm, whereas others can be produced by extrusion of the catalyst or catalyst precursor, resulting in a "catalyst in the wall" monolith structure. A relative comparison of CHFs and various monolithic catalyst structures is recommended to determine if one is more advantageous.

# References


Aguilar-Guerrero, V., Gates, B. C., 2008. Kinetics of CO oxidation catalyzed by supported gold: A tabular summary of the literature. *Journal of Catalysis*, 260, pp.351-357.

Aguilar-Guerrero, V., Gates, B. C., 2009. Kinetics of CO oxidation by supported gold: A tabular summary of the literature. *Catalysis Lett* , 130, pp. 108-120.

Alayon, E., Singh, J., Nachtegaal, M., Harfouche, M., van Bokhoven, J., 2009. On highly active partially oxidized platinum in carbon monoxide oxidation over supported platinum catalysts. *Journal of Catalysis*, 263, pp. 228-238.

Aris, R., 1957. On shape factors for irregular particles – I. *Chemical Engineering Science*, 6, pp. 262-268.

Avramescu, M., Borneman, Z., Wessling, M., 2008. Particle-loaded hollow fibre membrane adsorbers for lysozyme separation. *Journal of Membrane Science*, 322, pp. 306-313.

Baker, R. W.,2004. *Membrane Technology and Research, Inc.* West Sussex, England: John Wiley and Sons, Inc.

Bamwenda, G., Tsubota, S., Nakamura, T., Haruta, M., 1997. The influence of the preparation methods on the catalytic activity of platinum and gold supported on $TiO_2$ for CO oxidation. *Catalysis Letters*, 44, pp. 83-87.

Bennet, C., Myers, J., 1974. "*Momentum, Heat, and Mass Transfer*", 2nd Edition, New York, McGraw-Hill.

Bond, G.C., Louis, C., Thompson, D.T., 2006. *Catalysis by Gold*, Catalytic Science Series -Vol.-6. London: Imperial College Press.

Bond, G.C., Thompson, D.T., 2000. Gold- catalyzed oxidation of carbon monoxide. *Gold Bulletin*, 33(2), pp.41-51.

Brauer, J., 2008. Catalysis of CO oxidation by gold nanoparticles. *Literature Seminar, The University of Alabama, Department of Chemistry, Graduate Student Seminar Series*. February 12, The University of Alabama.

Carlsson, P., Skoglundh, M., Fridell, E., Jobson, E., Anderson, B., 2002. Induced low temperature catalytic ignition by transient changes in the gas composition. *Catalysis Today*, 73, pp.307-313.

Cerasari, S., 2000. *Kinetic and nonlinear effects associated with the catalytic CO oxidation on Pt surfaces*. Thesis (PhD.), Frei Universitat Berlin.

Chung, T., Qin, J., Gu, J., 2000. Effect of shear rate within the spinneret on morphology, separation performance and mechanical properties of ultrafiltration polyethersulfone hollow fibre membranes. *Chemical Engineering Science*, 55, pp.1077-1091.

Chung.T., Jiang, L. Y., Li, Y., Kulprathipanja, S., 2007. Mixed matrix membranes (MMMs) comprising organic polymers with dispersed inorganic fillers for gas separation. *Prog. Polym. Sci*. 32, pp. 483-507.

Denkwitz, Y., Makosch, M., Geserick, J., Hörmann, U., Selve, S., Kaiser, U., Hüsing, N., Behm, R., 2009. Influence of the crystalline phase and surface area of the $TiO_2$ support on the CO oxidation activity of mesoporous Au/$TiO_2$ catalysts. *Applied Catalysis B: Environmental* 91, pp. 470-480.

Dewil, R., Everaert, K., Baeyens, J., 2005. Theoretical assessment of the catalytic (Pt/$TiO_2$) oxidation of formaldehyde at ambient temperature. *Catalysis Communications* 6, 793-795.

Dwyer, S., Bennett, C., 1982. Transient infared studies of carbon monoxide oxidation on a supported platinum catalyst. *Journal of Catalysis*, 75, pp. 275-283.

Eiswirth, M., Ertl, G., 1986. Kinetic oscillations in the catalytic CO oxidation on Pt(100) surface. *Surf. Sci*. 177, pp. 90-100.

Farauto, R. J. and Bartholomew, C. H., 1997. *Fundamentals of Industrial Catalytic Processes*. 1st Edition. London, UK: Chapman and Hall.

Fogler, H.S.;1999. *Elements of Chemical Reaction Engineering*, 3rd Edition. New Jersey: Prentice Hall.

Fukumoto, K., Suzuki, T., 2002. Adsorption of formaldehyde using sepiolite-amino acid complex. *Nippon Kagagkkai Koen Ykoshu*, 81(1), p. 359.

Haruta, M., 1997. Size- and support- dependency in the catalysis of gold. *Catalysis Today,* 36, pp.153-166.

Haruta, M., 2003. When gold is not noble: catalysis by nanoparticles. *The Chemical Record,* 3, pp.75-87.

Haruta, M., Kobayashi, T., Sano, H., Yamada, N., 1987. Novel gold catalysts for the oxidation of carbon monoxide at a temperature far below 0ºC. *Chemistry Letters*, pp. 405-408.

Haruta, M., Tsubota, S., Kobayashi, T., Kageyama, H., Genet, M., and Delmon, B, 1993. Low-temperature oxidation of CO over gold supported on $TiO_2$, α-$Fe_2O_3$, and $Co_3O_4$. *Jour. Catal.,* 144, pp. 175-192.

Haruta, M., Ueda, A., Tsubta, S., Sanchez, R., 1996. Low-temperature catalytic combustión of methanol and its derivatives over supported gold catalysts. *Catalysis Today* 29, pp. 443-447.

Haruta, M., Yamada, N., Kobayashi, T., Iijima, S., 1989. Gold catalysts prepared by coprecipitation for low-temperature oxidation of hydrogen and of carbon monoxide. *J. Catal.*, 115, pp.301.

Hodgson, A.T., Destaillats, H., Sullivan, D.P., Fisk, W.J., 2007. Performance of ultraviolet photocatalytic oxidation for indoor air cleaning applications. *Indoor Air*, 17(4), pp. 305-316.

Hoflund, G.B., Gardner, S.D., 1995. Effect of $CO_2$ on the performance of au/$mno_x$ and pt/$sno_x$/$sio_2$ low temperature co oxidation catalysts. *Langmuir*, 11, pp. 3431-3434.

Hoflund, G.B., Gardner, S.D., Schryer,D.R., Upchurch, B.T., Kielin, E.J., 1996. Influence of promoters on the performance of $Au/MnO_x$ and $Pt/SnO_x/SiO_2$ low temperature CO oxidation catalysts. *React. Kinet.Catal.Lett*., Vol 58 (No.1), pp.19-26,.

Huber, H., McIntosh, D., Ozin, G., 1977. A metal atom model for the oxidation of carbon monoxide to carbon dioxide. The gold atom-carbon monoxide-dioxygen reaction and the gold atom-carbon dioxide reaction. *Inorg. Chem.,* 16 (5), pp. 975-979.

Husain, S., Koros, W., 2007. Mixed matrix hollow fibre membranes made with modified HSSZ-13 zeolite in polyethermide polymer matrix for gas separation. *Journal of Membrane Science*, 2888, pp. 195-207.

Jiang, L. Y., Chung, T. S., Cao, C., Huang, Z., Kultprathipanja, S., 2005. Fundamental understanding of nano-sized zeolite distribution in the formation of the mixed matrix single- and dual-layer asymmetric hollow fibre membranes. *Journal of Membrane Science,* 252, pp.89-100.

Kielin, E.J., 1998. *Platinized Tin Oxide: A Low Temperature Oxidation Catalyst. Dissertation (PhD)*. The College of William and Mary in Virginia.

Kittrell, J., 2002. *Final Report: Photocatalytic air cleaner for indoor air pollution control, EPA Contract 68D00275*. Available from: http://cfpub.epa.gov/ncer_abstracts/index.cfm/fuseaction/display.abstractDetail/abstract/1357/report/F [Accessed August 2008].

Koros, W., Fleming, G., 1993. Membrane-based gas separation. *Journal of Membrane Science,* 83, pp. 1-80.

Krämer, M., Schmidt, T., Stowe, K., Maier, W. F., 2006. Structural and catalytic aspects of sol–gel derived copper manganese oxides as low-temperature CO oxidation catalyst. *Applied Catalysis A: General,* 302, pp. 257–263.

Kulprathipanja, S., Nousil, R.W., Li, N.N., 1988. *Separation of fluids by means of mixed matrix membranes*. US patent 4,740,219.

Kulprathipanja, S., Nousil, R.W., Li, N.N., 1992. *Separation of gases by means of mixed matrix membranes*. US patent 5,127,925.

Lafyatis, D., Ansell, G., Bennett, C., Frost, J., Millington, P., Rajaram, R., Walker, A., Ballinger, T., 1998. Ambient temperature light-of for automobile emission control. *Applied Catalysis B: Environmental* 18, pp. 123-135.

Lamb, A.B., Bray, W.C., Frazer, J.C.,1920. The removal of carbon dioxide from the air. *Jour. Ind. Eng. Chem.*, 12, p. 213.

Laninovic, V. 2005. Relationship between type of nonsolvent additive and properties of polyethersulfone membranes. *Desalination*, 186, pp. 39-46.

Levenspiel, O., 1972. *Chemical Reaction Engineering*. 2nd Ed., Hoboken, N.J.: John Wiley & Sons, Chapter 14.

Levenspiel, O., 1984. *The Chemical Reactor Omnibook+,* Oregon:OSU Book Stores, Inc.

Li, C., Shen, Y., Jia, M., Sheng, S., Adebajo, M., Zhu, H., 2008. Catalytic combustion of formaldehyde on gold/iron-oxide catalysts. *Catal. Commun.,* 9, pp. 355-361.

Li, S., Liu, G., Lian, H., Jia, M., Zhao, G., Jiang, D., Zhang, W., 2008. Low-temperature CO oxidation over supported Pt catalysts prepared by colloid-deposition method. *Catalysis Communications*, 9, pp. 1045-1049.

Liao, P., Wolf, E., 1982. Self-sustained oscillations during CO oxidation on a Pt/$\gamma$-$Al_2O_3$ catalyst. *Chem. Eng. Comm.,* 13 (4), pp. 315-326.

Liu, Y., Koops, G., Strathmann, H., 2003. Characterization of morphology controlled polyethersulfone hollow fibre membranes by the addition of polyethylene glycol to the dope and bore liquid solution. *Journal of Membrane Science*, 223, pp. 187-199.

Lively, R., Chance, R., Deckman, H., Kelley, B., Koros, W., 2009. Hollow fibre adsorbent for the removal of $CO_2$ from flue gas. *Ind. Eng. Chem. Res*., 48 pp. 7312-7324.

Lockheed Missiles and Space Company, January 1977. *Investigation and testing of low temperature carbon monoxide catalysts, LMSC-D556669*. Lockheed Missiles and Space Company, CA.

Loeb,S., Sourirajan, S., 1962. Sea water demineralization by means of an osmotic membrane. *Adv. Chem. Ser*., 38, pp. 117.

Lu, J., Gao, H., Shaikhutdinov, S., Freund, H., 2007. Gold supported on well-ordered ceria films: nucleation, growth and morphology in CO oxidation reaction. *Catalyst Letters,* 114, pp. 8-16.

Machado, P., Habert, A., Borges, C., 1999. Membrane formation mechanism based on precipatation morphology: flat and hollow fibre polysulfone membranes. *Journal of Membrane Science,* 155, pp. 171-183.

McCarthy, E., Zahradnik, J., Kuczynski, G., Carberry, J., 1975. Some unique aspects of CO oxidation on supported Pt. *Journal of Catalysis,* 39, pp.29-35.

McPherson, J., Pattrick, G., Raphulu, M., Ntho, T., Moma, J., Ramdayal, D., Khumalo, T. Fredericks, N., Gqogqa, P., Beeming, B., Mafulako, P., Muhuma E., and van der Lingen, E., 2009. Gold catalysis at Mintek. *75th Council for Mineral Technology*, 5th June 2009, Project AuTEK, Advanced Materials Division. Randburg, South Africa.

Michaels, A., 1971. *High flow membrane*. US Patent 3,615,024.

Morrison and Boyd, 1973, pg 628-629. *Organic Chemistry*. 3rd edition. Boston: Allyn and Bacon Inc.

Nakayama, H., Hayashi, A., Eguchi , T., Nakamura, n., Tsuhakoa, M., 2002. Adsorption of formaldehyde by polyamine-intercallated α-zirconium phosphate. *Solid State Sciences*, 4(8), pp. 1067–1070.

Nalette, T., Thibaud-Erkey, C., 2003. Testing and development of new catalysts for vapor phase ammonia oxidation. SAE 2003-01-2502, *International Conference on Environmental Systems*, Vancouver, BC., Canada.

NASA AMES Research Center, 2004. *Advanced Life Support Division, In-House Life Support Technology Review Databook.* Section 2 – Air Revitalization Technologies. NASA AMES Research Center, Moffet Field, CA.

NASA Exploration web site. Available from http://www.nasa.gov/mission_pages/constellation/orion. [Accessed 2 November 2007].

Oh, S. J., Kim, N., Lee, Y. T., 2009. Preparation and characterization of PVDF/$TiO_2$ organic-inorganic composite membranes for fouling resistance improvement. *Journal of Membrane Science*, 345, pp.13-20.

Oh, S., Hoflund, G.B., 2006. Chemical state study of palladium powder and ceria-supported palladium during low- temperature CO oxidation. *J. Phys. Chem. A*, 110, pp.7609-7613.

Oh, S., Hoflund, G.B., 2007. Low-temperature catalytic carbon monoxide oxidation over hydrous and anhydrous palladium oxide powders. *Journal of Catalysis,* 245, pp. 35-44.

Olea, M., Tada, M., Iwasawa, Y., 2007. Temporal analysis of products (TAP) study on low temperature carbon monoxide oxidation on supported Au catalysts. *Topics in Catalysis*, 40 (1-2), pp.137-143.

Paul, Dr., Kemp, Dr., 1973. The diffusion time lag in polymer membranes containing adsorptive fillers. *J. Polym. Sci. Symp*., 41, pp. 79- 93.

Pavia, Lampman, and Kriz, 1996. *Spectroscopy*, 2nd Edition. Fort Worth, Texas: Harcourt Brace and Co.

Peng, J., Wang, S., 2007. Performance and characterization of supported metal catalysts for complete oxidation of formaldehyde at low temperature. *Applied Catalysis B; Environmental*, 73, pp.282-291.

Perry and Chilton, 1973. *Chemical Engineering Handbook*, 5th edition. New York: McGraw Hill, 1973.

Perry, J. L., 1998. *Elements of Spacecraft Air Quality Control Design. NASA/TP-1998-207978*. Marshall Space Flight Center, Huntsville, GA.

Perry, J., 2009a. A design basis for spacecraft cabin trace contaminant control. *39th International Conference on Environmental Systems*, Savannah, GA., July 2009. Warrendale PA., SAE International, ICES ICES 2009-01-2592.

Perry, J., 2009b. Status of the international space station (iss) trace contaminant control system., *39th International Conference on Environmental Systems*, Savannah, GA., July 2009. Warrendale PA., SAE International, ICES 2009-01-2353.

Qin, J., Chung, T., 2004. Effects of orientation relaxation and bore fluid chemistry on morphology and performance of polyethersulfone hollow fibre for gas separation. *Journal of Membrane Science,* 229, pp. 1-9.

Raphulu, M., McPherson, J., Pattrick, G., Ntho, T., Mokoena, L., Moma, J., van der Lingen, E., 2009. CO oxidation : Deactivation of $Au/TiO_2$ catalysts during storage. *Gold Bulletin*, 42(4), pp 328-336.

Reuvers, A., van den Berg, J., Smolders, C., 1987. Formation of membranes by means of immersion precipitation. Part I. A model to describe mass transfer during immersion precipitation. *Journal of Membrane Science,* 34, pp. 67-86.

Rubenfield, L., 1967. *Encyclopedia of Polymer Science and Technology*, Vol 16, pg 505. Hoboken, NJ: Interscience Publishers, a division of John Wiley and Sons, Inc.

Satterfield, C. N., 1980. *Heterogeneous Catalysis in Practice*. New York: McGraw-Hill Publishing Company.

Schryer,D.R., Hoflund, G.B., 1990. Low-temperature CO oxidation catalysts for long-life $CO_2$ lasers. International Conference held NASA Langley Research Center, Hampton, VA. October 17-19, 1989. NASA Conference Publication 3076, Washington, DC,1990.

Senkine, Y., 2002. Oxidative decomposition of formaldehyde by metal oxides at room temperature. *Atmospheric. Enivironment,* 36, p.5543.

Smith, J.,M., 1981. *Chemical Engineering Kinetics*, 3rd ed. New York: McGraw-Hill Book Company.

SSS 90-01, 1990. Ambient temperature catalytic oxidizer, Item 07, Hamilton Sundstrand Part# SV774230. *Component Data Handbook, Environmental Control and Life Support Systems*. Hamilton Sundstrand

STC Catalysts Inc. Available from www.stc-catalysts.com [Accessed December, 2007].

Steyn, J., Pattrick, G., Scurrell, M., Hildebrandt, D., Raphulu, M., van der Lingen, E., 2007. On-line deactivation of $Au/TiO_2$ for CO oxidation in $H_2$-rich gas streams. *Catalysis Today,* 122, pp. 254-259.

Sun, Y., Fang, L., Wyon, D., Wisthaler, A., Lagecrantz, L., Strom-Teisen, P., 2008. Experimental research on photocatalytic oxidation purification technology applied to aircraft cabins. *Building and Environment*, 43(3), pp. 258-268.

SVHS 8740, 1979. *Catalyst, platinum on carbon, purification process for*. Hamilton Sundstrand.

Tai, C., Perera, S., 2007. $CO_2$ recovery system using hollow fibres. *University of Bath/domnick hunter/Hamilton Sundstrand Project Report RE-CE 0124*.

Tai, Chin-Chih, 2007. *Novel Adsorbent Hollow Fibres.* Thesis (PhD). Department of Chemical Engineering, The University of Bath, Bath.

Taylor, S.H., Hutchings, G.J., and Mirzaei, A.A., 1999. Copper zinc oxide catalysis for ambient temperature carbon monoxide oxidation. *Chem. Commun,* pp.1373-1374.

The 3M Corporation, January, 2010.Technical data sheet 3M gold catalyst AUC-16-1 [online].Available from: http://multimedia.3m.com/mws/mediawebserver?mwsId=66666UuZjcFSLXTtnXMEnXT2EVuQEcuZgVs6EVs6E666666-- [Accessed 29 June 2010].

Thiele, E. W., 1939. Relationship between Catalytic Activity and Size of Particle. Industrial and Engineering Chemistry, 31(7), pp. 916-920.

Torrestiana- Sanchez, B., Ortiz-Basurtu, R., La Fuente, E., 1999. Effect of nonsolvents on properties of spinning Solutions and polyethersulfone hollow fibre ultrafiltration membranas. *Journal of Membrane Science,* 152, pp. 19-28.

Wang, D., Li, K., Teo, W., 1995. Relationship between mass ratio of nonsolvent-additive to solvent in membrane casting solution and its coagulation value. *Journal of Membrane Science,* 98, pp. 233-240.

Wang, D., Li, K., Teo, W., 1996. Polyethersulfone hollow fibre gas separation membranes prepared from NMP/alcohol solvent systems. *Journal of Membrane Science*, 115, pp. 85-108.

Wang, D., Teo, W., Li, K., 2002. Preparation and characterization of high-flux polysulfone hollow fibre gas separation membranes. *Journal of Membrane Science*, 2002, pp. 247-256.

Wang, L., Lui, Q., Huang, X., Lui, Y., Cao, Y., Fan, K., 2009. Gold nanoparticles supported on manganese oxides for low- temperature CO oxidation. *Applied Catalysis B : Environmental*, 88, pp.204-212.

Wickham, D.T., Engel, J., and Yu, J., Nalette, T., and Thibaud-Erkey, C., 2005. Results of VPCAR pilot scale and system level tests for the selective oxidation of ammonia to nitrogen and water; SAE paper No. 2005-01-3034. *35th International Conference on Environmental Systems*, Rome Italy.

Widjojo, N., Chung, T., Kulprathipanja, S., 2008. The fabrication of hollow fibre membranes with double-layer mixed-matrix materials for gas separation. *Journal of Membrane Science*, 325, pp. 326-335.

Wijmans, J., Baaij, J., Smolders, C., 1983. The mechanism of formation of microporous or skinned membranes produced by immersion precipitation. *Journal of Membrane Science*, 14, pp. 263-274.

Wu, K., Chung, Y., Chen, Yi-Ling, Chen, Yu-Wen, 2004. Catalytic oxidation of carbon monoxide over gold/iron hydroxide catalyst at ambient conditions. *Applied Catalysis B: Environmental*, 53, pp. 111-116.

Xiao, Y., Wang, K., Chung, T., Tan, J., 2006. Evolution of nano-particle distribution during the fabrication of mixed matrix TiO2-polyimide hollow fibre membranes. *Chemical Engineering Science*, 61, pp. 6228-6233.

Xu, C., Xu, X., Su, J., Ding, Y., 2007. Research on unsupported nanoporous gold catalyst for CO oxidation. *Journal of Catalysis,* 252, pp. 243-248.

Xu, Z., Qusay, A., 2004. Polyethersulfone (PES) hollow fibre ultrafiltration membranes prepared by PES/non-solvent/NMP solution. *Journal of Membrane Science*, 233, pp. 101-111.

Yang, L., Liu, Z., Shi, J., Hu, H., Shangguan, W., 2007. Design consideration of photocatalytic oxidation reactors using $TiO_2$-coated foam nickels for degrading indoor gaseous formaldehyde. *Catalysis Today,* 126, pp 359-368.

Yang, Q., Chung, T., Santoso, Y., 2007. Tailoring pore size and pore size distribution of hollow fibre membranes via dual-bath coagulation approach. Journal of Membrane Science, 290, pp 153-163.

Yang, R.T., 2003. *Adsorbents, Fundamentals and Applications*. Hoboken, NJ.: John Wiley and Sons.

Yu, C., Crump, D., 1998. A review of the emission of VOCs from polymeric materials used in buildings. *Build. Environ*. 33, p. 357.

Yung, M., Holmgreen, E., Ozkan, U., 2007. Low-temperature oxidation of carbon monoxide on Co/$ZrO_2$. *Catalysis Letters*, 118, pp 180-186.

Zeman, L., Tkacik, G., 1988. Thermodynamic analysis of a membrane-forming system water/n-methyl-2-pyrrolidone/polyethersulfone. *Journal of Membrane Science*, 36, pp.119-140.

Zhang, C., He, H., 2007. A comparative study of $TiO_2$ supported nobel metal catalysts for the oxidation of formaldehyde at room temperature. *Catalysis Today*, 126, pp345-350.

Zhang, C., He, H., Tanaka, K., 2005. Perfect catalytic oxidation of formaldehyde over a Pt/$TiO_2$ catalyst at room temperature. *Catalysis Communications*, 6(3), pp. 211-214.

Zhang, C., He, H., Tanaka, K., 2006. Catalytic performance and mechanism of a Pt/$TiO_2$ catalyst for the oxidation of formaldehyde at room temperature. *Applied Catalysis B; Environmental,* 65, pp.37- 43.

Zhang, Y., 2005. *Indoor Air Quality Engineering*, Boca Raton, Florida: CRC Press LLC.

# Appendixes

# Appendix 1 - Example Calculations

## A-1 Example Calculation for the Estimate of Reaction Rate and Deactivation Constants for the Oxidation of CO in Dry Air on $Pt/TiO_2$

The rate of a chemical reaction is proportional to the concentration of the reacting species and generally represented by equation A-1:

$$-r_a = [k_a(T)]\,a(t)[fn(C_a, C_b.....)] \qquad \text{A-1}$$

where: $r_a$ = rate of reaction of species a, mol $l^{-1}$ $s^{-1}$

$a$ = activity (=1 without deactivation, with deactivation $a$ is function of time)

$k_a$ = specific reaction rate constant which is a function of temperature $T$, $s^{-1}$

$C_a$, $C_b$ …= concentrations of reacting species $a$, $b$, mol $l^{-1}$,....

For the oxidation reactions and low concentrations of contaminants studied in this research, the rate of reaction can be considered first order in contaminant concentration (McCarthey et al. 1975, Dewil et al. 2005, Xu et al. 2007). Additionally, at the low concentrations associated with this research, the oxygen is present at concentrations much greater than stoichiometric and therefore can be considered constant and combined with the rate constant. This results in a rate equation that is a function of a single species with a pseudo rate constant, $k'$, and dropping the subscript "$a$" since the rate is essentially a function of CO concentration only. The low concentration of CO also allows the reaction to be considered isothermal and therefore equation A-1 for CO oxidation can be re-written as:

$$-r = k'\,a(t)[CO] \qquad \text{A-2}$$

For many reactions where poisoning occurs due to adsorption of reactants or products, the conversion decreases at an approximate linear rate with time, and the activity is considered to follow a first order decay law (Fogler 1999):

$$a = e^{-k_d t} \qquad \text{A-3}$$

where: $k_d$ = decay constant, mins$^{-1}$

$t$ = time, mins

Using the design equation for a packed bed reactor combined with the rate law for a first order reaction with deactivation yields:

$$v_0 \frac{d[CO]}{dW} = -k' a(t)[CO] \qquad \text{A-4}$$

where: $v_o$ = inlet volumetric flow rate, l min$^{-1}$

$W$ = weight of catalyst, g

Combining equations A-3 and A-4 and solving for the case where the activity is uniform throughout the reactor yields:

$$-k_d t = \ln\left(\frac{v_0}{Wk'}\right) + \ln\left(\ln\left(\frac{[CO]_0}{[CO]}\right)\right) \qquad \text{A-5}$$

where $[CO]_0$ is the inlet concentration of CO in mol l$^{-1}$.

From equation A-5 it can be seen that if the assumptions of first order decay rate and first order reaction are reasonable then a plot of $\ln\left(\ln\left(\frac{[CO]_0}{[CO]}\right)\right)$ as a function of time should yield a straight line with a slope of $-k_d$ and a y-intercept of $-\ln\left(\frac{v_0}{Wk'}\right)$ (Fogler 1999).

To estimate the specific rate and decay constants, a differential reactor was fabricated using 36.77 mg of catalyst particles that were crushed to less than 50 μm in diameter and dispersed in a matrix of glass wool which was subsequently formed into a plug and tested in a ½ inch (1.27 cm) diameter reactor. For the Pt/ $TiO_2$ catalyst, a test was run at a total flow rate ($v_o$) of 40 l $min^{-1}$ with an inlet concentration of 40 ppm CO. The result for the $Pt/TiO_2$ catalyst is shown in Figure A-1.

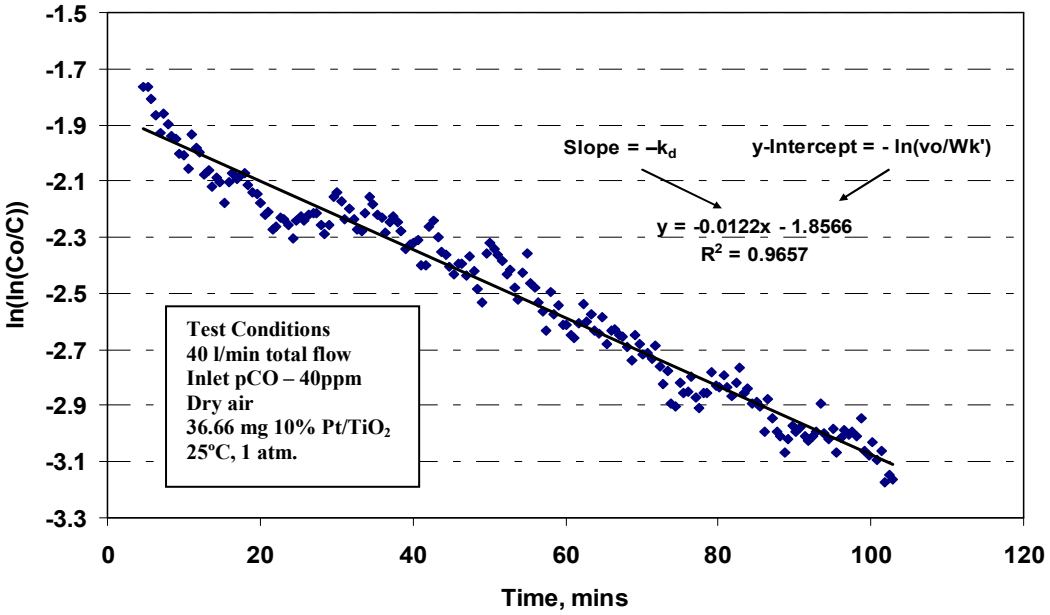


**Figure A-1 – Estimate of Specific Rate Constant and Decay Constant for CO Oxidation on 10% $Pt/TiO_2$ Powder Catalyst**

A linear regression of the data provides the values (slope and y-intercept) required to calculate the rate and decay constants. The decay constant, $k_d$, is the slope in Figure A-1 with the units of inverse time.

$$k_d = -0.0122 \text{ mins}^{-1}$$

The rate constant, *k'*, is calculated from the *y-intercept* which is equal to $-ln(v_o/Wk')$. Therefore,

$$-1.8566 = -ln(v_o/Wk')$$

$$k' = \frac{40\,\mathrm{l\,min^{-1}}}{0.037\mathrm{g}} e^{-1.8566} = 161.6\,\mathrm{l\,min^{-1}\,g^{-1}}$$

As calculated above, the decay constant, $k_d$ appears to be only dependent on the time on stream but this represents an over simplification in the analysis in many cases since the rate of decay is often a function of the concentration of the poison, or in the case where the reactants may act as a poison, the concentration of reactants (Fogler 1999). In this work, it is assumed that the activity is a function of the concentration of the CO concentration over the catalyst. Since the concentration in the differential reactor test was essentially constant at approximately 38 ppm (based on an approximate 10% conversion at an inlet concentration of 40 ppm), the decay constant must be adjusted based on an average concentration in the reactor. For the conversions tested in this research the correction is assumed linear and is simply based on the ratio of the average concentration in the reactor to that measured in the differential reactor.

$$k_d = k_{d\,(diifferntial\ test)} \frac{[CO]}{[CO]_{during\ differntial\ test}} \qquad \text{A-6}$$

**A-2 Estimate of Reaction Rate Constants for the Oxidation of HCHO in Dry Air on Pt/TiO2**

To estimate the reaction rate constant (also assumed as first order) for the oxidation of HCHO equation A-4 is used with the activity set equal to one since there was no significant indication of catalyst deactivation as:

$$v_0 \frac{d[CO]}{dW} = -k'[CO] \qquad \text{A-4}$$

which upon integration yields:

$$\ln \frac{C}{C_0} = -k' \frac{W}{v_0} \qquad \text{A-7}$$

Equation A-7 can be re-written in terms of the volume of catalyst instead of the weight of catalyst as:

$$\ln \frac{C}{C_0} = -k'' \frac{V_{cat}}{v_0} \qquad \text{A-8}$$

where the ratio $\frac{V_{cat}}{v_0}$ is the residence time in seconds, and *k''= k'* multiplied by the density of the catalyst. Therefore a plot of $\ln \frac{C}{C_0}$ versus the residence time will yield a straight line with a slope of *k''*. Data from for the oxidation of HCHO on $Pt/TiO_2$ is shown in Figure A-2 and the averages for the various flow conditions are listed below in Table A-1. Only the data at 0% relative humidity and conversions less than 100% were used in the calculation.

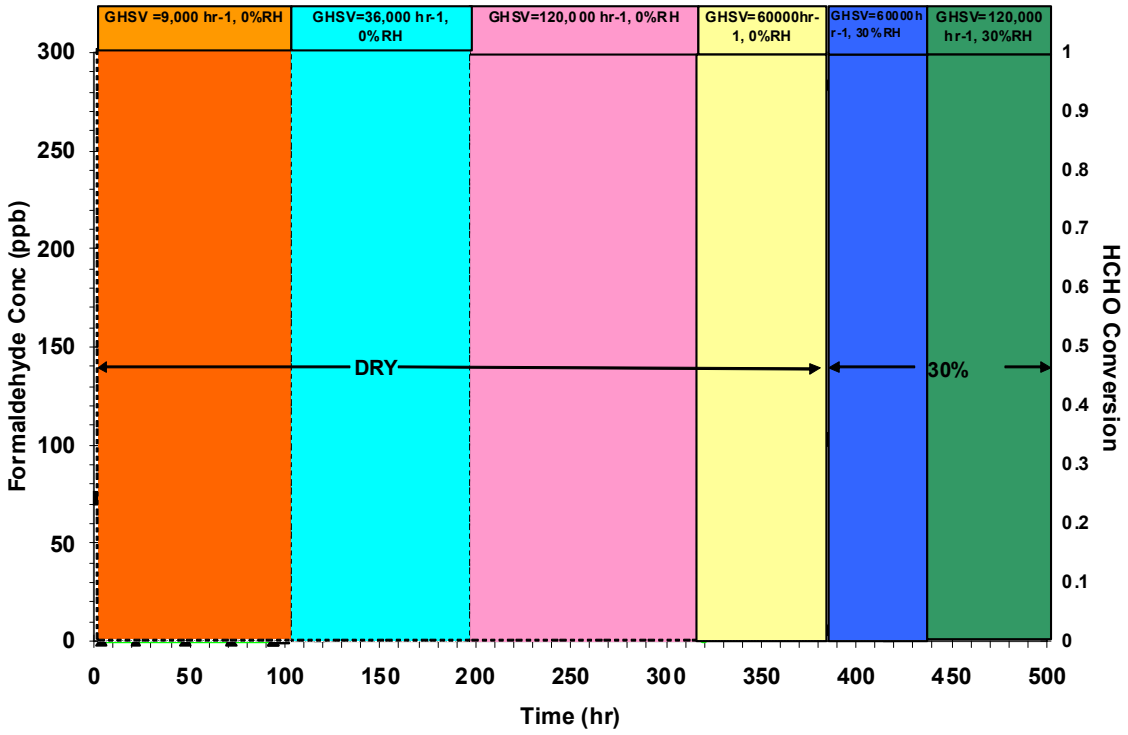


**Figure A-2 – Screening Trial for HCHO Oxidation on Pt/TiO2 Catalyst**

**Table A-1 Average Values Based on HCHO Oxidation Test**

| GHSV, $hr^{-1}$ | Residence time, s | $pCO_{in}$, ppm | $pCO_{out}$, ppm | $lnC/C_o$ |
|---|---|---|---|---|
| 36,000 | 0.1 | 106 | 3.4 | -3.44 |
| 60,000 | 0.06 | 105.5 | 7.23 | -2.67 |
| 120,000 | 0.03 | 110 | 35.31 | -1.14 |
| 120,000 | 0.03 | 285 | 117.42 | -0.89 |

Figure A-3 shows a plot of $ln(C/C_o)$ vs. the residence time with the results of a linear regression of the data, resulting in a slope of $k''$, the rate constant, with a value of 36.6 $s^{-1}$. Since it is analytically estimated that internal effectiveness factor is less than 1, and the bulk flow is in the transition region, inherent in the above calculated value of the rate constant is the overall effectiveness factor.

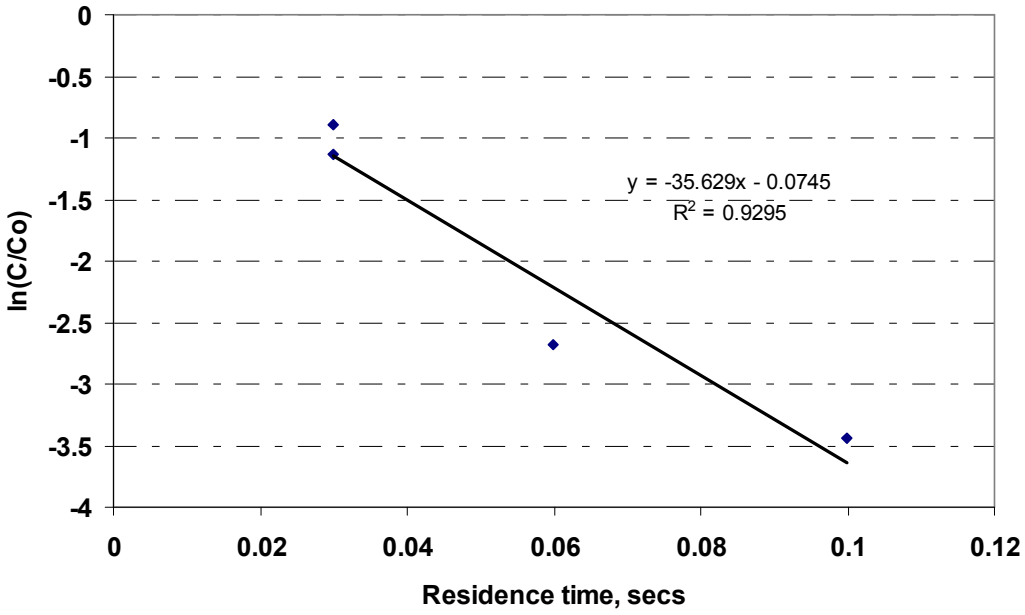


**Figure A-3 – Estimate of Reaction Rate Constant for the Oxidation of HCHO in Dry Air on $Pt/TiO_2$**

## A-3 Characteristic Length of Representative Catalytic Hollow Fibre Structure

The characteristic length, $L$, is a parameter used in the calculation of the Thiele modulus and is dependent on the geometry of a structure in which diffusion is occurring and is defined as

$$L = \frac{V_p}{A_r} \qquad \text{A-9}$$

where: $V_p$ = the volume of the catalyst structure (solid volume of the catalytic fibre), $cm^3$

$A_r$ = the exterior surface available for reactant penetration and diffusion, $cm^2$.

For the case of cylindrical catalysts, the calculation of the exterior surface area will include the area associated with the entire surface area of the cylinder including the ends, however in a potted hollow fibre configuration the area of the ends of the fibres is not included since it is negligible relative the area of the inner surface of the fibre.

For the cylindrical hollow fibre structures, $A_r$ is a function of the inside diameter and length of the fibre, and $V_p$ is the volume associated with the solid portion of the hollow fibre structure and therefore $L$ is given by:

$$L_{CHF} = \frac{V_p}{A_r} = \frac{(r_2{}^2 - r_1{}^2)\pi l_{CHF}}{2\pi r_1 l_{CHF}} = \frac{(r_2{}^2 - r_1{}^2)}{2r_1} \qquad \text{A-10}$$

where: $r_1$ = the radius associated with the inside diameter of the hollow fibre bore, cm

$r_2$ = the radius associated with the outside diameter of the hollow fibre bore, cm

$l_{CHF}$ = the length of the hollow fibre, cm

The initial CHF structures used in this research had an inside diameter of 0.8 mm ($r_1$ = 0.04 cm) and a nominal outside diameter of 2 mm ($r_2$ = 0.1cm) and therefore:

$$L_{CHF} = \frac{(0.1^2\ \text{cm}^2 - 0.04^2\ \text{cm}^2)}{2(0.04)\ \text{cm}} = 0.105\ \text{cm}$$

**A-4 Estimate of the Bulk Diffusivity of CO in Air**

The bulk diffusivity for a binary gas mixture (A, B) can be calculated using the *Chapman-Enskog formula* (Smith 1981):

$$D_{AB} = \frac{0.0018583 T^{3/2} \left( \frac{1}{M_A} + \frac{1}{M_B} \right)^{1/2}}{p_t \sigma_{AB}^{\,2} \Omega_{AB}} \qquad \text{A-11}$$

where: $D_{AB}$ = bulk diffusivity, $cm^2\ s^{-1}$

$T$ = temperature, ºK

$M_A$, $M_B$ = molecular weight of gases, $g\ mol^{-1}$

$p_t$ = total pressure of the gas mixture, atm

$\sigma_{AB}$, $\epsilon_{AB}$ = constants in the Lennard-Jones potential-energy function for the molecular pair $AB$; $\sigma_{AB}$ is in Å

$\Omega_{AB}$ = collision integral, which would be unity if the molecules were rigid spheres and is a function of $k_B T / \epsilon_{AB}$ for real gases ($k_B$ = Boltzmann constant)

The Lennard-Jones constants for the molecular pair $AB$ can be calculated from:

$$\sigma_{AB} = \frac{1}{2}(\sigma_A + \sigma_B) \qquad \text{A-12}$$

$$\varepsilon_{AB} = (\varepsilon_A \varepsilon_B)^{1/2} \qquad \text{A-13}$$

Where the subscripts represent the individual gases. The force constants for CO and Air taken from Smith (1981), are 3.590 Å and 3.617 Å, respectively and therefore substitution into equation A-12 yields:

$$\sigma_{CO:Air} = \frac{1}{2}(3.590 + 3.617) = 3.6035 \text{ Å}$$

Values of $\varepsilon/k_b$, (Smith 1981) for CO and air are 110 ºK and 97 ºK, respectively, which upon substitution into equation A-13 yields:

$$\varepsilon_{CO:air} = k_B(110x97)^{1/2} = k_B(103.29)\,^{o}\mathrm{K} \qquad \text{A-14}$$

The collision integral, $\Omega_{AB}$, is a function of $k_BT/\,\epsilon_{AB}$, which at ambient temperature can be calculated by substitution of equation A-14:

$$\frac{k_BT}{\varepsilon_{CO:air}} = \frac{k_B(298)}{k_B(103.29)} = 2.88$$

Based on the calculated value of $k_BT/\,\epsilon_{AB}$ for the molecular pair of CO and air of 2.88, the value of the collision integral, $\Omega_{CO:air}$ is 0.996 (Smith 1981).

The bulk diffusivity of CO in air can now be calculated by substitution into equation A-11:

$$D_{CO:air} = \frac{0.0018583(298)^{3/2}\left(\frac{1}{28.9}+\frac{1}{28}\right)^{1/2}}{1(3.6035)^2(0.996)} = 0.196\,\mathrm{cm}^2\,\mathrm{s}^{-1}$$

**A-5 Effective Diffusivity, Thiele Modulus and Internal Effectiveness Factor for Catalytic Hollow Fibre Structure.**

The Thiele Modulus, $M_T$, and internal effectiveness factors, $\eta$, are defined by equations A-15 and A-16 (Levenspiel 1972):

$$M_T = L\left(\frac{k}{D_e}\right)^{1/2} \qquad \text{A-14}$$

$$\eta = \frac{1}{M_T}(for M_T > 4) \qquad \text{A-15}$$

where: $D_e$ = effective diffusivity, $cm^2\ s^{-1}$

$k$ = rate constant, $s^{-1}$

$L$ = a characteristic length which is dependent on the catalyst geometry, cm

The effective diffusivity $D_e$, is used in diffusion calculations associated with porous catalysts and includes geometric correction factors which are applied to the diffusivity to account for the structure's properties.

$$D_e = \frac{D\varphi\sigma}{\tau} \qquad \text{A-16}$$

where: $D$ = diffusivity, $cm^2\ s^{-1}$

$\varphi$ = pellet porosity

$\tau$ = pellet tortuosity

$\sigma$ = constriction factor

The diffusivity within the structure includes both bulk and Knudsen diffusion and at steady state is defined by equation A-17 (Smith, 1981):

$$D = \frac{1}{\left(\frac{1}{D_{AB}} + \frac{1}{(K_k)_A}\right)} \qquad \text{A-17}$$

where; $D_{AB}$ = bulk diffusivity, $cm^2\ s^{-1}$

$(D_k)_A$ = the Knudsen diffusivity of species A, $cm^2\ s^{-1}$

The Knudsen diffusivity for diffusion in a circular pore of radius $a_p$ is (Smith 1981):

$$(D_k)_A = 9.70x10^3 a_p \left(\frac{T}{M_A}\right)^{1/2} \qquad \text{A-18}$$

where: $(D_k)_A$ = the Knudsen diffusivity of species A, $cm^2\ s^{-1}$

$a_p$ = radius of pore, cm

$T$ = temperature, ºK

Using an average pore radius for the CHF structures of 3.5 x $10^{-5}$ cm, based on the work of Tai (2007), the Knudsen diffusivity for the fibres can be estimated from equation A-18:

$$(D_k)_{CO} = 9.70x10^3 (3.5x10^{-5}) \left(\frac{298}{28}\right)^{1/2} = 1.108\ cm^2\ s^{-1}$$

The diffusivity of CO in the CHF is then calculated using equation A-17 and the value of the bulk diffusivity, $D_{CO:air}$, from Section A-4 as:

$$D = \frac{1}{\left(\frac{1}{0.196} + \frac{1}{1.108}\right)} = 0.167\ cm^2\ s^{-1}$$

The effective diffusivity for the CHF structure is then estimated using the following assumed values for the structural characteristics of catalytic supports (Fogler 1999) using equation A-16:

$\varphi = 0.4$

$\tau = 4$

$\sigma = 0.8$

$$D_e = \frac{0.167(0.4)(0.8)}{4} = 0.0134\,\text{cm}^2\,\text{s}^{-1}$$

The rate constant of the fibres, $k$, is calculated from the rate constant for the $Pt/TiO_2$ catalyst (previously calculated in Section A-1 above as $161.6\,\text{l}\,\text{min}^{-1}\,\text{g}^{-1}$ ) multiplied by the density in the catalytic structure, which was measured at 598 $\text{g}\,\text{l}^{-1}$ for a representative module containing 37 fibres in a 9/16 inch (1.43 cm) diameter tube that was 3.7 inches (9.4 cm) in length and contained 11.26 g of CHFs at 80% (wgt.) catalyst.

$$k = 161.6\,\text{l}\,\text{min}^{-1}\,\text{g}^{-1}\,(598\,g.l^{-1})\,(1\,\text{min})\,(60\,\text{s}^{-1}) = 1610.6\,\text{s}^{-1}$$

The Thiele modulus and internal effectiveness factor for the CHF fibre structure is then estimated using equations A-14 and A-15:

$$M_T = 0.105\,\text{cm}\left[\frac{1610.6\,\text{s}^{-1}}{0.0134\,\text{cm}^2\,\text{s}^{-1}}\right]^{1/2} = 36.4$$

$$\eta = \frac{1}{36.4} = 0.028$$

# Appendix 2 – Related Publications

Nalette, T., Elderidge, C., Yu, P., Alptekin, G., Graf, J., 2010. Advanced catalysts for the ambient temperature oxidation of carbon monoxide and formaldehyde. AIAA-2010-6306, *International Conference on Environmental Systems*, Barcelona, Spain.

# Advanced Catalysts for the Ambient Temperature Oxidation of Carbon Monoxide and Formaldehyde

Tim Nalette[1], Christopher Eldridge[2], Ping Yu[3]
*Hamilton Sundstrand – Space, Land &Sea, Windsor Locks, CT., 06096*

Gokhan Alptekin[4]
*TDA Research, Wheatridge CO., 80033*

*and*

John Graf[5],
*NASA Johnson Space Center, Houston, TX, 77058*

## I. Abstract

The primary applications for ambient temperature carbon monoxide (CO) oxidation catalysts include emergency breathing masks and closed loop life support systems, such as those employed on the Shuttle. While Hopcalite is typically used in emergency breathing masks for terrestrial applications, in the 1970s, NASA selected a 2% platinum on carbon for use on the Shuttle since it is more active and also more tolerant to water vapor.

In the last 10-15 years there have been significant advances in ambient temperature CO oxidation catalysts. Langley Research Center developed a monolithic catalyst for ambient temperature CO oxidation operating under stoichiometric conditions for closed loop $CO_2$ laser applications which is also advertised as having the potential to oxidize formaldehyde (HCHO) at ambient temperatures. In the last decade it has been discovered that appropriate sized nano-particles of gold are highly active for CO oxidation, even at sub-ambient temperatures, and as a result there has been a wealth of data reported in the literature relating to ambient/low temperature CO oxidation.

In the shorter term missions where CO concentrations are typically controlled via ambient temperature oxidation catalysts, formaldehyde is also a contaminant of concern, and requires a large amount of charcoal to control because of its low adsorption potential. This paper examines the activity of some of the newer ambient temperature CO and formaldehyde (HCHO) oxidation catalysts, and measures the performance of the catalysts relative to the NASA baseline ATCO catalyst at conditions of interest for closed loop trace contaminant control systems.

## II. Background

With the advent of closed cycle $CO_2$ lasers, a considerable body of literature exists related to low temperature CO oxidation catalysts. The high energy plasma of the laser results in decomposition of $CO_2$ into stoichiometric quantities of CO and $O_2$ which subsequently results in rapid power loss. To mitigate this phenomenon, low temperature CO oxidation catalysts have been developed to recombine the $O_2$ and CO, thereby maintaining the power output of the laser. While this application is targeting stoichiometric concentrations of CO and $O_2$, more recently some of these catalysts are being evaluated for ambient temperature oxidation of CO and HCHO[1-2].

Much of the research related to $CO_2$ lasers has focused on $Pt/SnO_2/SiO_2$ catalysts, however additional catalysts that have shown high activity include catalysts utilizing platinum or gold in combination with titanium dioxide, aluminum oxide, manganese dioxide, and iron oxide supports[3-6].

While the focus of this paper is on CO oxidation, in recent years there has been significant interest in the ambient temperature oxidation of HCHO targeting indoor air quality applications. Much of this work has identified platinum supported on tin oxide or titanium dioxide supports as the most promising. Since most short term NASA missions requiring trace contaminant control utilize activated charcoal for the adsorption of most of the organics, and the fact

that formaldehyde has a very low adsorption potential on activated charcoal, a catalyst that can perform ambient temperature oxidation of CO and HCHO is potentially advantageous from a design perspective.

Gold catalysts, developed by TDA Research and 3M, and platinum based catalysts developed by Hamilton Sundstrand, have been evaluated in preliminary screening tests to measure the relative activity compared to the NASA ATCO baseline ambient temperature CO oxidation catalyst which is 2% platinum on activated carbon. Additionally, limited testing for HCHO oxidation was also conducted for some of the catalysts. While the testing reported in this paper is focused on the low concentrations associated with trace contaminant control, TDA and 3M have performed additional testing of their gold catalysts at elevated CO concentrations ranging 1,000-10,000 ppm, some of which has been previously published[7].

## III. Discussion

Catalyst screening tests were conducted at approximate concentrations of interest to trace contaminant control systems consistent with the historical design requirements of the U.S. space program. Basic design requirements consider two sources of contamination – the crew and the equipment. The generation rates for numerous contaminants, compiled over the history of the U.S space program, along with the space maximum allowable concentrations (SMAC), are summarized by Perry[8]. The SMAC values for CO and HCHO are listed as 10mg/m3 (8ppm, ppm = mg/m3 x 22.4 liter/mole / molecular weight) and 0.10 mg/m3 (75ppb, ppb = ppm/1000) respectively. Nominal concentrations used in the catalyst screening tests reported in this study were approximately 10 ppm and 100 ppb, for CO and HCHO respectively.

### A. CO Oxidation Tests

The test rig used for the CO oxidation studies is shown below in Figure 1.

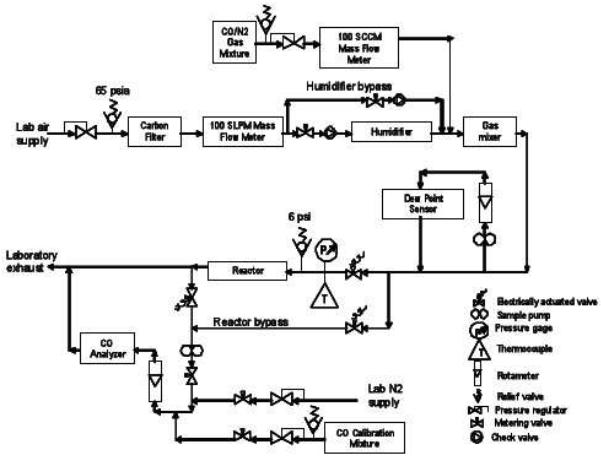


**Figure 1. CO Oxidation Test Rig**

The concentration of CO is controlled by adjusting the flow rate of a high concentration CO/nitrogen supply which is subsequently mixed with filtered laboratory air prior to feeding the CO/air mixture to the reactor. Humidity is added to the process air by diverting part of the process air flow through the humidifier.

To determine an appropriate flow rate to be used in the CO screening tests, the current NASA ATCO reactor design point flow rate and catalyst volume was used for scaling, which resulted in a gas hourly space velocity (GHSV) of 2,500 $hr^{-1}$. However, at this space velocity the conversion of all catalysts was 100% for 5 days and

therefore a relative comparison could not be made. To address this, the GHSV was increased until a conversion less than 100% was measured. A GHSV of 110,400 $hr^{-1}$ was determined sufficient to result in a measurable range of conversions for the various catalysts. All of the catalysts were initially tested in the "as received" form and size, with the exception of the TDA Au catalyst which was sieved to remove fines. The initial performance comparison utilized a volume of 15 cc for each of the catalysts tested. The results for the initial screening tests for the various catalysts in dry air at 10 ppm CO are shown in Figure 2.

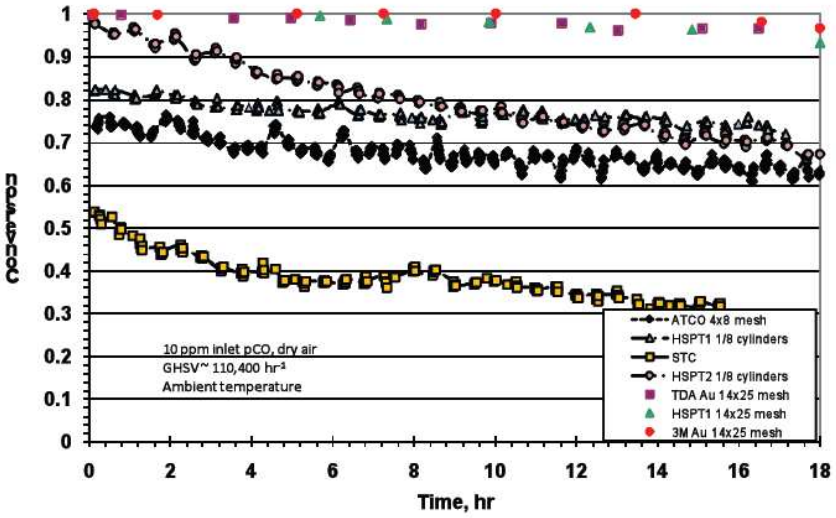


**Figure 2. Relative Activity of CO Oxidation Catalysts for Trace Contaminant Control Applications at GHSV of 110,400 $hrs^{-1}$, 10ppm Inlet CO, in Dry Air**

Figure 2 shows that catalysts with higher activities than the NASA baseline ATCO catalyst are readily available.

The STC monolith catalyst had the lowest conversion of all of the catalysts shown which is primarily assumed to be a result of lower active metal content per unit volume of catalyst, though the specific formulation was not available from the manufacturer.

As can be seen in Figure 2, particle size has a significant effect on the activity of the platinum catalyst HSPT1, and though not measured experimentally, it is assumed that this would be true for the other catalysts tested. This is due to the high intrinsic CO oxidation reaction rate being much higher than the diffusion rate of CO within the catalyst structure. To be able to distinguish the relative activities of the 14x25 mesh catalysts, a higher space velocity (1.85 x $10^6$ $hr^{-1}$) and higher CO concentration (40 ppm) were tested and the results shown in Figure 3.

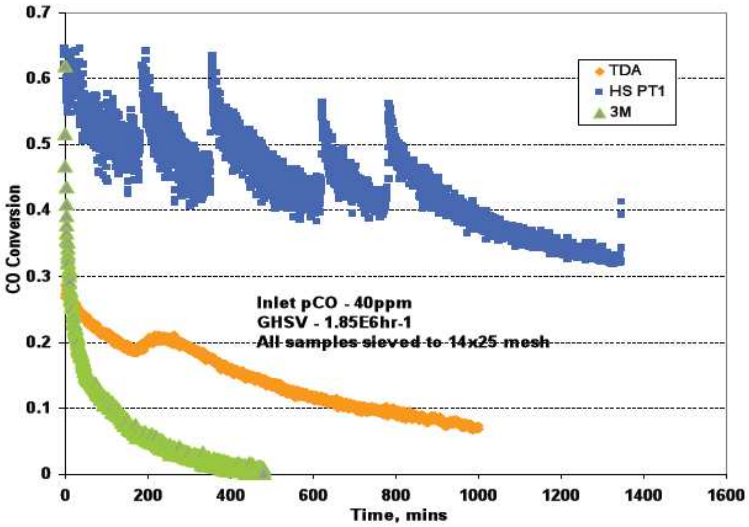


**Figure 3. Relative Activity of 14x25 mesh CO Oxidation Catalysts at GHSV of 1.85x$10^6$ $hrs^{-1}$, 40ppm Inlet CO, in Dry Air**

The oscillations noted for the platinum catalyst are consistent with similar observations for CO oxidation reported in the literature and is attributed to a periodic "restructuring" of the active species which are adsorbed on the platinum[9-10].

The effect of relative humidity was investigated in two separate tests due to the differences in measured conversion as a result of particle size. The larger catalyst particles, resulting in the lower conversions shown in Figure 2, were tested at a GHSV of 110,400 $hr^{-1}$, whereas the smaller catalyst particles were tested at higher space velocities and a higher CO concentration to provide some resolution of the relative activity of the catalysts. The results of these tests are shown in Figures 4 and 5. The HSPT1 14x25 mesh platinum catalyst resulted in 100% conversion at a GHSV of 160,000 $hr^{-1}$ but was not tested at 240,000 $hr^{-1}$.

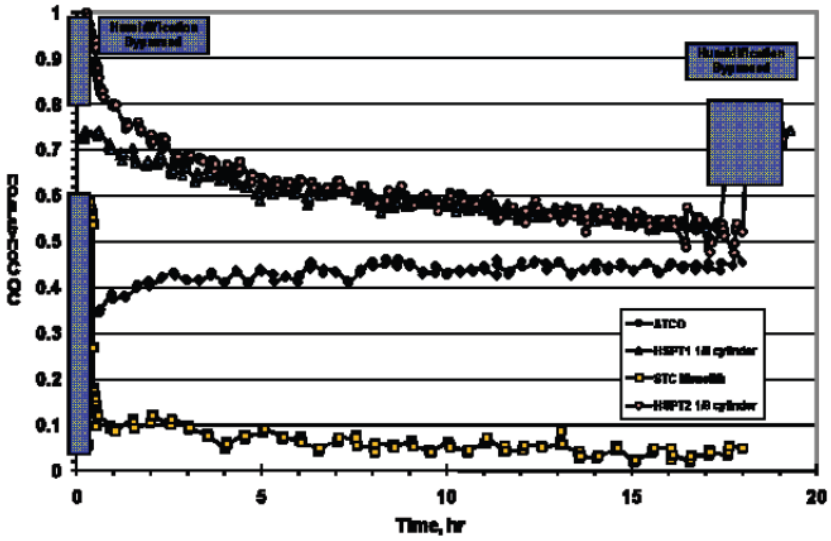


**Figure 4. Relative Activity of Larger Particle CO Oxidation Catalysts forTrace Contaminant Control at a GHSV of 110,400 $hr^{-1}$ at 50% Relative Humidity**

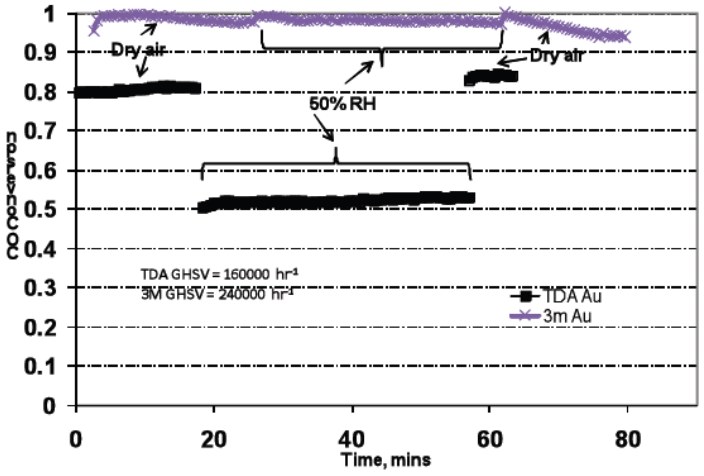


**Figure 5. Relative Activity of 14x25 mesh Au CO Oxidation Catalysts for Trace Contaminant Control Applications at Various GHSV, 40ppm Inlet CO, at 50% Relative Humidity**

At the conditions shown for the two gold catalysts in Figure 5, the 3M catalyst showed minimal effect due to the presence of water vapor, even with a 50% increase in GHSV, whereas the conversion of the TDA catalyst dropped approximately 38%. It is interesting to note that at higher space velocities in dry air, the TDA gold catalyst had a higher conversion as noted in Figure 3. This could be due to a couple of factors; first, the active metal content of the 3M catalyst may be lower than TDA's and therefore at the higher space velocity, there are insufficient active sites to sustain the high reaction rate, secondly, it is possible that due to the shorter duration of the tests conducted in the presence of water vapor, that the higher activity observed for the 3M catalyst is a result of its high initial activity (as seen in the dry testing) and if run for a longer test period, a decrease a decrease in activity would have been observed. Finally, it is noted that TDA has been involved in an extensive development activity associated with its gold catalyst and the catalyst used in this testing (fabricated in mid 2009) has been substantially improved recently but was not available for testing at the time of this publication.

### B. HCHO Oxidation Tests

The HCHO oxidation test set-up accommodated simultaneous testing of all candidate catalysts, using a series of 3-way valves on the outlet of each reactor to select the individual reactors for HCHO analysis of the effluent. A single, common synthetic air stream (20% O2, 80% N2) was used in all tests. Formaldehyde was generated by vaporizing paraformaldehyde. Formaldehyde generation is based on controlled diffusion of formaldehyde vapor. The formaldehyde generator consists of a vial, in which a quantity of paraformaldehyde is deposited, a diffusion tube attached to the vial, a containment vessel and a temperature controlled water bath. The vial is secured inside the containment vessel which is immersed in the water bath. Nitrogen carrier gas, preheated to the water bath operating temperature, enters the containment vessel and sweeps away formaldehyde from the end of the diffusion tube/vial before finally leaving the containment vessel. Humidity levels were controlled by passing part of the flow stream though a bubbler and then diluted with the balance of the flow stream and mixed prior to entering the bank of reactors. The HCHO test rig schematic is shown below in Figure 6.

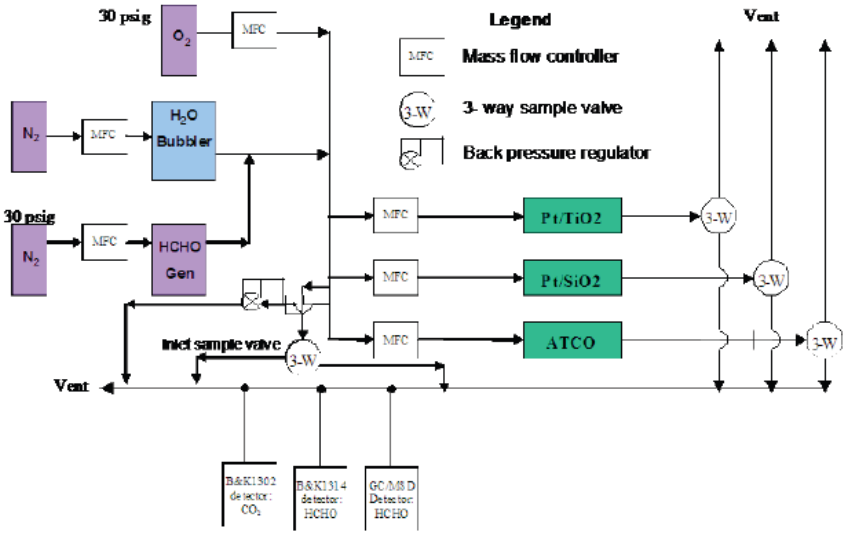


**Figure 6. Detailed Schematic of HCHO Oxidation Test Rig**

Due to the low CO oxidation activity of the STC catalyst relative to the granular platinum catalysts, HCHO oxidation tests were not conducted. Additionally, the 3M and TDA gold catalyst were not available at the time the HCHO testing was conducted so no HCHO data is available for them, and only the larger "as received" platinum catalyst structures were tested.

HCHO screening tests were conducted at GHSVs ranging from 6,000 – 120,000 $hr^{-1}$. Tests were conducted in dry air and at 30% RH, all at ambient temperature. Most of the tests were conducted at an inlet HCHO concentration of approximately 100 ppb while one test was conducted at an inlet HCHO concentration of approximately 300 ppb at a GHSV of 120,000 $hr^{-1}$. Since no significant deactivation was noted during the testing, the same catalyst was used for all tests. Moisture was introduced between hours 375 and 500. Results for the various tests are shown for the three catalysts in Figures 7-9.

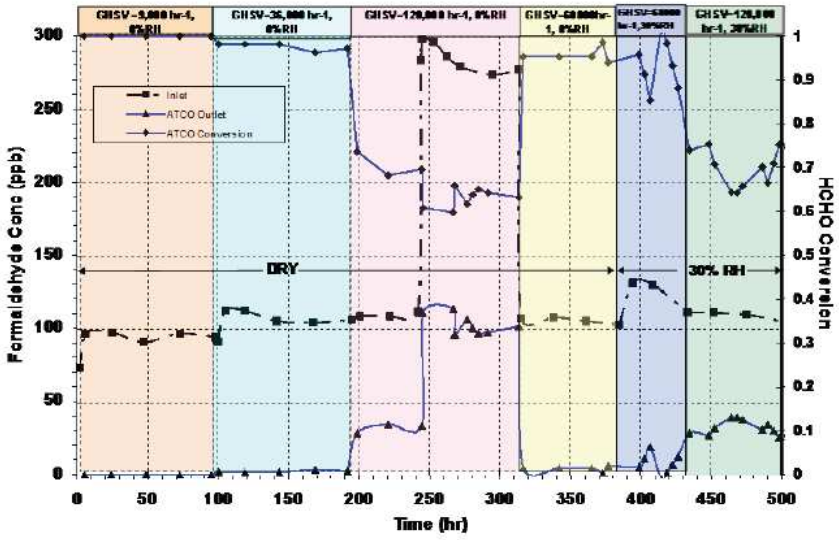


**Figure 7. Screening Test for HCHO Oxidation on ATCO Catalyst**

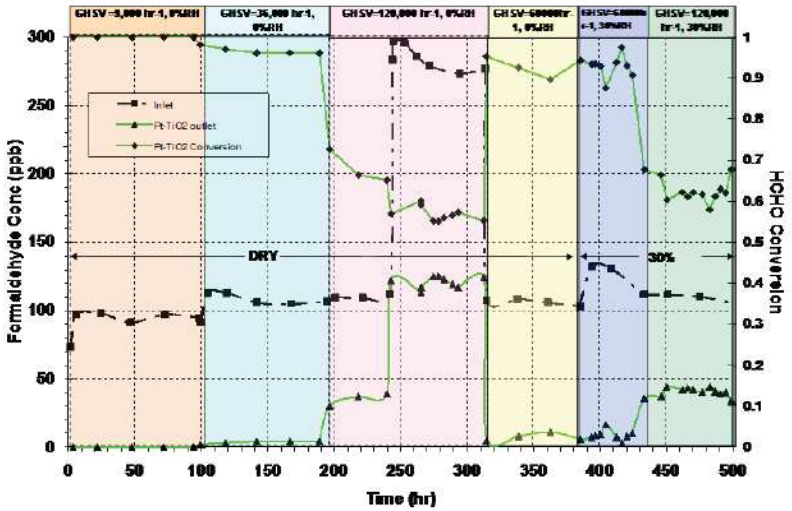


**Figure 8. Screening Test for HCHO Oxidation on HSPT1 1/8" Cylinder Catalyst**

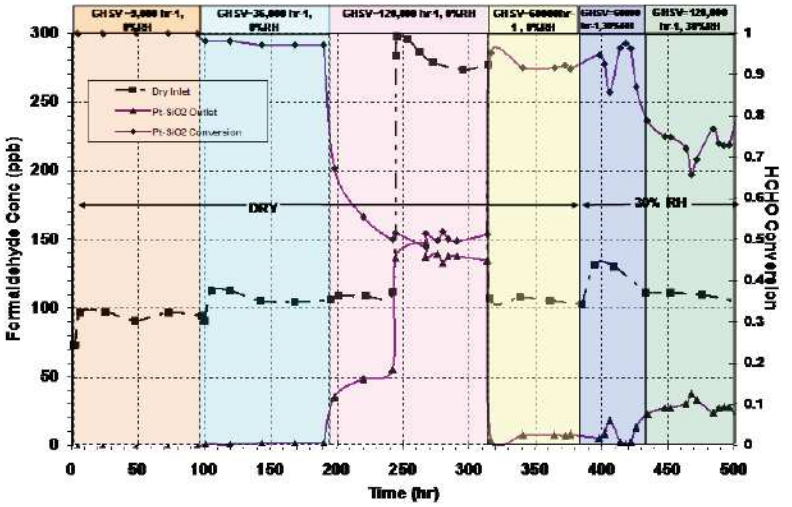


**Figure 9. Screening Test for HCHO Oxidation on HSPT2 1/8" Cylinder Catalyst**

For the three catalysts tested, there were no significant differences noted in performance over the range of conditions tested. At high space velocities, the dry HSPT2 performance was slightly lower than the others, however with the introduction of moisture, the oxidation efficiency increased to levels consistent with the others. In general the effect of moisture was relatively small and not as pronounced as in the CO oxidation screening tests. Upon changing the inlet HCHO concentration to 300 ppb, at approximately 250 hours into the test, there was no significant change in conversion.

In addition to the oxidation efficiency, the outlet CO2 concentration was also measured to allow for a mass balance to verify complete oxidation of the HCHO to CO2 and water without the formation of intermediate species. The outlet CO2 concentrations for the three catalysts are shown below in Figure 10 and shows that the HCHO is completely oxidized to CO2 within expected experimental accuracy. For complete oxidation of HCHO, the outlet CO2 concentration should be identical to the inlet HCHO concentration. The initial lower than expected CO2 concentration is believed to be due to an initial adsorption of the CO2 and/or HCHO as the surface species come to equilibrium on the catalyst surface, whereas the spike noted at approximately 80 hours into the test can be traced to an approximate 5° C increase in ambient temperature, most likely resulting in desorption of adsorbed CO2 from the catalysts.

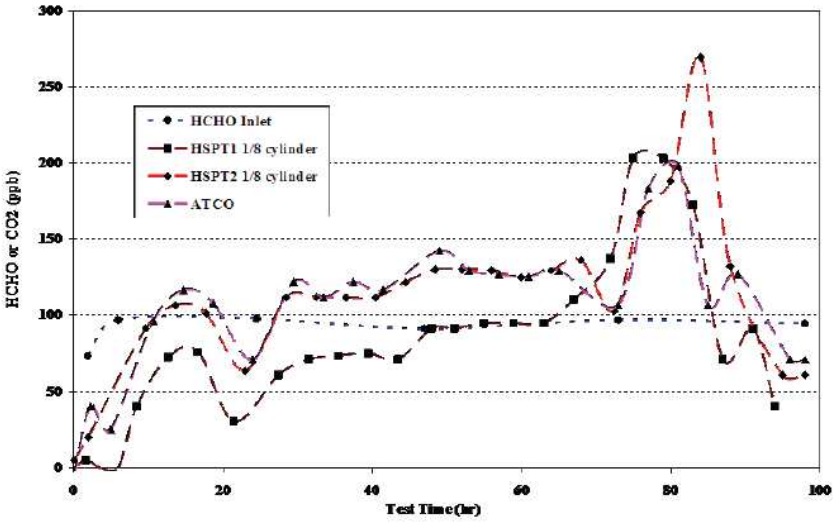


**Figure 10. Carbon Mass Balance during HCHO Oxidation – Effluent $CO_2$ Concentration**

## IV. Conclusion

For all the catalysts tested for CO oxidation at the nominal Shuttle design space velocity, 100% conversion was obtained for 5 days indicating that there is most likely significant margin in the current ATCO reactor. For the catalysts tested, the platinum catalyst were more active than gold catalysts, and a significant internal mass transfer resistance is demonstrated through the testing of smaller catalyst particles, indicating that additional enhancements are possible assuming that any increased pressure drop resulting from smaller particles can be addressed using appropriate reactor design. Additionally, catalyst supports with more open structures (higher effectiveness factor) may also warrant future investigation to reduce the required amount of catalyst.

The platinum catalysts were more active than the gold catalysts at high space velocity, while the TDA gold catalyst was more active than the 3M catalyst in dry air; however at lower space velocity the 3M catalyst was less susceptible to moisture than the TDA gold catalyst, though additional testing is needed to determine if this is sustainable for longer periods of time.

All of the platinum catalysts demonstrated similar activities for HCHO oxidation, with 100% conversion at 100ppb inlet concentrations up to a GHSV of 60,000$hr^{-1}$, with the conversion dropping to approximately 50% at a

GHSV of 120,000hr$^{-1}$. Minimal effect of moisture was noted at 30%RH for the HCHO oxidation on the platinum catalysts.

Based on the higher activity resulting from particle size for the platinum catalyst, a higher effectiveness catalyst would reduce bed size, though the potential impact on HCHO has not been validated.

In summary, advanced platinum and gold catalysts have demonstrated significantly higher ambient temperature oxidation efficiency for CO than the NASA baseline ATCO catalyst, and the platinum catalysts have demonstrated activity for ambient temperature oxidation of HCHO.

## Acknowledgments

The authors would like to thank the 3M Corporation for graciously providing gold catalyst samples used in this study and Tim Obee of the United Technologies Research Center for his extensive support in the conduct of the formaldehyde oxidation test studies.

## References

[1]Hoflund, G.B., Gardner, S.D., 1995. Effect of CO2 on the Performance of Au/MnOx and Pt/SnOx/SiO2 Low Temperature CO Oxidation Catalysts. *Langmuir*, 11, pp. 3431-3434.

[2]STC Catalysts Inc. Available from www.stc-catalysts.com [Accessed December, 2007].

[3]Haruta, M., 2003. When Gold Is Not Noble: Catalysis by Nanoparticles. *The Chemical Record,* 3, pp.75-87.

[4]Bond, G.C., Thompson, D.T., 2000. Gold- Catalyzed Oxidation of Carbon Monoxide. *Gold Bulletin*, 33(2), pp.41-51.

[5]Xu, C., Xu, X., Su, J., Ding, Y., 2007. Research on unsupported nanoporous gold catalyst for CO oxidation. *Journal of Catalysis*, 252, pp. 243-248.

[6]Aguilar-Guerrero, V., Gates, B. C., 2009. Kinetics of CO Oxidation by Supported Gold: A Tabular Summary of the Literature. *Catalysis Lett* , 130, pp. 108-120.

[7]Alptekin, G., Cates, M., Dubovik, M., Cesario, M., 2008. The Smoke Eater, A Sorbent/Catalyst for Recovery from Fires. *ICES 2008-01-2098*, San Francisco, CA.

[8]Perry, J. L., 1998. *Elements of Spacecraft Air Quality Control Design*. NASA/TP-1998-207978. Marshall Space Flight Center, Huntsville, GA.

[9]Eiswirth, M., Ertl, G., 1986. Kinetic oscillations in the catalytic CO oxidation on Pt(100) surface. *Surf. Sci*. 177, pp. 90-100.

[10]McCarthy, E., Zahradnik, J., Kuczynski, G., Carberry, J., 1975. Some Unique Aspects of CO Oxidation on Supported Pt. *Journal of Catalysis,* 39, pp.29-35.

# Appendix 3 - Publications

Allen, G., Baker, G., Nalette, T., Mankin, M., Thomas, G., 1999. Performance characteristics of the regenerable $CO_2$ removal system for the NASA EMU. SAE 1999-01-1997, *International Conference on Environmental Systems*, Denver, Colorada, US.

Colling, A., Nalette, T., Cusick, R., and Reysa, R., 1985. Development status of regenerable solid amine $CO_2$ control systems. SAE 851340, *International Conference on Environmental Systems*, San Francisco, California, US.

Filburn, T., Nalette, T., and Graf, J., 2001. The design and testing of a fully redundant regenerative $CO_2$ removal system (RCRS) for the shuttle orbiter. SAE 2001-01-2420, *International Conference on Environmental Systems*, Orlando Florida, US.

Filburn, T., Nalette, T., Genovese, J., Thomas, G., 1996. Advanced regenerable $CO_2$ removal technologies applicable to future EMUs. SAE 961484, *International Conference on Environmental Systems*, Monterey, California, US.

Flynn. M., Fisher, J., Kliss, M., Tleimat, B.,Tleimat, M., Quinn, G., Fort, J., Nalette, T., Baker, G., Genovese, J., 2004. The develoment of the vapor phase catalytic ammonia removal (VPCAR) engineering development unit. SAE 2004-01-2495, *International Conference on Environmental Systems*, Colorado Springs, Colorado, US.

Flynn. M., Tleimat, M., Nalette, T., Quinn, G., 2005. Performance testing of the vapor phase catalytic ammonia removal engineering development unit. SAE 2005-01-3033, *International Conference on Environmental Systems*, Rome, Italy.

Genovese, J., Nalette, T., 1994. Life characterization of advanced solid amine sorbents. SAE 941395, *International Conference on Environmental Systems*, Friedrichshafen, Germany.

Lin, A., Smith, F., Sweterlitsch, J., Graf, J., Nalette, T., Papale, W., Campbell, M., Lu, S., 2007. Testing of an amine-based pressure-swing system for carbon dioxide and humidity control. SAE 2007-01-3156, *International Conference on Environmental Systems*, Chicago, Illinois, US.

Lin, A., Smith, F., Sweterlitsch, J., Nalette, T., Papale, W., 2008. Further testing of an amine-based pressure-swing system for carbon dioxide and humidity control. SAE 2008-01-2101, *International Conference on Environmental Systems*, San Francisco, California, US.

Nalette, T., Filburn, T., 1992. Development of a regenerable metal oxide sheet matrix $CO_2$ removal system. SAE 921298, *International Conference on Environmental Systems* , Seattle, Washington, US.

Nalette, T., and Cusick, R., 1987. Development of a regenerable humidity and $CO_2$ control system for an advanced EMU. SAE 871471, *International Conference on Environmental Systems*, Seattle, Washington, US.

Nalette, T., Bedard, J., Carter, L., 2002. Catalyst development for the space station water processor assembly. SAE 2002-01-2362, *International Conference on Environmental Systems*, San Antonio, Texas, US.

Nalette, T., Blaser, R., Coleman, W., and Cusick, R.J., 1988. Development of an advanced solid amine humidity and CO2 control system for potential space station extravehicular activity application. SAE 881062, *International Conference on Environmental Systems*, San Francisco, California, US.

Nalette, T., Elderidge, C., Yu, P., Alptekin, G., Graf, J., 2010. Advanced catalysts for the ambient temperature oxidation of carbon monoxide and formaldehyde. AIAA-2010-6306, *International Conference on Environmental Systems*, Barcelona, Spain.

Nalette, T., Obee, T., 2007. A semi-continuous, regenerable system for trace contaminant control in closed atmospheres. SAE 2007-01-3155, *International Conference on Environmental Systems*, Chicago, Illinois, US.

Nalette, T., Papale, W., Smith, F., 2007. Development status of the carbon dioxide and moisture removal amine swing-bed (CAMRAS). SAE 2007-01-3157, *International Conference on Environmental Systems*, Chicago, Illinois, US.

Nalette, T., Papale, W., Smith, F., Perry, J., 2006. Development status of amine-based, combined humidity, $CO_2$ and trace contaminant control system for CEV. SAE 2006-01-2192, *International Conference on Environmental Systems*, Norfolk, Virginia, US.

Nalette, T., Reiss, J., Filburn, T., Mahan, E., Seery, T., Weisse, B., Smith, F., Perry, J., 2005. SAE 2005-01-2865 *International Conference on Environmental Systems*, Rome, Italy.

Nalette, T., Snowdon, D., Pickering, K., Callahan, M., 2007. The ISS water processor catalytic reactor as a post processor for advanced water reclamation systems. SAE 2007-01-3038, *International Conference on Environmental Systems*, Chicago, Illinois, US.

Papale, W., Nalette, T., Sweterlitsch, J., 2009. Development status of the carbon dioxide and moisture removal amine swing-bed (CAMRAS). SAE 2009-01-2442, *International Conference on Environmental Systems*, Savannah, Georgia, US.

Scribnik, F., Birbara, P., Faszcza, J., Nalette, T., 1990. Smoke and contaminant removal system for space station. SAE 901391, *International Conference on Environmental Systems*, Williamsburg, Virginia, US.

Sundstrom, D., Klei, H., Nalette, T., Reidy, D., and Weir, B., 1986. Destruction of halogenated aliphatics by ultraviolet catalyzed oxidation with hydrogen peroxide. *Hazardous Waste and Hazardous Materials*, Vol 3, No. 1.

Thibaud-Erkey, C., Nalette, T., 2003. Testing and development of new catalysts for vapor phase ammonia oxidation. SAE 2003-01-2502, *International Conference on Environmental Systems*, Vancouver, BC., Canada.

Tsai, C., Guray, I., Tang, X., Nalette, T., Thibaud-Erkey, C., Brinker, C., Xomeritakis, G., 2003. Novel amine-functional membrane for metabolic $CO_2$ removal from spacesuit breathing loop. Proceedings : Space Technology and Applications International Forum, 654, pp. 861-868.

Wickham, D.T., Engel, J., and Yu, J., Nalette, T., and Thibaud-Erkey, C., 2005. Results of VPCAR pilot scale and system level tests for the selective oxidation of ammonia to nitrogen and water. SAE paper No. 2005-01-3034, *35th International Conference on Environmental Systems*, Rome Italy.

Wickham, D.T., Engel, J., and Yu, J., Nalette, T., and Thibaud-Erkey, C., 2004. Development of a pilot scale reactor for the selective oxidation of ammonia to nitrogen and water. SAE paper No. 2004-01-2406, *International Conference on Environmental Systems*, Colorado Springs, Colorado, US.

# Appendix 4 - Patents

| U.S. Patent # | Title |
|---|---|
| 7,759,275 | Sorbent system for water removal from air |
| 7,736,416 | Thermally lined molecular sieve beds for $CO_2$ removal |
| 7,089,933 | $CO_2$ sorbent for inhalation drug therapy |
| 6,797,043 | Encapsulated $CO_2$ $H_2O$ sorbent |
| 6,755,892 | Carbon dioxide scrubber for fuel and gas emissions |
| 6,364,938 | Sorbent system and method for absorbing carbon dioxide from the atmosphere of a closed habitable environment |
| 5,876,488 | Regenerable Solid Amine Sorbent |
| 5,681,503 | Flat Sheet $CO_2$ Sorbent |
| 5,620,940 | Process for Forming a Regenerable Supported Amine-Polyol Sorbent |
| 5,525,237 | Process for Removing Free and Dissolved $CO_2$ from Aqueous Solutions |
| 5,518,626 | Process Employing Thermally Sterilizable Aqueous Polishing Agents |
| 5,492,683 | Regenerable Supported Amine-Polyol Sorbent |
| 5,480,625 | Enhancing Carbon Dioxide Sorption Rates using Hygroscopic Additives |
| 5,454,968 | Flat Sheet $CO_2$ Sorbent |
| 5,427,751 | Method for Using High Capacity Unsupported Regenerable $CO_2$ Sorbent |
| 5,376,614 | A Regenerable Supported Amine - Polyol Sorbent |
| 5,281,254 | Continuous Carbon Dioxide and Water Removal System |
| 5,214,019 | Enhancing Carbon Dioxide Sorption Rates Using Hygroscopic Additives |
| 5,174,974 | Regenerable $CO_2/H_2O$ Solid Sorbent |
| 5,106,754 | Zero Gravity Compatible Total Organic and Inorganic Carbon Analyzer |
| 5,104,810 | Zero Gravity Purge and Trap for Monitoring Volatile Organic Compounds |
| 5,091,358 | Regenerable $CO_2/H_2O$ Solid Sorbent |
| 5,081,047 | Zero Gravity Compatible Total Organic Carbon Analyzer |
| 5,079,209 | Preparation of High Capacity Unsupported Regenerable $CO_2$ Sorbent |
| 5,073,505 | Eluent Storage and Preparation Apparatus and Method for Using the Same in a Zero Gravity Environment |